



UNIVERSIDAD DE CANTABRIA

PROGRAMA DE DOCTORADO

EN BIOLOGÍA MOLECULAR Y BIOMEDICINA

TESIS DOCTORAL

**NUEVOS MECANISMOS DE TUMOROGÉNESIS Y
PROGRESIÓN DEL LINFOMA CUTÁNEO DE CÉLULAS T: PAPEL
DE LA RED DE SEÑALIZACIÓN PLCG1-PRKCQ-STAT3**

PhD THESIS

**NOVEL MECHANISMS OF TUMORIGENESIS AND
PROGRESSION OF CUTANEOUS T CELL LYMPHOMA: ROLE
OF PLCG1-PRKCQ-STAT3 SIGNALLING NETWORK**

NURIA GARCÍA DÍAZ

Dirigida por:

Dr. JOSÉ P. VAQUÉ DÍEZ

Dr. MIGUEL Á. PIRIS PINILLA

Escuela de Doctorado de la Universidad de Cantabria

Santander 2019



UNIVERSIDAD DE CANTABRIA

PROGRAMA DE DOCTORADO

EN BIOLOGÍA MOLECULAR Y BIOMEDICINA

TESIS DOCTORAL

**NUEVOS MECANISMOS DE TUMOROGÉNESIS Y
PROGRESIÓN DEL LINFOMA CUTÁNEO DE CÉLULAS T:
PAPEL DE LA RED DE SEÑALIZACIÓN PLCG1-PRKCQ-STAT3**

PhD THESIS

**NOVEL MECHANISMS OF TUMORIGENESIS AND
PROGRESSION OF CUTANEOUS T CELL LYMPHOMA:
ROLE OF PLCG1-PRKCQ-STAT3 SIGNALLING NETWORK**

NURIA GARCÍA DÍAZ

Dirigida por:

Dr. JOSÉ P. VAQUÉ DÍEZ

Dr. MIGUEL Á. PIRIS PINILLA

Escuela de Doctorado de la Universidad de Cantabria

Santander 2019

Dr. José P. Vaqué Díez, investigador Ramón y Cajal en el Departamento de Biología Molecular de la Universidad de Cantabria,

Dr. Miguel Á. Piris Pinilla, Patólogo del Servicio de Patología de la Fundación Jiménez Díaz de Madrid y director del Máster de Oncología Molecular de la Universidad Rey Juan Carlos de Madrid,

EXPONEN:

Que han llevado a cabo las funciones de CO-DIRECTORES del trabajo de TESIS DOCTORAL realizado por la graduada Nuria García Díaz en el Instituto de Investigación Marqués de Valdecilla (IDIVAL) y el Departamento de Biología Molecular de la Universidad de Cantabria, titulado “NUEVOS MECANISMOS DE TUMOROGÉNESIS Y PROGRESIÓN DEL LINFOMA CUTÁNEO DE CÉLULAS T: PAPEL DE LA RED DE SEÑALIZACIÓN PLCG1-PRKCQ-STAT3”.

Consideramos que los objetivos planteados y los resultados obtenidos en dicho trabajo, fundamentan las conclusiones a las que se llegan. Por lo tanto, el trabajo reúne los requisitos necesarios para su presentación como memoria de Doctorado por la interesada, al objeto de poder optar al título de DOCTOR por la Universidad de Cantabria.

En Santander, a veintiuno de noviembre de dos mil diecinueve.

José P. Vaqué Díez

Miguel Á. Piris Pinilla

Esta Tesis Doctoral ha sido realizada conjuntamente en el Instituto de Investigación Marqués de Valdecilla (IDIVAL) y el Departamento de Biología Molecular de la Facultad de Medicina de la Universidad de Cantabria en Santander.

La financiación necesaria para la realización de esta Tesis Doctoral ha sido aportada por el Instituto Carlos III mediante los proyectos PI16/00156 y PIE15/00081, y por la asociación Luchemos por la Vida mediante los proyectos concedidos en 2016, 2018 y 2019.

La autora de esta Tesis ha disfrutado de contrato del Programa de Personal Investigador en formación predoctoral, referencia MPREVAL18/01 concedido por la Universidad de Cantabria, el IDIVAL y la Consejería de Educación del Gobierno de Cantabria.

A mis padres,
A mi hermana.
Gracias

"I neither know nor think that I know"

Socrates



UNIVERSIDAD DE CANTABRIA

PROGRAMA DE DOCTORADO

EN BIOLOGÍA MOLECULAR Y BIOMEDICINA

PhD THESIS

**NOVEL MECHANISMS OF TUMORIGENESIS AND
PROGRESSION OF CUTANEOUS T CELL LYMPHOMA:
ROLE OF PLCG1-PRKCQ-STAT3 SIGNALLING NETWORK**

NURIA GARCÍA DÍAZ

Escuela de Doctorado de la Universidad de Cantabria

Santander 2019

INDEX

ABBREVIATIONS	i
1. INTRODUCTION	1
1.1 Primary cutaneous lymphomas.....	3
1.2 Mycosis Fungoides and Sézary Syndrome.....	5
1.2.1 Diagnosis	5
1.2.2 Prognosis	7
1.2.3 Treatment	8
1.3 Pathogenesis	18
1.3.1 Immunophenotype	18
1.3.2 Tumour microenvironment.....	19
1.3.3 Molecular pathogenesis.....	23
1.4 Malignant signalling network comprising potential mechanisms of CTCL biology ...	28
1.4.1 TCR-PLCy1 signalling pathway.....	30
1.4.2 Role of PRKCQ in T-cell signalling	33
1.4.3 JAK/STAT signalling pathway.....	36
2. HYPOTHESIS AND OBJECTIVES	41
2.1 Hypothesis.....	43
2.2 Objectives.....	43
3. MATERIALS AND METHODS.....	45
3.1 Human samples.....	47
3.2 Chick embryo model for <i>in vivo</i> studies	47
3.2.1 Eggs preparation for xenografting tumour cells	48
3.2.2 Cells preparation for xenografting	48
3.2.3 Tumour cells grafting onto the CAM.....	50
3.2.4 Primary tumours and chick embryo tissues collection	50
3.2.5 Human tumour cells quantification	50
3.3 Cell culture for <i>in vitro</i> studies	51
3.3.1 Cell lines and maintenance	51
3.3.2 Reagents.....	53

3.3.3 Transfection	54
3.3.4 Lentivirus production and transduction.....	55
3.4 Cell viability assays	58
3.4.1 Cell proliferation assay.....	58
3.4.2 Synergism assay	59
3.4.3 Apoptosis assay	59
3.5 DNA and RNA analysis	60
3.5.1 Bacterial transformation and plasmid DNA purification.....	60
3.5.2 DNA isolation and purification from <i>in vivo</i> samples	62
3.5.3 Site-directed mutagenesis.....	62
3.5.4 DNA sequencing	63
3.5.5 Quanti-Blue™ assay.....	65
3.5.6 Luciferase reporter assay	65
3.5.7 Fluorescence in situ hybridization.....	67
3.5.8 RNA extraction and purification.....	67
3.5.9 Reverse transcription and quantitative polymerase chain reaction (RT-qPCR) ..	69
3.5.10 RNA sequencing	71
3.6 Protein analysis	72
3.6.1 Western blotting	72
3.6.2 Immunohistochemical staining.....	74
3.6.3 Nuclear-cytoplasmic fractionation.....	74
3.6.4 STAT3 transcription factor ELISA-based binding assay	76
3.6.5 Immunoprecipitation	77
3.6.6 Mass spectrometry	78
3.7 Statistical analyses.....	80
4. RESULTS	83
4.1 Correlation of clinical stage with biomarker expression in MF patients' samples....	85
4.1.1 Clinical characteristics at diagnosis of the MF patients' cohort.....	85
4.1.2 IHC analyses show differential STAT activation in patients with advanced-stage MF	86

4.2 HEK-Blue™ IL-6 cells as a model to study STAT3 activation	89
4.2.1 HEK-Blue™ IL-6 cell line set-up.....	89
4.2.2 JAK1 Y654F increase STAT3 activation upon IL-6 stimulation in HEK-IL6 cells...	91
4.3 PLCG1 downstream signalling towards NFAT, NF-κB and STAT3 transcriptional activity	93
4.3.1 PLCG1 S345F activates NFAT and NF-κB-mediated transcription by a PRKCQ dependent manner in HEK-IL6 cells.	93
4.3.2 PLCG1 S345F promotes activation of STAT3 in HEK-IL6 cells.....	95
4.4 TPA-mediated signalling towards NFAT, NF-κB and STAT3.....	97
4.4.1 TPA increases NFAT- and NF-κB-mediated transcription in HEK-IL6 cells.....	97
4.4.2 TPA increases STAT3-mediated transcription through PRKCQ and not through JAKs in HEK-IL6 cells.	100
4.4.3 JAK-dependent and -independent regulation of STAT3 activity in T cells	103
4.5 PRKCQ downstream signalling towards NFAT and STAT3 activation	105
4.5.1 PRKCQ expression in HEK-IL6, Jurkat and CTCL cell lines.....	105
4.5.2 A constitutively active PRKCQ mutant activates NFAT but not NF-κB	107
4.5.3 PRKCQ activates STAT3 through a mechanism that depends on its kinase activity	108
4.6 Effects of sotrastaurin and ruxolitinib in CTCL proliferation and apoptosis	110
4.6.1 Sotrastaurin inhibits cell proliferation and promotes apoptosis in HEK-IL6, Jurkat and CTCL cells.....	110
4.6.2 Ruxolitinib inhibits cell proliferation and promotes apoptosis in CTCL cells. ..	112
4.6.3 Synergistic activity of combined PRKCQ and JAK inhibition in cell proliferation	112
4.7 PRKCQ deficiency negatively affects CTCL cell proliferation and STAT3 activation	114
4.7.1 PRKCQ knockdown impairs STAT3 activation in HEK-IL6 and proliferation of T cells	114
4.7.2 PRKCQ knockdown impairs cell proliferation and STAT3 activation in CTCL cells	115
4.8 PRKCQ interacting proteins in CTCL cells	117
4.8.1 PRKCQ does not interact with STAT3.....	117
4.8.2 PRKCQ interactome.....	118

4.9 Biological CTCL effects of PRKCQ <i>in vivo</i>	122
4.9.1 PRKCQ knockdown effects in CTCL tumour growth, intravasation and metastasis <i>in vivo</i>	122
4.9.2 PRKCQ pharmacological inhibition exerts potent anti-CTCL effects regarding tumour growth and metastasis <i>in vivo</i>	123
4.10 Gene regulation by PRKCQ in CTCL cells	127
4.10.1 PRKCQ expression in CTCL cell samples used for RNA sequencing.....	127
4.10.2 Gene regulation by PRKCQ in basal conditions in CTCL cells	127
4.10.3 Gene regulation by PRKCQ in TPA-stimulated CTCL cells.	130
5. DISCUSSION.....	133
5.1 STAT3 as a marker of MF progression.....	135
5.2 Role of JAK/STAT signalling in CTCL.....	137
5.3 PLCG1/PRKCQ signalling towards NFAT and NF-κB activation.....	139
5.4 PLCG1/PRKCQ signalling towards STAT3 activation	140
5.5 PRKCQ participates in essential CTCL activities <i>ex vivo</i> and <i>in vivo</i>	143
6. CONCLUSIONS	147
7. BIBLIOGRAPHY	151
8. RESUMEN EN CASTELLANO.....	165
8.1 Introducción	167
8.2 Hipótesis y objetivos	170
8.3 Resultados y discusión	171
8.4 Conclusiones.....	175
ANNEXES.....	177
PUBLICATIONS.....	195

ABBREVIATIONS

7-AAD	7-aminoactinomycin D
AKT	Protein kinase B, PKB
AlloSCT	Allogenic stem cell transplantation
AP-1	Activator protein 1
APC	Anaphase-promoting complex
ASK1	Apoptosis Signal-Regulating Kinase 1, MAP3K5
ATP	Adenosine triphosphate
BCL3	B-Cell Lymphoma 3-Encoded Protein
BSA	Bovine serum albumin
BTK	Bruton's tyrosine kinase
BV	Brentuximab vedotin
CAM	Chorioallantoic membrane
CaN	Calcineurin
CARD	Caspase recruitment domain-containing protein 11
CCL	CC motif chemokine ligand
CCR	CC chemokine receptor
CD	Cluster of differentiation
CDKN2A/2B	Cyclin-dependent kinase Inhibitor 2A/2B
cDNA	Complementary deoxyribonucleic acid
CI	Combination index
CIT	Citron Rho-Interacting Serine/Threonine Kinase
CLA	Cutaneous Lymphocyte Antigen
CR	Complete response
Ct	Threshold cycle
CTCL	Cutaneous T cell lymphoma
CTLA-4	Cytotoxic T-Lymphocyte Antigen 4
CXCR	CXC chemokine receptor
DAG	Diacylglycerol
DAS	Dasatinib
DMEM	Dulbecco's Modified Eagle Medium
DMSO	Dimethyl sulfoxide
DNA	Deoxyribonucleic acid
dNTP	Deoxynucleotide triphosphates

DSS	Disease-specific survival
DUSP	Dual-specificity phosphatase
E. Coli	Escherichia coli
ECP	Extracorporeal photopheresis
EGFR	Epidermal growth factor receptor
ELISA	Enzyme-linked immunosorbent assay
EMA	European Medicines Agency
EORTC	European Organization for Research and Treatment of Cancer
ERK	Extracellular signal-regulated kinases
FACS	Fluorescence-activated cell sorting
FBS	Fetal bovine serum
Fc	Fragment crystallizable region
FDA	Food and Drug Administration
FDR	False discovery rate
FFPE	Formalin-fixed paraffin-embedded
FISH	Fluorescence in situ hybridization
FOS	Fostamatinib
FOXP3	Forkhead Box P3
g	Gravitational force
GAPDH	Glyceraldehyde 3-phosphate dehydrogenase
G-CSF	Granulocyte-colony stimulating factor
Gy	Gray (unit)
HDAC	Histone deacetylases
HEK293T	Human embryonic kidney 293T
HEK-IL6	Human embryonic kidney-Blue IL-6 cells
HF	High fidelity
HNRNPK	Heterogeneous Nuclear Ribonucleoprotein K
IBR	Ibrutinib
IC50	Half maximal inhibitory concentration
IFN	Interferon
IgG	Immunoglobulin G
IHC	Immunohistochemistry
IKK	I κ B kinase
IL	Interleukin
IL6ST	Interleukin 6 receptor
IP3	Inositol 1,4,5-trisphosphate
IS	Immunological synapse

ISCL	International Society for Cutaneous Lymphomas
ITK	IL2 Inducible T Cell Kinase
JAK	Janus kinase
kb	Kilobase
KIR3DL2	Killer Cell Immunoglobulin Like Receptor
LAR	Luciferase Assay Reagent
LAT	Linker for activation of T cells
LB	Luria-Bertani broth
LCK	Lymphocyte Cell-Specific Protein-Tyrosine Kinase
LIMK	LIM Domain Kinase
LSP	Lymphocyte Specific Protein
MAPK	Mitogen-activated protein kinase
MEK	Mitogen-activated protein kinase kinase
MF	Myosis fungoides
MHC	Major histocompatibility complex
min	Minutes
MK	MK-2206
MMAE	Monomethyl auristatin E
mRNA	Messenger ribonucleic acid
MS	Mass Spectrometry
mTOR	Mechanistic target of rapamycin kinase
MTX	Methotrexate
nbUVB	Narrowband ultraviolet B
NFAT	Nuclear factor of activated T cells
NFKB	Nuclear Factor Kappa B
NGS	Next generation sequencing
NM	Nitrogen mustard
NTC	Non-targeting control
OD	Optical density
ORR	Overall response rate
p	Protein
PBS	Phosphate-buffered saline
PCR	Polymerase chain reaction
PD-1	Programmed death 1
PFS	Progression-free survival
PGAM5	Phosphoglycerate Mutase Family Member 5
PI3K	Phosphatidylinositol-4,5-bisphosphate 3-kinase

PIAS	Protein inhibitors of activated STATs
PIP2	Phosphatidylinositol 4,5-bisphosphate
PKC	Protein kinase C
PLB	Passive lysis buffer
PLCG1/PLCy1	Phospholipase C gamma 1
PPM	Parts per million
PRKCQ	Protein kinase C, isoform θ
PTEN	Phosphatase and tensin homolog
PTP	Phospho-tyrosine phosphatases
PUVA	Plus ultraviolet A
QB	Quanti-blue
qPCR	Quantitative polymerase chain reaction
RA	Retinoic acid
RACK	Receptor for activated C kinase 1
REAL	Revised European-American Lymphoma
RIN	RNA integrity number
RLU	Relative light units
RNA	Ribonucleic acid
RNA-seq	RNA sequencing
ROR γ	Retinoic acid receptor-related orphan receptor gamma
rpm	Revolutions per minute
RPMI	Roswell Park Memorial Institute medium
rRNA	Ribosomal RNA
RT	Room temperature
RT-qPCR	Reverse transcription qPCR
RUX	Ruxolitinib
s	Seconds
SCNVs	Somatic copy number variations
SDS-PAGE	Polyacrylamide-SDS gel electrophoresis
SEAP	Secreted embryonic alkaline phosphatase
Seq	Sequencing
SH2	Src Homology 2
shRNA	Short hairpin RNA
SN	Supernatant
SOCS	Suppressor of cytokine signalling
SOT	Sotrastaurin
SS	Sézary syndrome

SSNVs	Somatic single-nucleotide variations
STAT	Signal Transducer and Activator of Transcription
SYK	Spleen tyrosine kinase
TAC	Tacrolimus
TANK	TRAF family member-associated NF-kappa-B activator
TBS-T	Tris-buffered saline-Tween
T _{cm}	Central memory T cells
TCR	T cell receptor
T _{em}	Effector memory T cells
TFA	Trifluoroacetic
Tfh	Follicular helper T cells
TGFB	Transforming growth factor beta
tGFP	Turbo green fluorescent protein
Th	Helper T cell
Tm	Melting temperature
TNF	Tumour necrosis factor
TNFRSF	Tumour necrosis factor receptor superfamily
TNMB	Tumour, node, metastasis, blood staging system
TP53	Tumour protein 53
TPA	12-O-tetradecanoyl-phorbol-13-acetate
TRAF	TNF receptor-associated factor
Treg	Regulatory T cell
Trm	Tissue-resident memory T cells
TS	Targeted sequencing
TSEB	Total skin electron beam
Tyk	Non-receptor tyrosine-protein kinase
Tyr	Tyrosine
USA	United States of America
UVA	Ultraviolet A
UVB	Ultraviolet B
WB	Western blot
WES	Whole exome sequencing
WGS	Whole genome sequencing
WHO	World health organization
ZAP-70	Zeta-chain-associated protein kinase 70
ZEB1	Zinc finger E-box-binding homeobox 1

INTRODUCTION

1. INTRODUCTION

1.1 Primary cutaneous lymphomas

Primary cutaneous lymphomas constitute a heterogeneous group of non-Hodgkin lymphomas affecting the skin with no evidence of concurrent extracutaneous disease at the time of diagnosis. After the gastrointestinal tract, the skin is the second most common site of extranodal non-Hodgkin lymphoma, with an estimated annual incidence of 1:100,000 (Willemze et al. 2005; Hristov et al. 2019).

In the last decades, the classification of cutaneous lymphomas has evolved and has been updated with the incorporation of new entities. In 1994, the Revised European-American Lymphoma (REAL) classification categorized the lymphoid malignancies in three types: B-cell, T-cell and Hodgkin's disease defining them for the first time with histologic, immunologic and genetic features (Lee Harris et al. 1994). Then, in 1997, the European Organization for Research and Treatment of Cancer (EORTC) Cutaneous Lymphoma Study Group proposed for the first time to distinguish between primary and secondary cutaneous lymphomas as the clinical behaviour and prognosis of these entities were clearly different from those systemic lymphomas that migrate to the skin secondarily (Willemze et al. 1997). In 2005, the World Health Organization (WHO) and the EORTC reached an agreement on a consensus cutaneous lymphomas' classification based on a combination of clinical, histologic, immunophenotypical and genetic features (Willemze et al. 2005). This classification, recently updated (Willemze et al. 2019), is worldwide used nowadays for the diagnosis of primary cutaneous lymphomas.

Currently, Cutaneous T cell lymphomas (CTCLs hereon) are considered a group of non-Hodgkin lymphomas characterised by the clonal proliferation of malignant CD4⁺ T cells in

INTRODUCTION

the skin. While nodal non-Hodgkin lymphomas are mostly B-cell derived, approximately 75-80% of primary cutaneous lymphomas are T-cell derived.

CTCLs are divided into three main categories: i) classical CTCLs, that includes the most common subtypes: Mycosis Fungoides (MF), MF variants and Sézary Syndrome (SS), ii) primary cutaneous CD30⁺ lymphoproliferative disorders (LPDs) and iii) the remaining group of rare CTCLs. The classification of the latter group is complex as they are very rare diseases that only accounts for less than 10% of all CTCLs. In **table 1.1** the classification of CTCLs is summarised alongside the frequency and the disease-specific 5-year survival of each subtype (Willemze et al. 2019).

Table 1.1. WHO-EORTC CTCL classification, its relative frequency and disease-specific 5-year survival.

*Data of all primary cutaneous lymphomas included in Dutch and Austrian registries between 2002 and 2017. N/A, not available; NOS, not otherwise specified. Table Adapted from Willemze *et al.* 2005 and Willemze *et al.* 2019.

WHO-EORTC classification	Frequency (%)*	Disease-specific 5-year survival (%)
Classical CTCLs		
MF	39	88
MF variants		
Folliculotropic MF	5	75
Pagetoid reticulosis	<1	100
Granulomatous slack skin	<1	100
SS	2	36
Primary cutaneous CD30⁺ LPDs		
Cutaneous anaplastic large cell lymphoma	8	95
Lymphomatoid papulosis	12	99
Rare CTCLs		
Adult T-cell leukemia/lymphoma	<1	N/A
Subcutaneous panniculitis-like T-cell lymphoma	1	87
Extranodal NK/T-cell lymphoma, nasal type	<1	16
Chronic active EBV infection	<1	N/A
Primary cutaneous peripheral T-cell lymphoma, rare si	6	11-100
Primary cutaneous peripheral T-cell lymphoma, NOS	2	15

1.2 Mycosis Fungoides and Sézary Syndrome

MF is the most common CTCL subtype accounting for approximately 45% of them. It has been classically described as a clonal expansion of tissue-resident helper T cells in the skin. It has an indolent clinical course with slow progression over years and can be presented in different forms ranging from unique patches (**figure 1.1A**) to more extended skin involvement with plaques (**figure 1.1B**) and tumours (**figure 1.1C**), but furthermore, it can also progress to extracutaneous localizations. MF has an annual incidence rate (IR) of 4.1/1.000.000 people being more prevalent in males than females (male-female IR ratio of 1.72) (Bradford et al. 2009). This IR increases among black patients (5.9/1.000.000). Generally, it can typically affect adults with a median age at diagnosis of 55-60 years (Willemze et al. 2005).

SS is a rare leukemic type of CTCL, only accounting for 2% of them (Willemze et al. 2019), and characterized by erythroderma (**figure 1.1D**), generalized lymphadenopathy, hyperkeratosis (**figure 1.1E**) and the presence of neoplastic T cells with cerebriform nuclei (Sézary cells, **figure 1.1F**) in the skin, lymph nodes and peripheral blood (Willemze et al. 2005; Willemze et al. 2019).

1.2.1 Diagnosis

Although MF and SS are classified as separate entities, the same clinical staging system has been used to assure a uniform diagnosis and management of the patients. To that end, the International Society for Cutaneous Lymphomas (ISCL) and EORTC proposed an updated staging system based on the TNMB classification that evaluates the involvement of skin

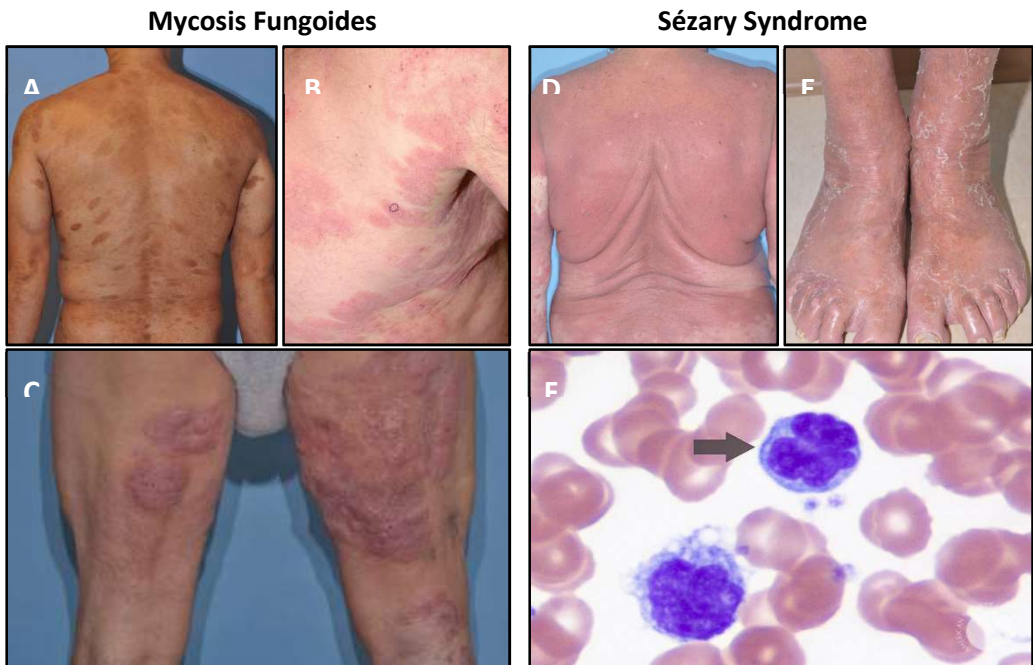


Figure 1.1. Clinical manifestations of Mycosis Fungoides and Sézary Syndrome. MF patients presenting patches (A), plaques (B) and tumours (C). SS patient presenting generalized erythroderma (D) and hyperkeratosis (E), and Sézary cells from peripheral blood (F). Patient images adapted from Jawed *et al.* 2014 and Sézary cell image from <https://imagebank.hematology.org/>

lesions (T, tumour), lymph nodes (N), visceral organs (M, metastasis), and peripheral blood (B) in a range of 0-4 (Olsen *et al.* 2007) and by establishing stages from IA to IVB. Stages IA, IB and IIA are considered early stage disease, whereas stages IIB to IVB constitute advanced disease. In **table 1.2** the most relevant TNMB features of each stage are summarised (Agar *et al.* 2010; Trautinger *et al.* 2017).

Early stages of MF can be difficult to diagnose because patients develop clinical features very similar to other benign skin diseases and the final diagnosis can be delayed up to 3 years, although this delay does not necessarily imply progression to more advanced stages (Scarlsbrick *et al.* 2018 Nov 25). The ISCL proposed a MF diagnosis based on an algorithm including clinical, histopathologic, molecular and immunopathologic features. Some of the clinical criteria used focuses on the variability in size, shape and colour of individual lesions

and /or the number and distribution of these lesions. Among the histopathological features, the presence of atypical lymphoid cells within the epidermis, surrounding a Langerhans cell in the so-called Pautrier's microabscesses, or the increase in the number of lymphocytes (not necessarily atypical) are the most characteristic events. Nevertheless, these features are the most difficult and debated ones because, in many cases, biopsies from multiple sites overtime are required to clearly identify a MF diagnosis (Kim et al. 2005). As ancillary studies for diagnosis, PCR-based analysis of the T cell receptor gamma (TCR γ) gene rearrangements and the loss of expression of some T cell surface antigens such as CD2, CD3, CD5 and CD7 are used to help with the definite MF diagnosis although the sensitivity and specificity of these immunohistologic criteria are highly variable. In conjunction, MF diagnosis usually requires an integrated clinical, morphological, immunohistochemical and molecular analysis (Pimpinelli et al. 2005).

The diagnosis of SS requires also the presence of clinical, analytical, immunohistochemical and molecular studies. Eventually, the identification of the same clonal T cell in the skin and peripheral blood is crucial to exclude patients with benign inflammatory conditions (Vonderheid et al. 2002). In addition, this evidence has to be confirmed with an absolute Sézary cell account of at least 1000 cells/mm³ and/or the presence of immunophenotypical abnormalities such as expanded CD4⁺ T cell population (with a CD4/CD8 ratio more than 10) and the loss of mature T cell antigens such as CD7 and CD26. Also, the infiltration of Sézary cells in the lymph nodes involved, erythroderma and palmoplantar hyperkeratosis are commonly present in SS patients (Willemze et al. 2005).

1.2.2 Prognosis

Whereas the prognosis of MF patients depends on stage, particularly the type and extent of skin lesions, and the involvement of the disease at extracutaneous localizations, the

INTRODUCTION

prognosis of SS patients is generally poor. The median survival of MF patients is 20 years, whereas a SS patient has a median survival of approximately only 3.13 years and a higher progression risk than MF patients (Agar et al. 2010). Based on the stage, patients with limited patch/plaque disease (covering less than 10% of the skin surface, stage IA) have a 5-year disease-specific survival (DSS) of 98% which decreases to 89% if the skin surface affected is more than 10% (stage IB). 5-year DSS for patients with one or more tumours (stage IIB) is only 56% and decreases to 23% when there is a histologically documented lymph node involvement of high grade (stage IVA₂). When metastasis affects any visceral organ, the 5-year DSS decreases to only 18% (**table 1.2**).

Additionally, the infiltration of hair follicles (folliculotropism) and the presence of >25% of large cells in the dermal infiltrate (large cell transformation) have a prognostic value, both associated with a poorer outcome (Agar et al. 2010; Pérez et al. 2019).

1.2.3 Treatment

Currently, there is no curative treatment for CTCL. The treatment of MF and SS patients is merely palliative and focused on improving symptoms and quality of life, with the exception for allogeneic stem cell transplantation that could achieve curative intentions. Following a stepwise, stage-adapted approach is recommended for the treatment of these patients, considering age, patient general status, extent of lesions, rate of disease progression and prior therapies (Wilcox 2017). For very early stages, mainly when only patches are present, the best option is to apply a 'watch and wait' expectant policy as patients with stage IA have a low risk of progression (only 10% within 10 years) (Agar et al. 2010). In general, skin-directed therapies are the best option for early stages of MF as a first-line treatment, while systemic therapies, usually combined with skin-directed treatment, are more commonly used for more advanced stages of MF and SS. The choice of the different treatment options

Table 1.2. ISCL/EORTC staging for MF/SS. Table showing the most relevant characteristics of skin (T: tumour), nodal (N), visceral (M: metastasis) and blood (B) involvement for each stage, the median overall survival (OS) and the 5-year disease-specific survival (DSS). Table adapted from Trautinger *et al.* 2017 and Agar *et al.* 2010.

Stage	TNMB classification				Median OS (years)	5-year DSS (%)
	T	N	M	B		
Early	IA	Limited patches or plaques covering < 10% skin surface	No clinically abnormal peripheral lymph nodes	No visceral organ involvement	Absence or low blood burden	35.5 98
	IB	Patches or plaques covering ≥ 10% skin surface	No clinically abnormal peripheral lymph nodes	No visceral organ involvement	Absence or low blood burden	21.5 89
	IIA	Any patches or plaques	Clinically abnormal peripheral lymph nodes, grade 2 or less	No visceral organ involvement	Absence or low blood burden	15.8 89
Advanced	IIB	One or more tumour ≥ 1 cm diameter	None to clinically abnormal peripheral lymph nodes, grade 2 or less	No visceral organ involvement	Absence or low blood burden	4.7 56
	IIIA	Erythroderma covering ≥ 80% body area	None to clinically abnormal peripheral lymph nodes, grade 2 or less	No visceral organ involvement	No blood burden	4.7 54
	IIIB	Erythroderma covering ≥ 80% body area	None to clinically abnormal peripheral lymph nodes, grade 2 or less	No visceral organ involvement	Low blood burden (>5% peripheral blood lymphocytes atypical)	3.4 48
	IVA ₁	Any skin involvement	None to clinically abnormal peripheral lymph nodes, grade 2 or less	No visceral organ involvement	High blood burden (≥1000/μl Sézary cells)	3.8 41
	IVA ₂	Any skin involvement	Clinically abnormal peripheral lymph nodes, grade 3-4	No visceral organ involvement	Low to high tumour burden	2.1 23
	IVB	Any skin involvement	None to clinically abnormal peripheral lymph nodes, grade 3-5	Visceral involvement	Low to high tumour burden	1.4 18

INTRODUCTION

for CTCL is dependent on social and scientific grounds; for that reason, I will focus on those available and commonly used in Europe (a summarized first- and second-line treatment options are shown in **table 1.3**).

Table 1.3. First- and second-line treatment options in MF/SS. Adapted from Trautinger *et al.* 2017

	Stage	First-line	Second-line
Early	IA-IIA	Expectant policy or SDT: Topical corticosteroids, nbUVB, PUVA, Localised RT,	SDT: TSEB Systemic: retinoids, IFN α , low- dose MTX
	IIB	SDT: TSEB, Localised RT Systemic: retinoids, IFN α , low- dose MTX, monochemotherapy	Systemic: polychemotherapy, alloSCT
Advanced	IIIA-IIIB	SDT: TSEB Systemic: retinoids, IFN α , low- dose MTX, ECP	Systemic: monochemotherapy, alloSCT
	IVA-IVB	Radiotherapy (TSEB and localised) Systemic: chemotherapy	Radiotherapy (TSEB and localised) Systemic: chemotherapy,
	SS	Systemic: retinoids and IFN α (in combination with ECP or PUVA), low-dose MTX	Systemic: chemotherapy, alemtuzumab, alloSCT
	Maintenance after remission	ECP, IFN α , low-dose MTX, NM, PUVA, retinoids, topical corticosteroids, UVB	

1.2.3.1 Skin-directed therapies (SDT)

Topical corticosteroids

Corticosteroids have an immunosuppressive effect by inhibiting lymphocyte binding to the endothelium and intercellular adhesion. They are widely used as palliative treatment for individual lesions in early patch/plaque disease. In a single study of 79 patients with stage IA/IB, the twice-daily use of high-potency topical corticosteroids showed an overall response rate of 94% for IA stage and 82% for IB, with complete response (CR) rates of 63% and 25% respectively (Zackheim *et al.* 1998). The most common cutaneous side-effects of

the treatment with corticosteroids are irritant dermatitis, purpura (purple-coloured spots) and in some cases reversible suppression of cortisol levels.

Topical mechlorethamine

Mechlorethamine, also known as nitrogen mustard (NM), is a cytotoxic chemotherapy agent approved by the United States (US) Food and Drug Administration (FDA) for the treatment of MF stage IA/IB who have received prior skin-directed therapy. The 0.02% gel preparation showed response rates of 58.5% with 13.8% of CR (Lessin et al. 2013). In Europe, it has recently been authorised as a first line treatment for early MF stages (https://www.ema.europa.eu/en/documents/assessment-report/ledaga-epar-public-assessment-report_en.pdf). Topical NM is well tolerated but some side-effects are observed such as allergic contact dermatitis.

Ultraviolet phototherapy

A consensus guideline for the use of phototherapy in MF/SS, for both clinical practice and for clinical trials, has been recently published by the US Cutaneous Lymphoma Consortium (Olsen et al. 2016). 8-Methoxypsoralen, supplied orally, plus ultraviolet A (PUVA) and narrowband ultraviolet B (nbUVB) are the most widely available phototherapy options. nbUVB is recommended for early MF/SS stages characterized by patches only, as it cannot penetrate deeper than UVA in the skin. For plaque disease and for dark skin patients PUVA is the phototherapy recommended.

The CR of nbUVB range from 54% to 90% of patients (average: 84%), depending on the study and the variable definition of disease clearance. CR rates for PUVA are 85% for stage IA, 65% for stage IB and 85% for stage IIA (Olsen et al. 2016). If the patient shows insufficient

INTRODUCTION

response or immediate relapse, phototherapy can be combined with systemic options such as retinoids or interferon α , described below.

Patients treated with phototherapy can develop erythema and pruritus, but the most important side effect is the development of secondary skin cancer. Although there are large studies analysing the potential risk of acquiring skin cancer after phototherapy treatment in patients with psoriasis and other skin disorders (Lee et al. 2005), these studies in MF/SS patients are limited. In a follow-up study on early stage MF patients treated with PUVA in a continuous maintenance of about every 6 weeks, 26% developed non-melanoma skin cancer, including squamous cell carcinoma and basal cell carcinoma (Querfeld et al. 2005). A long-term follow up of patients or alternative treatment should be considered to prevent and/or treat possible adverse effects by phototherapy in MF patients.

Total skin electron beam therapy

Total skin electron beam (TSEB) therapy is used when the distribution of disease is along the entire skin surface. In this technique electrons are generated in a linear accelerator and attenuated to penetrate the skin to a limited depth so toxicity to internal organs is largely reduced. TSEB is recommended for first-line treatment of MF from stage IIB to IVB and as a second-line treatment for IA, IB and IIA stages. The standard dose of 30-36 Gy is able to induce remission rates, particularly in T2 and T3 disease (Maingon et al. 2000). Recently, the reduction in radiation doses (12 Gy) have been compared to the standard ones for their clinical efficacy with similar successful results in treatment outcome (overall response rate (ORR) for both treatment regimens was over 87.5%) but with lower toxicity (Georgakopoulos et al. 2018). Common side effects of standard dosing include desquamation, erythroderma, alopecia, nail changes and limb edema.

Localised radiotherapy

Localised and superficial radiotherapy (RT) provides effective palliative treatment for individual lesions inducing long-term remission in unilesional disease (Micaily et al. 1998). It can be used alone or as adjuvant treatment in combination with other skin-directed or systemic therapies for patients with early stages of MF. Side effects of local radiation are dose dependent but minimal. Most reported ones are erythema, desquamation, atrophy and skin dryness.

1.2.3.2 Systemic therapies***Retinoids***

Retinoids are derivatives of vitamin A that exert their activities by interacting with nuclear receptors (both retinoic acid and retinoic X receptors). Bexarotene, the only retinoid specifically developed and approved for the treatment of refractory, advanced-stage CTCL (Duvic et al. 2017), is an inducer of apoptosis and inhibits metastasis and angiogenesis that has shown an ORR of 45%, although it is commonly used in combination or in maintenance. The most common side effects observed are drying of the skin and mucous membranes and central hypothyroidism. All retinoids are teratogenic.

Interferon α

Interferons (IFN) are polypeptides with antiviral, cytostatic and immunomodulating functions. Among all, IFN- α is the one approved for the treatment of MF/SS with partial remission rates of more than 50% and complete responses of about 20% (Olsen 2003). It has dose dependent side-effects such as flu-like symptoms, elevated transaminases, leukopenia and thrombocytopenia.

INTRODUCTION

Chemotherapy

Single-agent and combination chemotherapy regimens have been used for the treatment of non-Hodgkin lymphomas since the 1970s, but their activity in CTCL is far from long-lasting and has been associated with high toxicity and risk of infection (Hughes et al. 2015). This therapeutic approach is being used in patients with advanced-stage MF (IVA and IVB) or SS who have had multiple relapses, but more than 90% of them will receive alternative treatment within 1 year, so usually alternative options are preferred. On the other hand, methotrexate (MTX), a cytotoxic antifolate, has been used in non-oncological diseases such as psoriasis and rheumatoid arthritis, and in low dosages, are well tolerated for the treatment of MF/SS (Benedek 2010).

Extracorporeal photopheresis (ECP)

This phototherapy consists in extracorporeal blood exposure to the photoactivated drug 8-methoxypsoralen with an excellent safety profile and very rare adverse events. It has shown a good efficacy (with ORR around 60%) and prolonged survival in patients with advanced stages either as monotherapy or combined with other treatment options such as retinoids, interferons or PUVA, although it can be also used in early stages of the disease and as maintenance after remission achievement (Knobler et al. 2014).

Allogeneic stem cell transplantation (AlloSCT)

AlloSCT is based on the transplant of hematopoietic stem cells from a matching donor, in order to suppress the disease and restore the patient immune system, being considered the only treatment option in MF/SS with curative intention. It is used as second-line treatment for advanced stages of MF and SS, preferably in young patients with low tumour burden and a high predictable risk of progression at the same time (Trautinger et al. 2017).

Although it is available just for a very small patient population, it has a 5-year overall survival of 46% (Duarte et al. 2014) and it has been observed that 80% of patients will not require further treatment options within a year (Hughes et al. 2015).

1.2.3.3 Novel therapies

Due to the lack of curative treatment options in CTCL, there are many novel targeted therapies under research. In the last few years, a number of agents have been approved for the treatment of CTCL in USA and Japan such as vorinostat and romidepsin, two Histone Deacetylase (HDAC) inhibitors. But the access to these treatments in Europe is limited. Recently, the European Medicines Agency (EMA) has approved two monoclonal antibodies that showed promising results, and a number of other compounds are currently being investigated. Here, some of the most important ones are summarized.

Monoclonal antibodies

In 2017 and 2018, two monoclonal antibodies have been approved in Europe showing clinical benefit for CTCL patients: brentuximab vedotin and mogamulizumab (Oka and Miyagaki 2019).

Brentuximab vedotin (BV) is an antibody-drug conjugate composed of monomethyl auristatin E (MMAE), a cytotoxic anti-tubulin agent, and a chimeric monoclonal anti-CD30 antibody. CD30 is a cell membrane protein belonging to the tumour necrosis factor receptor superfamily, which has been shown to be expressed on tumour cells of MF/SS patients. BV specifically binds to CD30 and, once internalized and cleaved, releases the MMAE disrupting the microtubule network and causing cell cycle arrest and apoptosis (Deng et al. 2013). In the ALCANZA study, an international randomized phase 3 trial, the median progression-free survival (PFS) was 15.9 months (versus 3.5 months for patients treated with the physician's

INTRODUCTION

choice agent), and 5% of the patients achieved CR after BV treatment (Prince et al. 2017), suggesting that this treatment can be an appropriate option in patients with malignant cells expressing CD30 in at least in 10% of the skin infiltrate.

On the other hand, mogamulizumab is a humanized IgG1 monoclonal κ antibody with a defucosylated Fc region which selectively binds to C-C chemokine receptor 4 (CCR4). CCR4 is the receptor for thymus and activation-regulated chemokine and macrophage-derived chemokine and is involved in the migration of type 2 helper T cells and regulatory T cells to the skin. Mogamulizumab exerts an enhanced antibody-dependent cellular cytotoxicity in CCR4-expressing tumoral cells (Ishii et al. 2010). In the MAVORIC study, this antibody has shown an ORR of 21% in MF and 37% in SS patients with relapsed or refractory disease, suggesting that this treatment is especially effective for those patients with blood involvement; reaching a median PFS of 7.7 months as compared with 3.1 for vorinostat, a HDAC inhibitor (Kim et al. 2018).

Other antibodies are currently being investigated for CTCL patients such as inhibitors of the immune checkpoint and a KIR3DL2 inhibitor. Immune checkpoints molecules, such as cytotoxic T lymphocyte-associated protein 4 (CTLA-4) and programmed cell death protein 1 (PD-1), are negative regulators of T cell responses. Thus, targeting these molecules, the anti-tumour immune T cell responses can be improved. A recent phase 2 study conducted in advanced and refractory CTCL patients has shown an 37.5% ORR for *pembrolizumab*, a PD-1-blocking antibody, suggesting that inhibiting immune checkpoints can be a novel strategy for advanced MF/SS treatment (Khodadoust et al. 2019). KIR3DL2 (also known as CD158k) is a member of the killer-cell immunoglobuline-like receptor family that binds to HLA-class I ligands and negatively modulates immune cell functions. This receptor is widely expressed in malignant T cells in SS and advanced MF, and results from phase I trials have

shown an ORR in 44% in patients treated with *IPH4102*, an anti-KIR3DL2 antibody (Oka and Miyagaki 2019; Bagot et al. 2019). Thus, these promising results make it a potential novel therapy for these patients.

Other targeted inhibitors

Currently, other clinical trials assessing the efficacy of targeted inhibitors such as duvelisib, everolimus or topical pimecrolimus are being conducted. Duvelisib and everolimus are oral inhibitors of PI3K and mTOR respectively. These are being studied in the treatment of patients with relapsed or refractory CTCL and are showing partial responses with ORR of 31.6% for duvelisib and 44% for everolimus (Oka and Miyagaki 2019). Topical pimecrolimus, a calcineurin (CaN) inhibitor, is currently being studied as first-line treatment in patients with early stages of MF. Downstream of TCR-PLCG1 signalling (see below), activated CaN dephosphorylates and activates Nuclear Factor of Activated T cells (NFAT), a transcription factor that is a key regulator of T cell functions. Therefore, inhibition of CaN might be a therapeutic option for CTCL. Pimecrolimus has been approved for the treatment of a number of dermatologic disorders like for example atopic dermatitis (Guenther et al. 2019), so its efficacy is being studied in a multicentre, single-arm, phase 2 study (PimTo-MF study, EudraCT number: 2014-001377-14) in 39 patients with early stages (IA-IIA) of MF. The preliminary results are promising (manuscript in preparation): only 1 patient (2.5%) showed progression disease, 16 (41%) stable disease, 21 (54%) partial response and 1 (2.5%) showed a complete response.

These clinical results suggest that CTCL patients with activated PI3K, mTOR or CaN signalling pathways might be beneficiary for targeted therapy.

1.3 Pathogenesis

1.3.1 Immunophenotype

Cutaneous lymphomas are characterized by the epidermal infiltration of atypical T cells forming the characteristic Pautrier's microabscesses (intraepidermal clusters of clonal T cells), a highly distinctive feature of MF but only observed in a minority of cases (Willemze et al. 2005). In a physiological context, upon encountering antigen in the lymph nodes, activated naïve T cells express cutaneous lymphocyte antigen (CLA) and chemokine receptors such as CCR4 that binds to endothelial surface receptor E-selectin and CC ligand 17 (CCL17) respectively, thus facilitating their homing to the skin (Girardi et al. 2004). Activated T cells can differentiate into multiple T cell subsets of effector and memory cells, depending on the cytokine production. Central memory T cells (T_{CM}) access peripheral blood and lymph nodes and effector memory T cells (T_{EM}) migrate into extranodal regions such as the skin where the majority will remain as tissue-resident memory T cells (T_{RM}) (Clark et al. 2006; Watanabe et al. 2015). In a CTCL context, it has been demonstrated that SS and MF can arise from different T cell subsets probably giving evidence of the distinct clinical behaviour of both CTCL subtypes. While malignant T cells from SS patients have a T_{CM} phenotype capable of circulating between skin, lymph nodes and blood, which is consistent with SS clinical manifestations (lymphadenopathy and presence of malignant T cell in the peripheral blood), T cells from MF have a T_{EM} phenotype and remain in the skin where they can produce inflammatory cytokines that facilitate the recruitment of other non-malignant T cells and the formation of the characteristic patches and plaques of this subtype (Campbell et al. 2010). Nevertheless, it has been shown that many characteristics of the malignant T cells can change during disease progression and the phenotypical heterogeneity and plasticity within the malignant population seems to be relatively high

(Krejsgaard et al. 2012). Interestingly, in two very recent studies, it has been proposed that the initial transformation in MF does not seem to occur at the level of mature skin-resident memory T cells, as currently believed, but in some cases probably at a much earlier stage during lymphocyte development. More specifically, it has been suggested that it occurs after completion of TCR γ rearrangements but before the initiation of TCR β and TCR α recombination. These observations are supported by the identification of identical sequences of TCR γ but multiple TCR β and TCR α clonotypes, hence, suggesting a potential polyclonal origin of this type of lymphoma (Iyer et al. 2019; Hamrouni et al. 2019).

1.3.2 Tumour microenvironment

1.3.2.1 Th1-Th2 transition

Naïve CD4⁺ T-cell can differentiate into T helper 1 (Th1), Th2, Th17, induced regulatory T cell (iTreg) and follicular helper T cells (Tfh) depending on the cytokines produced: interleukin 12 (IL-12) and IFN- γ are important for Th1 cell differentiation, IL-4 for Th2 cell differentiation, TGF- β together with IL-6 induces Th17 cell differentiation, TGF- β , retinoic acid (RA), and IL-2 regulates iTreg differentiation whereas Tfh differentiation is induced by IL-21. Alongside these and as part of intricate signalling events, activation of specific transcription factors can trigger differentiation programs for each T helper cell subset like T-bet for Th1 cells, GATA3 for Th2 cells, ROR γ t for Th17 cells and Foxp3 for iTreg (Zhou et al. 2009).

It has been described that Th1 cell lineage predominates in early MF together with a high expression of IL-2, IL-12 and IFN- γ . However, as disease progresses to more advanced stages or in SS cases, the phenotype changes to Th2 with an increased IL-4, IL-5, IL-10 and IL-13 expression that occurs concomitantly with a decrease in the expression of Th1 factors (Saed et al. 1994; Papadavid et al. 2003; Guenova et al. 2013). In parallel to this shift in the

INTRODUCTION

phenotype balance, a switch in the expression of chemokines favouring the progression of the disease has been shown and is explained as follows: there is a decrease in chemokines that preferentially attract CXCR3- and CCR5-expressing Th1 inflammatory cells, such as CXC ligand 9 (CXCL9) and CXCL10, and an increase in chemokines that primarily attract CCR3-, CCR4- and CCR8-expressing Th2 cells such as CC ligand 17 (CCL17), CCL18, CCL22 and CCL26 (Krejsgaard et al. 2017).

One of the mechanisms that have been proposed for the Th1-Th2 transition is the distinct proportion of T cell population that can be detected in the skin lesions (**figure 1.2**). In early stages of CTCL, the skin lesions contain a small population of malignant CD4⁺ T cells within a dense infiltrate of activated CD8⁺ cytotoxic T cells and Th1 cells expressing cytotoxic molecules that mediates anti-tumour responses and consequently suppressing the expansion of malignant cells. But in the progression of the disease, a reduction in CD8⁺ cells as a result of a clonal CD4⁺ expansion presumably driving the acquisition of a Th2 phenotype has been shown (Kim et al. 2005). Supporting this information, CD8⁺ T cell number has been correlated with good prognosis in patients with MF. A plausible explanation for this, may consists of considering that early-stage disease with a high number of infiltrating reactive T cells and a Th1 phenotype is associated with a skin-restricted disease, whilst progressive disease is associated with a Th2 phenotype and systemic immunological deficiencies (Vermeer et al. 2001).

1.3.2.2 Role of interleukins

Besides the increase in Th2-associated cytokines and chemokines, the expression of a range of interleukins increase during the clinical course of the disease. These have been shown to play important pathogenic roles by paracrine and autocrine mechanisms. In this regard and to show a number of examples, IL-4 and IL-13 have been found to promote tumour cell

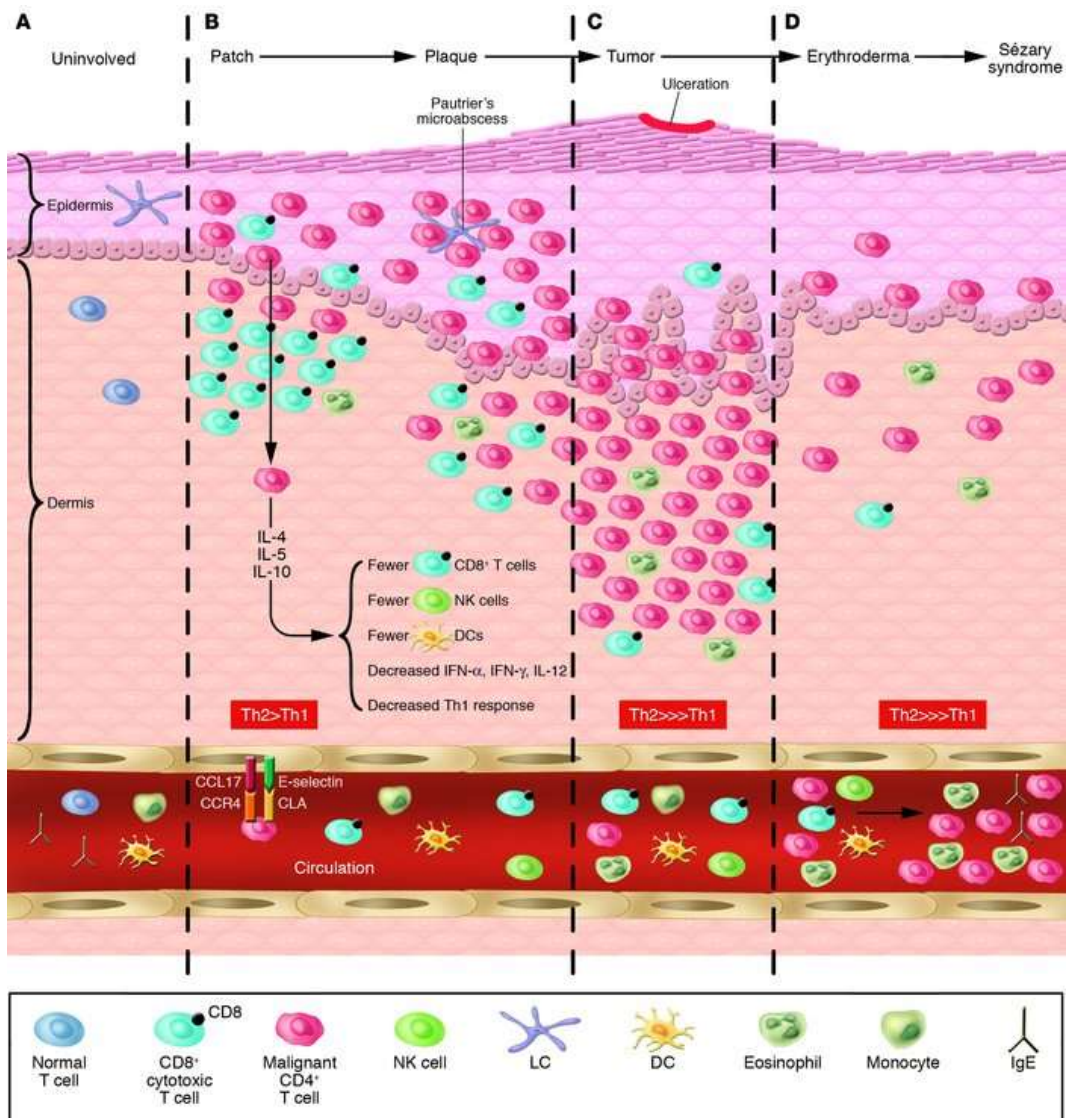


Figure 1.2. Tumour microenvironment in MF progression and SS. A) Normal skin showing resident Langerhans cells in the epidermis and skin-homing T cells in the dermis and circulation. B) Patch and plaque MF in which the CD4⁺ malignant T cells home to the epidermis around Langerhans cells. In these stages, CD8⁺ T cells are frequently found in the infiltrate as part of the host immune response. C) Tumour MF comprised of primarily malignant T cells and few CD8⁺ T cells. D) Erythrodermic MF and SS with detectable circulating malignant T cells that elaborate Th2 cytokines that affect CD8⁺ T cell, natural killer (NK) cells, and dendritic cells (DC) numbers and function, and consequently, the host immune response. Image adapted from Kim E *et al.* 2005.

INTRODUCTION

proliferation in a signal transducer and activator of transcription 6 (STAT6)-dependent manner (Geskin et al. 2015). In addition, IL-15 can be produced by malignant T cells but also by activated epidermal keratinocytes in the tumour microenvironment, it can contribute to the aberrant activation of the transcription factors STAT3 and STAT5 in advanced CTCLs (Netchiporouk et al. 2014). Following this line of evidence regarding aberrant STAT activation, Th17 phenotype acquisition and IL-17 expression, which are both controlled by Janus kinase 3 (JAK3)/STAT3 signalling, have been associated with advanced stages or increased risk of disease progression (Krejsgaard et al. 2011; Krejsgaard et al. 2013). Furthermore, IL-16 induces the recruitment of CD4⁺ T cells to the skin (Tuzova et al. 2015) whereas IL-10 expression contributes to the suppression of cellular immunity and anti-tumour responses (Fiorentino et al. 1991). In summary, all these interleukins not only impair cellular immunity and anti-tumour responses but can also contribute to the proliferation of malignant T cells by triggering key pro-oncogenic signalling mechanisms, like JAK/STAT, that may be essential for the progression of the disease.

1.3.2.3 *Staphylococcus aureus* infections

Due to a compromised cutaneous barrier and the dysfunction in the immune responses, the skin of CTCL patients is often colonized with enterotoxin-producing *Staphylococcus aureus* (Axelrod et al. 1992; Nguyen et al. 2008). It has been observed that staphylococcal enterotoxins induce an increased proliferation, activation of STAT3 and expression of STAT3-regulated cytokines in the malignant T cells thus probably promoting malignant transformation or progression (Willerslev-Olsen, Krejsgaard, Lise M Lindahl, et al. 2016). Although the infection with these bacteria is not specific of CTCL patients (as its colonization has been also observed in benign diseases such as atopic dermatitis), the infectious events are a major cause of morbidity and mortality (Blaizot et al. 2018) and the treatment of these

patients with antibiotics has been associated with significant clinical improvement (Talpur et al. 2008),

1.3.3 Molecular pathogenesis

1.3.3.1 Cytogenetic aberrations

Before the next generation sequencing (NGS) era, both cytogenetic and molecular studies revealed a high degree of chromosomal instability in both MF and SS. Amongst these, recurrent hotspot chromosomal abnormalities have been identified and include: loss of 9p21 (involving *CDKN2A-CDKN2B*), 10q (loss of *PTEN* and *FAS*), 17p (loss of *TP53*), 19p (loss of *E2A*); and 8q and 17q gains (affecting *MYC* and *STAT3/STAT5* respectively) (Mao et al. 2003; Vermeer et al. 2008; Laharanne et al. 2010). More recently, it has been described that a high proportion of the oncogenic abnormalities identified in MF and SS correspond to somatic copy number variations (SCNVs) as compared to somatic single-nucleotide variations (SSNVs) (an average of 11.8 versus 1.0 respectively) (Choi et al. 2015). This frequency is significantly higher than those observed in other adult cancer types (Elenitoba-Johnson and Wilcox 2017). In this regard, the ratio of *TP53* deletions to mutations is significantly higher in CTCL (5.1 vs. 1) than in other tumours where the prevalence of *TP53* deletion and mutation are almost equivalent. Also, the percentage of patients with *STAT3* and *STAT5B* amplifications (up to 60%) largely overcome that of mutations (0.9% and 3.6% for each gene respectively). Also, *JAK2* and *PRKCQ* (gene encoding for the isoform θ of Protein Kinase C, PKC θ) are amplified in 12.5% and 30% of CTCL samples analysed respectively whereas mutations were detected in only 0.9% of the cases for *PRKCQ* and undetectable in *JAK2* (Park et al. 2017).

Following the above-mentioned line of evidence, deletions in *ZEB1* (60% patients) were also detected more frequently than mutations (Choi et al. 2015). *ZEB1* is a transcription factor

INTRODUCTION

that exerts tumour suppressor activities in CTCL. Interestingly, ZEB1 DNA binding sites are located upstream of the transcription initiation site of *GATA3*, a transcription factor crucial for Th2 cell differentiation. Thus, *ZEB1* loss might contribute to *GATA3* overexpression and a subsequent acquisition of a Th2 phenotype, which, as aforementioned, has been correlated with advanced CTCL stages (Saed et al. 1994; Guenova et al. 2013). Finally and to provide further evidence regarding the complex and heterogeneous landscape of inter- and intrachromosomal rearrangements compared to SSNVs in CTCL lesions, and regarding the focus of this work, recurrent deletions have been detected in *HNRNPK* and *SOCS1* (in 37% and 33% of the MF patients analysed respectively) (Bastidas Torres et al. 2018). Interestingly both genes codify for proteins that are negative regulators of JAK/STAT signalling and therefore highlight the potential malignant role that this signalling pathway may play in the biology of this disease.

1.3.3.2 Mutational landscape

Recently, genome-wide studies based on NGS techniques have greatly improved our understanding of the genomic and mutational landscape of CTCL. Most of the studies have focused on SS cases while some others included also MF cases (see **table 1.4** for more details). The most commonly used approaches have been whole exon sequencing (WES; 218 cases) that characterized the exomes of coding genes, targeted sequencing (TS; 282 cases), that specifically characterised a defined group of genes/locus, and whole genome sequencing (WGS; 32 cases).

Overall, the majority of somatic single nucleotide substitutions observed in MF/SS are C > T transitions (between 40% and 74%) (Choi et al. 2015; Wang et al. 2015; McGirt et al. 2015; Prasad et al. 2016). This mutational signature, which is much less common in other haematological cancers, is considered to be caused by UV light exposure when occurring at

NpCpG sites but, remarkably, no correlation was observed between the presence of UVB signature and history of therapeutic UV exposure (localised radiotherapy or ECP) (Choi et al. 2015; Wang et al. 2015).

Taking together all these recent genomic studies, including our own, they have revealed that the deregulated genes can cluster mainly into 5 cellular processes: cell cycle regulation, JAK/STAT signalling, mitogen-activated protein kinases (MAPK) signalling, TCR/Nuclear factor kappa b (NF- κ B) signalling and chromatin modification, probably indicating the importance of such mechanisms in CTCL lymphomagenesis. In **figure 1.3** the most recurrent oncogenes and tumour suppressor genes with SCNVs and/or SSNVs are represented as part of the above-mentioned clusters. Of note, and after *TP53*, the most frequently mutated gene is *PLCG1*, a major effector of TCR downstream signalling. The average percentage of CTCL cases harbouring mutations in *PLCG1* is 10% and ranges from 5.5% to 21% (Vaqué et al. 2014; Choi et al. 2015; Ungewickell et al. 2015; McGirt et al. 2015; Woollard et al. 2016).

Specifically, alterations in TCR-PLCG1 and JAK/STAT pathways in CTCL were firstly unravelled by our laboratory contributing to the field by identifying recurrent mutations in PLCG1 and JAK kinases (Vaqué et al. 2014; C. Pérez et al. 2015). They were the initial mutational studies performed in a cohort of SS and MF patients by using an NGS approach. A targeted-enriched sequencing analysis for coding and regulatory regions of a selection of genes was performed in 11 CTCL patients (4 SS and 7 MF). The mutated genes belonged to well-known intracellular signalling pathways with biological relevance in T cells such as TCR signalling, cytokine activity, NF- κ B, JAK/STAT and MAPK signalling pathways among others. Missense mutations in *PLCG1*, *TP53*, *IL6ST*, *CCR4*, *JAK1*, *JAK3*, *RELB*, *TRAF6* and *CARD11* among others were identified (**figure 1.4**). Two genes were recurrently mutated: *TP53* (in different positions in 2 of 11 cases) and *PLCG1* (in 3 cases, 2 mutated in S345 and 1 in S520).

INTRODUCTION

PLCG1 S345F mutation was validated in a larger cohort of 42 CTCL patients, and together

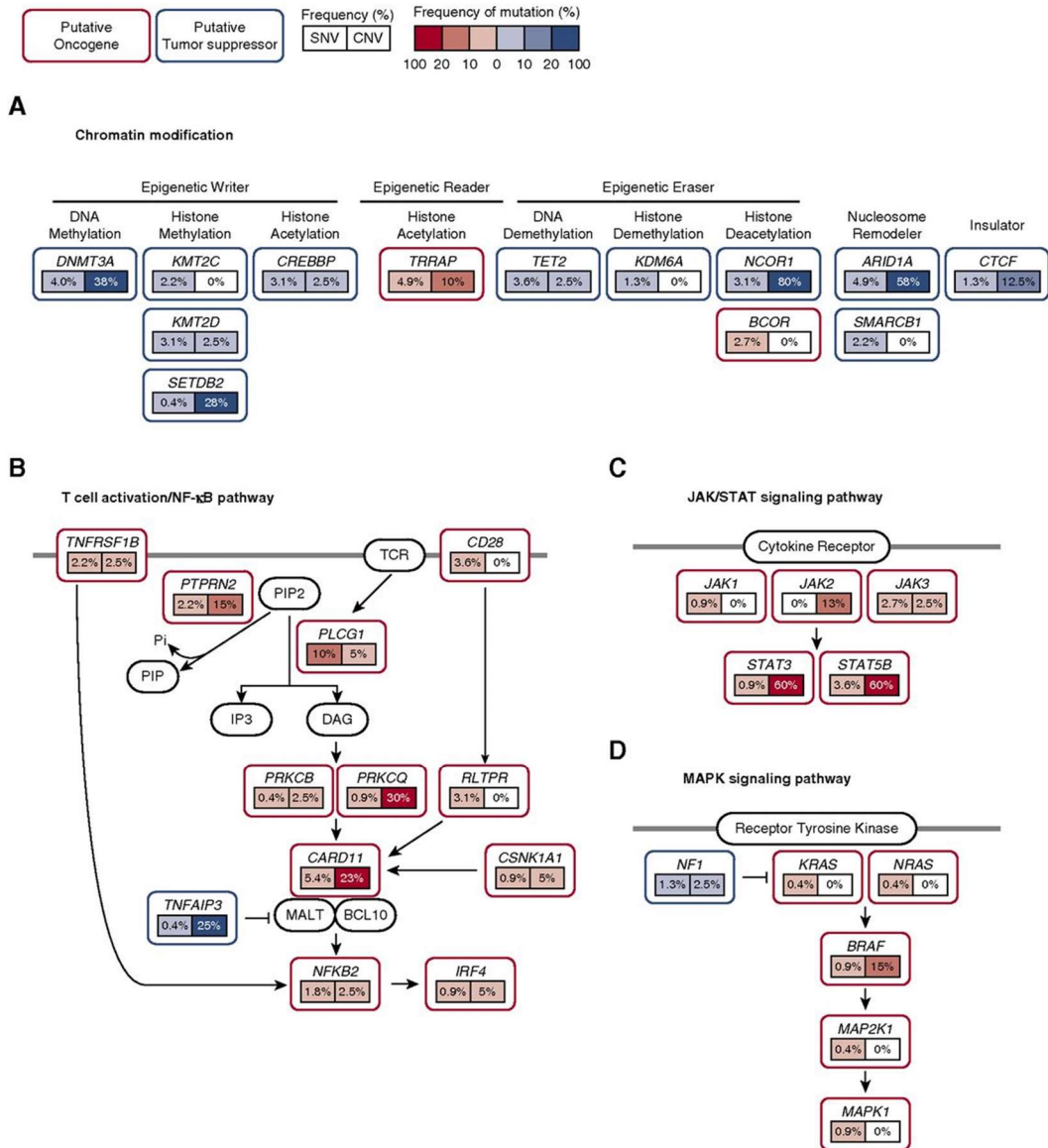


Figure 1.3. Schematic mutations and copy number variations in recurrently altered signalling pathways in CTCL. CTCL harbours recurrent mutations that are predicted to affect A) chromatin, B) T-cell activation/NF- κ B signalling, C) JAK/STAT signalling, and D) MAPK signalling. Putative oncogenes and tumour suppressor genes are indicated in red and blue boxes, respectively. Frequencies of single nucleotide variants and copy number variants are indicated as percentages in left and right boxes under the genes, respectively. SNV, single nucleotide variant; CNV, copy number variant. Adapted from Park et al 2017.

INTRODUCTION

with the previous cohort, this gene was recurrently mutated in 21% of the cases (11 out of 53). Interestingly, PLCG1 S345F mutation and nuclear staining of NFAT by immunochemistry (IHC) was identified in a consecutive sample taken from a relapsed patient that was originally negative for the mutation and with a cytoplasmatic staining of NFAT, probably suggesting that activated PLCG1 could play a role in the pathogenesis and/or progression of CTCL. The gain of function of PLCG1 S345F mutant (but also of S520F) was confirmed by an increased NFAT transcriptional activity (Vaqué et al. 2014).

In the other study performed by our laboratory, a targeted gene-enrichment sequencing of the pseudokinase domain of *JAK1*, *JAK2* and *JAK3* genes were performed in a total of 46 CTCL patients (including the 11 patients from Vaqué et al.). Mutations in *JAK1* and *JAK3* were found in up to 7 patients and in a CTCL cell line (HuT 78, *JAK1* Y654F mutation). Interestingly, *JAK1* were recurrently mutated in two patients in position R659 but the consequence of these mutations regarding the activation of the pathway is still not studied. In both studies, cells harbouring the mutations (293T cells overexpressing PLCG1 mutants and HuT 78 inherently harbouring *JAK1*/*JAK3* mutants) were highly sensitive to PLCG1 and *JAK* signalling inhibition by Tacrolimus (CaN inhibitor) and Ruxolitinib (*JAK* inhibitor) respectively, supporting the idea that targeting specific PLCG1 and *JAK* downstream signalling could be a therapeutic option for the treatment of patients carrying alterations in these pathways.

1.4 Malignant signalling network comprising potential mechanisms of CTCL biology

The NGS studies described above have revealed a number of deregulated pathways potentially promoting essential T cell activities including cell proliferation, survival or

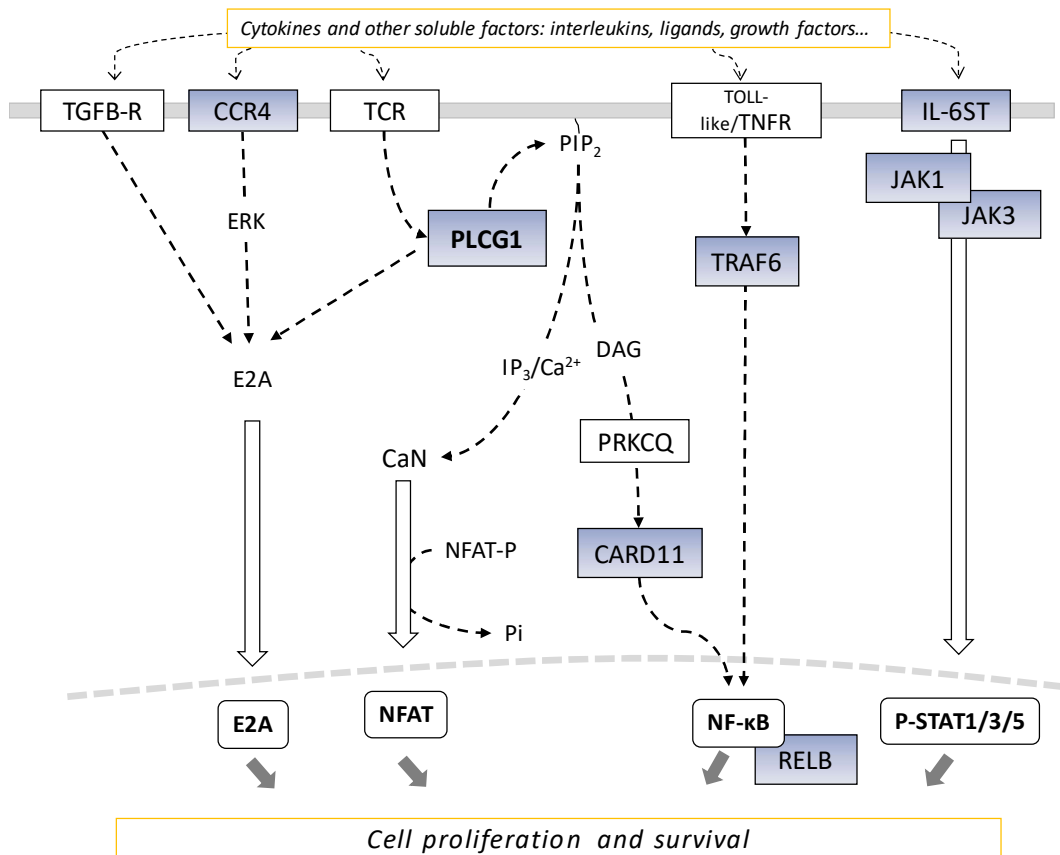


Figure 1.4. CTCL signalling network affected by somatic mutations in previous studies by our group. Schematic representation showing key T-cell signalling pathways harbouring some of the mutations identified in Vaqué et al 2014 and Pérez et al 2015. Genes in blue are mutated genes identified in the analyses. Image adapted from Vaqué et al 2014.

differentiation processes towards the acquisition of specific T cell lineages such as Th2 and Th17. These pathways can be summarized as follows (**figure 1.4**): i) TCR/PLCG1-NFAT, ii) PRKCQ- and/ or TNFR-NF-κB, and iii) JAK-STAT (see further explanations below). From a functional perspective, we can envision these pathways to participate as part of a malignant signalling network driving essential CTCL mechanisms and biological activities. These mechanisms can be triggered by multiple alteration including: i) aberrant autocrine or paracrine stimulation of T cell receptors (such as CCR4, TCR, TNFR or interleukin receptors) by cytokines, interleukins or growth factors generated by the transformed T cells and/or by

INTRODUCTION

the tumoral microenvironment; ii) by the acquisition of multiple genetic alterations in key genes to trigger the activation of downstream signals towards the activation of transcription factors such as NFAT, NF- κ B and STATs (**figure 1.4**).

1.4.1 TCR-PLC γ 1 signalling pathway

1.4.1.1 TCR activation

T cell receptors (TCRs) are protein complexes composed by six different polypeptides. The TCRs of most T cells are composed by TCR α , TCR β , CD3 γ , CD3 δ , CD3 ϵ and CD3 ζ , but some T cells, mostly located in the mucosal compartments, carry $\gamma\delta$ TCRs (Vantourout and Hayday 2013; Alcover et al. 2018). TCR $\alpha\beta$ subunits have immunoglobulin-like variable domains that recognize peptide antigens associated with major histocompatibility complex (MHC) molecules expressed on the surface of antigen-presenting cells (APCs). These subunits are associated with the CD3 complex subunits (γ , δ , ϵ and ζ , not to be confused with TCR $\gamma\delta$ variable subunits), which are invariable and ensure signal transduction. When T cells interact with APCs, the TCR complex is assembled and triggers the formation of immunological synapse (IS) (**figure 1.5**), which controls T cell activation as well as helper and cytotoxic effector functions. TCR-CD3 complexes can recruit the SRC family protein tyrosine kinases such as the lymphocyte-specific protein tyrosine kinase LCK, which phosphorylate immunoreceptor tyrosine-based activation motifs located in the cytoplasmatic domains of CD3 (Dong et al. 2019). LCK is constitutively active and maintains the signalling required for the survival of naïve T cells, but the T-cell activation is orchestrated by the relative abundance and spatiotemporal organization of the tyrosine kinases and phosphatases (such as CD45 and dual-specific phosphatase 22, DUSP22) that regulate its activity. LCK phosphorylates Zeta-chain-associated protein kinase 70 (ZAP-70)

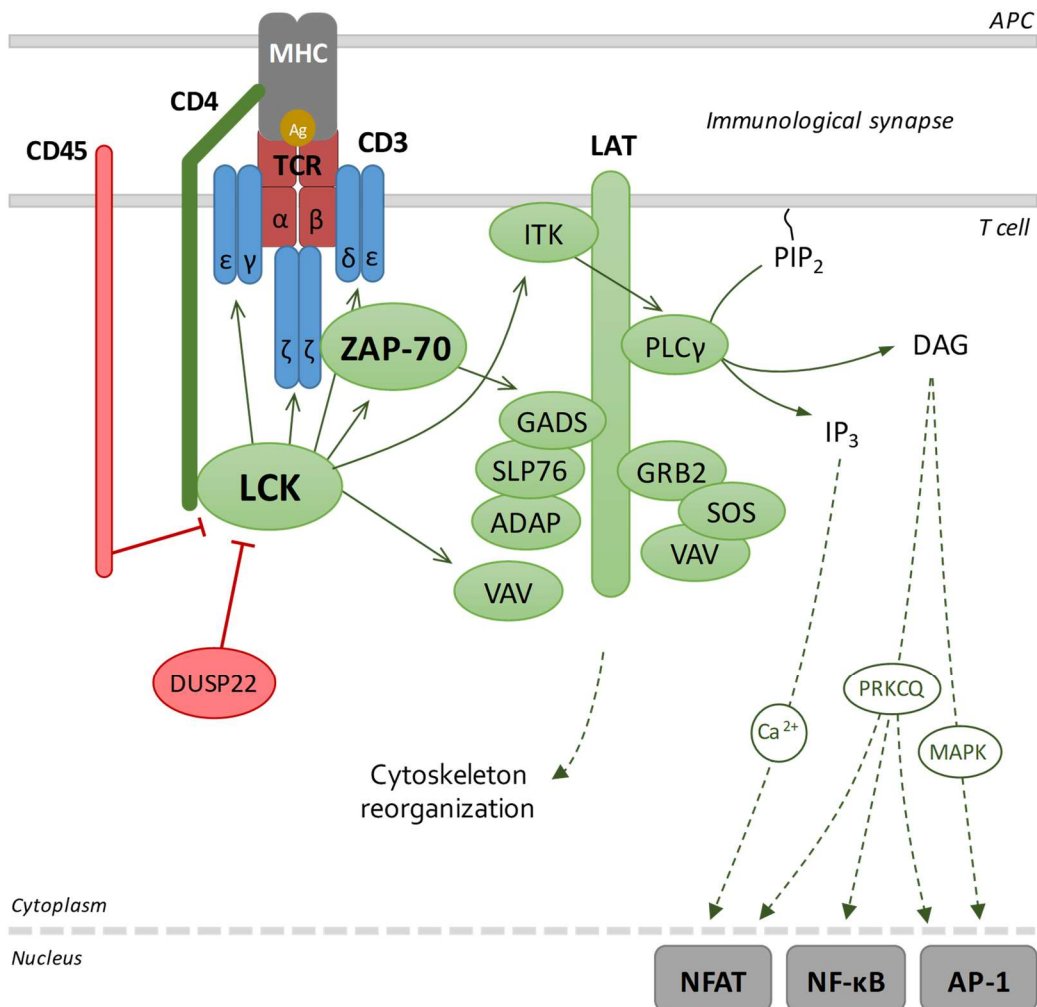


Figure 1.5. Key elements in TCR signalling. TCR signalling is initiated by engagement of TCR with MHC-peptide complexes on the surface of antigen-presenting cells (APCs), together with coreceptors such as CD4. TCR-CD3 complex consists on TCRαβ subunits and the CD3 subunits in dimeric form: εγ, δε, and ζζ. LCK is recruited to the complex, which then phosphorylates the cytoplasmic tails of the CD3 subunits and ZAP-70. ZAP-70 phosphorylates LAT causing the assembly of the LAT signalosome. PLCγ1, assembled to LAT, cleaves PIP₂ into DAG and IP₃ resulting in the activation of PKC and MAPK, and the release of calcium, important for downstream signalling events and transcriptional activation. Together these events set off a complex and tightly regulated signalling cascade leading to transcription of genes involved in cytoskeleton reorganization, proliferation, cytokine production, and other effector T-cell functions.

INTRODUCTION

which activates the linker for activation of T cells (LAT), an adaptor protein that assemble multiple proteins, such as Phospholipase Cy1 (PLC γ 1) (Weiss et al. 1991).

In Cutaneous T-cell lymphomas, activation of TCR signalling can be triggered by multiple mechanisms: by TCR-MHC interaction by cell within the tumour microenvironment (such as dendritic cells and macrophages) promoting the survival of malignant T cells (Wilcox et al. 2009) and by the acquisition of genetic alterations of TCR downstream pathways such as mutations in *PLCG1*, and/or in costimulatory receptors such as CD28. These mechanisms can lead to the aberrant activation of multiple growth and survival intracellular mechanisms including NF- κ B, NFAT, PI3K and MAPK pathways. These in turn promote cytokine production (mostly IL-2) and regulate the actin cytoskeleton reorganization promoting the formation of the IS (Wilcox 2016).

1.4.1.2 PLC γ 1

PLC γ 1, is encoded by the gene *PLCG1*, (**figure 1.6**), a member of the phospholipase C family of enzymes that is ubiquitously expressed (Kadamur and Ross 2013). PLC γ 1 is maintained in an inactive state, but upon T cell activation, an IL-2-inducible tyrosine kinase (ITK) can phosphorylate it on Tyr783 which changes the protein structure to an open conformation. In this setting, PLC γ 1 catalyses the cleavage of phosphatidylinositol 4,5-bisphosphate (PIP $_2$) to inositol 1,4,5-trisphosphate (IP $_3$) and diacylglycerol (DAG). Both DAG and IP $_3$ are essential second messengers for the transduction of T cell signaling: DAG is a cofactor for several PKC



Figure 1.6. Schematic representation of PLC γ 1 protein domains. PH: pleckstrin homology domain essential for phospholipid binding, PLCXc and PLCYc: catalytic activity domains and SH2/SH3: Src homology 2/3 domains essential for protein-protein interaction.

family enzymes, such as PKC θ , while IP₃ regulates the release of Ca²⁺ from the endoplasmic reticulum (which itself controls a major regulatory network) but also stimulate protein kinases, transcription and mRNA processing.

As aforementioned, *PLCG1* has been found recurrently mutated in between 5.5% - 21% of patients (mostly in SS cases). One of the more frequent mutation, PLCG1 S345F, has been confirmed as a gain-of-function mutation as shown by an increased NFAT, Activator protein-1 (AP-1) and NF- κ B activities, although other alterations such as S520F mutation or the VYEEDM1161V indel has been also identified as activators of downstream signalling (Vaqué et al. 2014; Patel et al. 2019).

1.4.2 Role of PRKCQ in T-cell signalling

1.4.2.1 PRKCQ structure and expression

PKC θ (PRKCQ from hereon), was originally cloned in 1993 as a novel member of the PKC family enzymes (Baier et al. 1993). This family of serine/threonine kinases consists of 12 related isoforms that are divided in three groups based on isoform structure and their corresponding activators: conventional PKCs including isoforms α , β and γ which are activated by DAG, phorbol esters (such as 12-O-Tetradecanoylphorbol-13-acetate, TPA) and Ca²⁺ in the presence of phosphatidylserine; novel PKCs including ϵ , η , δ and θ , only activated by DAG and phorbol esters and the atypical PKCs group, which include ζ and ι/λ and are only activated by protein-protein interactions (Altman and Kong 2016).

Novel PKCs share the protein structure (**figure 1.7**). These kinases contain a highly conserved catalytic domain and a regulatory domain that maintains the enzyme in an inactive conformation (Steinberg 2008). The regulatory domain is composed by C2-like domain, which interacts with phospholipids independently of Ca²⁺ binding, and C1

INTRODUCTION

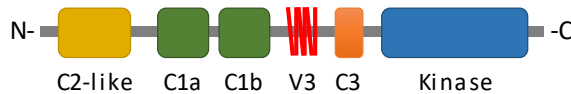


Figure 1.7. Schematic representation of PKCθ protein domains. C2-like: phosphotyrosine interaction with SH2 domain-containing proteins; C1a and C1b: TPA/DAG binding; V3: hinge region involved in the indirect association with CD28, C3: ATP-binding pocket and kinase: catalytic activity

domains which are the molecular sensors of TPA/DAG. These domains are separated from the catalytic domain by the V3 or hinge region, important for the interaction with CD28 in the IS. The catalytic domain is composed by C3, an ATP-binding pocket and the kinase domain.

PRKCQ is expressed in skeletal muscle and lymphoid organs, predominantly in the thymus and lymph nodes. Among hematopoietic cells, PRKCQ is most abundant in T cells and is expressed at much lower levels or even undetectable in B-cells, macrophages, neutrophils and erythrocytes (Meller et al. 1998; Altman and Kong 2016).

1.4.2.2 PRKCQ function

PRKCQ has several unique properties that distinguish it from other T cell-expressed PKCs: first, is the only member of the PKC family that has the ability to translocate to the IS between T-cells and APCs upon TCR and MHC recognition and second, this translocations can be selectively regulated by Vav/Rac pathway, which is associated with the actin cytoskeleton. Interestingly, this translocation is positively correlated with its kinase activity, thus highlighting its crucial role in T-cell signalling (Monks et al. 1997; Isakov and Altman 2002; Kong et al. 2011). These features suggest an independent mechanism of PRKCQ activation in addition to the conventional DAG- and PLCγ1-dependent pathway.

Activated PRKCQ positively regulates NF-κB, AP-1 and NFAT transcription factors leading to T-cell activation, proliferation, survival and differentiation processes (Wang et al. 2012; Phetsouphanh and Kelleher 2015). NF-κB is a major target of activated PRKCQ, which

activates the inhibitor κ B kinases (IKK) leading to the nuclear translocation of NF- κ B. AP-1, a dimer of the Jun and Fos family proteins, is also induced by PRKCQ activation in a Ras-dependent manner, and NFAT that is dephosphorylated and translocated to the nucleus by calcineurin in a functional partnership with PRKCQ (G Werlen et al. 1998). All these pathways promote the production of IL-2 which induces pro-mitogenic effects through the regulation of cell cycle genes and facilitates cell survival by promoting the expression of anti-apoptotic factors (Monks et al. 1997).

PRKCQ is also required for Th2 and Th17 (but not Th1) cell differentiation. Mice deficient for PRKCQ have a defective immune response against helminth infection or model allergens and are also protected from Th17-mediated autoimmune diseases (Marsland et al. 2004; Tan et al. 2006). Interestingly, Th17 differentiation has been suggested to be induced via AP-1 and NF- κ B-dependent upregulation of STAT3 (Kwon et al. 2012).

In addition to the role of PRKCQ in transducing signals elicited by the triggering of many cell receptors, it has also been described some other functions in the nucleus such as the induction of cytokine genes expression and microRNAs in association with the chromatin in T cells (Sutcliffe et al. 2011).

As aforementioned, PRKCQ was found amplified in up to 30% of CTCL patients analysed (Choi et al. 2015; Woollard et al. 2016) and furthermore, its expression was 5-fold upregulated in SS patients (Wang et al. 2015). Interestingly these alterations are non-overlapping with PLCG1 and JAK1/JAK3 mutations hence suggesting that these proteins might participate in a coordinated fashion as part of the same intracellular signalling pathways or network. To date, the disease implications of deregulated PRKCQ alongside its potential mechanistic interplay with PLCG1 and JAK/STAT signalling has not been studied yet in CTCL.

1.4.3 JAK/STAT signalling pathway

1.4.3.1 JAK/STAT family members

Members of the Janus associated kinase/signal transducer and activator of transcription (JAK-STAT) family play multiple roles in a number of cellular processes such as inflammation and cancer (including haematological malignancies) but also in haematopoiesis, fertility or growth. The JAK family consists of 4 cytoplasmic tyrosine kinases members (JAK1, JAK2, JAK3, Tyk2), which form hetero and homodimers in the cell membrane, transducing signals towards STAT proteins through several transmembrane receptor families. Type I receptors include the granulocyte colony stimulating factor (G-CSF) and the erythropoietin receptor, type II receptors are subdivided into type IIa and type IIb receptors which include granulocyte-macrophage colony-stimulating factor receptor (type IIa) and the IL2/6 and leukaemia inhibitory factor receptors (type IIb). JAK proteins are composed by 4 domains: FERM and SH2 domains necessarily for the interaction with the receptors and the pseudokinase domain, which interact with the kinase domain for the catalytic activity (figure 1.8) (Yamaoka et al. 2004).

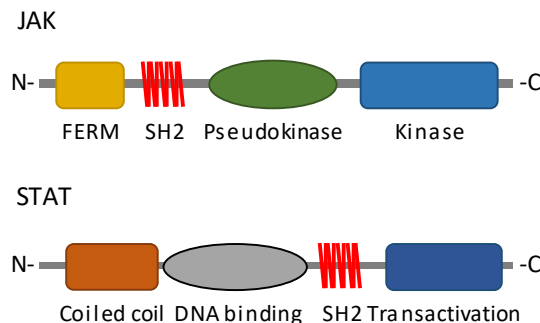


Figure 1.8. Schematic representation of JAK and STAT protein domains. JAK domains: FERM and SH2: JAK-receptor interaction; pseudokinase: interact with kinase domain; kinase: catalytic activity. STAT domains: Coiled coil: interaction with other proteins; DNA binding domain, SH2: dimerization and transactivation domain: transcriptional activation.

On the other hand, seven STAT proteins have been identified in human cells: STAT1, STAT2, STAT3, STAT4, STAT5A, STAT5B, STAT6. The functional domains of STATs include a coiled coil necessarily for the interaction with other proteins, a DNA binding domain, a SH2 domain, which mediates binding to phosphorylated tyrosine residues of other STATs (dimerization) and a C-terminal transactivation domain required for full transcriptional activation (**figure 1.8**) (Goswami and Kaplan 2017).

1.4.3.2 JAK/STAT pathway activation

The intracellular tails of the transmembrane receptors described above are constitutively associated with inactive JAKs. Upon activation of the receptor, JAKs are tyrosine phosphorylated becoming catalytically active tyrosine kinases capable of recruiting members of the STAT family in the cytoplasmic region of the receptors and phosphorylating them. Upon phosphorylation by JAK kinases, the STATs form dimers, which translocate to the nucleus and act as transcription factors inducing gene expression of factors involved in apoptosis/survival, angiogenesis, proliferation and differentiation via the DNA-binding domain (Calò et al. 2003). In some cases, signalling through STATs can be activated by receptors with intrinsic tyrosine kinase activity such as epidermal growth factor receptor (EGFR) (Thomas et al. 2015) (**figure 1.9**).

The ‘canonical’ signalling phosphorylation cascade at tyrosine residues (like Y701 in STAT1, Y705 in STAT3, Y694 in STAT5A and Y699 in STAT5B) (Lim and Cao 2006) and subsequent SH2 domain-mediated homo- or heterodimerization of STATs has been historically described as the essential requisite for biological activity of the proteins. However, it has also been studied that phosphorylation in serine residues, unphosphorylated STATs and chemical modifications have also important roles. For example, it has been reported that methylation of STAT3 was described in IL-6-driven gene transcription, and that

INTRODUCTION

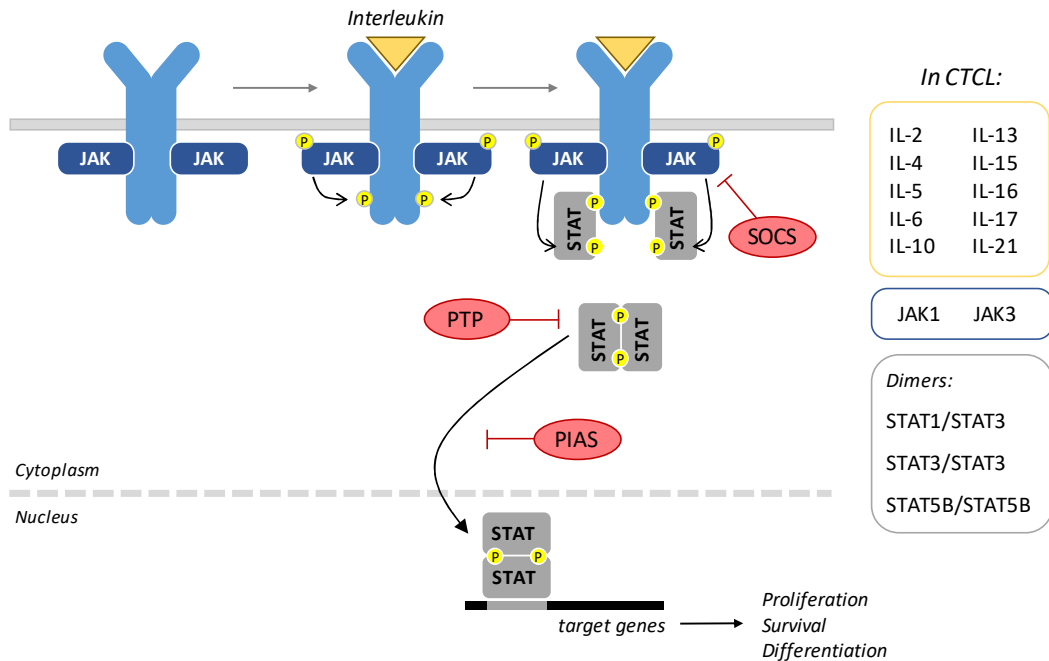


Figure 1.9. 'Canonical' JAK/STAT signalling activation. JAK proteins are constitutively associated with the receptor, which is activated upon cytokine binding. Activated JAKs recruit and phosphorylate STAT proteins at tyrosine residues. STAT proteins dimerize and translocate to the nucleus where induce the expression of its target genes. Suppressor of cytokine signalling (SOCS), phospho-tyrosine phosphatases (PTP) and protein inhibitors of activated STATs (PIAS) are negative regulators of the signalling. The principal interleukins, JAK kinases and STAT dimers involved in CTCL are represented.

unphosphorylated STAT3 and STAT5A are critical for stem cell haematopoiesis (Dawson et al. 2009; Hu et al. 2013; Villarino et al. 2017). On the other hand, phosphorylation in serine 727 of STAT1 and STAT3 is essential for maximal transcription activation (Wen et al. 1995) and for the activity of the electron transport chain in the mitochondria upon Ras/Raf/MEK/ERK cascade (Gough et al. 2009; Gough et al. 2013). Finally, It has been described that serine phosphorylation of STAT3 by growth factors and interleukins can be attributed to ERKs like ERK2, JNK1 and p38 and PKC δ (Lim and Cao 2006).

1.4.3.3 JAK/STAT pathway regulation

Three major mechanisms have been identified to negatively regulate the signalling of JAK/STAT pathway at multiple levels: i) SH2-containing phospho-tyrosine phosphatases (PTP) and CD45 tyrosine phosphatase that remove phosphate groups from JAKs and STATs, ii) protein inhibitors of activated STATs (PIAS), that inhibit STAT-DNA binding, control STAT cellular localization and promote post-transcriptional modifications of STATs, and iii) the suppressor of cytokine signalling (SOCS) proteins that are cytokine-induced competitive inhibitors of STAT receptor binding, also inhibiting JAK kinase activity, and also can target different pathway components for proteosomal degradation (Furqan et al. 2013).

1.4.3.4 JAK/STAT signalling in CTCL

Due to the crucial role of this pathway in the T-cell biology and immunity, the deregulation of the JAK/STAT pathway has been described in multiple haematological malignancies presumably providing a selective advantage to drive transformation to a malignant precursor cell. It has been well described that the aberrant activation of JAK1/3-STAT3/5 pathway in T cells is an important feature of T cell lymphomas including CTCL (Netchiporouk et al. 2014; Waldmann and Chen 2017).

As aforementioned in section 1.3.3, frequent SSNVs and SCNVs targeting JAK and STAT genes have been reported in CTCL (Vaqué et al. 2014; Choi et al. 2015; McGirt et al. 2015; Park et al. 2017; Bastidas Torres et al. 2018). Of note, STAT3 and STAT5B were amplified in 60% of patients (Park et al. 2017). Mutations in STAT proteins have been also identified but to a lesser extent. They are predominantly localized in the highly conserved SH2 domain, necessary for protein dimerization (Shahmarvand et al. 2018). Mutations in JAK proteins have been also identified in CTCL, more frequently in JAK1 and JAK3. In a deep sequencing study performed to detect low frequency somatic mutations, carried out by our group, JAK1

INTRODUCTION

and JAK3 mutations were detected in 15% of CTCL tumours. Interestingly, these mutations were located in hotspots affecting the pseudokinase domain of the proteins, which have regulatory functions (C. Pérez et al. 2015), but its contribution to the activation of the pathway has not been yet studied.

Also, constitutive JAK3 phosphorylation and constitutive STAT3 activation has been identified in both MF and SS (Sommer et al. 2004; R C T McKenzie et al. 2012). Indeed, STAT3 is considered an oncogene as shown by the formation of tumours in nude mice after transplantation of normal mouse fibroblast expressing a mutated STAT3 that constitutively form dimers (Bromberg et al. 1999).

HYPOTHESIS AND OBJECTIVES

2. HYPOTHESIS AND OBJECTIVES

2.1 Hypothesis

Cutaneous T cell lymphoma (CTCL) is a heterogeneous group of entities with a difficult diagnosis and a variety of treatment options that greatly depend on clinical experience and accessibility but that are merely palliative. Although some molecular mechanisms leading to lymphoma genesis or progression of the disease have been elucidated, the underlying mechanisms are not well understood.

We hypothesized that a malignant network of signalling mechanisms, acting downstream of PLCG1, drives tumorigenesis and progression of CTCL. PRKCQ may be playing an essential role leading to the activation of the transcriptional endpoints NFAT, NF- κ B and STAT towards an effective neoplastic role.

2.2 Objectives

In order to dissect the interplay between members of the malignant network that may participate as progression mechanisms in CTCL and to better understand the role of PRKCQ in this disease, we have focused in the following objectives:

1. To explore the biological role of NFAT, NF- κ B and STAT genes and challenge their potential use as biomarkers for diagnosis in a CTCL patient cohort.
2. To study the activity of NFAT, NF- κ B and STAT3 in cell-based models.
3. To identify proteins interacting with PRKCQ in CTCL cells.
4. To investigate the biological implications of PRKCQ activity *in vivo*.
5. To determine the potential genes regulated by PRKCQ in CTCL cells.

MATERIALS AND METHODS

3. MATERIALS AND METHODS

3.1 Human samples

Cases submitted for a Mycosis Fungoides (MF) diagnosis or a second opinion in different institutions of the Spanish national health system between 2001 and 2018 were included in the study. Diagnostic criteria were based on World Health Organization–European Organisation for Research and Treatment of Cancer (WHO–EORTC) classification (Willemze et al. 2005). Cases of CTCL other than MF were excluded. Clinical stage was established based on the TNMB classification previously described (Olsen et al. 2007). Formalin-fixed paraffin-embedded (FFPE) skin biopsies of a total of 78 MF patients were used for the diagnosis by histological examination and for the immunohistochemical study.

This study was conducted in accordance with the Declaration of Helsinki and supervised by the ethical committee of the Hospital Universitario Marqués de Valdecilla, Santander, Spain.

3.2 Chick embryo model for *in vivo* studies

In order to study effects of PRKCQ deficiency and sotrastaurin in tumoral formation and growth, tumour cells intravasation and metastasis, chicken embryo model was performed in collaboration with Berta Casar from Piero Crespo's laboratory (IBBTEC – CSIC), as previously described (Crespo and Casar 2016). Below, chicken eggs and cells preparation for tumour grafting as well as sample harvesting are detailed.

3.2.1 Eggs preparation for xenografting tumour cells

The chicken eggs were prepared as shown in **figure 3.1**. Freshly fertilized chicken eggs (from Gilbert Farm, Tarragona, Spain) were incubated on their side in a rotating incubator (rotating three times per hour) at 37 °C and 60% humidity for 10 days. On day 10 when the chick embryos are still naturally immunodeficient, were placed on their side on an egg rack and the allantoic vein is localized at the top of the eggshell. The embryo is located at the bottom of the egg and the air sack on its right (**figure 3.1A**). After cleaning the area with iodine, a small hole through the eggshell into the air sack was made with a 30-gauge (G) syringe needle (**figure 3.1A**), and another hole near the allantoic vein was made without penetrating the chorioallantoic membrane (CAM), with a Dremel rotary tool kit (**figure 3.1B**). Then, a 20G syringe needle with a small hook was used to make a third very small hole in the eggshell membrane (**figure 3.1C**). In order to separate the CAM from the shell and let it drop, a mild vacuum with an automatic pipette was made in the air sack hole (**figure 3.1D**). Once the CAM was dropped, a square window (of approximately 1 cm²) was made with a Dremel cut off wheel (**figure 3.1E**) at the top of the egg to make the CAM accessible. This hole was sealed with laboratory tape and eggs were placed into a stationary incubator at 37 °C and 60% humidity until being grafted (**figure 3.1F**).

3.2.2 Cells preparation for xenografting

On one hand, in order to study PRKCQ knockdown effects, non-targeting control (NTC) and short hairpin RNA against PRKCQ (shPRKCQ) MyLa cells were used. The establishment of these cells are fully explained in section 3.3.4. Briefly, both NTC and shPRKCQ cells were treated with 1 ug/ml doxycycline in order to knockdown (or not) PRKCQ. After 96 h, cells were counted with a Neubauer chamber, washed with phosphate buffered saline (PBS) twice and resuspended at 40·10⁶ cells/ml in serum-free media with Matrigel™ at 20%.

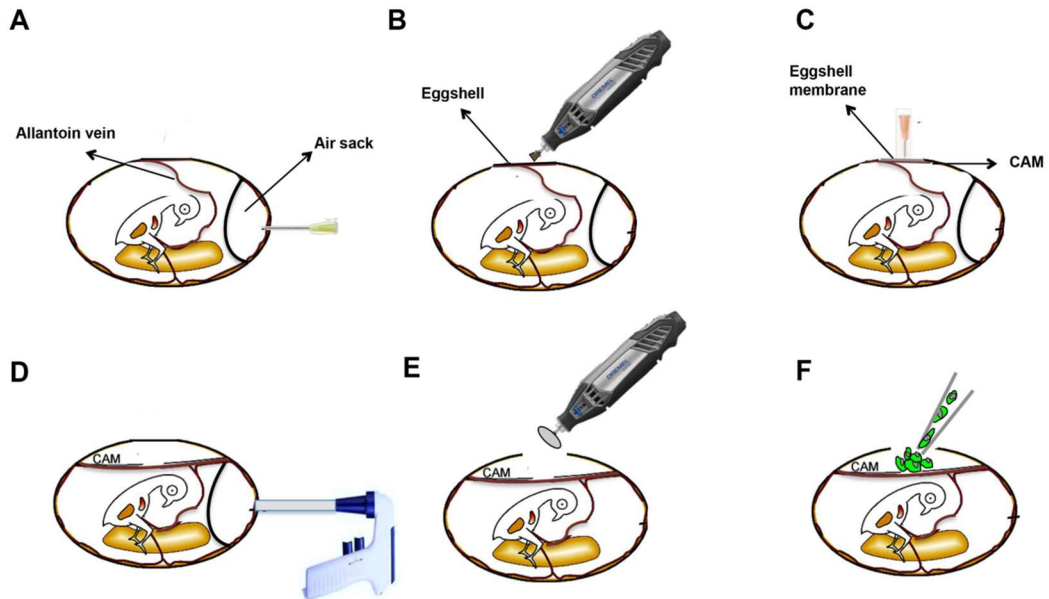


Figure 3.1. Chick embryo model procedure. A) After 10 days of incubation, the allantoic vein is positioned against the top of the egg. A hole in the eggshell is made into the air sack using a 30 G syringe needle. B) Another hole using a Dremel rotary tool kit is made adjacent to the attachment point for the allantoic vein. C) A third small hole in the eggshell membrane is made using a 20 G syringe needle. D) A mild vacuum is applied into the hole over the air sack to evacuate the air and drop the chorioallantoic membrane (CAM). E) A square window (1 cm²) is made using a Dremel cut off wheel to expose the CAM. F) Tumour cells are grafted onto the CAM. Image adapted from Crespo & Casar, *Bio-protocol*, 2016.

Matrigel™ is composed by structural proteins resembling the complex extracellular environment found in many tissues.

On the other hand, to study the effects of the PRKCQ pharmacological inhibition with sotrastaurin (Selleckchem), MyLa cells were used for xenografting. Exponentially growing MyLa cells were counted with a Neubauer chamber, washed PBS twice and resuspended at 40·10⁶ cells/ml in serum-free media with Matrigel™ at 20%.

In both cases, cells were placed on ice until grafted.

3.2.3 Tumour cells grafting onto the CAM

The hole at the top of the eggshell was unsealed and 25 µl of cell suspension ($1 \cdot 10^6$ of total cells approximately) were placed onto a small area of the CAM. The shell window was re-sealed with laboratory tape, and the embryo was returned to the stationary incubator after 10 min of repose allowing the cells to settle.

3.2.4 Primary tumours and chick embryo tissues collection

After 7 days, chick embryo samples were harvested. The hole made previously at the top of the eggshell was enlarged, primary tumour was resected from the CAM and weighted. The chick embryo was removed from the eggshell by cutting the shell radially into equal halves and then a piece of the lower CAM and liver and the lungs were harvested to proceed to genomic DNA isolation (detailed in section 3.5.2).

3.2.5 Human tumour cells quantification

In order to detect human tumour cell DNA in the chick tissues a quantitative polymerase chain reaction (qPCR) for human *Alu* sequences was performed using 30 ng of DNA, *Alu*-specific primers (see **table 3.1**) and SYBR® Green Master Mix (Applied Biosystems). Chicken GAPDH primers were used as internal control. The PCR was run as follows:

Time	Temperature	Cycles
2 min	95 °C	1
30 s	95 °C	40
30 s	63 °C	
30 s	72 °C	
∞	4 °C	hold

Quantitative PCRs were analysed using the SDS 2.2.2 software (Applied Biosystems). A standard curve, using a dilution series of human DNA (10^2 , 10^3 , 10^4) from the original

tumour cells, was generated to quantify human tumour cells comparing the Ct values obtained from the standard dilution against the ones from the chick embryo samples, in triplicate. Water was used as negative control.

Table 3.1. Primer sequences used in this thesis.

Name	Forward 5'-3'	Reverse 5'-3'	Use	Amplicon (bp)
Alu	ACGCTGTAAATCCCAGGACTT	TCGCCCAGGCTGGCTGGGTGCA	RT-qPCR	220
chicken GAPDH	GAGGAAAGGTCGCCTGGTGATCG	GGTGAGGACAAGCAGTGAGGAACG	RT-qPCR	297
PRKCQ-A148E	CTTTGCCTGCTTGATC <u>TCACCCCGCGCTGAT</u>	ATCAGCGCCGGGGTGAGATCAAGCAGGCAAAG	Mutagenesis	-
JAK1-R659C	AGTCTTAGACCCAGCCACA	GCGATGTCCTTACCACACCA	Sequencing	202
JAK1-Y654F	AGTCTTAGACCCAGCCACA	GCGATGTCCTTACCACACCA	Sequencing	202
PLCG1-S345F	GTCCTTCCTGAGTTCCAGC	GTCCTGCACACCATCAAGGA	Sequencing	450
PRKCQ-A148E	ACTTCTGGAAATGAGTGACACAA	CTTCTTCCACAGCCACAT	Sequencing	153
PRKCQ	CCATGTCGCCATTCTTCGG	GCCCGTTCTTGATTGACA	RT-qPCR	129
ACTB	AGTGTGACGTGGACATCCGCAAAG	ATCCACATCTGCTGGAAGGTGGAC	RT-qPCR	163

3.3 Cell culture for *in vitro* studies

3.3.1 Cell lines and maintenance

Adherent or non-adherent cell lines were grown in Dulbecco's Modified Eagle Medium (DMEM) or RPMI-1640 medium respectively supplemented with 10% heat-inactivated fetal bovine serum (FBS, Gibco, Thermo Fisher Scientific), glucose (4.5 g/L), L-glutamine (292 mg/L), streptomycin sulphate (10 mg/L) and potassium penicillin (10000 U/L) (Lonza) (see **table 3.2** for details).

HEK-Blue™ IL-6 cells (HEK-IL6 from here on) were cultured in DMEM medium supplemented with 10% FBS and supplemented with glucose (4.5 g/L), L-glutamine (292 mg/L), streptomycin sulphate (10 mg/L), potassium penicillin (10000 U/L) (Lonza), 100 µg/ml Normocin™, 200 µg/ml Hygromycin B Gold and 100 µg/ml Zeocin™ (InvivoGen). This cell line, specifically designed to monitor the activation of JAK/STAT pathway induced by IL-6,

Table 3.2. Cell lines used in this thesis.

Cell line	Description	Culture medium	Origin/Source
HEK-Blue™ IL-6	Human embryonic kidney cells expressing constitutively IL-6 receptor and SEAP reporter gene	DMEM 10% FBS + 100 µg/ml Normocin™ + 200 µg/ml Hygromycin B Gold + 100 µg/ml Zeocin™	InvivoGen
Jurkat	Acute T cell leukemia	RPMI 10% FBS	Laboratory collection
MyLa	Cutaneous T cell lymphoma - Mycosis fungoides	RPMI 10% FBS	ECACC
HuT 78	Cutaneous T cell lymphoma - Sézary syndrome	RPMI 10% FBS	ATCC
HEK293T	Human embryonic kidney 293 expressing T antigen	DMEM 10% FBS	Laboratory collection
HEK-Blue™ IL-6 NTC	HEK-Blue™ IL-6 cells expressing stable vector of doxycycline-inducible non-targeting control shRNA	DMEM 10% FBS + 100 µg/ml Normocin™ + 200 µg/ml Hygromycin B Gold + 100 µg/ml Zeocin™ + 1 µg/ml puromycin	This thesis
HEK-Blue™ IL-6 shPRKCQ 1	HEK-Blue™ IL-6 cells expressing stable vector of doxycycline-inducible shRNA 1 against PRKCQ	DMEM 10% FBS + 100 µg/ml Normocin™ + 200 µg/ml Hygromycin B Gold + 100 µg/ml Zeocin™ + 1 µg/ml puromycin	This thesis
HEK-Blue™ IL-6 shPRKCQ 2	HEK-Blue™ IL-6 cells expressing stable vector of doxycycline-inducible shRNA against PRKCQ	DMEM 10% FBS + 100 µg/ml Normocin™ + 200 µg/ml Hygromycin B Gold + 100 µg/ml Zeocin™ + 1 µg/ml puromycin	This thesis
HEK-Blue™ IL-6 shPRKCQ 3	HEK-Blue™ IL-6 cells expressing stable vector of doxycycline-inducible shRNA against PRKCQ	DMEM 10% FBS + 100 µg/ml Normocin™ + 200 µg/ml Hygromycin B Gold + 100 µg/ml Zeocin™ + 1 µg/ml puromycin	This thesis
Jurkat NTC	Jurkat cells expressing stable vector of doxycycline-inducible non-targeting control shRNA	RPMI 10% FBS + 1 µg/ml puromycin	This thesis
Jurkat shPRKCQ 1	Jurkat cells expressing stable vector of doxycycline-inducible shRNA against PRKCQ	RPMI 10% FBS + 1 µg/ml puromycin	This thesis
Jurkat shPRKCQ 2	Jurkat cells expressing stable vector of doxycycline-inducible shRNA against PRKCQ	RPMI 10% FBS + 1 µg/ml puromycin	This thesis
Jurkat shPRKCQ 3	Jurkat cells expressing stable vector of doxycycline-inducible shRNA against PRKCQ	RPMI 10% FBS + 1 µg/ml puromycin	This thesis

MyLa NTC	MyLa cells expressing stable vector of doxycycline-inducible non-targeting control shRNA	RPMI 10% FBS + 1 µg/ml puromycin	This thesis
MyLa shPRKCQ 1	MyLa cells expressing stable vector of doxycycline-inducible shRNA against PRKCQ	RPMI 10% FBS + 1 µg/ml puromycin	This thesis
MyLa shPRKCQ 2	MyLa cells expressing stable vector of doxycycline-inducible shRNA against PRKCQ	RPMI 10% FBS + 1 µg/ml puromycin	This thesis
MyLa shPRKCQ 3	MyLa cells expressing stable vector of doxycycline-inducible shRNA against PRKCQ	RPMI 10% FBS + 1 µg/ml puromycin	This thesis
HuT 78 NTC	HuT 78 cells expressing stable vector of doxycycline-inducible non-targeting control shRNA	RPMI 10% FBS + 1 µg/ml puromycin	This thesis
HuT 78 shPRKCQ 1	HuT 78 cells expressing stable vector of doxycycline-inducible shRNA against PRKCQ	RPMI 10% FBS + 1 µg/ml puromycin	This thesis
HuT 78 shPRKCQ 2	HuT 78 cells expressing stable vector of doxycycline-inducible shRNA against PRKCQ	RPMI 10% FBS + 1 µg/ml puromycin	This thesis
HuT 78 shPRKCQ 3	HuT 78 cells expressing stable vector of doxycycline-inducible shRNA against PRKCQ	RPMI 10% FBS + 1 µg/ml puromycin	This thesis

constitutively expresses IL-6 receptor and a reporter gene expressing a secreted embryonic alkaline phosphatase (SEAP) under the control of the IFN- β minimal promoter fused to four signal transducer and transcription activator 3 (STAT3) binding sites (**figure 3.2**). The detection of activated STAT3 in these cells by Quanti-Blue™ assay is fully explained in section 3.5.5.

All cells were maintained exponentially growing in a humidified atmosphere at 37 °C and 5% CO₂.

3.3.2 Reagents

Tacrolimus, sotrastaurin, ruxolitinib, ibrutinib, dasatinib, fostamatinib and MK-2206 were used at 1 µM as inhibitors of calcineurin, PRKCQ, JAK, BTK, Src, Syk and Akt signalling pathways respectively.

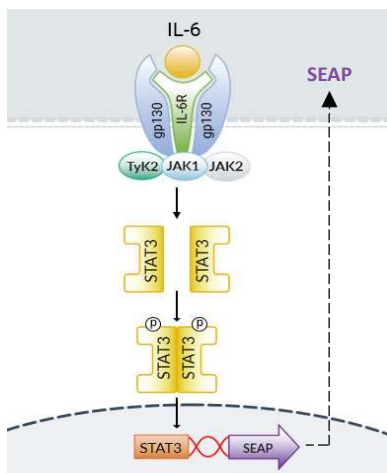


Figure 3.2. HEK-Blue™ IL-6 cell model used in this thesis. Schematic representation of IL-6R/JAK/STAT3/SEAP pathway of HEK293 cells transfected with human IL-6R gene and SEAP reporter gene. Image adapted from <https://www.invivogen.com/>

TPA and IL-6 were used at 10 ng/ml to induce PKC and JAK/STAT pathways activation respectively.

Stock preparation: all reagents were dissolved in DMSO (VWR) to a final concentration of 10 mM (for inhibitors) or 10 µg/ml (for TPA), except for IL-6 that was dissolved in distilled water (Qiagen) to a final concentration of 10 µg/ml.

All stock solutions were aliquoted and stored at -20 °C until used.

Table 3.3 provides a list of the reagents used in this thesis and its related information.

3.3.3 Transfection

Lipofectamine LTX with PLUS reagents (Invitrogen) was used for transfecting HEK-IL6 cells. The day before transfection, cells were seed at 20-30% of confluence in 6-well culture plates or 60 mm culture dishes. The day of transfection 0.5 or 1 µg of DNA was diluted in 300 or 1000 µl of DMEM medium with 0.5 or 1 µl of PLUS reagent, mixed by vortexing and

Table 3.3. Reagents (inhibitors and activators) used in this thesis

Reagent	Synonym	Target	Source	Reference
Tacrolimus	FK506	FKBP12	Selleckchem	S5003
Sotrastaurin	AEB071	pan-PKC (mostly for PKC θ)	Selleckchem	S2791
Ruxolitinib	INCB018424	JAK1/2	Selleckchem	S1378
Ibrutinib	PCI-32765	BTk	Selleckchem	S2680
Dasatinib	BMS-354825	Abl, Src, c-Kit	Selleckchem	S1021
Fostamatinib	R788	Syk	Selleckchem	S2625
MK-2206 2HCl		Akt1/2/3	Selleckchem	S1078
TPA	PMA	PKC	Sigma	P1585
IL-6		IL-6R	Sigma	SRP3096

incubated for 5 min at RT. Then, 1.5 or 2.5 μ l of Lipofectamine LTX reagent was added to the dilution, mixed by vortexing again and incubated for at least 30 min at RT. Finally, dilution was added dropwise to the cells after medium remove and incubated for 3 h. After that, fresh growing medium was added to the cells. Cells were collected for analysis between 24 to 48 h after transfection according to the experiment.

In case of selecting stably cell lines, 48 h post transfection medium was removed, and fresh growing medium supplemented with 1 μ g/ml puromycin was added.

The expression vectors used for transfection and its related information are shown in **table 3.4**, and the expressed mutants in HEK-IL6 are analysed by western blot in **figure 3.3**.

3.3.4 Lentivirus production and transduction

3.3.4.1 Lentivirus production

Lentivirus particles were produced to transduce HEK-IL6, Jurkat, MyLa and HuT 78 cells with inducible short hairpin (sh) sequences constructs against human PRKCQ mRNA. SMARTvector™ carrying tGFP and doxycycline-inducible non-targeting control (NTC) shRNA or shRNA against human PRKCQ mRNA, both under mEF1 α promoter regulation, constructs were used in this study (Dharmacon). See **table 3.4** for more information about DNA constructs.

Table 3.4. Constructs for transfections used in this thesis

Name	Construct	Origin/Source
pCMV6-Entry vector	Empty vector	Laboratory collection (described in Vaqué JP. <i>et al</i> 2014)
pCMV6-PLCG1 WT	PLCG1 wild type gene	Laboratory collection (described in Vaqué JP. <i>et al</i> 2014)
pCMV6-PLCG1 S345F	PLCG1 S345F mutant gene	Laboratory collection (described in Vaqué JP. <i>et al</i> 2014)
pCMV6-JAK1 WT	JAK1 wild type gene	Origene
pCMV6-JAK1 R659C	JAK1 R659C mutant gene	Origene/BioNova (mutagenesis)
pCMV6-JAK1 Y654F	JAK1 Y654F mutant gene	Origene/BioNova (mutagenesis)
pCMV6-PRKCQ WT	PRKCQ wild type gene	Origene
pCMV6-PRKCQ A148E	PRKCQ A148E mutant gene	This thesis
pRL-Null	<i>Renilla</i> luciferase reporter gene regulated by the T7 promoter	Promega
pGL4.30 NFAT-RE	Firefly luciferase reporter gene regulated by NFAT response element	Promega
pGL4.32 NF- κ B-RE	Firefly luciferase reporter gene regulated by NF- κ B response element	Promega
pGL4.47 SIE	Firefly luciferase reporter gene regulated by sis-inducible element (STAT3:STAT3)	Promega
shRNA NTC ID: VSC11654	shRNA non-targeting control regulated by mEF1 α promoter	Dharmacon
shRNA PRKCQ 1 ID: V3SH11252-226034596	shRNA against human PRKCQ gene regulated by mEF1 α promoter	Dharmacon
shRNA PRKCQ 2 ID: V3SH11252-228441253	shRNA against human PRKCQ gene regulated by mEF1 α promoter	Dharmacon
shRNA PRKCQ 3 ID: V3SH11252-229785178	shRNA against human PRKCQ gene regulated by mEF1 α promoter	Dharmacon

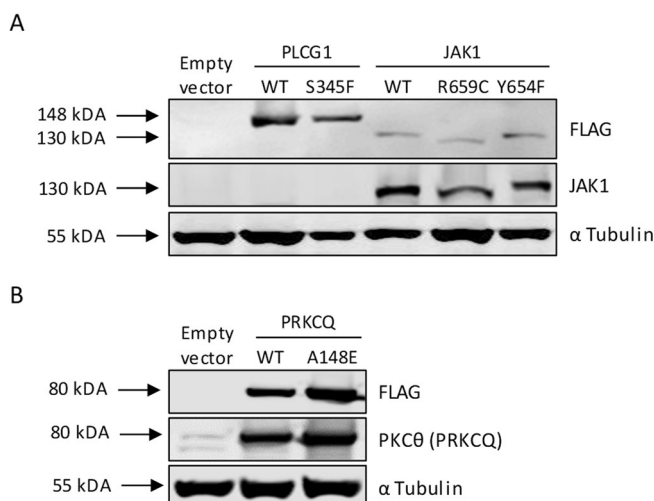


Figure 3.3. Vectors protein expressions in HEK-Blue™ IL-6 cells. Western blot analyses of whole HEK-IL6 cell lysates transfected for 24 h with wild type (WT) and mutant vectors containing A) PLCG1 and JAK1 genes and B) PRKCQ gene and incubated with the indicated antibodies. Images are representative of each western blot.

Lentiviral particles were produced by transfecting HEK293T cells with the Trans-Lentiviral shRNA Packaging System kit (Dharmacon), following the manufacturer's instructions. The day before transfection, HEK293T cells were seeded at 70% of confluence in 100 mm culture dishes. The day of transfection, 42 µg of each DNA construct and 30 µl of Trans-lentiviral packaging mix were diluted in 1 ml of water. Then, 105 µl CaCl₂, and 1050 µl HBSS 2X solution were added sequentially in a drop wise manner. After 3 min of incubation at RT, the dilution was added to the cells, which were incubated for a maximum of 16 h with the mixture. Finally, medium was removed and replaced with fresh DMEM medium supplemented with 5% FBS and 1% P/S.

Two days after transfection, lentivirus-containing supernatant was collected, centrifuged at 4 °C 1600 g for 10 min and filtered through 0.45 µm pore size sterile syringe filter (Merck Millipore). Finally, lentivirus solution was stored at -80 °C until used.

3.3.4.2 Cell transduction

For cell transduction, cells were seeded at 20% of confluence in 6-wells culture plates. Next day, culture medium was removed, and new mix was added: 1 ml of complete DMEM medium, 1 ml of lentivirus-containing supernatant and 8 µg/ml polybrene. 48 h post transduction, medium was removed, and fresh medium was added supplemented with 1 µg/ml puromycin to select stably cell lines. After 7 days post-selection, cells were harvested and checked for short hairpin sequence construct acquisition and functionality by RT-qPCR and western blot.

3.4 Cell viability assays

3.4.1 Cell proliferation assay

To study the inhibitors effects over cell proliferation, CellTiter-Glo® Luminescent Cell Viability Assay kit (Promega) was used following the manufacturer's instructions. This method enables the identification of viable cells in culture based on quantification of the free-ATP present as indicator of metabolically active cells. Cells were seeded in 96-well plates (1000 cells/well) in growing conditions and incubated overnight in a humidified atmosphere at 37 °C and 5% CO₂. The following day, cells were treated with increasing concentrations of the inhibitors for 48 h. Luminometric changes were quantified using the Synergy™ HTX Multi-Mode Microplate Reader (Biotek).

The half maximal inhibitory concentration (IC₅₀) was estimated at 48 h of drug treatment by using GraphPad Prism 6 software.

3.4.2 Synergism assay

To assess the drug synergism of sotrastaurin and ruxolitinib in MyLa and HuT 78 cells, the effects in proliferation of each inhibitor alone and the combination of both were analysed as described in the previous section. Then, the combination indexes (CI) were calculated with CalcuSyn software, as previously described (Chou and Talalay 1984). This software determines the CI by considering the fraction of affected cells of both inhibitors alone and compares it with the fraction of affected cells of the combination treatment, and assesses whether a combination of two drugs results in a synergistic ($CI < 1$), additive ($CI = 1$) or antagonistic effect ($CI > 1$).

3.4.3 Apoptosis assay

Induction of apoptosis by ruxolitinib and sotrastaurin was evaluated using FlowCollect™ Annexin Red Kit (Merck Millipore), according to the manufacturer's instructions. This kit assesses both early and late apoptosis and includes recombinant Annexin V, a calcium-dependent phospholipid binding protein with high affinity for phosphatidyl serine expressed on the apoptotic cell membrane, conjugated to a red sensitive dye CF647 (for detecting early apoptosis) and 7-Aminoactinomycin (7-AAD), a membrane impermeant dead cell dye, which is an indicator of cell membrane structural integrity (for detecting late apoptosis).

Cells were seeded in 24-well plates (100000 cells/well) in growing conditions and incubated overnight in a humidified atmosphere at 37 °C and 5% CO₂. The following day, cells were treated with the indicated inhibitor and 24 h after were collected for flow cytometer analysis. Cell samples were resuspended 1X Assay Buffer HSC (made from the provided 10X Assay Buffer HSC) at a final concentration of $1 \cdot 10^6$ cells/ml. Then, 100 µl of cell suspension

were incubated with 100 µl of Annexin Red Working Solution¹ at 37 °C for 15 min. Cells were washed once with 1X Assay Buffer HSC, resuspended in 195 µl of 1X Assay Buffer HSC together with 5 µl of 7-AAD and incubated at RT for 5 min in the dark. Finally, cells were analysed by a flow cytometer. In the case of evaluating ruxolitinib effects, data were collected using a FACS-Calibur flow cytometer (BD Biosciences) and analysed using CellQuest Pro software (BD Biosciences). For the evaluation of sotrastaurin effects, data were collected using a CytoFLEX flow cytometer (Beckman Coulter) and analysed by CytExpert™ software (Beckman Coulter).

3.5 DNA and RNA analysis

3.5.1 Bacterial transformation and plasmid DNA purification

3.5.1.1 Bacterial transformation

Plasmid DNA was transformed using heat-shock method into Escherichia coli (E. Coli) DH5α competent cells (Invitrogen) for DNA amplification.

To that end, 50 µl E. coli DH5α cells were mixed with 1 µg of plasmid DNA. The mixture was incubated on ice for 5 min. After that, a heat shock of 40 sec at 42 °C was performed followed by other 2 min incubation on ice. Transformed E. coli DH5α cells were then supplemented with 1 ml SOC medium (Invitrogen) containing no antibiotics and incubated in a shaking incubator at 37 °C 200 rpm for 1 h, allowing the antibiotic resistant gene to be expressed. Then, E. coli cells were spread on LB-agar growth media plates containing the corresponding antibiotic selection (100 µg/ml ampicillin or 50 µg/ml kanamycin depending on the case) and incubated overnight at 37 °C.

¹ *Annexin red working solution*: Annexin V, CF647 stock solution 1:20 in 1X Assay Buffer HSC.

The following day, three selected single colonies were both seeded again on LB-agar growth media “master” plates containing the corresponding antibiotic and incubated overnight at 37 °C. Then, some cells from these separated single colonies were inoculated in 5 ml LB growth media bottles containing the corresponding antibiotic selection in an orbital shaking incubator at 37 °C 150 rpm to let them grow separately overnight. Next day, the bacterial culture was harvested by centrifugation at 4 °C 3000 rpm for 15 min and plasmid DNA was purified with the QIAamp DNA Mini kit (Qiagen) following manufacturer’s instructions.

For preparation of glycerol stocks of the verified DNA plasmid-transformed bacteria, positive single colonies that were seeded on LB-agar “master” plates were inoculated and let them grow overnight in 5 ml LB growth media containing the corresponding antibiotic selection in an orbital shaking incubator at 37 °C 150 rpm. Next day, LB media grown cells were centrifuged at 3000 rpm for 10 min and the supernatant was discarded. Bacteria pellet was resuspended 1ml of LB-glycerol 1:1 (v/v), added to a cryotube and stored at -80 °C until used.

3.5.1.2 Plasmid DNA purification

To prepare higher amounts of plasmids DNA for transfections, a little amount of the glycerol stock of the desire plasmid was inoculated into 5 ml LB growth medium containing the appropriate antibiotic and incubated for 8 h in an orbital shaking incubator at 37 °C and 150 rpm. Then, the starter culture was used to inoculate 200 ml LB growth media containing the same selection antibiotic and grown overnight in the same culture conditions (37 °C and 150 rpm). The following day, bacterial culture was centrifuged at 6000 g for 15 min and plasmid DNA was purified using the EndoFree Plasmid Maxi kit (Qiagen) following manufacturer’s instructions. Plasmid DNA concentration was determined by measuring A_{260nm} using a microvolume spectrophotometer (NanoDrop 2000).

3.5.2 DNA isolation and purification from *in vivo* samples

To extract genomic DNA from chick embryo tissues, a Polytron™ homogenizer (Kinematica) was used in order to process the tissues. Once the samples were mechanically digested, QIAamp genomic DNA purification kit (Qiagen) was used, following manufacturer's instructions. Genomic DNA was stored at -20 °C until used.

3.5.3 Site-directed mutagenesis

To generate the PRKCQ A148E mutant, alanine (GCC) was changed by glutamine (GAG) at position 148 of human PRKCQ gene, mimicking the union of the cofactor and therefore constitutively activating the protein, as previously described (Baier-Bitterlich et al. 1996). To that end, the QuikChange Lightning Site-Directed Mutagenesis Kit (Agilent Technologies) was used, following the manufacturer's instructions. First, the mutant strand synthesis reaction was performed by mixing: 5 µl of 10x reaction buffer, 50 ng of DNA template (pCMV6-PRKCQ), 125 ng of forward primer, 125 ng of reverse primer, 1 µl of dNTP mix, 1.5 µl of QuickSolution reagent distilled water to a final volume of 50 µl and finally 1 µl of QuickChange Lightning Enzyme (*PfuUltra* HF DNA polymerase). Then, the cycle used for the synthesis reaction was the following:

Time	Temperature	Cycles
2 min	95 °C	1
20 s	95 °C	18
10 s	60 °C	
3 min 30 s	68 °C	
(30 s*7kb, plasmid length)	68 °C	
5 min	68 °C	1

The primers used for the mutagenesis are shown in **table 3.1**. Then, the digestion of the amplification products was performed by adding 2 µl of the provided *Dpn* I restriction

enzyme directly to each amplification reaction, mixing it by pipetting up and down and incubating it at 37 °C for 5 min in order to digest the parental (and non-mutated) DNA. The *Dpn* I endonuclease is specific for methylated and hemimethylated DNA and is used to digest the parental DNA template and to select for mutation-containing synthesized DNA. Finally, the vector DNA containing the desired mutation is then transformed into XL10-Gold ultracompetent cells. To that end, 45 µl of the cells were gently mixed with 2 µl of the provided β-mercaptoethanol and incubated on ice for 2 min. Then, 2 µl of the *Dpn* I-treated DNA was transferred to the mixture, gently mixed it and incubated on ice for 30 min. DNA was transformed using heat-shock method as previously described in section 3.5.1.

3.5.4 DNA sequencing

In order to confirm the mutations of each vector used in this study, including the mutated by site-directed mutagenesis, Sanger sequencing of the plasmids was performed. To that end, DNA plasmids were sequenced using BigDye™ Terminator v3.1 Cycle Sequencing Kit (ThermoFisher Scientific) and 5 µM of primer (for the primers used see **table 3.1**). Then, the cycle used for the amplification reaction was the following:

Time	Temperature	Cycles
2 min	94 °C	1
10 s	96 °C	25
5 s	50 °C	
4 min	60 °C	
∞	4 °C	hold

Then, the samples were purified with CENTRI-SEP Spin Columns (Princeton Separations) following the manufacturer's instructions prior to denature the DNA with formamide and sequence it at Pathology Anatomy Service from Hospital Universitario Marqués de

Valdecilla. The chromatograms of the plasmids (wild types and mutants) and the position of the mutant along the protein structure are shown in **figure 3.4**.

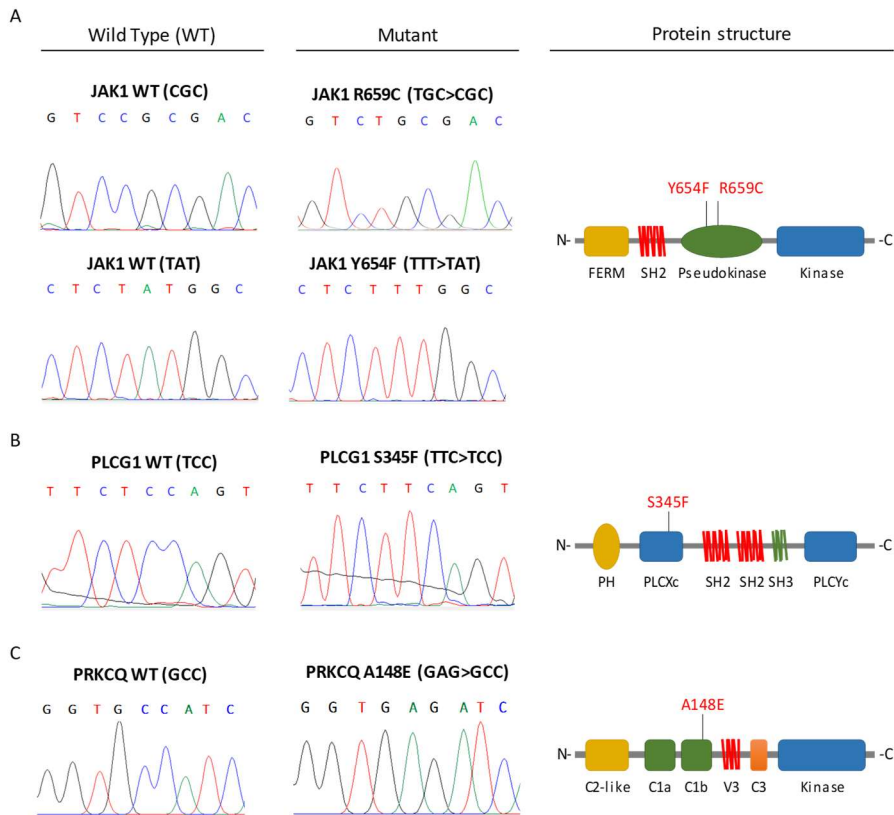


Figure 3.4. Mutant sequences used in this thesis. Chromatograms of sequenced wild type (WT, left) and mutant (middle) vectors containing A) JAK1, B) PLCG1 and C) PRKCQ genes. Schematic protein domains and mutant localization (right) are represented for each gene and mutant. JAK1 domains: FERM and SH2: JAK-receptor interaction; pseudokinase: interact with kinase domain; kinase: catalytic activity. PLCG1 domains: PH: phospholipid binding; PLCXc and PLCYc: catalytic activity; SH2 and SH3: protein-protein interaction. PKC θ domains: C2-like: phosphotyrosine interaction; C1a and C1b: TPA/DAG binding; V3: hinge region and kinase: catalytic activity.

3.5.5 Quanti-Blue™ assay

Activation of STAT3 in HEK-IL6 cells is assessed by the quantification of SEAP release in the supernatant (SN) of the cells by determining its alkaline phosphatase activity by this colorimetric enzyme assay (standard procedure is summarised in **figure 3.5**). Quanti-Blue™ (QB) solution is prepared by dissolving one pouch of the provided powder to 50 ml of sterile endotoxin-free water (Sigma), gently swirling it and incubating it at 37 °C for 30-60 min. The solution is kept at 37 °C before used or stored at 4 °C for up to 2 weeks. In a flat-bottom 96-well plate, 180 µl of the QB solution is mixed with 20 µl of the cell supernatant and incubated at 37 °C for 90 min. Then, the SEAP levels are determined by measuring optical density (OD) at 620-655 nm in a spectrophotometer.

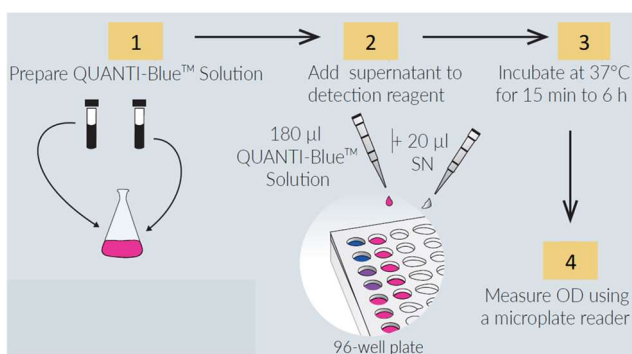


Figure 3.5. Quanti-Blue™ assay. Standard procedure using QUANTI-Blue™ Solution (QB) for the detection of secreted SEAP from supernatant (SN). Image adapted from <https://www.invivogen.com/>

3.5.6 Luciferase reporter assay

Luciferase report assay was performed to analyse and quantify transcription factor NFAT, NF-κB and STAT3 activities in HEK-IL6 cells, using Dual-Glo® Luciferase Assay System (Promega).

MATERIALS AND METHODS

Cells were seeded in 12-well plates and, the day after, were transfected in transient conditions with Lipofectamine LTX with PLUS reagents (Invitrogen), as described above, with a mix of DNA plasmids specific for each experiment, generally:

- 0.3 µg of firefly (*Photinus pyralis*) luciferase gene reporter vector carrying the 5' transcription regulatory sequence of the desired transcription factor
- 0.1 µg of pRL-Null containing *Renilla* (*Renilla reniformis*) luciferase gene construct that is constitutively expressed used as control of transfection efficiency.
- 1 µg of the specific gene or control constructs used for each experiment.

Also, cells without DNA plasmids transfected were used as blank to reduce background luminescence signals from cells. See **table 3.4** for more information about DNA constructs.

48 h post-transfection, passive lysis and quantification of *Renilla* and firefly levels were performed following the manufacturer's instructions. Cells were lysed on ice with 100 µl of 1X Passive Lysis Buffer (PLB) diluted in distilled water for each well, harvested in a 96-well plate and stored at -80 °C until assayed. To measure the luminescence levels, plate was thawed, centrifuged at 14000 rpm for 1 min and then, 20 µl of supernatant cell lysate was loaded into a 96-well white plate. Then, 100 µl of Luciferase Assay Reagent (LARII) containing luciferin (firefly luciferase substrate) was added and luminescence was measured within 1 min after addition. After that, firefly luciferase reaction was quenched with 100 µl of Stop&Glo® reagent that also contains coelenterazine (*Renilla* luciferase substrate), initiating the second luciferase reaction. Luminescence from both reactions was measured with GloMax®-Multi reader (Promega).

Firefly luminescence values were normalized against *Renilla* luminescence values used as control of transfection for each sample. Samples were blanked using the blank wells. Measurements were done in parallel triplicates and values were averaged. Relative light

units (RLU) were obtained of experimental values related to empty vector or untreated (controls) values.

3.5.7 Fluorescence in situ hybridization

PRKCQ amplification or polysomy of the arm of the chromosome where PRKCQ is located was assessed on 35 patient samples of the MF cohort by fluorescence in situ hybridization (FISH) by our collaborator Alejandro A. Gru from University of Virginia, USA. Briefly, FISH was conducted (as previously described in (Luo et al. 2017)) on tissue sections (5 or 6 μm thick) after deparaffinization and target retrieval using steam cooking in citrate buffer for 20 minutes, followed by a 20-minute cool-down period and a 5-minute wash with distilled water, then pepsin digestion (37 °C, 30 min) and a subsequent wash in 2x standard saline citrate. PRKCQ (10p15.1) and CEP10 (10p11) FISH probes (Abbott Molecular) were codenatured with the tissues at 90 °C for 13 min and hybridized at 37 °C overnight. After hybridization, slides were washed in 50% formamide/1x standard saline citrate (5 min) and 2x standard saline citrate (5 min) at room temperature, air dried, counterstained with DAPI (0.5 I/ml), and examined on an Olympus BX60 fluorescent microscope with appropriate filters (Olympus).

3.5.8 RNA extraction and purification

Total RNA extraction from human cell lines was performed using TRIzol reagent (Invitrogen). Adherent cells were lysed in the plate: growing medium was removed by aspiration and 0.5 ml TRIzol was directly added to the plate. In the case of non-adherent cells, approximately $5 \cdot 10^6$ of cells were collected, centrifuged at 200 g for 5 min, medium was removed, and cells were lysed with 0.5 ml of TRIzol reagent. After 5 min of incubation at room temperature, cells were scratched from the plate or mixed with the pipette up and down for the non-adherent cells and the homogenized samples were collected in a 1.5 ml

tube. Next, 0.2 ml chloroform per 1 mL TRIzol was added and vigorously mixed for 15 s. TRIzol-chloroform mixture was incubated 2-3 min at room temperature and then centrifuged 12000 g for 15 min at 4 °C. The upper aqueous phase was collected and transferred to a new 1.5 mL tube. Then, 0.3 mL of 100% 2-propanol was added, mixed by inversion and incubated for 10 min at room temperature in order to precipitate the RNA. After this, it was centrifuged 12000 g for 10 min at 4 °C. Supernatant was discarded and the RNA pellet was washed once with 0.5 mL of 75% ice-cold ethanol by vortexing and then centrifuged at 7500 g 5 min at 4 °C. Ethanol was discarded, and the RNA pellet was resuspended in a final volume of 20-50 µl with RNase-free water (depending on the RNA pellet observed). Finally, RNA resuspended was incubated in a heat block set at 55 °C for 10 min to homogenise and then stored at -80 °C. RNA concentration was determined by measuring A260nm using a microvolume spectrophotometer (Nanodrop 2000, Thermo Scientific). RNA integrity was checked by subjecting samples to electrophoresis separation in a conventional agarose gel. Low-Agarose (Conda) was melting in 1X TAE buffer² at 1% (w/v) and, prior to gel casting, "Real Safe Dye" (Real laboratory) was added (dilution 1:20000). RNA samples were prepared as following: 0.2-1 µg of RNA was diluted in 5 µl RNase-free water and 5 µl of RNA loading buffer (Thermo Scientific), heated for 10 min at 65 °C, loaded into a gel and run for 20 min at 100 V in 1X TAE buffer¹. Finally, resulting separation was visualized in an UV-transilluminator and recorded using a Gel-Doc EZImager (Bio-Rad). Two bands corresponding to the 28S and 18S rRNA subunits should be observed.

RNA integrity of RNA-sequencing samples was determined by High Sensitivity RNA ScreenTape analysis (Agilent). Only samples with a RNA integrity number (RIN) more than 8 were chosen for sequencing.

² TAE buffer: 400 mM Tris, 200 mM acetic acid, 10 mM EDTA pH 8; stock concentration 10X and pH 8.3; stored at room temperature.

3.5.9 Reverse transcription and quantitative polymerase chain reaction (RT-qPCR)

In order to analyse the expression of specific genes at the mRNA level, quantitative reverse transcription polymerase chain reaction (RT-qPCR) was performed.

First, reverse transcription (RT) was performed using total extracted RNA from cells. Complementary DNA (cDNA) was obtained from 1 µg of total RNA as template using the SuperScript IV reverse transcriptase and random primers approach (Invitrogen), following the manufacturer's instruction in a total volume of 20 µl. Reaction was divided in a preincubation step at 65 °C for 5 min and an incubation with RTase as follows:

Time	Temperature
10 min	23 °C
10 min	55 °C
10 min	80 °C

The obtained cDNA was stored at -20 °C until used.

To quantify the levels of a specific mRNA in an experimental condition, cDNA was amplified by SYBR Green dye-based quantitative PCR using specific primers for the gene of interest. Primers were designed using the online PrimerBlast (NCBI; <https://www.ncbi.nlm.nih.gov/tools/primer-blast/>) software tool, according to PCR standard guidelines: length 18 to 25 bp, GC content 40 to 65%, no G at the 5' end, no secondary structures and T_m= 50-65 °C. To check correct design and theoretical conditions of PCR, an *in silico* assay was performed using the online UCSC In-Silico PCR tool (UCSC, <https://genome.ucsc.edu/cgi-bin/hgPcr>). PCR conditions and primers efficiency were experimentally determined depending on the nature and complexity of each sequence. Primer sequences and amplicon sizes used in RT-qPCR assays are shown in **table 3.1**.

MATERIALS AND METHODS

The Power SYBR™ Green PCR Master Mix (Applied Biosystems) supplied in a 2X concentration premix (containing SYBR™ GreenER dye, AmpliTaq DNA polymerase, UP (Ultra-Pure) with a proprietary hot start mechanism, heat-labile Uracil-DNA glycosylase, ROX dye passive reference, dNTP blend containing dUTP/dTTP and optimized buffer components) was used to amplify the cDNA in a 7300 Fast Real-Time PCR System (Applied Biosystems). The qPCR reaction was prepared as follows: 5 µl of Power SYBR™ Green PCR Master Mix were mixed with 0.3 µM of each primer (forward and reverse; stock concentration 10 µM), 1 µl of cDNA and DEPC-water until 10 µl of final volume. Then, reaction mix was added to a 384-well PCR plate in triplicates. Reaction mix without cDNA was used as no template control (NTC) to detect possible amplification signals from contaminant DNA or primer dimers. The protocol used for amplification and real time melting curve was the following:

Time	Temperature	Cycles
10 min	95 °C	1
15 s	95 °C	40
10 min	60 °C	
15 s	95 °C	Melt curve (+0.5 °C x 80 cycles)
15 s	60 °C	
15 s	95 °C	

Quantitative PCRs were analysed using the SDS 2.2.2 software (Applied Biosystems). Threshold cycles (Ct) were determined by default at the beginning of DNA amplification in the exponential phase. The mRNA expression of genes of interest was normalized to mRNA expression of housekeeping genes (GAPDH and/or β-actin) using the comparative $2^{-\Delta\Delta C_t}$ method (described in (Livak and Schmittgen 2001)):

$$\Delta\Delta Ct = (Ct_{target\ gene} - Ct_{house\ keeping})_{condition} - (Ct_{target\ gene} - Ct_{house\ keeping})_{control}$$

$$Relative\ expression\ level\ (Fold\ Change) = 2^{-\Delta\Delta Ct}$$

3.5.10 RNA sequencing

Total RNA was extracted as described above. The RNA-Seq libraries were prepared at Centro Nacional de Análisis Genómico (CNAG) following the TruSeq®Stranded mRNA LT Sample Prep Kit protocol (Illumina). Briefly, total RNA (500ng) was enriched for the polyA mRNA fraction and fragmented by divalent metal cations at high temperature. In order to achieve the directionality, the second strand cDNA synthesis was performed in the presence of dUTP. The blunt-ended double stranded cDNA was 3'adenylated and Illumina platform compatible adaptors with Unique Dual Indexes and Unique Molecular Identifiers (Integrated DNA Technologies) were ligated. The ligation product was enriched with 15 PCR cycles and the final library was validated on an Agilent 2100 Bioanalyzer with the DNA 7500 assay (Agilent).

The libraries were sequenced on HiSeq4000 (Illumina, Inc) in a fraction of a HiSeq 4000 PE Cluster kit sequencing flow cell lane, following the manufacturer's protocol for dual indexing. Image analysis, base calling and quality scoring of the run were processed using the manufacturer's software Real Time Analysis (RTA 2.7.7) and followed by generation of FASTQ sequence files.

RNA-seq paired-end reads were mapped against the human reference genome (GRCh38) using STAR version 2.5.3a (Dobin et al. 2013) with ENCODE parameters for long RNA. Annotated genes (gencode version 29) were quantified using RSEM version 1.3.0 with default parameters (Li and Dewey 2014). Differential expression analysis was performed with DESeq2 version 1.18.1 (Love et al. 2014).

3.6 Protein analysis

3.6.1 Western blotting

Phosphorylation and protein level quantification were analysed by immunoblotting (Western blot).

Cell lysis was performed using RIPA buffer (Sigma) supplemented with phosphatase and protease inhibitors cocktails (Roche). Adherent cells were lysed directly in the plate: culture media was removed by aspiration, cells were washed once with 1X PBS and removed by aspiration, lysis buffer was added to the plate directly placed on ice and cells were scratched and collected to a 1.5 ml tube. Homogenized samples were kept on ice for 20 min and clarified by centrifuging at 14000 rpm for 15 min at 4 °C. Proteins-containing supernatant was collected and transferred to a new tube and stored at -20 °C until used.

Quantification of protein concentration was carried out using DC protein assay reagent kit (Bio-Rad). Standard curve was established using 0-10 µg/µl of BSA (concentration stock 1mg/ml, diluted in distilled water). Measurement of standards and samples was performed in a 96-wells plate mixing 1 µl of sample, 25 µl of reagent A and 200 µl of reagent B. Samples were incubated 5 min protected from light at room temperature and protein quantification was determined measuring absorbance at 595 nm in a Spark Multimode Microplate Reader (Tecan Trading AG). Protein concentration of experimental samples was estimated interpolating $A_{595\text{ nm}}$ values in the standard curve with concentration samples.

Protein samples were prepared at a final concentration of 1 µg/µl by mixing the corresponding volume of protein extracts filled with lysis buffer until the total volume desired and 4X Laemmli buffer (Bio-Rad) supplemented with 2-mercaptoethanol (VWR) as loading buffer, added to a final 1X of working concentration. Then, samples were boiled at

95 °C for 5 min to denaturize proteins and kept on ice until used in order to avoid protein renaturation.

Samples were loaded and separated according to their molecular weight in a polyacrylamide-SDS gel electrophoresis (SDS-PAGE). Percentage of acrylamide/bis-acrylamide solution (29:1) (stock solution= 40%, w/v) (Bio-Basic) used for the gel preparation was dependent on the molecular weight of the protein to be analysed (ranging from 8-12 %). Electrophoresis was carried out in a Mini-PROTEAN Tetra cell cuvette (Bio-Rad) powered by a basic PowerPAC supply (Bio-Rad) at constant voltage of 100-150 V for 2-3 hours, using electrophoresis running buffer³. PageRuler plus pre-stained protein ladder (Thermo Scientific) was used to evaluate protein migration and separation during gel electrophoresis. Proteins were transferred from acrylamide gel to a 0.45 µm nitrocellulose blotting membrane (Amersham Protran, GE Healthcare) in a Mini-Trans blot cell (Bio-Rad) using cold transfer buffer⁴ at 4 °C and constant amperage of 350 mA for 60-120 min depending on the molecular weight of the proteins of interest. After protein transference, proteins-containing nitrocellulose membrane was stained with Red Ponceau⁵ solution for 5 min at room temperature and destained with distilled water until proteins bands were seen to check protein load and integrity. Then, membrane was blocked for 30 min in 5 % non-fat dry milk-TBS-T⁶ buffer (w/v) in agitation at room temperature in order to avoid unspecific antibody binding during the following steps. Membrane was washed three times with TBS-T for 10 min and incubated with the specific primary antibody diluted in 5% BSA-TBS-T (w/v)

³ *Running buffer*: 25 mM Tris pH 8.3, 192 mM glycine, 0.1 % SDS (w/v); stock concentration 10X, stored at room temperature.

⁴ *Transfer buffer*: 25 mM Tris pH 8.3, 192 mM glycine, 10 % methanol (v/v); stock solution 1X, stored at 4 °C.

⁵ *Red Ponceau solution*: 0.1% Ponceau S (w/v) (Bio-Rad) in 5 % acetic acid (v/v); stock solution 1X, stored at room temperature.

⁶ *TBS-T*: 0.05 % Tween 20 (v/v) diluted in TBS (20 mM Tris-HCl pH 7.5, 150 mM NaCl); stock solution 1X, stored at room temperature.

overnight at 4 °C in agitation (see **table 3.5** for more details). After that, membrane was washed three times with TBS-T for 10 min and then, incubated at room temperature for 1 hour with the corresponding secondary fluorochrome-conjugated antibody diluted in 5% BSA-TBS-T (w/v) as indicated in **table 3.5**. Finally, membrane was washed three times for 10 min with TBS-T and proteins of interest were detected and recorded with an Odyssey Infrared Imaging scanner (Li-Cor biosciences). Immunoblot densitometry analysis on every band was calculated using Image Studio Software (LI-COR). Phosphorylation and total protein densitometry values were normalized to α -Tubulin signal.

3.6.2 Immunohistochemical staining

Immunohistochemical (IHC) staining of Nuclear Factor of Activated T cells Cytoplasmic 1 (NFATc1), Phospho Signal Transducer and Activator of Transcription 1 (P-STAT1), P-STAT3, P-STAT5, p50, p65, p52 and RelB (see **table 3.5** for more details) was performed on tissue microarray sections and was assessed using routine IHC techniques for 78 tumoral patient samples in Pathology Service from Hospital Universitario Marqués de Valdecilla. A positive staining was defined as a score higher than 1 (score 0: < 5% cells positively stained, score 1: 5-25%, score 2: 25-50% and score 3: > 50%). Each slide was reviewed by two independent pathologists, who examined the nuclear staining in each case.

3.6.3 Nuclear-cytoplasmic fractionation

Fractionation of nuclear-cytoplasmic proteins was performed with the Nuclear Extract Kit (Active Motif) following the manufacturer's instructions. Approximately $3 \cdot 10^6$ of non-adherent cells were collected and centrifuged at 4 °C 200 g for 5 min. Supernatant was discarded and cells were washed twice with ice-cold PBS/Phosphatase Inhibitors⁷,

⁷ *PBS/Phosphatase inhibitor*: 0.4 ml 10X PBS + 0.2 ml phosphatase inhibitor (both provided by kit), add water to a final volume of 4 ml per sample.

Table 3.5. Antibodies used in this thesis

Antibody	Immunogen	Type	Species	Source	Reference	Use	Dilution
C-Rel		Primary	Rabbit (monoclonal)	Abcam	ab227519	IHC	1:25
NFATc1	197-304 aa (human)	Primary	Mouse (monoclonal)	BD Biosciences	556602	IHC	1:100
p50	1-12 aa (human)	Primary	Rabbit (polyclonal)	Millipore	06-886-I-25UG	IHC	1:1000
p52	1-444 aa (human)	Primary	Mouse (monoclonal)	Millipore	05-361	IHC	1:600
p65	1-286 (human)	Primary	Rabbit (monoclonal)	Santa Cruz Biotech	sc-8008	IHC	1:250
Phospho STAT1 Y701	residues surrounding Tyr701 (human)	Primary	Rabbit (monoclonal)	Cell Signaling	9167	IHC	1:100
Phospho STAT3 Y705	residues surrounding Tyr705 (human)	Primary	Rabbit (monoclonal)	Cell Signaling	9145	IHC	1:400
Phospho STAT5 Y694	residues surrounding Tyr694	Primary	Rabbit (monoclonal)	Cell Signaling	9314	IHC	1:100
RelB	380-579 (human)	Primary	Rabbit (monoclonal)	Santa Cruz Biotech	sc-48366	IHC	1:200
PKCθ		Primary	Mouse (monoclonal)	BD Biosciences		IP	1:200
ASK1	residues surrounding Ile280 (human)	Primary	Rabbit (monoclonal)	Cell Signaling	8662	IP/WB	1:200 (IP) 1:1000 (WB)
STAT3		Primary	Rabbit	Active Motif	45196	TransAM	1:1000
Anti-rabbit HRP-conjugated IgG		Secondary		Active Motif	45196	TransAM	1:1000
FLAG (DDK)	produced by immunizing mice with a synthetic peptide (DYKDDDDK) coupled to KLH	Primary	Mouse (monoclonal)	Origene	TA50011-100	WB	1:1000
JAK1	residues surrounding Tyr1022/1023 (human)	Primary	Rabbit (polyclonal)	Cell Signaling	3332	WB	1:1000
Phospho STAT1 Y701	residues surrounding Tyr701 (human)	Primary	Rabbit (monoclonal)	Cell Signaling	9167	WB	1:1000
Phospho STAT3 Y705	residues surrounding Tyr705 (human)	Primary	Rabbit (monoclonal)	Cell Signaling	9145	WB	1:1000
Phospho STAT3 S727	residues surrounding Ser727 (human)	Primary	Rabbit (monoclonal)	Cell Signaling	94994	WB	1:1000
PKCθ	residues surrounding Pro632 (human)	Primary	Rabbit (monoclonal)	Cell Signaling	13643	WB	1:1000
STAT1		Primary	Rabbit (polyclonal)	Cell Signaling	9172	WB	1:1000
STAT3		Primary	Rabbit (monoclonal)	Cell Signaling	4904	WB	1:1000
α Tubulin	Raised against Sarkosyl-resistant ribbons from Sea Urchin sperm axonemes	Primary	Mouse (monoclonal)	Santa Cruz Biotech	sc-23948	WB	1:5000
Goat anti-mouse IgG DyLight™ 800		Secondary	Goat (polyclonal)	Invitrogen	SA535521	WB	1:10000
Goat anti-rabbit IgG DyLight™ 680		Secondary	Goat (polyclonal)	Invitrogen	35569	WB	1:10000

centrifuged again and supernatant discarded keeping cell pellet on ice. Then, cells were gently resuspended in 250 µl of 1X Hypotonic Buffer⁸ and incubated on ice for 15 min. 25 µl of Detergent was added to the cells, which were greatly vortexed for 10 s and centrifuged at 4 °C 14000 g for 30 s. Then, the supernatant (cytoplasmic fraction) was transferred to a new tube and stored at -80 °C. The nuclear proteins are in the pellet, which were resuspended in 50 µl of Complete Lysis Buffer⁹ by pipetting up and down and incubated for 30 min on ice on a rocking platform set at 100 rpm. After that, suspension was greatly vortex

⁸ *Hypotonic buffer*: 25 µl of 10X hypotonic buffer (provided by kit) and 225 µl of water, per sample.

⁹ *Complete Lysis Buffer*: 2.5 µl 10mM DTT + 22.25 µl Lysis Buffer AM1 + 0.25 µl Protease Inhibitor Cocktail (provided by kit). Must be prepared fresh.

for 30 s and centrifuged at 4 °C 14000 g for 10 min. The nuclear fraction-containing supernatant was transferred to a new tube and stored at -80 °C until used.

3.6.4 STAT3 transcription factor ELISA-based binding assay

To detect and quantify transcription factor STAT3 binding capacity to its consensus binding sites in HuT 78 cells, an ELISA-based assay was performed using a TransAM STAT3 transcription factor assay kit (Active Motif), following the manufacturer's instructions (STAT3-TransAM from here on). This ELISA-based method consists in a 96-well plate on which oligonucleotides containing the STAT consensus binding site (5'-TTCCCGGAA-3') has been immobilized. The active form of STAT3 from nuclear extracts specifically binds to these oligonucleotides. To that end, nuclear proteins were lysate using Nuclear Extract Kit (Active Motif) and protein concentration was determined using DC protein assay reagent kit (Bio-Rad), as described above.

30 µl of complete binding buffer¹⁰ was added to each well. Next, 5 µg of sample or positive control (provided by kit) diluted in 20 µl of complete lysis buffer² were added and incubated for 3 hours at room temperature with mild agitation (rocking platform). For blank, 20 µl complete lysis buffer² was added in a well. Next, each well was washed three times with 1X wash buffer (prepared from the provided 10X wash buffer diluted in distilled water), flicking the plate over a sink to empty the wells. Then, each well was incubated with the specific primary antibody (STAT3 1:1000) (see **table 3.5**) diluted in 100 µl of 1X antibody binding buffer (prepared from the provided 10X antibody binding buffer diluted in distilled water) for 1 hour at room temperature without agitation. After that, wells were washed three times with 1X wash buffer as described above and then, incubated at room temperature

¹⁰ *Complete binding buffer*: 0.07 µl DTT + 0.34 µl Herring Sperm DNA in 33.4 µl Binding buffer AM3, per well. Must be prepared fresh.

for 1 hour with the corresponding secondary HRP-conjugated antibody (anti-rabbit IgG for STAT3, see **table 3.5**) diluted in 1X antibody binding buffer. Then, wells were washed four times, developing solution was added at each well and incubated for 10 min at room temperature protected from light to develop blue colour of each reaction. Finally, stop solution was added to each well (in presence of acid the blue colour turns yellow) and absorbance was read on a Spark Multimode Microplate Reader (Tecan Trading AG) within 5 min at 450 nm with an optimal reference wavelength of 655 nm. Plate was blanked using the blank wells.

3.6.5 Immunoprecipitation

$5 \cdot 10^6$ cells were used for each protein immunoprecipitation assay. Cells were collected, washed with PBS, centrifuged at 4 °C 200 g for 5 min and lysed. 500 µl of lysis buffer¹¹ was added to the cell pellet and incubated on ice for 20 min. After incubation, cell lysate was centrifuged at 4 °C, 18000 g for 5 min. Proteins-containing supernatant was transferred to a new tube for protein immunoprecipitation and 50 µl of total cell lysate (10% of input) was kept at -20 °C until used as positive control.

450 µl of cell lysate was used for a single immunoprecipitation and 2 µg of specific antibody or unspecific immunoglobulins (IgGs) used as control were added. Also, 10 µl of Protein G Sepharose™ 4 Fast Flow (GE Healthcare) beads, previously washed with lysis buffer, were added in order to capture protein-antibody immunocomplexes. The protein-antibody-beads mix was incubated for 3 h at 4 °C under end-to-end rotation. After incubation, mix was centrifuged at 4 °C, 5000 g for 1 min, supernatant was discarded and pellet containing

¹¹ *Lysis buffer*: 20mM HEPES, 150 mM NaCl, 1% NP-40, 1:100 β-glycerophosphate and 1:1000 of sodium orthovanadate, leupeptin and aprotinin. The proteases inhibitors must be added fresh.

immunocomplexes-beads mix was washed twice with wash buffer¹². Finally, proteins were eluted from beads with 50 µl of 2X Laemmli Buffer¹³. At this point, non-immunoprecipitated total lysate (10% of input) was also mixed with 4X Laemmli buffer to a 1X final concentration. Samples were heated 5 min at 95 °C in order to denaturalise proteins and separate beads, were centrifuged in a spinner and were then subjected to immunoblot analysis.

Detection of immunoprecipitated or co-immunoprecipitated proteins was determined by western blot with specific antibodies, as described above. Total lysate (10% of input) was used as positive control and IgG from the same species than the specific antibody was used as negative control in order to discard unspecific protein bindings.

3.6.6 Mass spectrometry

3.6.6.1 Immunoprecipitation for mass spectrometry analysis

Protein immunoprecipitation for mass spectrometry analysis was carried out as described before but with an additional two washing steps without NP-40 (only 20mM HEPES, 150 mM NaCl), in order to remove the detergent from samples and unspecific binders, and with a different elution step.

3.6.6.2 Enzymatic digestion and elution

Elution of proteins subjected to mass spectrometry analysis was carried out according to the “On-beads digestion” protocol used by Turriziani B. et al. (Turriziani et al. 2014). Beads-immunocomplexes were trypsinized, in order to digest the baits and the interacting proteins in 60 µl of Elution Buffer I¹⁴. Digestion was performed at 27 °C for 30 min in a

¹² *Wash buffer*: 20mM HEPES, 150 mM NaCl, 1% NP-40

¹³ *2X Laemmli buffer*: 4X Laemmli buffer diluted to 2X with wash buffer

¹⁴ *Elution Buffer I*: 2 M urea, 50 mM Tris-HCl pH 7.5 and 5 µg/ml Trypsin

shaker at 800 rpm. After the initial digestion, samples were centrifuged at 7000 rpm for 1 min and supernatant was transferred to a new tube. Beads were washed twice in Elution Buffer II¹⁵ and the supernatants were pooled. Samples were left on bench to continue the digestion overnight at room temperature.

3.6.6.3 Stage Tips purification

The following day, 20 µl of Iodoacetamide (5 mg/ml, freshly prepared) was added to the samples and then incubated for 30 min in the dark. Samples were treated with 1 µl trifluoroacetic (TFA) to stop the digestion and desalted in C18 stagetips. Briefly, the tips were prepared as following: a small disc of Empore material 3 M were placed in an ordinary pipette tip, preparing a single tip for each sample. Tips were activated with 50 µl of 50% acetonitrile, 0.1% TFA and washed with 50 µl of 0.1% TFA. 130 µl of sample was added to the column and washed twice with 50 µl 0.1% TFA. Liquid was passed through the pipette tip manually with the aid of a syringe or with a light centrifugation step. Peptides were then eluted using 25 µl of 50% acetonitrile, 0.1% TFA solution passed twice through the tip. This last step was performed manually with the help of a syringe. Samples were evaporated in a Speedvac concentrator (Thermo Scientific) and resuspended in 15 µl 0.1% TFA solution and then analysed by mass spectrometry.

3.6.6.4 Mass spectrometry analysis

The peptides were analysed on a Q-Exactive mass spectrometer connected to an Ultimate Ultra3000 chromatography system (both Thermo Scientific) incorporating an autosampler. 5 µl of the peptides, for each sample, was loaded on a homemade column packed with 1.9 µm ReprosilAQ C18 (Dr. Maisch) and separated by an increasing acetonitrile gradient, using a 40 min reverse-phase gradient (from 3%–32% acetonitrile) at a flow rate of 250 nl/min.

¹⁵ *Elution Buffer II*: 2 M urea, 50 mM Tris-HCl pH 7.5 and 1 mM DTT

The mass spectrometer was operated in positive ion mode with a capillary temperature of 220 °C, with a potential of 2000 V applied to the column. Data were acquired with the mass spectrometer operating in automatic data-dependent switching mode, selecting the 12 most intense ions prior to tandem MS (MS/MS) analysis. The intensity of each ion is a relative measurement of the peptide concentration in the sample. Protein concentration is then calculated as the sum of all peptide intensities normalized by the size or number of observable peptides.

3.6.6.5 Data analysis

Mass spectra were analysed using the MaxQuant Software package of two technical and biological replicates of the experimental and control samples. Raw data files were searched against a human database (Uniprot HUMAN), using a mass accuracy of 6 parts per million (ppm) and 0.01 false discovery rate (FDR) at both peptide and protein level. Every single file was considered as separate in the experimental design; the replicates of each condition were grouped for the subsequent statistical analysis. Results were cleaned for reverse and contaminants and missing values (0) were replaced by a constant (1) in order to allow the following statistical analysis.

3.7 Statistical analyses

For patients' studies, chi-square (χ^2) or Fisher's Exact test were used, as appropriate, to determine correlations between the presence and absence of markers used in patient samples using a two-sided test with a statistical significance of $p < 0.05$ (95% confidence interval). P values: * < 0.05 and ** < 0.005 .

For *in vitro* studies, unless otherwise specified, all experiments were independent and numerical data were summarized as the mean \pm SEM (standard error of the mean) using GraphPad Prism6 software. Each global mean was compared using two-tailed unpaired Student's t-test with a statistical significance of $p < 0.05$ (95% confidence interval). P values: * < 0.05 , ** < 0.005 and *** < 0.001 .

For the proteomic analysis, all experiments were independent, and the list of significant interactions was determined based on a fold change in peptide abundance in relation to negative control ≥ 2 and a p value < 0.05 (by Student's t-test).

For the transcriptome analysis, principal component analysis was done using the top 500 most variable genes with the 'prcomp' R function and 'ggplot2' R library. Heatmaps with the top 50 differentially expressed genes were performed with the 'pheatmap' R package.

RESULTS

4. RESULTS

4.1 Correlation of clinical stage with biomarker expression in MF patients' samples.

The malignant mechanisms that control the development and progression of CTCLs are not fully understood, although some of them have been identified in the last few years. Our group have contributed in the field by identifying recurrent mutations with activating effects over phospholipase C gamma 1 (PLCG1) (Vaqué et al. 2014) and Janus kinases/signal transducer and activator of transcription (JAK/STAT) signalling pathways (Vaqué et al. 2014) (C. Pérez et al. 2015). In addition, other studies have identified recurrent activating mutations in T-cell receptor (TCR) and tumour necrosis factor receptor (TNFR) signaling pathways as well as recurrent amplifications of protein kinase C theta (*PRKCQ*) and deletions of nuclear factor kappa B2 (NFkB2) leading to the activation of NF-κB pathway (Elenitoba-Johnson and Wilcox 2017)(Izban et al. 2000).

To challenge the ability of a number of transcription factors to participate as disease mechanisms acting downstream of the afore mentioned signalling network (described in figure 1.4), we decided to study samples from a cohort of 78 clinically characterized MF patients paying special attention to the tumour stages. The status of *PRKCQ* gene was also analysed in 35 patients of the cohort.

4.1.1 Clinical characteristics at diagnosis of the MF patients' cohort

The clinical characteristics of the patients are summarized in **table 4.1**. The median age is 64 years (ranging from 12 to 87), 60% are male and 38% female (the sex of 1 patient is not available). 78% of the patients (61/78) were diagnosed with early stages (stage IA, IB or IIA) and 22% (17/78) with advanced stages (stage IIB, IIIA, IIIB, IVA₁, IVA₂ or IVB). Most of the

RESULTS

Table 4.1. Clinical characteristics of patients included in the study.

	All		Early stages		Advanced stages		p value (χ^2)
Age at MF diagnosis	Median	Range	Median	Range	Median	Range	
Years	64	(12-87)	63	(12-87)	66	(38-87)	-
Sex	n	%	n	%	n	%	
Male	47	60	36	59	11	65	0.57
Female	30	38	25	41	5	29	
Not available	1				1		
Clinical stage at diagnosis							
Early (IA-IIA)	61	78	61	100			-
Advanced (IIB-IVB)	17	22			17	100	
MF skin lesions							
Patches/plaques	61	78	57	93	4	24	<0.001
Follicular lesions	5	6.5	4	7	1	6	> 0.99
Erythroderma	5	6.5	0		5	29	<0.001
Tumour	7	9	0		7	41	<0.001

early stage patients (93%) presented patches/plaques with 7% displaying follicular lesions. Among advanced stage patients, 24% showed patches/plaques, and also follicular lesions, erythroderma and tumours (6%, 29% and 41% respectively).

4.1.2 IHC analyses show differential STAT activation in patients with advanced-stage MF

To study the activation status of these pathways in CTCL, immunohistochemical analyses of a specific transcription factors were used as endpoints for the activity of each pathway, as follows: Nuclear Factor of Activated T cells Cytoplasmic 1 (NFATc1, NFAT hereon), Phosphorylated Signal Transducer and Activator of Transcription 1 (P-STAT1), P-STAT3, and P-STAT5, together with p50, p65, p52 and RelB. These serve to analyse TCR-PLCG1, JAK/STAT and the canonical and non-canonical NF- κ B pathways respectively. To this end skin biopsies were collected, fixed in formalin and embedded in paraffin for further studies. Each nuclear staining was reviewed by two independent pathologists. The antibodies and dilutions used are described in materials and methods section 3.6.2 (**table 3.5**). The amplification of *PRKCQ* and the polysomy of the chromosome region were the gene is

located were also analysed by fluorescence in situ hybridization (FISH) in 35 patients of the cohort (26 early-stage and 9 advanced-stage patients).

The staining and FISH results and their correlation with the clinical stage are shown in **figure 4.1 and table 4.2**. Interestingly, P-STAT3 expression correlated with advanced stages of the disease at diagnosis ($p = 0.004$, **table 4.2**) as it was positively stained in 7 out of 58 early-stage patients (12%) and in 8 out of 17 advanced-stage patients (47%). P-STAT1 was positively stained in 23% of advanced-stage patients versus 5.4% in early-stage patients, although this difference is not significant ($p = 0.08$). But if P-STAT1 and P-STAT3 proteins expression were analysed together, the correlation between stages would be significant: 8 out of 55 early-stage patients (14.5%) with positive staining versus 7 out of 13 in advanced-stage cases (53.8%) ($p = 0.005$). Finally, if all P-STAT proteins were analysed together, this signalling pathway would still be significantly activated in advanced stages (53.8% versus 20.4%, $p = 0.03$). Among the rest of the transcription factors, no significant differences were found between clinical stages, even if the proteins from the canonical and non-canonical NF- κ B pathways were analysed together.

On the other hand, *PRKCQ* amplification or polysomy was not significantly correlated between CTCL stages: the positive hybridization was identified in 9 out of 26 (34.6%) early-stage patients and in 2 out of 9 (22.2%) advanced-stage patients.

All together, these results support the role of TCR/PLCG1-NFAT, *PRKCQ*, NF κ B and JAK-STAT to participate alongside early and advanced stages of the disease and highlight the role of STAT activity, more specifically that of STAT3, in the progression of the disease towards advanced stages.

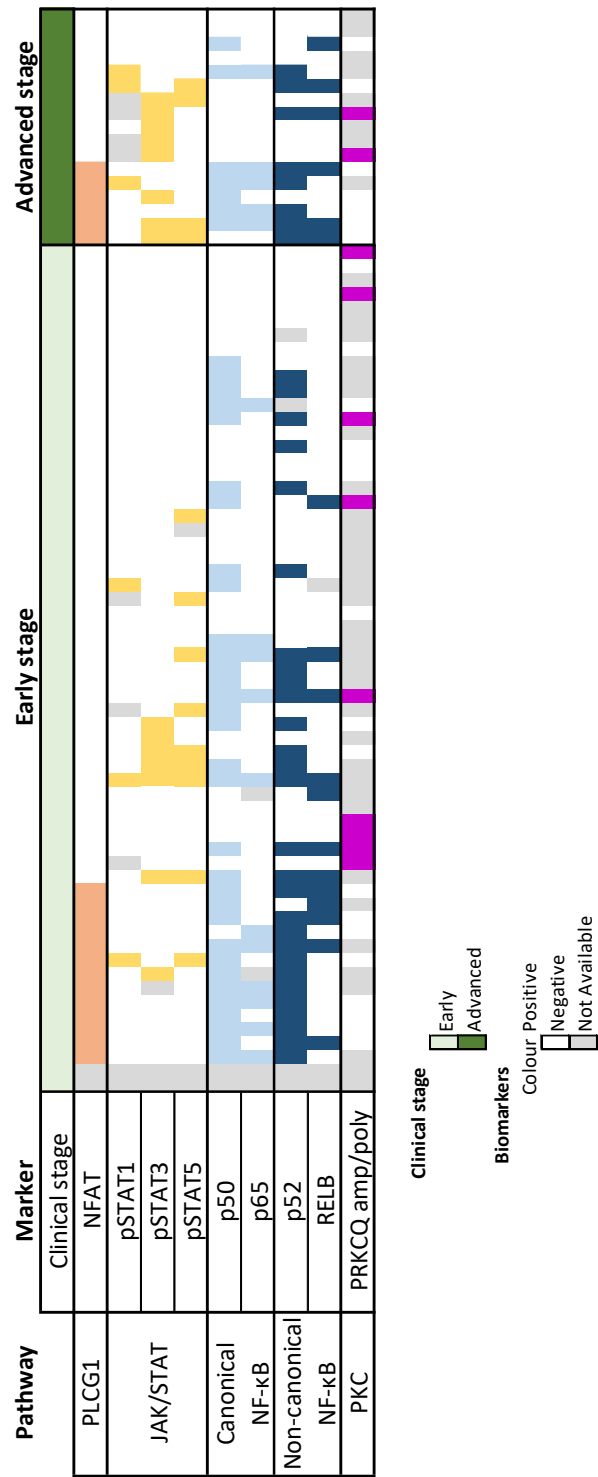


Figure 4.1. See legend on next page

See figure in previous page.

Figure 4.1. Summary of immunohistochemical data from patients with clinical information. Patients showing status of the studied markers (colour: positive, white: negative, grey: data not available) and clinical stage (light green: early stage, dark green: advanced).

Table 4.2. Correlation between immunohistochemical markers and clinical stages in MF patients. Positively and total stained cases and its percentage are shown for early and advanced stages. The significant statistics are bolded (* $p \leq 0.05$, ** $p \leq 0.005$).

Pathway	Marker	Early stage		Advanced stage		p value (χ^2)
		n	%	n	%	
PLCG1	NFAT	13/59	22	6/17	35.3	0.341
JAK/STAT	P-STAT1	3/56	5.4	3/13	23	0.08
	P-STAT3	7/58	12	8/17	47	0.004 **
	P-STAT5	9/58	15.5	3/17	17.6	0.48
	P-STAT1/3	8/55	14.5	7/13	53.8	0.005 **
	P-STAT1/3/5	11/54	20.4	7/13	53.8	0.03 *
Canonical NF- κ B	p50	32/59	54.2	7/17	41.1	0.41
	p65	11/57	19.3	5/17	29.4	0.5
	p50/p65	32/57	56	7/17	41	0.41
Non-canonical NF- κ B	p52	28/57	49.1	8/17	47	>0.99
	RelB	12/58	20.7	6/17	35.3	0.33
	p52/RelB	31/56	55.4	9/17	53	>0.99
PKC	PRKCQ amp/poly	9/26	34.6	2/9	22.2	0.69

4.2 HEK-Blue™ IL-6 cells as a model to study STAT3 activation

4.2.1 HEK-Blue™ IL-6 cell line set-up.

As described before, phosphorylated STAT3 is a marker of advanced stages in MF patients. To study the implication of the activation of this transcription factor in the pathogenesis of the disease, we took advantage of HEK-Blue™ IL-6 (HEK-IL6 from here on) cells (see **figure 3.2** in materials and methods section 3.3.1). These HEK293 cells constitutively express a human IL-6 receptor gene and a reporter gene construct expressing a secreted embryonic alkaline phosphatase (SEAP) fused to four STAT3 binding sites. Once STAT3 is activated, SEAP reporter gene is expressed and secreted into cell culture supernatant. The

RESULTS

quantification of activated STAT3 is easily measured by a colorimetric enzyme assay (using the QUANTI-Blue™ solution, quanti-blue from here on, see **figure 3.5** for more details) that determines the alkaline phosphatase activity in the supernatant of the cell culture.

To study the dynamics of STAT3 activation in this system, HEK-IL6 cells were incubated with increasing concentrations of IL-6 for 24 h (**figure 4.2A**) and with 10 ng/ml at different time points (**figure 4.2B**) and the SEAP levels were measured. STAT3 is most activated in HEK-IL6 treated for 48 h with 10 ng/ml of IL-6. It is known that to activate its targets genes, phosphorylated STAT3 can homodimerized or heterodimerized with STAT1 upon IL-6 stimulation. In this regard, phosphorylation of STAT1 and STAT3 in Y701 and Y705 respectively, upon IL-6 treatment at different time points was also determined by western blot (**figure 4.2C**). Both STAT1 and STAT3 are most phosphorylated, in these residues, after 60 min of IL-6 stimulation.

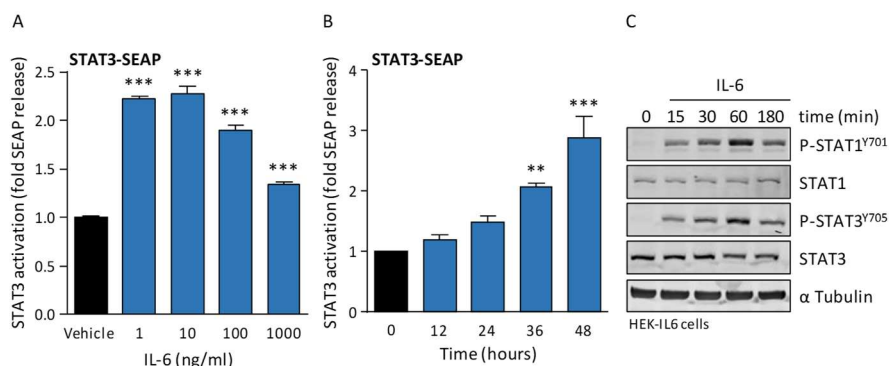


Figure 4.2. HEK-IL6 cells set-up for the detection of STAT3 activation. Quantification of SEAP release in HEK-IL6 cells A) treated with increasing concentrations and B) at different time points of IL-6 (10 ng/ml). Error bars show SEM. * compared with the control vehicle (** $p < 0.01$, *** $p < 0.001$). C) Western blot of whole cell lysates starved, treated for 1 h with IL-6 (10 ng/ml) at indicated time points and incubated with the indicated antibodies. Images are representative of each western blot.

4.2.2 JAK1 Y654F increase STAT3 activation upon IL-6 stimulation in HEK-IL6 cells.

Previous results from our laboratory have highlighted a potential role for JAK/STAT signalling pathway in CTCL. In this regard we detected mutations in the pseudokinase domains of *JAK1* and *JAK3* kinases using two different cohorts of CTCL cases (C. Pérez et al. 2015)(Vaqué et al. 2014). In these studies, *JAK1* was found recurrently mutated in CTCL patients (R659C), and in HuT 78 (Y654F), a human SS cell line. To study their contribution towards STAT activation, we first generated both *JAK1* cDNA mutants. We confirmed mutations by Sanger sequencing (**figure 3.4A**) and their protein expression by western blot (**figure 3.3A**). Then, HEK-IL6 cells were transfected with FLAG-*JAK1* wild type (WT), FLAG-*JAK1* R659C and FLAG-*JAK1* Y654F mutants and empty vector (EV) as control, incubated with control vehicle or IL-6 (10 ng/ml) and the STAT3 activity and phosphorylation was determined by quanti-blue and western blot respectively (**figure 4.3A and 4.3B**). In these settings, only *JAK1* Y654F mutant significantly activated STAT3, and this activation as well as the increase in phosphorylation (Y705) was enhanced upon IL-6 stimulation. This can suggest that this mutation confers a greater transduction potential of extracellular signals, like IL-6 in this case, towards STAT3 activation. The activation of STAT3 by this mutant was confirmed by luciferase reporter assay (STAT3-luc, **figure 4.3C**). Furthermore, HEK-IL6 cells expressing *JAK1* Y654F mutant and treated for 24 h with the JAK inhibitor, ruxolitinib, significantly decrease the activation of STAT3, suggesting that this activation is dependent on its kinase activity (**figure 4.3D**).

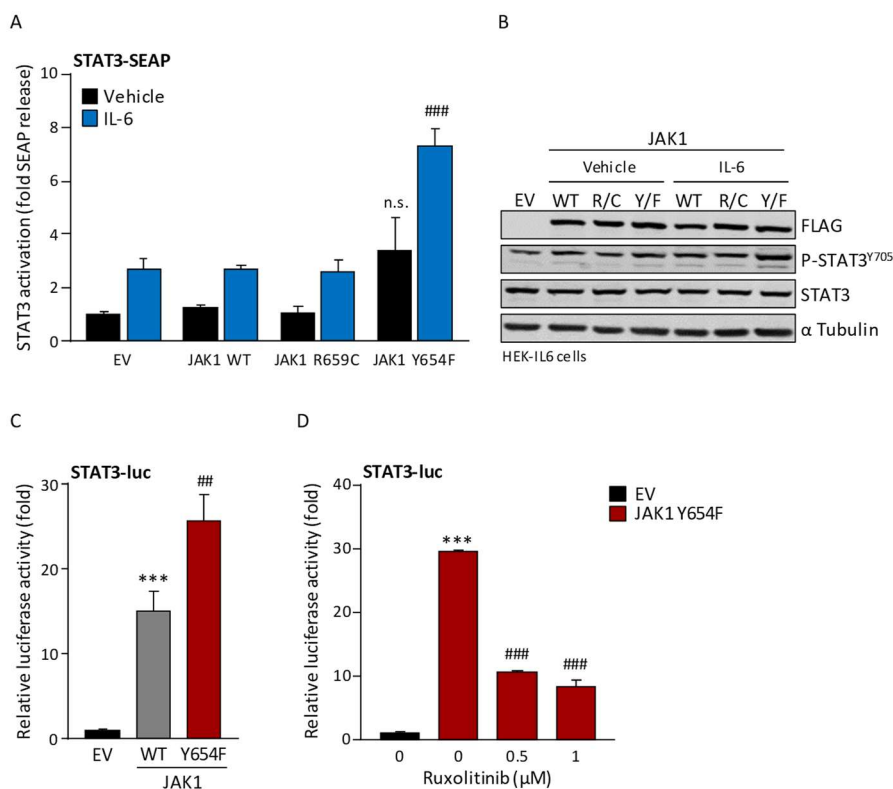


Figure 4.3. JAK1-Y654F activates STAT3-mediated transcription. A) Quantification of SEAP release in cells transfected with empty vector (EV) as control, JAK1 WT and JAK1 R659C and Y654F mutants, treated for 48 h with control vehicle or IL-6 (10 ng/ml). Error bars show SEM. N.s. = compared with JAK1 WT treated with control vehicle (n.s. $p > 0.05$). # compared with JAK1 WT treated with IL-6 (### $p < 0.001$). B) Western blot of whole cell lysates transfected with same constructions as A), treated for 1 h with control vehicle or IL-6 (10 ng/ml) and incubated with indicated antibodies. Images are representative of each western blot. STAT3 luciferase activity in HEK-IL6 cells transfected with C) EV, JAK1 WT or JAK1 Y654F mutant; or D) EV and JAK1 Y654F mutant and treated for 24 h with control vehicle or ruxolitinib. Error bars show SEM. * compared with EV (***) $p < 0.001$. # compared with JAK1 WT or JAK1 Y654F treated with control vehicle (## $p < 0.01$, ### $p < 0.001$).

4.3 PLCG1 downstream signalling towards NFAT, NF- κ B and STAT3 transcriptional activity

4.3.1 PLCG1 S345F activates NFAT and NF- κ B-mediated transcription by a PRKCQ dependent manner in HEK-IL6 cells.

Recurrent PLCG1 S345F mutations can be frequently detected among MF and SS cases (Vaqué et al. 2014). This mutation localises in one of the catalytic domains of PLCG1 (**figure 3.4B**) and has been widely confirmed by other studies (Choi et al. 2015; Ungewickell et al. 2015; Mcgirt et al. 2015; Woollard et al. 2016). From a mechanistic perspective, the contribution of activated PLCG1 to the disease pathogenesis and/or progression is still not fully understood. To that end, we studied the effects of PLCG1 S345F over potential downstream effectors. First, mutant sequence was confirmed by Sanger sequencing (**figure 3.4B**), and the WT and mutant protein expression was analysed by western blot (**figure 3.3A**). Then, HEK-IL6 cells were co-transfected with this PLCG1 mutant alongside NFAT or NF- κ B luciferase reporter gene constructs (NFAT-luc, NF- κ B-luc hereon) and their activity was measured 48 h after. As could be anticipated, PLCG1 S345F significantly activated NFAT- and NF- κ B-mediated transcription compared to PLCG1 WT (**figure 4.4A**).

In addition to the above mentioned experimental settings, cells were treated with specific inhibitors of each pathway as follows: 1) tacrolimus, that in a complex with FK506 binding protein (FKBP12) inhibits the phosphatase activity of calcineurin (CaN) towards the activation of NFAT proteins, blocking its nuclear translocation and further activation of its target genes; 2) sotrastaurin, pan-protein kinase C (PKC) inhibitor (inactive to PKC ζ) with an increased 3-fold selectivity for the isoform PKC θ (PRKCQ hereon) versus PKC β 1 and other isoforms; and 3) ruxolitinib, a pan-JAK inhibitor with much more sensitivity to JAK1/2 versus JAK3. To that end, HEK-IL6 cells co-transfected with PLCG1 S345F and NFAT-luc were

RESULTS

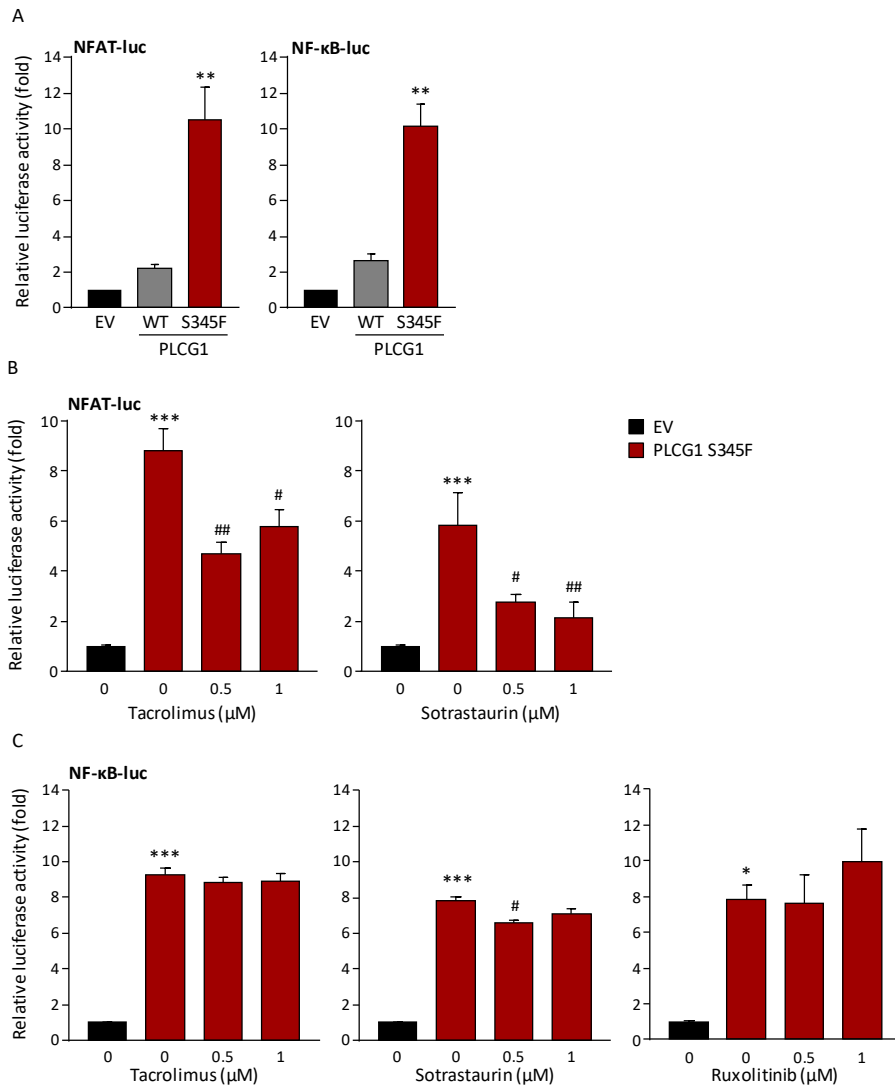


Figure 4.4. PLCG1 S345F promotes NFAT- and NF-κB-mediated transcription. A) NFAT and NF-κB luciferase activity in HEK-IL6 cells transfected with empty vector (EV), PLCG1 wild type (WT) or S345F mutant. B) NFAT luciferase activity of HEK-IL6 cells transfected with EV or PLCG1 S345F mutant and treated for 24 h with control vehicle and different concentrations of Tacrolimus or sotrastaurin. C) NF-κB luciferase activity of HEK-IL6 cells transfected with EV or PLCG1 S345F mutant and treated for 24 h with control vehicle and different concentrations of tacrolimus, sotrastaurin or ruxolitinib. Error bars show SEM. * compared with PLCG1 WT or EV (* $p < 0.05$, ** $p < 0.01$, *** $p < 0.001$). # compared with PLCG1 S345F treated with control vehicle (# $p < 0.05$, ## $p < 0.01$).

treated for 24 h with tacrolimus or sotrastaurin before assessing NFAT activity. As shown in **figure 4.4B**, both inhibitors abrogated the activation of NFAT-mediated transcription by PLCG1 S345F, suggesting that, as previously described, downstream of PLCG1, both CaN and PRKCQ can participate in its activation. Alongside this, HEK-IL6 cells were also co-transfected with the mutant and NF- κ B-luc and treated for 24 h with tacrolimus, sotrastaurin or ruxolitinib (**figure 4.4C**). Our results, as could be anticipated, inhibition of CaN and JAK did not affect NF- κ B activation by PLCG1, whereas abrogating PRKCQ activity did. To our surprise this effect, despite being significant, was very modest and therefore might suggest that PRKCQ may not participate as a central mediator of NF- κ B activation downstream PLCG1 signalling.

4.3.2 PLCG1 S345F promotes activation of STAT3 in HEK-IL6 cells.

As describe in section 4.1, activated STAT3 is a significant marker of advanced disease in MF patients. Furthermore, activating PLCG1 S345F mutation may be acquired along the progression of the disease as it was detected in advanced MF or in SS lesions. Interestingly, a patient sample that was found negative for the mutation, showed this mutation 14 months later (Vaqué et al. 2014). Thus, the connection between PLCG1 signalling pathway and the activation of STAT3 was investigated in the setting of the deregulated CTCL network described in the introduction (**figure 1.4**).

First, HEK-IL6 were transfected with PLCG1 WT, PLCG1 S345F mutant and EV (negative control) and phosphorylation of STAT3 proteins was analysed. Since it has been described that both tyrosine 705 (Y705) and serine 727 (S727) phosphorylations of STAT3 are required for maximal transcriptional activation (Wen et al. 1995), we decided to study both. As shown in **figure 4.5**, overexpressing both PLCG1 WT and S345F mutant significantly increase STAT3 phosphorylation in both residues.

RESULTS

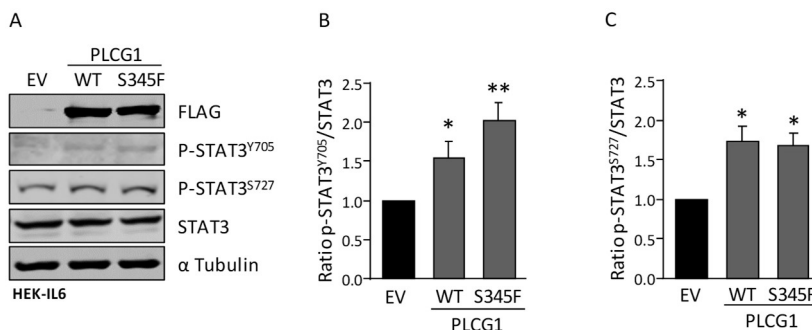


Figure 4.5. PLCG1 S345F promotes STAT3 phosphorylation in Y705 and S727 residues. A) Western blot analyses of whole HEK-IL6 cells lysates transfected with empty vector (EV), PLCG1 wild type (WT) or S345F mutant, starved overnight and incubated with indicated antibodies. Images are representative of each western blot. Quantification of protein expression of STAT3 phosphorylated at B) Y705F or C) S727 residues relative to total STAT3 of HEK-IL6 cells transfected as A) (n=3). Error bars show SEM. * compared with EV (* $p < 0.05$, ** $p < 0.01$).

Taking advantage of the quanti-blue and luciferase reporter assay systems, we studied STAT3 transcriptional activity downstream of PLCG1. HEK-IL6 cells were transfected with EV, PLCG1 WT and PLCG1 S345F mutant and STAT3-mediated transcription was determined 48 h after by using quanti-blue (**figure 4.6A**) or by luciferase using STAT3 luciferase reporter (STAT3-luc from here on, **figure 4.6B**). In both settings, PLCG1 S345F significantly activated STAT3.

To gain further insight into the mechanisms that participate downstream PLCG1 in STAT3 activation, we incubated transfected cells with the inhibitors described above: tacrolimus (CaN), sotrastaurin (PRKCQ) and ruxolitinib (JAK). Thus, HEK-IL6 cells were transfected with PLCG1 S345F and EV and incubated for 24 h with increasing concentrations of each inhibitor after which STAT3-luc was measured (**figure 4.7A**). In these conditions, only inhibitors of PRKCQ and JAKs blocked STAT3 activation downstream of activated PLCG1. The levels of phosphorylated STAT3 were also analysed by western blot in HEK-IL6 cells starved

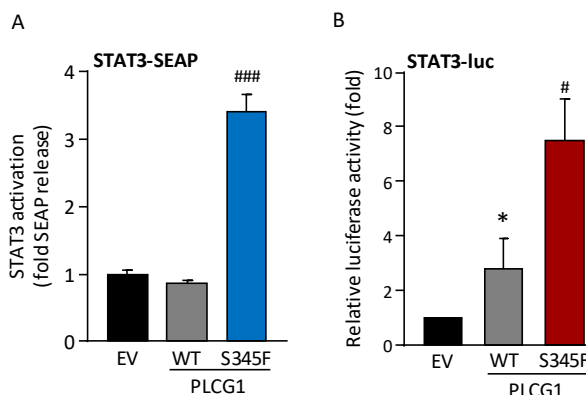


Figure 4.6. PLCG1 S345F promotes STAT3-mediated transcription. Quantification of A) SEAP release or B) STAT3 luciferase activity in HEK-IL6 cells transfected with empty vector (EV), PLCG1 wild type (WT) or S345F mutant. Error bars show SEM. * compared with EV (* $p < 0.05$), # compared with PLCG1 WT (# $p < 0.05$, ###, $p < 0.001$).

overnight and incubated with sotrastaurin for 3 h (**figure 4.7B**). The changes of phosphorylated signals in Y705 and S727 residues were quantified and related to total levels of STAT3, all normalised to α -tubulin signals (**figure 4.7C and 4.7D**, respectively). Our data show that PLCG1 S345F increases the phosphorylation of STAT3 in both Y705 and S727 residues and inhibition of PRKCQ significantly reduces these.

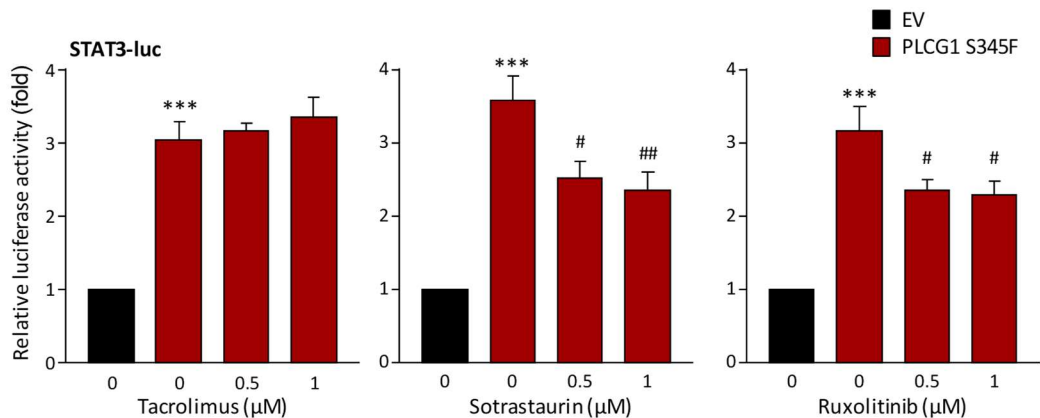
4.4 TPA-mediated signalling towards NFAT, NF- κ B and STAT3

4.4.1 TPA increases NFAT- and NF- κ B-mediated transcription in HEK-IL6 cells.

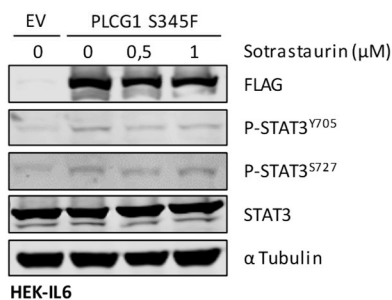
Since PRKCQ seems to be implicated in the activation of NFAT and NF- κ B downstream of PLCG1 (see **figure 4.4**), we decided to use 12-O-tetradecanoylphorbol-13-acetate (TPA from here on) in our system. TPA is a diester phorbol that activates PKCs, we used it in HEK-IL6

RESULTS

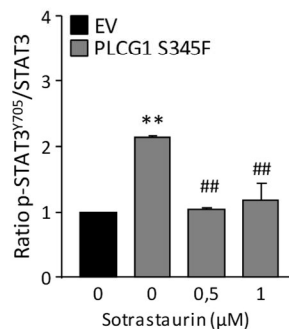
A



B



C



D

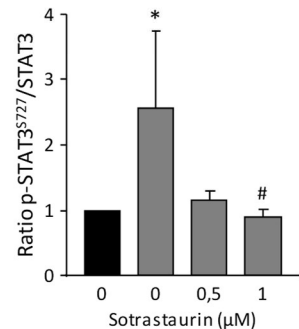


Figure 4.7. PLCG1 S345F promotes STAT3-mediated transcription through a mechanism involving PRKQC and JAK kinases in HEK-Blue™ IL-6 cells. A) STAT3 luciferase activity in HEK-IL6 cells transfected with empty vector (EV) or PLCG1 S345F mutant and treated for 24h with control vehicle and tacrolimus, sotrastaurin or ruxolitinib at the indicated concentrations. B) Western blotting analyses of whole cells lysates transfected as A), starved overnight, treated for 3h with control vehicle or Sotrastaurin and incubated with the indicated antibodies. Images are representative of each western blot. Quantification of protein expression of STAT3 phosphorylated at C) Y705F (n=4) or D) S727 (n=3) residues relative to total STAT3 of HEK-IL6 cells transfected as B). Error bars show SEM. * compared with EV (* p < 0.05, ** p < 0.01, *** p < 0.001). # compared with PLCG1 S345F treated with control vehicle. (# p < 0.05, ## p < 0.01).

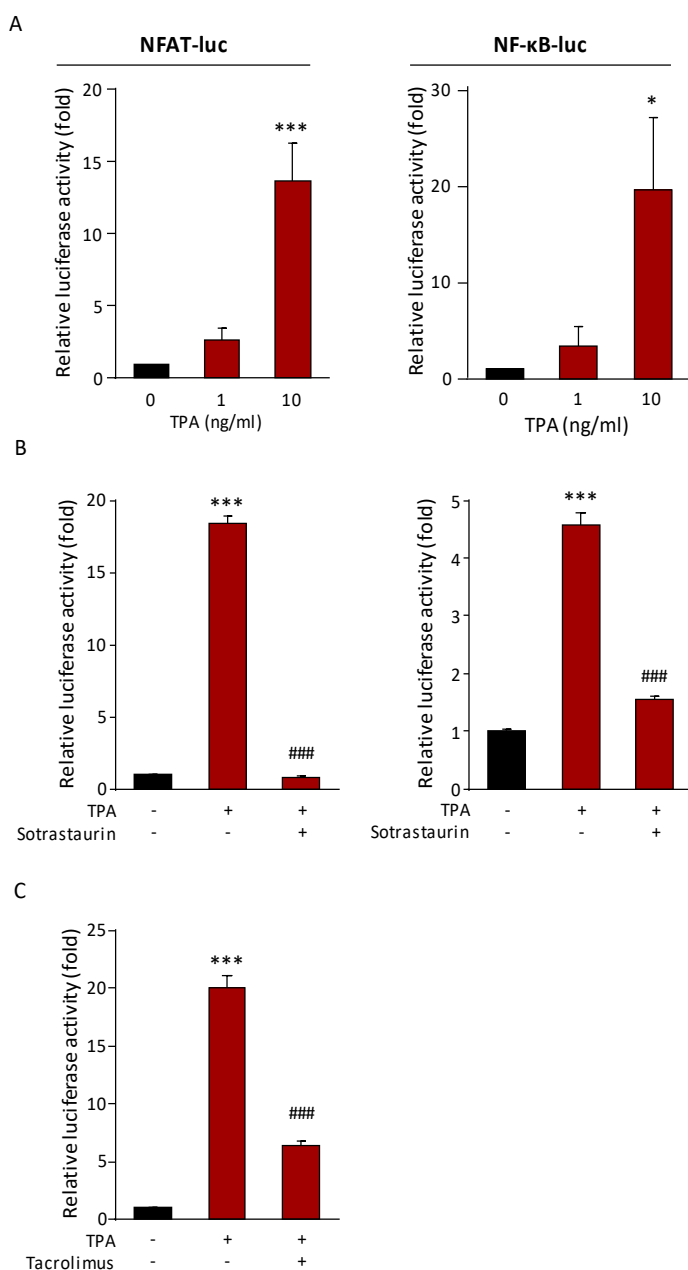


Figure 4.8. TPA activates NFAT- and NF-κB-mediated transcription through mechanism involving PRKCQ activity. NFAT (left) and NF-κB (right) luciferase activities in HEK-IL6 cells A) treated with control vehicle or TPA at indicated concentrations and B) treated with control vehicle or sotrastaurin and with control vehicle or TPA. C) NFAT luciferase activity of HEK-IL6 cells treated with control vehicle or TPA and with control vehicle or Tacrolimus. All treatments were performed for 2 h with control vehicle or inhibitor (1 μM) and then for 24 h with control vehicle or TPA (10 ng/ml). Error bars show SEM. * compared with control vehicle (* $p < 0,05$, *** $p < 0.001$). # compared TPA alone (### $p < 0.001$).

transfected with the luciferase reporter genes, at increasing concentrations during 24 h (**figure 4.8A**). TPA (10 ng/ml) significantly activated NFAT-luc and NFkB-luc. Then, the participation of PRKCQ was analysed in the same conditions but including a pre-incubation of 2 h with sotrastaurin (PRKCQ inhibitor), before using TPA. As shown in **figure 4.8B**, sotrastaurin abrogated NFAT- and NF- κ B activities elicited by TPA. As control for NFAT activity, cells were transfected with NFAT-luc and incubated with tacrolimus and TPA. As previously described, the TPA-induced NFAT activation is also dependent on CaN (**figure 4.8C**).

4.4.2 TPA increases STAT3-mediated transcription through PRKCQ and not through JAKs in HEK-IL6 cells.

We have previously shown that PLCG1 can activate STAT3 in a PKC- and JAK-dependent fashion **figure 4.7** so we decided to study the implication of PRKCQ towards STAT3 activity more in detail. To that end, HEK-IL6 cells were transfected with STAT3-luc and treated with increasing concentrations of TPA for 24 h. As shown in **figure 4.9A**, TPA mediates STAT3 activation. Using specific inhibitors, we observed that this is abrogated by sotrastaurin (**figure 4.9B left**) but, remarkably, the specific JAK inhibitor did not (**figure 4.9B right**). These results suggest that, in our experimental settings, the increase of STAT3-mediated transcription, downstream PRKCQ activation can occur independently of JAK kinases.

To further confirm these results, protein levels of phosphorylated STAT1 and STAT3 were analysed alongside transcriptional STAT3 activity using quanti-blue assay in HEK-IL6 cells treated with TPA. This time we decided to pre-incubate cells with several inhibitors in order to investigate the potential implication of other signaling pathways that have been implicated in the regulation of STAT3 activation. The inhibitors used, apart from the ones

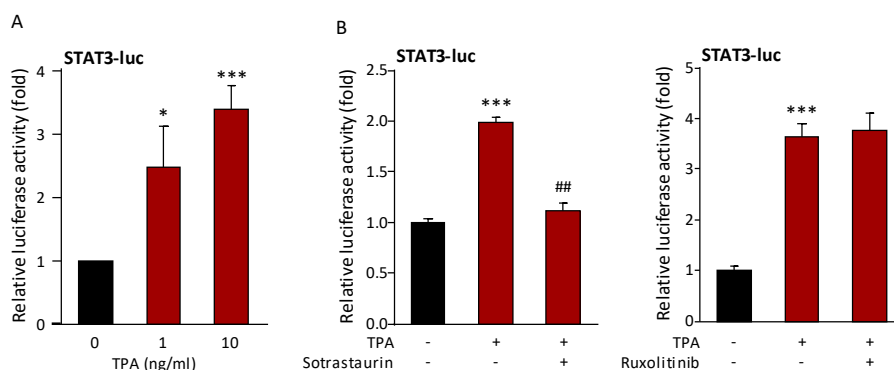
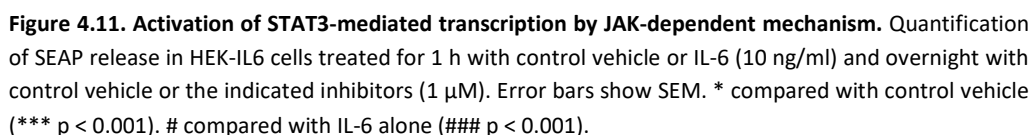
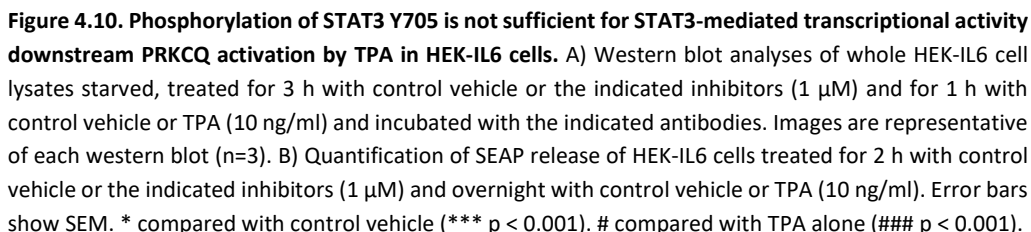


Figure 4.9. TPA activates STAT3-mediated transcription through mechanism involving PRKCQ activity. STAT3 luciferase activities in HEK-IL6 cells A) treated with control vehicle or TPA at indicated concentrations and B) treated for 2 h with control vehicle, sotrastaurin (left) or ruxolitinib (right) (1 μM) and for 24 h with control vehicle or TPA (10 ng/ml). Error bars show SEM. * compared with control vehicle (* $p < 0.05$, *** $p < 0.001$). # compared TPA alone (## $p < 0.01$, ### $p < 0.001$).

already described and used before, were: ibrutinib (targeting BTK), dasatinib (targeting Abl, Src and c-Kit), fostamatinib (targeting Syk) and MK-2206 (targeting Akt1/2/3).

To analyse the phospho-protein levels, HEK-IL6 were pre-treated for 3 h with each inhibitor (1 μM) and then incubated for 1 h with TPA (10 ng/ml) (**figure 4.10A**). TPA increases tyrosine phosphorylation of STAT1 (Y701) and STAT3 (Y705), which was abrogated by specific PRKCQ, JAK and Syk inhibitors. TPA also promotes STAT3 phosphorylation at S727, but interestingly, only the PRKCQ inhibitor abrogated it. Thus, regarding PRKCQ, our data show that it can promote STAT3 phosphorylation by JAK or SYK-dependent (Y705) and JAK-independent (S727) mechanisms. Regarding STAT3 transcriptional activity, only sotrastaurin (PRKCQ inhibitor) completely abrogated STAT3 activation downstream of PKC activation by TPA (**figure 4.10B**). This is a surprising result that strongly suggests that, STAT3 phosphorylation at S727 can be a mayor mechanism to control STAT3 activity downstream of PRKCQ.

A



Furthermore, JAK-dependent STAT3 activation was measured by quanti-blue as positive control of ruxolitinib. To that end, HEK-IL6 were treated for 2 h with tacrolimus, sotrastaurin or ruxolitinib and then incubated overnight with IL-6. As shown in **figure 4.11**, only ruxolitinib was able to abrogate IL-6-dependent STAT3 activation as expected.

Thus, in the context of PLCG1/PRKCQ signalling network, activation of STAT3 can be triggered by JAK-dependent and JAK-independent mechanisms.

4.4.3 JAK-dependent and -independent regulation of STAT3 activity in T cells

As shown before, regulation of STAT3 activity, downstream of PRKCQ, can occur through the acquisition of phosphorylations in residues Y705 and S727. In order to study STAT3 activation and transcriptional activity, downstream PRKCQ in a human CTCL setting, we took advantage of Jurkat (Acute T Cell Leukemia), MyLa (advanced MF) and HuT 78 (SS) cell lines. To study phosphorylation affecting STAT3, cells were starved and pre-incubated for 3 h with tacrolimus, sotrastaurin or ruxolitinib and then treated for 1 h with TPA, and whole cell lysates were incubated with the indicated antibodies. As shown in **figure 4.12A**, TPA increases the phosphorylation of STAT1 (Y701) and STAT3 (only at S727) in Jurkat cells, and only sotrastaurin, abrogates both phosphorylations. In contrast, ruxolitinib only decreases STAT1 phosphorylation at Y701. Phosphorylation of STAT3 at Y705 is not detectable upon TPA stimulation in these cells.

In the case of CTCL cells, TPA promoted the phosphorylation of STAT1-Y701, STAT3-Y705 and STAT3-S727, perhaps with the exception of STAT3-Y705 in MyLa cells since these cells display an increased and steady level of phosphorylated STAT3 Y705 even under starvation conditions (**figure 4.12B and C**). Also, in both cell lines, ruxolitinib suppressed TPA-mediated

RESULTS

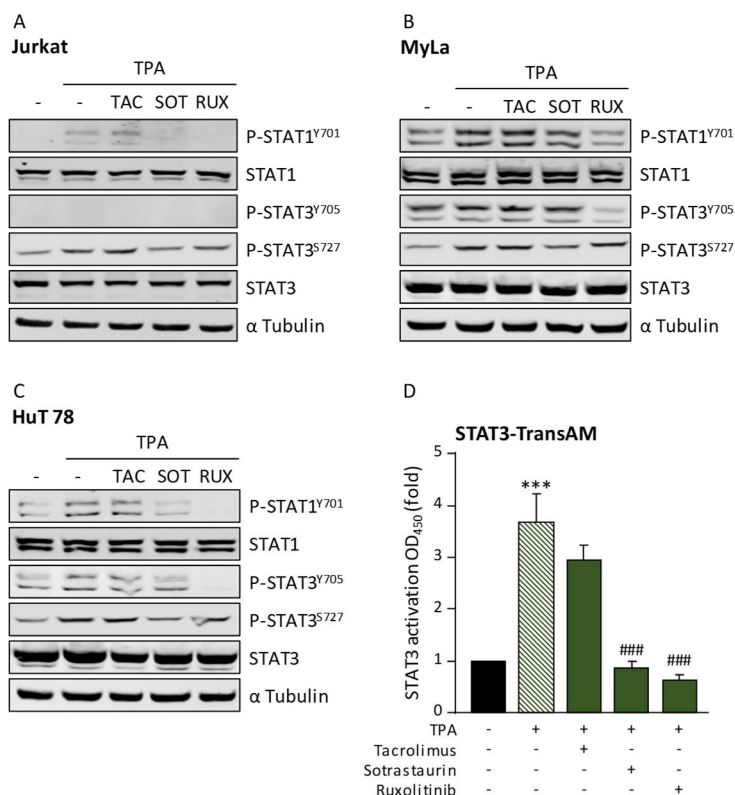


Figure 4.12. JAK-dependent and -independent regulation of STAT3 activity in Jurkat, MyLa and HuT 78 cells. Western blot analyses of starved A) Jurkat, B) MyLa and C) HuT 78 cells treated for 3 h with control vehicle or the indicated inhibitors (1 μ M) and for 1 h with control vehicle or TPA (10 ng/ml) and incubated with the indicated antibodies. Images are representative of each western blot (n=3). D) Quantification of STAT3 activity in HuT 78 cells treated for 3 h with control vehicle or the indicated inhibitors (1 μ M) and overnight with control vehicle or TPA (10 ng/ml) (n=3). Error bars show SEM. * compared with the control vehicle (**p < 0.001). # compared with TPA alone (###p < 0.001).

STAT1 and STAT3 phosphorylation at tyrosine residues. By contrast, sotrastaurin suppressed STAT3-S727 and STAT1-Y701 phosphorylation in both cell lines and in STAT3-Y705 only in Hut 78. These results, we believe are aligned to our previous observations in HEK IL6 cells and robust the idea that downstream PLCG1/PRKCQ, STAT3 activation can be triggered by JAK-dependent and JAK-independent mechanisms in a CTCL context.

In order to explore how these mechanisms can regulate STAT3 transcriptional activity, we performed a TransAM assay (STAT3-TransAM from here on) in HuT 78 cells. This is an ELISA-

based method consisting in a 96-well plate on which oligonucleotides containing the STAT3 consensus binding site (5'-TTCCCGGAA-3') has been immobilized. The active form of STAT3 from nuclear extracts specifically binds to these oligonucleotides. The nuclear extracts are incubated with a primary antibody that recognizes an epitope on STAT3 that is accessible only when STAT3 is activated and bound to the DNA. Then, a secondary antibody conjugated with a horseradish peroxidase (HRP) is added providing a sensitive and easily colorimetric quantification. So, HuT 78 cells were pre-incubated for 3 h with tacrolimus, sotrastaurin or ruxolitinib, and then treated overnight with TPA. Then nuclear extracts were obtained and incubated in the STAT3-TransAM well plate. Our data show that TPA can increase STAT3 activity in these cells, which is abrogated by PRKCQ and JAK inhibitors (sotrastaurin and ruxolitinib respectively, **figure 4.12D**). Our data suggest that both signalling axis are implicated in the control of STAT3 transcriptional activity upon TPA stimulation in these cells. As expected, and in these settings, CaN is not implicated in STAT3 activation upon TPA treatment.

4.5 PRKCQ downstream signalling towards NFAT and STAT3 activation

4.5.1 PRKCQ expression in HEK-IL6, Jurkat and CTCL cell lines

PRKCQ has been found amplified in 20-30% of CTCL patients in two independent genomic studies and, interestingly, occurred in a mutually exclusive manner with PLCG1 mutations (Choi et al. 2015; Woollard et al. 2016). We decided to study *PRKCQ* gene amplification and mRNA and protein expression in HEK-IL6, Jurkat, MyLa and HuT 78 cells (*PRKCQ* amplification was not studied in HEK-IL6). Both polysomy of chromosome 10 where *PRKCQ*

RESULTS

is located and *PRKCQ* amplification were studied by fluorescence *in situ* hybridization (FISH) in collaboration with Dr. Alejandro A. Gru from Department of Pathology, University of Virginia, USA. As shown in **figure 4.13A**, Jurkat cells show both chromosome 10 polysomy and *PRKCQ* amplification whereas HuT 78 cells only have chromosome 10 polysomy and MyLa none of them. These results correlate well with mRNA (**figure 4.13B**) and protein (**figure 4.13C**) expression, where the highest *PRKCQ* expression is found in Jurkat cells, followed by HuT 78, HEK-IL6 and MyLa cell lines.

Thus, expression levels of *PRKCQ* is detectable in all cell models used with marked differences between MyLa (lower) and HuT 78 (higher) CTCL cells.

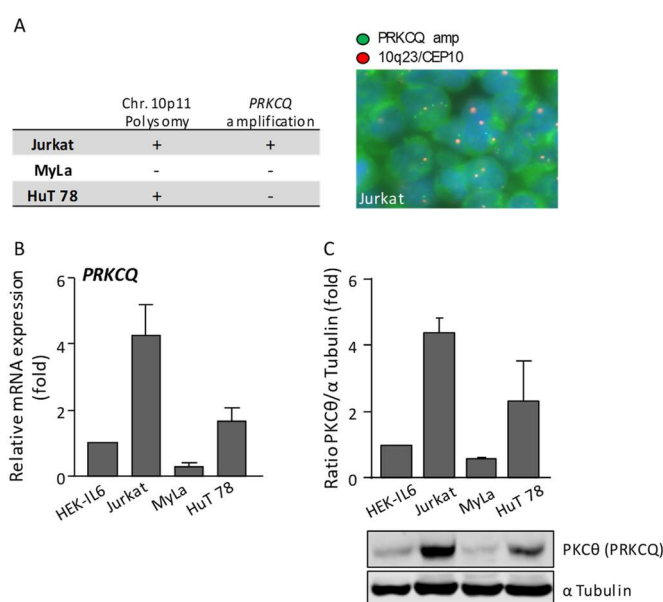


Figure 4.13. Expression of *PRKCQ* in HEK-IL6, Jurkat, MyLa and HuT 78 cells. A) Study of chromosome 10p11 polysomy and *PRKCQ* amplification in Jurkat, MyLa and HuT 78 cells by fluorescence *in situ* hybridization. Representative image of *PRKCQ* (green) and 10q23/CEP10 (red) probes in Jurkat cells. B) mRNA expression of *PRKCQ* in HEK-IL6, Jurkat, MyLa and HuT 78 cells. C) Basal protein expression and quantification (n=2) of PKCθ (*PRKCQ*) in same cells as B). Images are representative of each western blot. Error bars show SEM.

4.5.2 A constitutively active PRKCQ mutant activates NFAT but not NF- κ B

In order to study whether PRKCQ by itself is sufficient to activate NFAT and NF- κ B, a constitutively active mutant was generated by direct mutagenesis. The construct pCMV6-FLAG-PRKCQ was mutated in residue 148, changing from wild type GCC (A, alanine) to mutant GAG (E, glutamic acid), (see methods). To confirm this mutation, pCMV6-FLAG-PRKCQ A148E (PRKCQ A148E hereon) and its WT counterpart (PRKCQ WT hereon) were sequenced (chromatograms and localization of mutant within protein domains are represented in **figure 3.4C**) and their protein expression was analysed by western blot (**figure 3.3B**). Then, HEK-IL6 cells were co-transfected with empty vector (EV), PRKCQ WT and PRKCQ A148E mutant alongside NFAT- or NF- κ B-luc reporter genes and their activity was measured. As previously described, activated PRKCQ significantly increased NFAT-mediated transcription (**figure 4.14A**), probably synergizing with that of CaN (Guy Werlen et al. 1998). This activation was dependent in its kinase activity as sotrastaurin abrogated PRKCQ-mediated NFAT activation (**figure 4.14B**). On the other hand and surprisingly, mutant PRKCQ did not activate NF- κ B-mediated transcription (**figure 4.14C**) despite it has been described that PRKCQ can activate NF- κ B by TCR/CD28 co-stimulation in mature T cells (Lin et al. 2000; Sun et al. 2000).

Given this unexpected result and considering the biological data regarding CTCL progression and its association with STAT3, previously shown in this thesis, we decided to focus on the mechanisms used by PRKCQ to promote STAT3 activation.

RESULTS

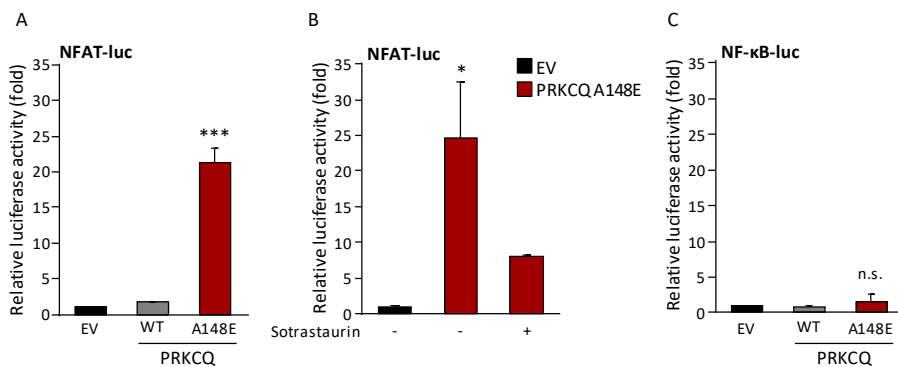


Figure 4.14. Constitutively active PKC θ mutant activates NFAT-mediated transcription but not that of NF- κ B. NFAT luciferase activity in HEK-IL6 cells A) transfected with empty vector (EV), PRKCQ wild type (WT) or PRKCQ A148E mutant and B) transfected with EV and PRKCQ A148E and treated 24 h with control vehicle or sotrastaurin (1 μ M). C) NF- κ B luciferase activity in HEK-IL6 transfected with same conditions as A). Error bars show SEM. * compared with EV (n.s. $p > 0,05$, * $p < 0,05$, *** $p < 0.001$).

4.5.3 PRKCQ activates STAT3 through a mechanism that depends on its kinase activity

As described in section 4.1, only activated STAT3 correlates with CTCL progression to advanced stages. Furthermore, as described in section 4.4.3 and downstream of PLCG1, STAT3 activation is triggered, at least in part, by PRKCQ-dependent mechanisms in CTCL cells. So, PRKCQ WT was transfected in HEK-IL6 cells, alongside STAT3-luc, and then cells were stimulated with TPA. As shown in **figure 4.15A**, overexpression of PRKCQ upon TPA stimulation increased 7-fold STAT3-mediated transcription whereas, when PRKCQ was not overexpressed, TPA only increased it 3-fold. Furthermore, expression of the PRKCQ active mutant induced STAT3-luc (**figure 4.15B**) and STAT3 phosphorylation (**figure 4.15C**) in S727, in the absence of TPA. Also, and as expected, sotrastaurin inhibited STAT3-luc activation elicited by PRKCQ A148E in HEK-IL6 cells (**figure 4.15D**).

Thus, as part of the signaling network activated downstream of PLCG1, PRKCQ can trigger STAT3 phosphorylation and transcriptional activity through a mechanism that depends on its kinase activity.

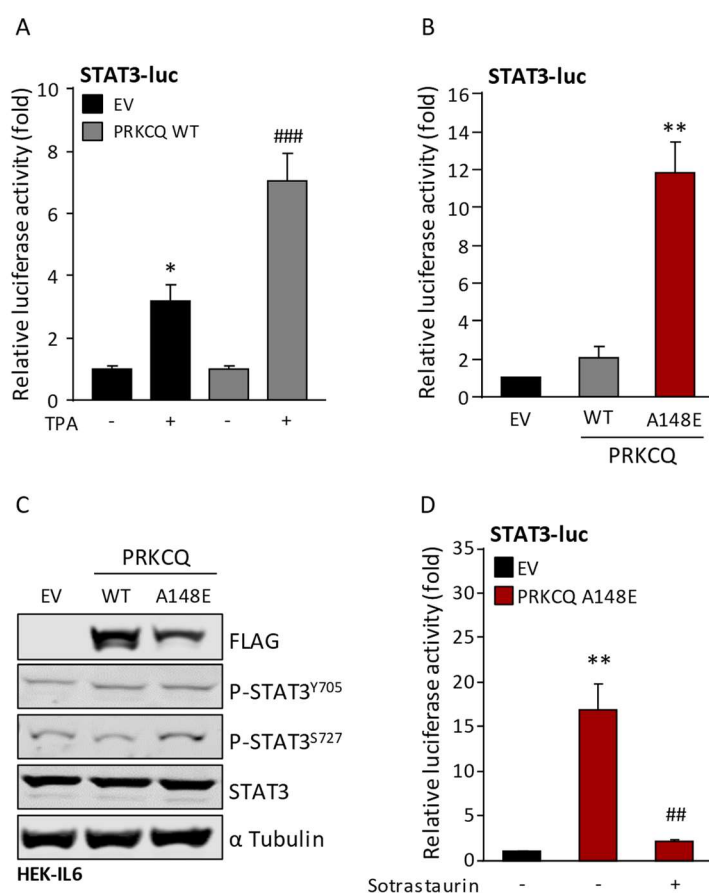


Figure 4.15. PRKCQ activates STAT3 through a mechanism that depends on its kinase activity. STAT3 luciferase activity in HEK-IL6 cells transfected with A) empty vector (EV) or PRKCQ WT (2 ug) and treated overnight with control vehicle or TPA (10 ng/ml); B) EV, PRKCQ WT or PRKCQ A148E and D) EV or PRKCQ A148E and treated overnight with control vehicle or sotrastaurin (1 μ M). C) Western blot analyses of whole HEK-IL6 cells lysates transfected with EV, PRKCQ WT or PRKCQ A148E and incubated with indicated antibodies. Images are representative of each western blot. Error bars show SEM. * compared with EV treated with control vehicle (A,D) or with EV (B) (* $p < 0.05$, ** $p < 0.01$). # compared with EV treated with TPA (A) or with PRKCQ A148E treated with control vehicle (D) (## $p < 0.01$, ### $p < 0.001$).

4.6 Effects of sotrastaurin and ruxolitinib in CTCL proliferation and apoptosis

4.6.1 Sotrastaurin inhibits cell proliferation and promotes apoptosis in HEK-IL6, Jurkat and CTCL cells.

Since PRKCQ can promote STAT3-mediated transcription in CTCL cells and its inhibition counteracts STAT3 activation, the effects of sotrastaurin in cell proliferation and apoptosis were analysed. To that end, HEK-IL6, Jurkat, MyLa and HuT 78 cells were incubated with increasing concentrations of this inhibitor and the proliferation effects were measured at 24 and 48 h by quantifying the ATP presence in cell culture with a luminescent assay (CellTiter-Glo). The data enabled to calculate the IC_{50} concentration at 48 h using GraphPad Prism 6 software. As shown in **figure 4.16**, sotrastaurin impaired cell proliferation in a concentration-dependent manner. The IC_{50} concentration of sotrastaurin is indicated for

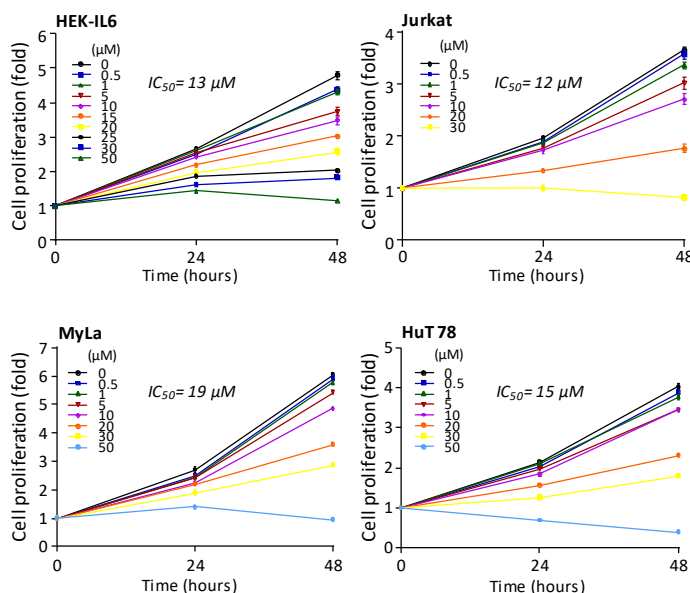


Figure 4.16. Antiproliferative effects of Sotrastaurin in HEK-IL6, Jurkat, MyLa and HuT 78 cells. Proliferation analyses in HEK-IL6, Jurkat, MyLa and HuT 78 cells at 0, 24 and 48 h treated with increasing concentrations of sotrastaurin. IC_{50} concentrations at 48 h are indicated for each cell line. Error bars show SEM.

each cell line and ranges between 12 and 19 μM . In order to study the effects of sotrastaurin in apoptosis, MyLa (**figure 4.17A**) and HuT 78 (**figure 4.17B**) cells were incubated with control vehicle, IC_{50} or double IC_{50} ($2 \times \text{IC}_{50}$) of sotrastaurin in each case and early (annexin V, Y axis) and late (7-AAD, X axis) apoptosis was analysed by flow cytometry. As shown in **figure 17**, top panels show a significant decrease of CTCL cell viability due to incubation with the PRKCQ inhibitor, which in turn, can be explained by a mixture of early and late apoptotic markers as shown in the data plots (bottom panels).

Thus, inhibiting PRKCQ activity using a specific inhibitor exerts anti-CTCL effects in terms of inhibiting cell proliferation alongside activating apoptosis.

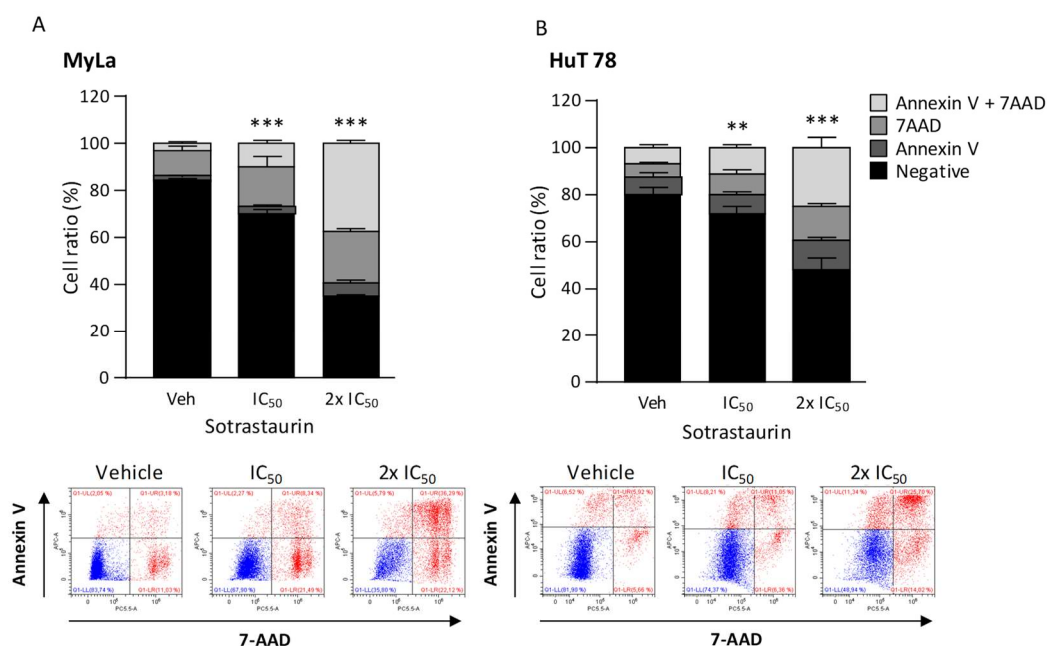


Figure 4.17. Pro-apoptotic effects of sotrastaurin in CTCL cells. Percentage of early (Annexin V) or late (7-AAD) apoptotic A) MyLa and B) HuT 78 cells incubated for 24 h with control vehicle (Veh), IC_{50} or double IC_{50} ($2 \times \text{IC}_{50}$) of sotrastaurin (n=3). Representative plots of Annexin V (Y axis) and 7AAD (X axis) staining data of each condition are shown. Error bars show SEM. *comparison between viable cells (negative staining) treated with sotrastaurin and viable cells treated with control vehicle (** $p < 0.01$; *** $p < 0.001$).

4.6.2 Ruxolitinib inhibits cell proliferation and promotes apoptosis in CTCL cells.

As described before, STAT3 activation in CTCL is also triggered by JAK-dependent mechanisms, so the effects in proliferation and apoptosis of JAK inhibition by ruxolitinib were investigated in CTCL cell lines by using the same methods as above. Thus, increasing concentrations of ruxolitinib impairs CTCL cell proliferation in a concentration-dependent manner (**figure 4.18A**, the IC_{50} concentration is indicated for each cell line). Also, the percentage of viable MyLa and HuT 78 cells (**figure 4.18B**) is decreased when treated with IC_{50} or $2x IC_{50}$ concentrations. Representative early (annexin V, X axis) and late (7-AAD, Y axis) apoptosis staining plots are shown.

Thus, inhibiting JAK activity using a specific inhibitor also elicits anti-CTCL effects by inhibiting cell proliferation and activating apoptosis.

4.6.3 Synergistic activity of combined PRKCQ and JAK inhibition in cell proliferation

Based on our data where inhibition of PRKCQ and JAK with sotrastaurin and ruxolitinib respectively, exert anti-proliferative and pro-apoptotic effects separately, the combination effects of inhibiting both signalling pathways were investigated and the combination index (CI) was calculated by CalcuSyn software. To that end, the proliferation effects of inhibitors alone and in combination were analysed with CellTiter-Glo after 48 h of treatment and the fraction of affected cells were calculated. This method assesses whether a combination of two drugs results in a synergistic ($CI < 1$), additive ($CI = 1$) or antagonistic effect ($CI > 1$) considering the fraction of affected cells of both inhibitors alone and comparing it with the fraction of affected cells of the combination treatment. The combination indexes were

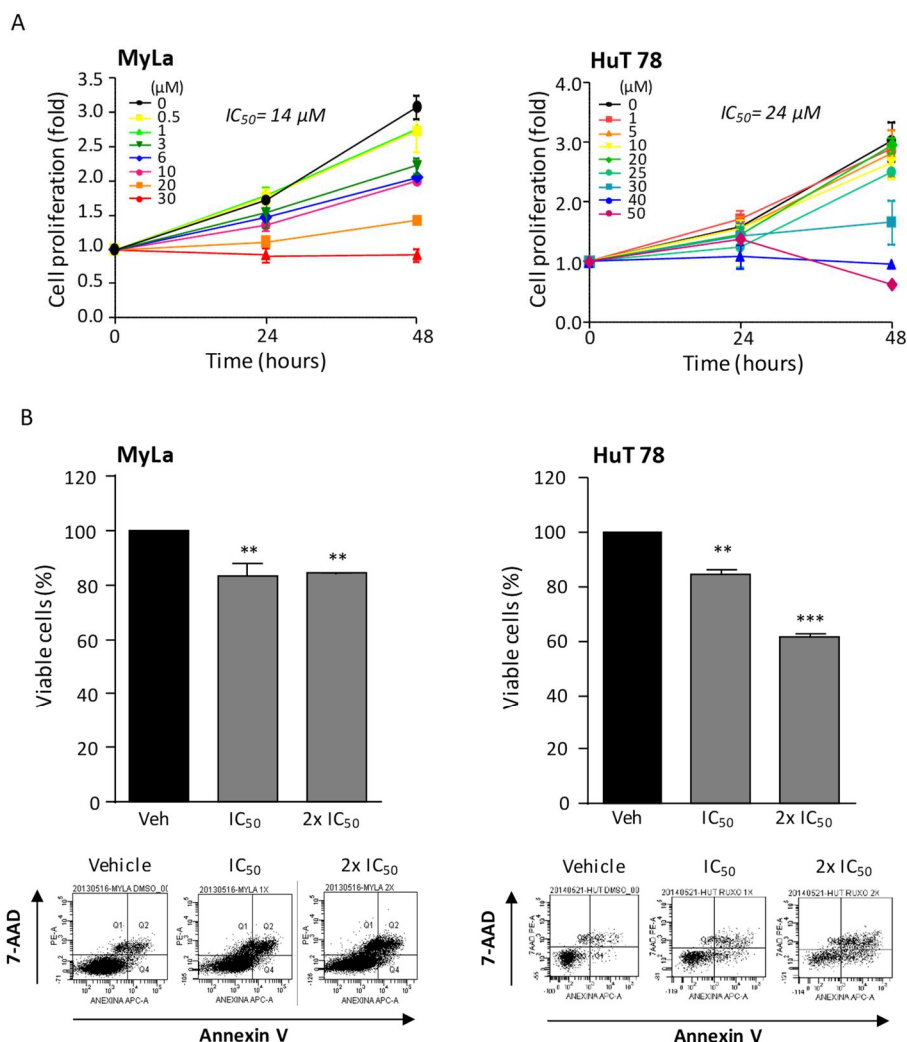


Figure 4.18. Antiproliferative and pro-apoptotic effects of ruxolitinib in CTCL cells. A) Proliferation analyses in MyLa and HuT 78 cells treated with increasing concentrations of ruxolitinib at 0, 24 or 48 h. IC_{50} concentrations at 48 h are indicated for each cell line. B) Percentage of viable MyLa and HuT 78 cells incubated for 24 h with control vehicle (Veh), IC_{50} or double IC_{50} ($2x IC_{50}$) of ruxolitinib ($n=3$). Representative plots of annexin V (X axis) and 7AAD (Y axis) staining data of each condition are shown. Error bars show SEM. * viable cells compared with control vehicle (** $p < 0.01$; *** $p < 0.001$).

RESULTS

calculated at median effect dose (ED_{50}), or at 75% (ED_{75}) and 90% (ED_{90}) effect dose and represented in **figure 4.19**. In all cases combination therapy induces synergistic effects in both cell lines, except for HuT 78 cells at ED_{50} where the effect is additive.

Thus, the combination of inhibitors targeting two independent signalling pathways that can trigger STAT3 activation, a marker of advanced stages of the disease as previously shown, might have important clinical implications.

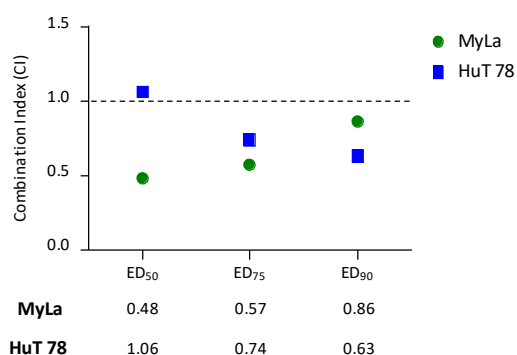


Figure 4.19. Synergistic anti-proliferative effects of combining sotrastaurin and ruxolitinib in CTCL cells. ED_{50} , ED_{75} and ED_{90} combination indexes (CI) of MyLa and HuT 78 cells treated for 24 h with sotrastaurin and ruxolitinib. $CI < 1$ synergism; $CI = 1$ additive effect and $CI > 1$ antagonism.

4.7 PRKCQ deficiency negatively affects CTCL cell proliferation and STAT3 activation

4.7.1 PRKCQ knockdown impairs STAT3 activation in HEK-IL6 and proliferation of T cells

To further understand the role of PRKCQ in CTCL cells, an inducible knockdown of PRKCQ expression was performed by using lentiviral particles containing short hairpin RNA against human *PRKCQ* gene (shPRKCQ hereon). To that end, lentiviral particles of three different

shPRKCQ and the non-targeting control (NTC) were generated and used to transduce cell lines in culture. The two best shPRKCQ constructs were selected for each cell line to perform the following experiments. After lentiviral transduction, shPRKCQ cell lines were stably selected with puromycin (1 µg/ml) and, unless otherwise stated, PRKCQ knockdown was performed upon incubating transduced cells with doxycycline (1 µg/ml) 96 h before performing the experiments.

Thus, in these conditions, knockdown of PRKCQ protein expression was assessed in stably transduced HEK-IL6 and Jurkat cells after incubation with doxycycline (**figure 4.20A**). We decided to use these cell lines to study the role of PRKCQ in STAT3 activation (HEK-IL6; mechanistically) and T-Cell proliferation (Jurkat; biologically) respectively, each in a suitable model. Then, and under these same settings, STAT3 transcriptional activity was analysed in HEK-IL6 cells with impaired PRKCQ expression in response to TPA. As shown in **figure 4.20B** STAT3 activation by TPA was significantly impaired by PRKCQ deficiency in HEK-IL6 cells. We also attempted to study the biologic impact that PRKCQ deficiency could cause in Jurkat cells. As shown in **figure 4.20B**, the reduction of PRKCQ impaired cell proliferation.

These results highlight the potential role of PRKCQ at controlling STAT3 activation and T-cell proliferation thereby increasing the scope of our previous observations.

4.7.2 PRKCQ knockdown impairs cell proliferation and STAT3 activation in CTCL cells

We next explored the effects of PRKCQ deficiency in CTCL cell lines by generating lentiviral inducible shPRKCQ MyLa and HuT 78 cell lines and its negative controls, following the previously described method. As shown in **figure 4.21A**, doxycycline-inducible shPRKCQ greatly impairs PRKCQ protein expression in both cell lines. Consistent with our previous

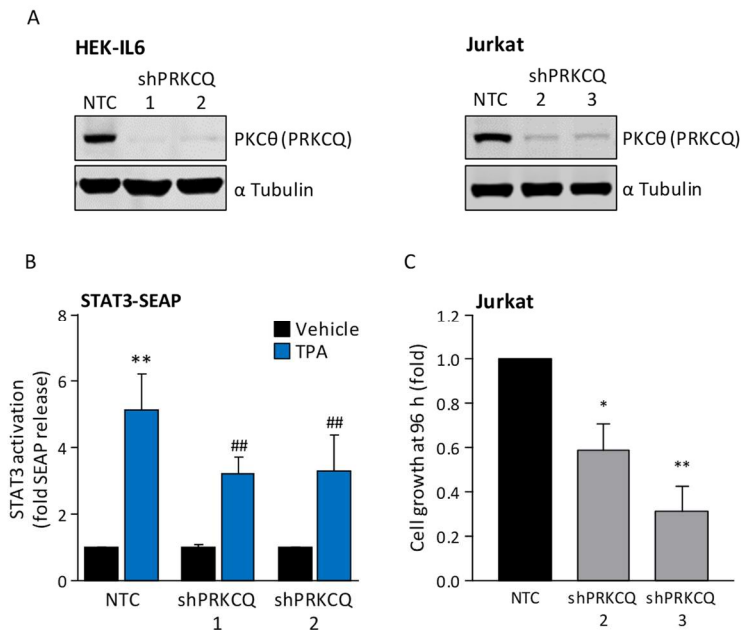


Figure 4.20. PRKCQ knockdown expression inhibits STAT3 activity and T-cell proliferation in HEK-IL6 and Jurkat cells, respectively. A) PRKCQ protein expression in inducible non-targeted control (NTC) or short hairpin PRKCQ (shPRKCQ) HEK-IL6 and Jurkat cells (n=3). Images are representative of each western blot. B) Quantification of SEAP release at 96 h after induction of PRKCQ knockdown in NTC or shPRKCQ HEK-IL6 cells treated overnight with control vehicle or TPA (10 ng/ml). C) Proliferation analysis at 96 h after induction of PRKCQ knockdown in NTC and shPRKCQ Jurkat cells. Error bars show SEM. * compared with vehicle (B) or NTC (C) (* p < 0,05, ** p < 0.01). # compared with NTC treated with TPA (## p < 0.01).

results, phosphorylation of STAT3 at S727 was negatively affected by PRKCQ knockdown in both cell lines whereas phosphorylation of STAT3 Y705 was also affected but to a lesser extent. Moreover, in HuT 78 cells STAT3 transcriptional activity was reduced after shPRKCQ induction as assessed by STAT3-TransAM method (**figure 4.21B**). Biologically, impaired PRKCQ expression negatively affected cell proliferation in MyLa and HuT 78 cells after 72 h and 96 h of knockdown induction respectively (**figure 4.21C**).

Taking together these results, our data shows that in CTCL cells STAT3 activation can be triggered, at least in part, by PRKCQ-dependent mechanisms which occurs alongside an impaired ability to proliferate.

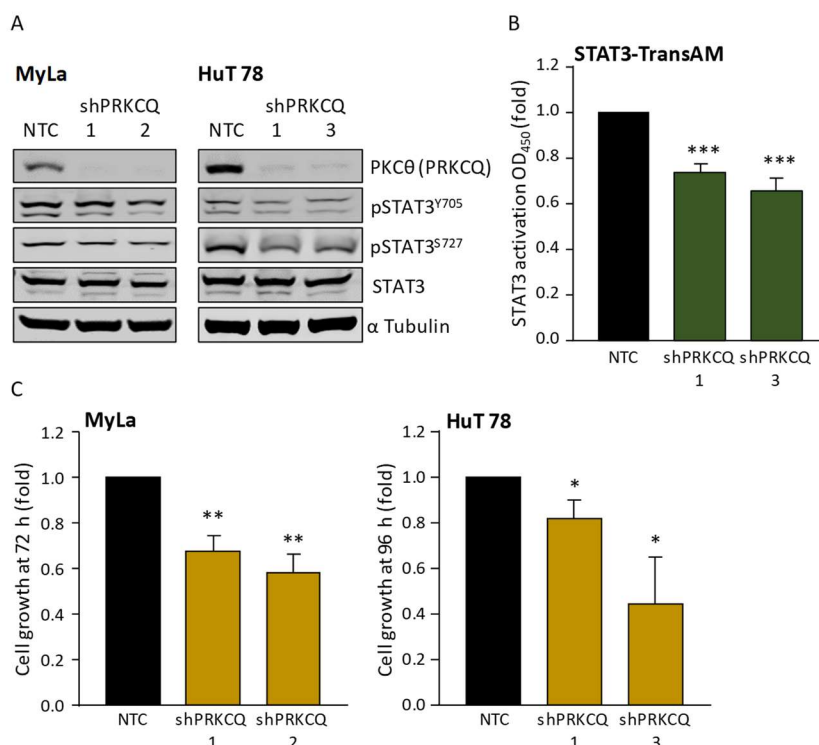


Figure 4.21. PRKCQ knockdown expression inhibits cell proliferation and STAT3 activation in CTCL cells.

A) Western blot analyses of whole cells lysates of inducible non-targeting control (NTC) or short hairpin PRKCQ (shPRKCQ) MyLa and HuT 78 cells incubated with the indicated antibodies (n=2). Images are representative of each western blot. B) Quantification of STAT3 activity in NTC and shPRKCQ HuT 78 cells 96 h after PRKCQ knockdown induction (n=4). C) Proliferation analyses of NTC or shPRKCQ MyLa and HuT 78 at 72 h and 96 h respectively after PRKCQ knockdown induction (n=4). Error bars show SEM. T-test * compared with NTC (* p < 0.05, ** p < 0.01, *** p < 0.001).

4.8 PRKCQ interacting proteins in CTCL cells

4.8.1 PRKCQ does not interact with STAT3

It has been previously demonstrated that some PKC isoforms interact with and phosphorylates STAT3, such as PKCδ, PKCε and PKCζ, (Aziz et al. 2007; Kim et al. 2008; Li et al. 2016; Cathcart Ashish Bhattacharjee et al. 2019) so we wondered if PRKCQ (PKCθ) does too in HuT 78 cells. We decided to work with this cell line since these are CTCL cells with

RESULTS

higher levels of PRKCQ (see **figure 4.13**). To that end, total lysates were endogenously co-immunoprecipitated with PRKCQ or STAT3 and the presence of STAT3 and PRKCQ were respectively assessed by western blot. As shown in **figure 4.22** and in these settings, there is no interaction between both proteins suggesting that there might be other proteins activating STAT3 downstream PRKCQ.

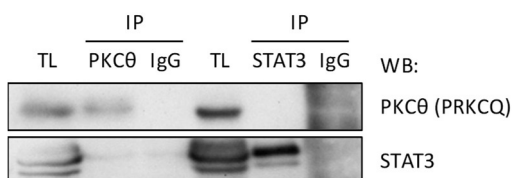


Figure 4.22. PRKCQ does not interact with STAT3 in HuT 78 cells. Co-immunoprecipitation of PKCθ (PRKCQ) and STAT3 in HuT 78 cells. Protein lysates were immunoprecipitated with anti-PKCθ and anti-STAT3 antibodies and the presence of STAT3 and PKCθ, respectively, in the immunocomplexes were assessed by western blot. Total lysates (TL) were used as loading control and IgG was immunoprecipitated as negative control.

4.8.2 PRKCQ interactome

In order to study the candidate proteins interacting with PRKCQ that could be participating in STAT3 activation, mass spectrometry analysis was performed in David Gomez-Matallanas' laboratory in Dublin, as part of my international stay. This technique identifies and quantifies proteins within a sample by measuring the mass-to-charge ratio of ions. To this end, PRKCQ was endogenously immunoprecipitated in both NTC and shPRKCQ (as negative control) HuT 78 cells in the presence of doxycycline and starved and treated or not with TPA, in two independent replicates. Immunocomplexes were digested and mass spectra were quantified twice, as described in Materials and Methods section 3.6.6. The data obtained from shPRKCQ HuT 78 cells constitute the non-specific protein-protein interactions, which are eliminated to get the specific ones (significant interactions was determined based on a fold change in peptide abundance in relation to negative control \geq

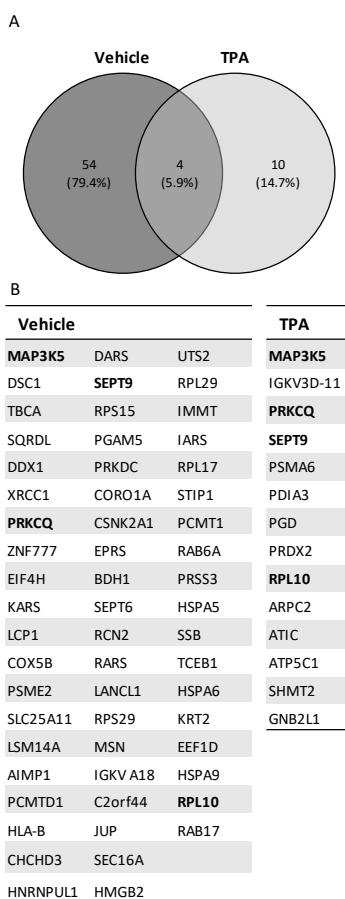


Figure 4.23. Proteins interacting with PRKCQ in starved or TPA-stimulated HuT 78 cells. A) Venn diagram of significantly proteins interacting with PRKCQ in inducible non targeting control (NTC) HuT 78 cells starved and treated with control vehicle (black circumference) and starved and treated for 1 h with TPA (10 ng/ml, grey circumference) from mass spectrometry assay. B) List of genes represented in A. Bold genes are present in both conditions. Inducible short hairpin PRKCQ (shPRKCQ) HuT 78 cells starved and treated both with vehicle or TPA were used as negative controls.

2 and a p value < 0.05 by Student's t-test). A total of 58 proteins are significantly interacting with PRKCQ in non-stimulated cells whereas only 14 proteins are interacting after TPA stimulation (**figure 4.23A**). In **figure 4.23B** the gene names of proteins interacting with PRKCQ are listed, both treated with control vehicle and TPA (see **annexes 1 and 2** for further details). Interestingly, three proteins (Mitogen-activated protein kinase kinase kinase 5, MAP3K5 [also known as Apoptosis signal-regulating kinase 1, ASK1], Septin-9 [SEPT9] and

RESULTS

Ribosomal Protein L10 [RPL10]) are interacting both before and after TPA stimulation. In this regard, PRKCQ-MAP3K5 interaction was confirmed by co-immunoprecipitating MAP3K5 in 293T cells overexpressed with PRKCQ WT or active A148E mutant and incubated with MAP3K5 and PRKCQ antibodies, to confirm the immunoprecipitation and the interaction, respectively (**figure 4.24**).

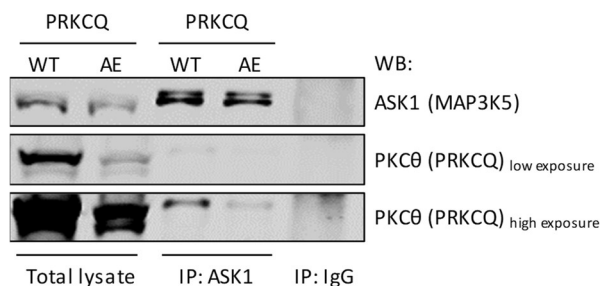
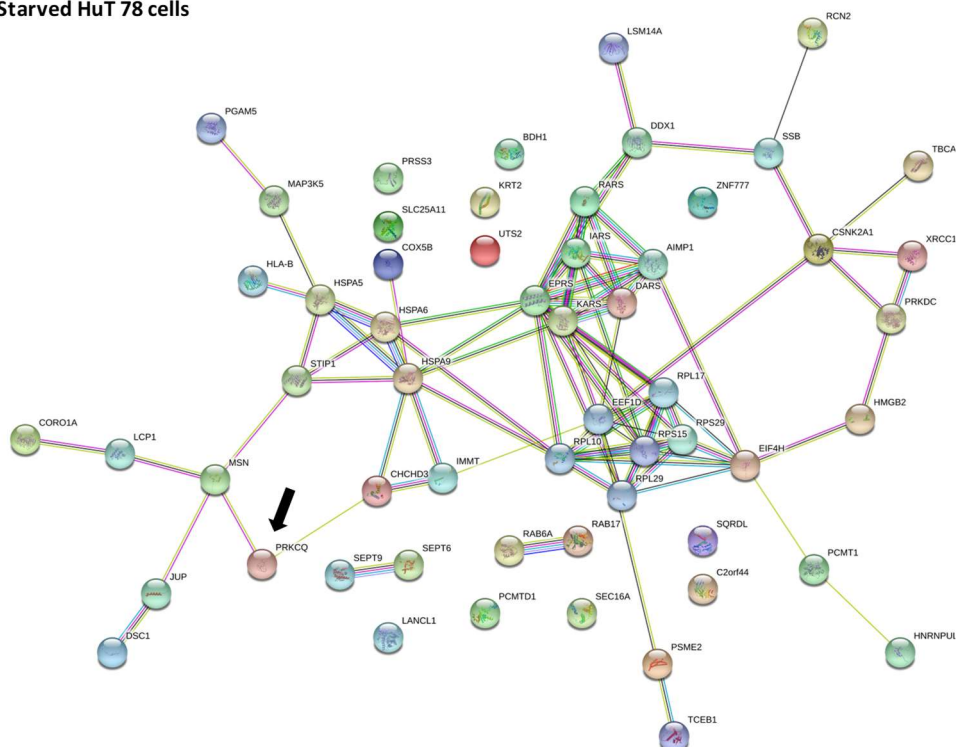


Figure 4.24. MAP3K5-PRKCQ interaction validation. Co-immunoprecipitation of PKCθ (PRKCQ) and ASK1 (MAP3K5) in HEK293T cells transfected with PRKCQ WT and A148E mutant. Total lysates were immunoprecipitated with anti-ASK1 antibody and the presence of ASK1 and PKCθ in the immunocomplexes were assessed by western blot. Total lysates were used as loading control and IgG was immunoprecipitated as negative control.

Once the proteins interacting with PRKCQ were obtained by mass spectrometry, *in silico* functional enrichment analyses were performed using STRING software (<https://string-db.org/>), a database of known and predicted protein-protein interactions. The functional networks of proteins are represented in **figure 4.25** (black arrow shows PRKCQ). Among the proteins, there are only two that are known interactors of PRKCQ (represented with pink edge): Moesin (MSN, **figure 4.25A**), a cross-linker between plasma membranes and actin-based cytoskeletons (Pietromonaco SF et al J Biol Chem, 1998) and Receptor For Activated C Kinase 1 (RACK1, gene name: GNB2L1, **figure 4.25B**) a scaffolding protein that binds to and stabilizes activated PKCs, increasing PKC-mediated phosphorylation (Lopez-Bergami et al. 2005).

A

Starved HuT 78 cells



B

TPA-stimulated HuT 78 cells

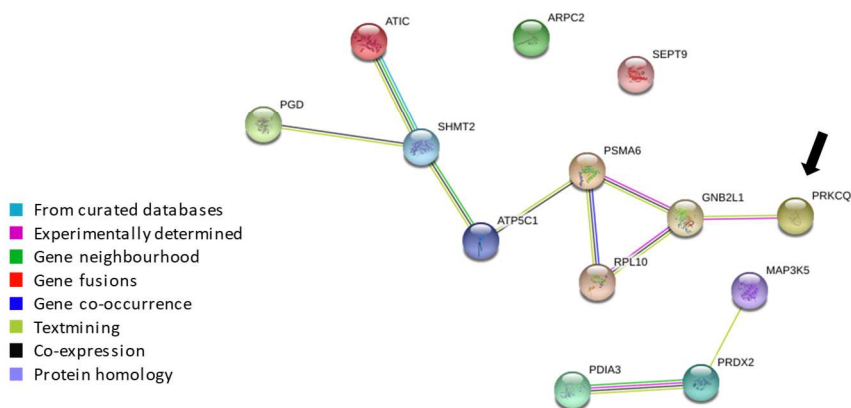


Figure 4.25. STRING functional network of proteins interacting with PKC θ in starved and TPA-stimulated HuT 78 cells. Protein interactions of significantly genes associated with PKC θ (PRKQ) in inducible non targeting control (NTC) HuT 78 cells A) starved for 2 h and treated for 1 h with control vehicle and B) starved for 2 h and treated for 1 h with TPA (10 ng/ml) from STRING software (<https://string-db.org/>). Edges represents protein-protein interactions: from curated databases and experimentally determined (both known interactions), from gene neighbourhood, gene fusions and gene co-occurrence (predicted interactions) and textmining, co-expression and protein homology (other type of sources).

4.9 Biological CTCL effects of PRKCQ *in vivo*

4.9.1 PRKCQ knockdown effects in CTCL tumour growth, intravasation and metastasis *in vivo*

In order to study the CTCL biological processes where PRKCQ could be playing a role we decided to take advantage of a chicken embryo model that enables a quick and reproducible experimental approach where to study tumour growth, tumour cells intravasation and the establishment of liver and lung metastases. This is a unique and beneficial experimental model to study the metastatic processes due to the accessibility of the chorioallantoic membrane (CAM), a highly vascularized extra-embryonic tissue located under the eggshell, and its receptiveness for xenografting human tumour cells. Within 5-7 days, sizable tumours can be formed, escape the primary site, invade surrounding stroma, intravasate into blood vessels, and reach the distal CAM and internal organs, where disseminated cells extravasate and form micro metastasis foci (see methods).

To that end, chicken embryos were prepared to establish xenograft tumour cells. Briefly, at least 5 embryos for each condition, and in three independent replicates, were incubated at 37 °C and 60% humidity for 10 days. At that time, embryos are naturally immunodeficient, as the lymphoid system is not fully developed yet, so the human tissues and cells are able to graft without species-species restrictions. Here, non-targeting control (NTC) and shPRKCQ MyLa cells were treated, 96 h before grafting them, with doxycycline (1 ug/ml) to induce PRKCQ knockdown. Then, $1 \cdot 10^6$ cells were xenografted onto the CAM and primary tumours were allowed to grow for 7 days (experimental time course is summarized in **figure 4.26A**). Representative images from NTC and shPRKCQ chick embryos groups are shown in **figure 4.26B**. In NTC, a visible tumour is formed (circled) after 7 days of incubation, whereas in the shPRKCQ embryo, no tumour formation is observed. Interestingly, it is quite

remarkable the novo formation of blood vessels surrounding and radially converging towards the tumour in the NTC embryo suggesting the important angiogenic potential of these CTCL-derived tumours. Primary tumour formation and growth, tumour cell intravasation to distal CAM and lung and liver metastases were assessed. Primary tumours were weighted and quantitative PCR for human *Alu* sequences from distal CAM, liver and lung genomic DNA samples were performed in order to detect human (MyLa) cells. PRKCQ deficiency significantly decreases MyLa-derived tumour growth (**figure 4.26C**). Primary tumours of control group (NTC) weighed an average of 82 mg (range 52-126 mg, n=16) whereas the primary tumours of shPRKCQ group weighed an average of 27 mg (range 12-61 mg, n=14). PRKCQ deficiency also significantly decreases intravasation to distal CAM as the median number of human cells in this tissue decreased from 383 cells/10⁶ chicken cells to 25 cells/10⁶ chicken cells (**figure 4.26D**). When analysing the metastatic process, PRKCQ knockdown completely abrogated the dissemination of tumour cells to liver and lung organs (**figure 4.26E**). Cancer human cells decrease from 310 to 18 cells/10⁶ chicken cells in the liver and from 121 to 10 cells/10⁶ chicken cells in the lungs.

Thus, applying this novel *in vivo* experimental approach to the field of CTCL enabled the identification of PRKCQ playing an essential role in CTCL tumour development and metastatic progression.

4.9.2 PRKCQ pharmacological inhibition exerts potent anti-CTCL effects regarding tumour growth and metastasis *in vivo*

As shown before in section 4.6.1 sotrastaurin, a highly specific PRKCQ inhibitor, exerts anti-proliferative and pro-apoptotic effects in CTCL cells. To address this question *in vivo*, we also took advantage of the chick embryo model described above. To that end, 1.10⁶ of MyLa

RESULTS

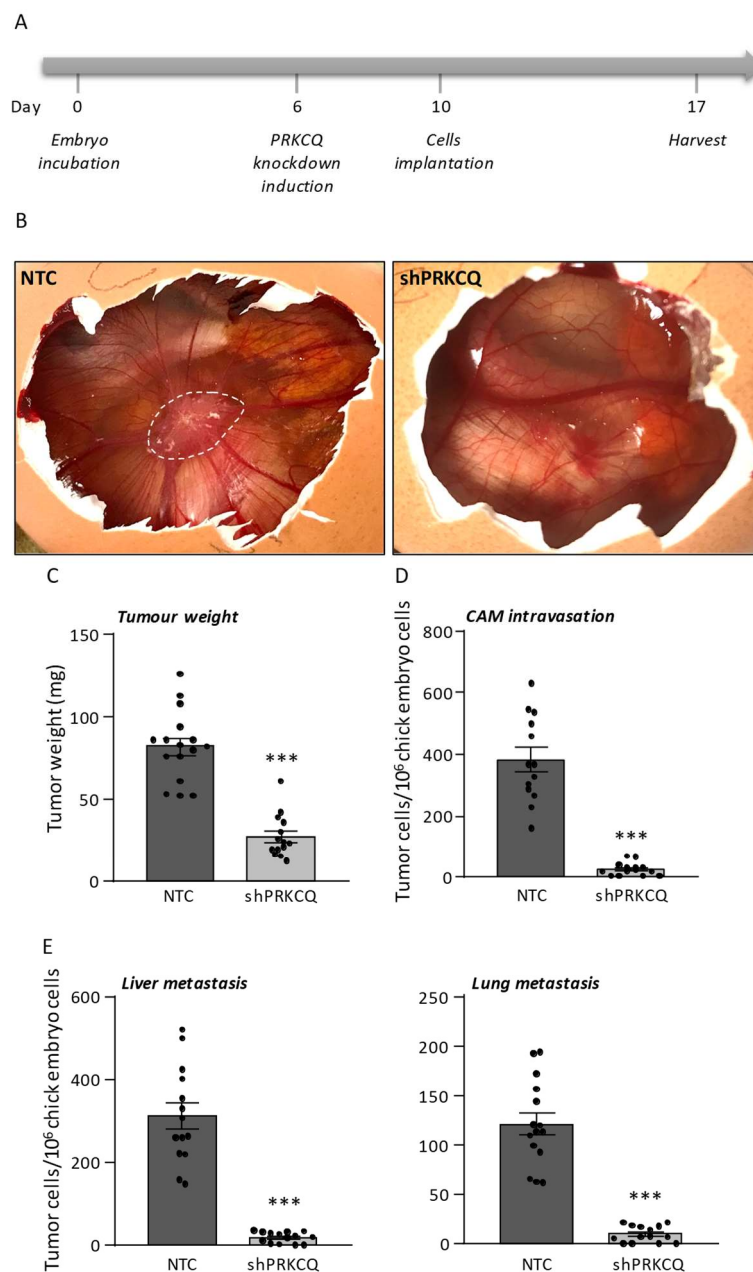


Figure 4.26. Antitumoral and antimetastatic effects of PRKCQ knockdown *in vivo*. A) Schematic tumour cells implantation procedure of inducible non-targeting control (NTC) or short hairpin PRKCQ (shPRKCQ) MyLa cells xenografted on chicken embryo chorioallantoic membrane (CAM) after 4 days of PRKCQ knockdown induction. Tumours were allowed to progress for 7 days before harvesting. B) Representative images of NTC and shPRKCQ chick embryos. PRKCQ knockdown effects on C) tumour size, D) tumour cell intravasation to distal CAM, and E) liver and lung metastases. Error bars show SEM. * compared with NTC (***) $p < 0.001$).

cells were xenografted onto CAM at day 10 of embryo development, and then two treatment experimental conditions were performed: one group treated with sotrastaurin every two days (a total of two days, shown as twice) and another group treated only once, two days before harvesting the samples (the experimental procedure is summarized in **figure 4.27A**). The latest treatment group was performed in order to study if once the primary tumour is established; sotrastaurin is able to abrogate the metastatic process. Primary tumours were topically treated with 10 μ M of sotrastaurin or the control vehicle (DMSO). All groups were treated with vehicle at the same time points as its counterparts meaning that control group (vehicle) was treated with DMSO at days 12, 14 and 15, the 'twice' group was also treated with DMSO at day 15 and the 'once' group was treated with vehicle at days 12 and 14. Tumours were allowed to grow for 7 days and then primary tumour formation and growth, tumour cell intravasation to distal CAM and lung and liver metastases were analysed. Sotrastaurin significantly impairs tumour growth used both once and twice (**figure 4.27B**). Primary tumours of control group weighted an average of 62 mg (range 40-93 mg, n=18) whereas the primary tumours of treatment groups weighted 48 mg (range 21-81 mg, n=18) when treated once and 35 mg (range 6-67 mg, n=17) when treated twice. Sotrastaurin also impaired tumour cell intravasation to distal CAM (**figure 4.27C**). This intravasation was completely abrogated when primary tumours were treated from the beginning ('twice' group) as number of cells decreases from a mean of 520 to 18 cells/ 10^6 chicken cells. Moreover, sotrastaurin also impaired liver and lung metastases in both treatment groups (**figure 4.27D**). Treating embryos with sotrastaurin only once (two days before harvesting the samples) significantly decreased the number of tumoral cells in the lung from a mean of 140 to 65 cells/ 10^6 chicken cells. Interestingly, this effect was even higher when analysing liver metastasis (only 22 tumoral cells/ 10^6 chicken cells were found

RESULTS

compared to 338 cells/ 10^6 chicken cells from control group), hence suggesting that the lung is occupied earlier than the liver during the metastatic process.

Thus, using this embryo chicken model for CTCL tumorigenesis and metastasis, we show that pharmacological inhibition of PRKCQ can constitute a plausible approach to treat CTCL patients even at more advanced stages of the disease.

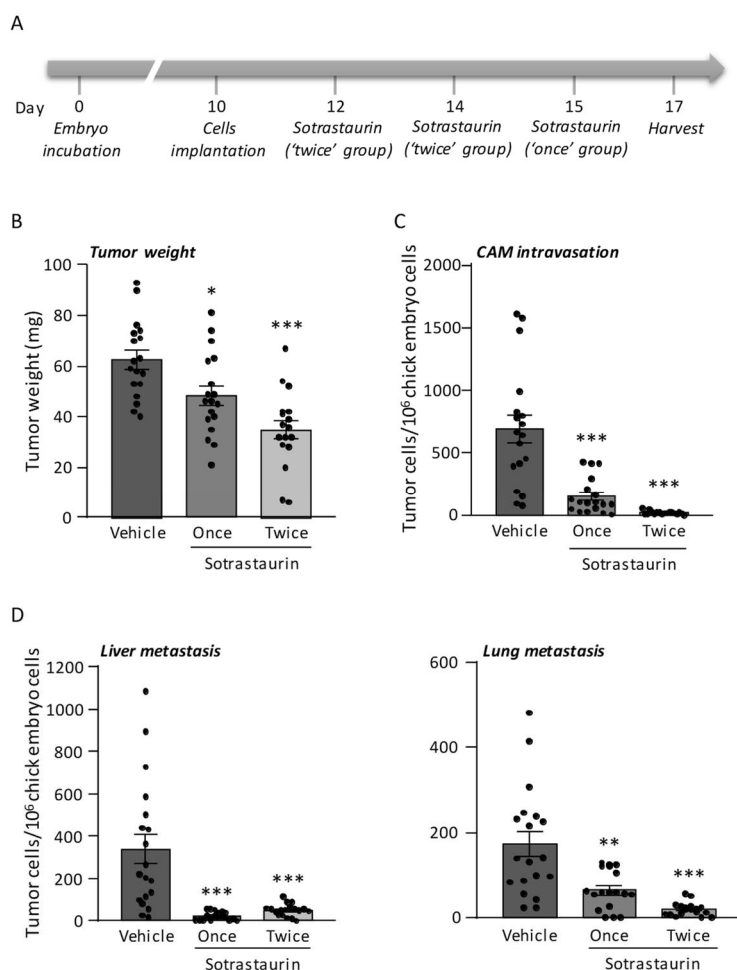


Figure 4.27. Antitumoral and antimetastatic effects of sotrastaurin *in vivo*. A) Schematic tumour cells implantation and treatment procedure of MyLa cells xenografted on chicken embryo chorioallantoic membrane (CAM), treated with 10 μ M of sotrastaurin two days before harvest (once) or every 2 days (twice) and allowed to progress for 7 days before harvesting. Sotrastaurin effects on B) tumour size, C) tumour cell intravasation to distal CAM, and D) liver and lung metastases. Error bars show SEM. * compared with control vehicle (* $p < 0.05$, ** $p < 0.01$, *** $p < 0.001$).

4.10 Gene regulation by PRKCQ in CTCL cells

4.10.1 PRKCQ expression in CTCL cell samples used for RNA sequencing

In order to study the genes that are transcriptionally controlled by PRKCQ in CTCL and that can be participating in the progression of the disease by activating STAT3, mRNA sequencing was performed in NTC and shPRKCQ MyLa and HuT 78 cells both with and without TPA stimulation. To that end, NTC and shPRKCQ cells were treated with control vehicle or TPA (10 ng/ml) for 24 h in three independent replicates and PRKCQ expression was analysed by quantitative reverse transcription PCR (RT-qPCR) after mRNA extraction (figure 4.28). PRKCQ expression in both cell lines and experimental conditions was significantly depleted.

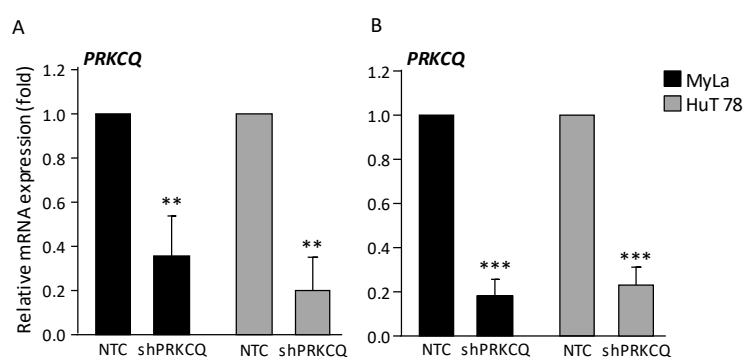


Figure 4.28. PRKCQ knockdown expression in RNA-seq samples. mRNA expression of PRKCQ in inducible NTC and short hairpin PRKCQ (shPRKCQ) MyLa and HuT 78 cells treated A) with control vehicle and B) TPA (10 ng/ml) for 24 h from samples used for RNA sequencing (n=3). Error bars show SEM. * compared with NTC (** $p < 0.01$, *** $p < 0.001$).

4.10.2 Gene regulation by PRKCQ in basal conditions in CTCL cells

The mRNA of NTC and shPRKCQ MyLa and HuT 78 cells was sequenced and the mRNA levels of whole transcriptome were analysed by our collaborators in Centre de Regulació Genòmica del Centre Nacional d'Anàlisi Genòmica (CNAG-CRG). A total of 241 genes were

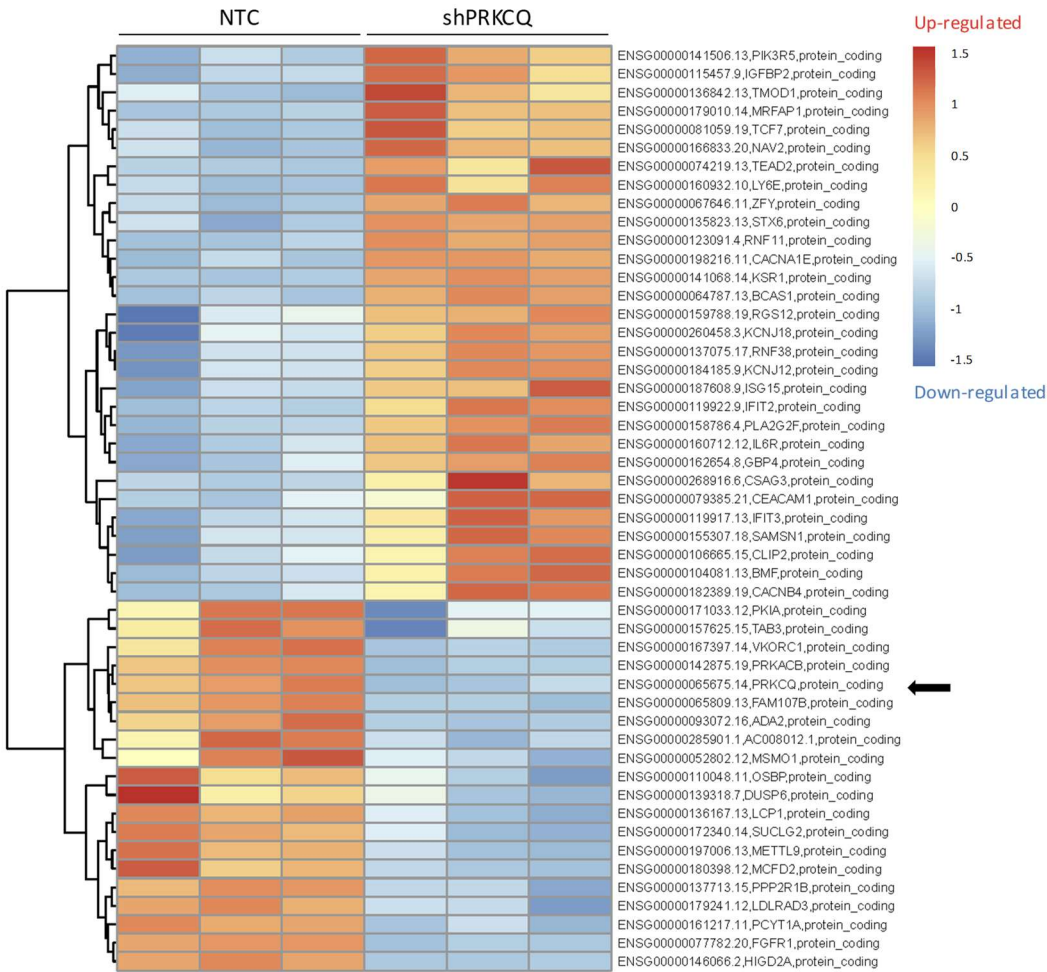


Figure 4.29. Gene expression controlled by PRKCQ in MyLa cells. Gene expression of the top 50 more significantly deregulated genes in inducible non targeting control (NTC) and short hairpin PRKCQ (shPRKCQ) MyLa cells (n=3). Black arrow shows PRKCQ gene.

significantly deregulated by PRKCQ in MyLa cells, 92 down-regulated and 149 up-regulated, and a total of 182 genes in Hut 78 cells, 149 down-regulated and 33 up-regulated (see **annex 3** for details). In **figures 4.29 and 4.30**, top 50 most significantly deregulated genes in MyLa and HuT 78 cells respectively are represented.

To name but a few, genes that are found downregulated include receptors with cytoplasmic kinase activity such as fibroblast growth factor receptors 1 and 3 (FGFR1 and FGFR3), which

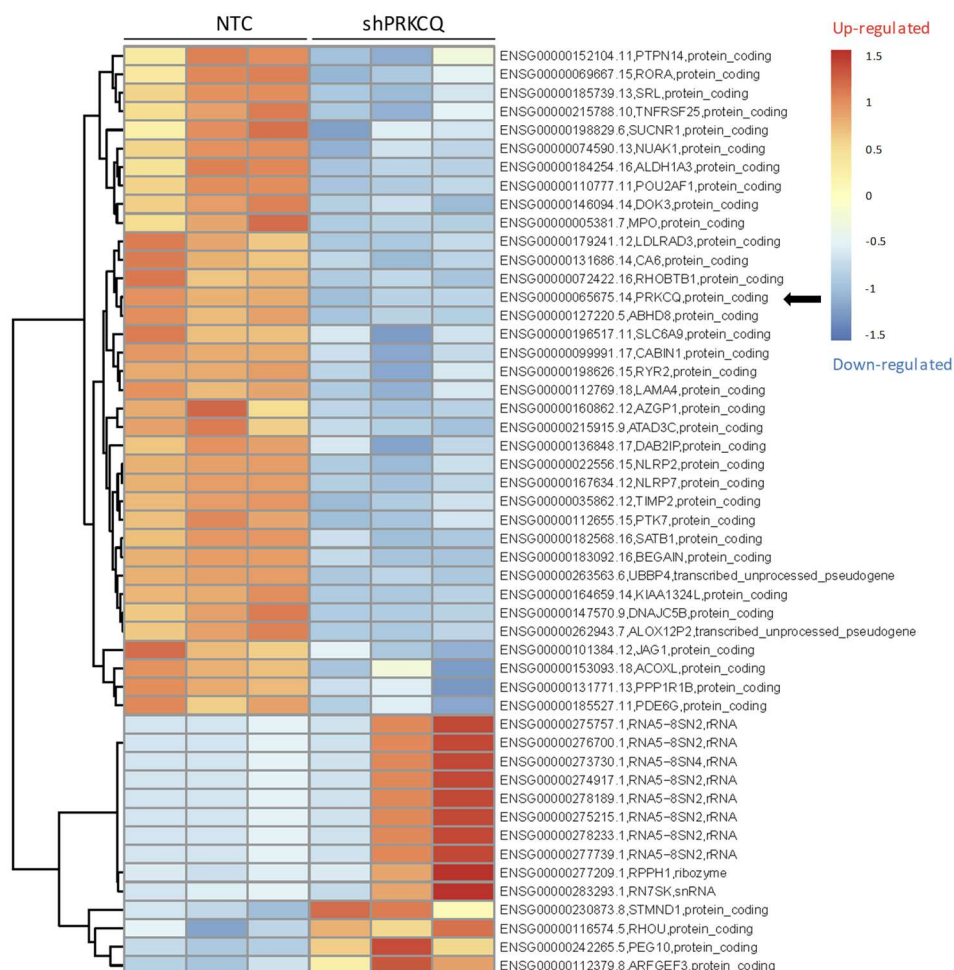


Figure 4.30. Gene expression controlled by PRKCQ in HuT 78 cells. Gene expression of the top 50 more significantly deregulated genes in inducible non targeting control (NTC) and short hairpin PRKCQ (shPRKCQ) HuT 78 cells (n=3). Black arrow shows PRKCQ gene.

in turns activate PLCG1 and STAT signalling, and Tumour Necrosis Factor Receptor Superfamily Member 25 (TNFRSF25), which is primarily involved in apoptosis and inflammation. Another interesting gene related to inflammation and T cell functions are NFATC2, found downregulated in both MyLa and HuT 78 cells. Furthermore, Dual Specific Phosphatases 6 and 15 (DUSP6 and DUSP15) are downregulated in MyLa and HuT 78 cells respectively, which regulate ERK activation, and Lymphocyte Cytosolic Protein 1 (LCP-1, also known as L-Plastin) in MyLa, which is a regulator of the immune cell function regulating the

stability of actin-based structures. On the other hand, some of the genes that are found upregulated are the receptor of IL-6 (IL6R), the Mitogen-Activated Proteins Kinase Kinase Kinase 4 (MAP3K4, also known as MEKK4) and Kinase Kinase Kinase Kinase 4 (MAP4K4, also known as MEKKK4), which both have been described to activate JNK kinases; and receptors that regulate immune responses transducing inhibitory signals such as the Killer cell immunoglobulin-like receptors KIR2DL3 and KIR3DL1.

4.10.3 Gene regulation by PRKCQ in TPA-stimulated CTCL cells.

Whole mRNA levels were also analysed in NTC and shPRKCQ MyLa and HuT 78 cells after 24 h stimulation with TPA (10 ng/ml). A total of 355 genes were deregulated by PRKCQ after pathway activation with TPA in MyLa cells, 152 down-regulated and 203 up-regulated, and 147 were deregulated in HuT 78 cells, 115 down-regulated and 32 up-regulated (see **annex 4 for details**). In **figures 4.31 and 4.32**, top 50 most significantly deregulated genes in MyLa and HuT 78 cells respectively, after TPA stimulation, are represented.

In general terms, some of the genes that are found deregulated include genes involved in cytoskeleton, TNF signalling and NF- κ B signalling pathways. Interestingly, a number of genes involved in the actin/cytoskeleton signalling are found downregulated including MYH10, LIMA1, NRCAM, CORO1B, SYNPO, PALLD and LSP1. Furthermore, genes involved in the JAK/STAT pathways are also deregulated. For example, in HuT 78 cells, SOCS2, a phosphatase that inhibits JAK kinase activities is found upregulated thus probably enhancing JAK/STAT signalling; and IL-10 is found downregulated, which has been associated with induction of Th2 phenotype. In contrast, genes involved in chemokine signalling have been also found upregulated such as IL-15 and CCR8 in MyLa cells.

Interestingly, Vascular Endothelial Growth Factor B (VEGFB), a gene that regulates the formation of blood vessels, has been found downregulated in MyLa cells, which is consistent with our previous results from the chick embryo model where the formation of vessels surrounding the tumour was observed.

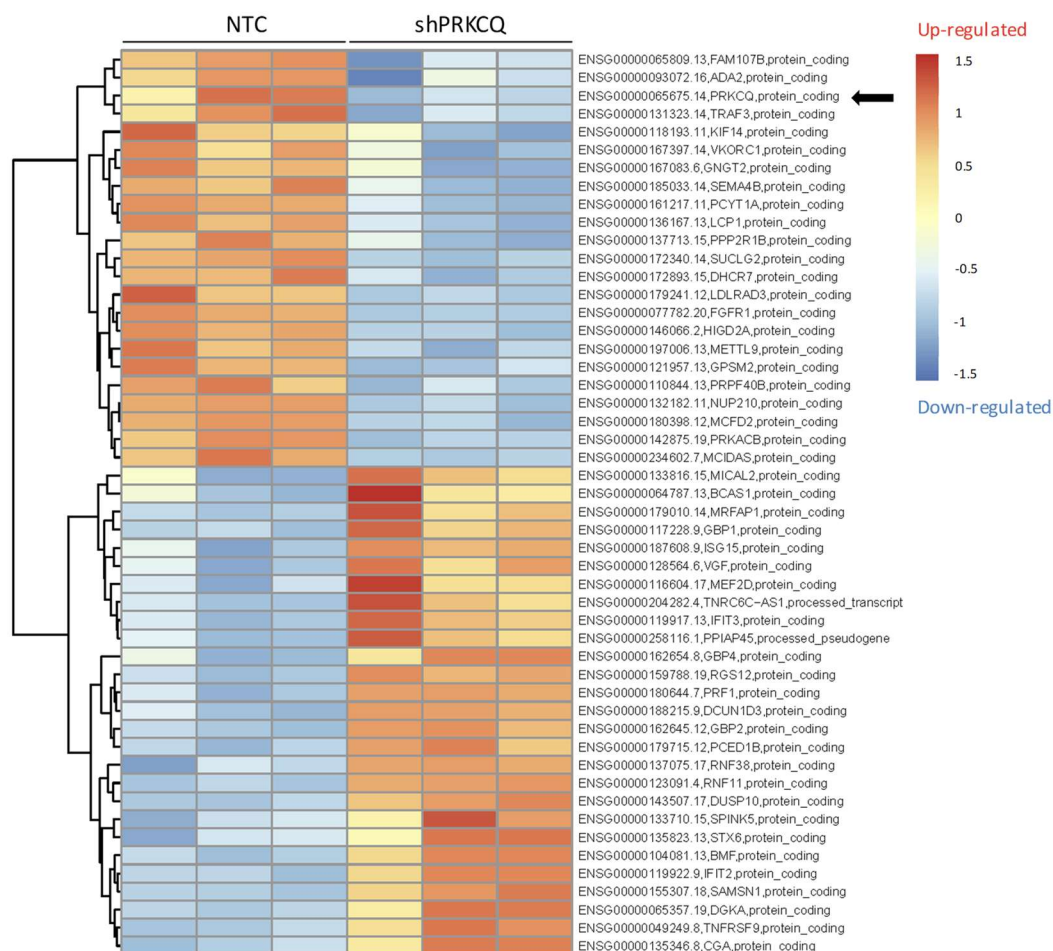


Figure 4.31. TPA-induced gene expression controlled by PRKCQ in MyLa cells. Gene expression of the top 50 more significantly deregulated genes in MyLa cells in inducible non targeting control (NTC) and short hairpin PRKCQ (shPRKCQ) and treated for 24 h with TPA (10 ng/ml) (n=3). Black arrow shows PRKCQ gene.

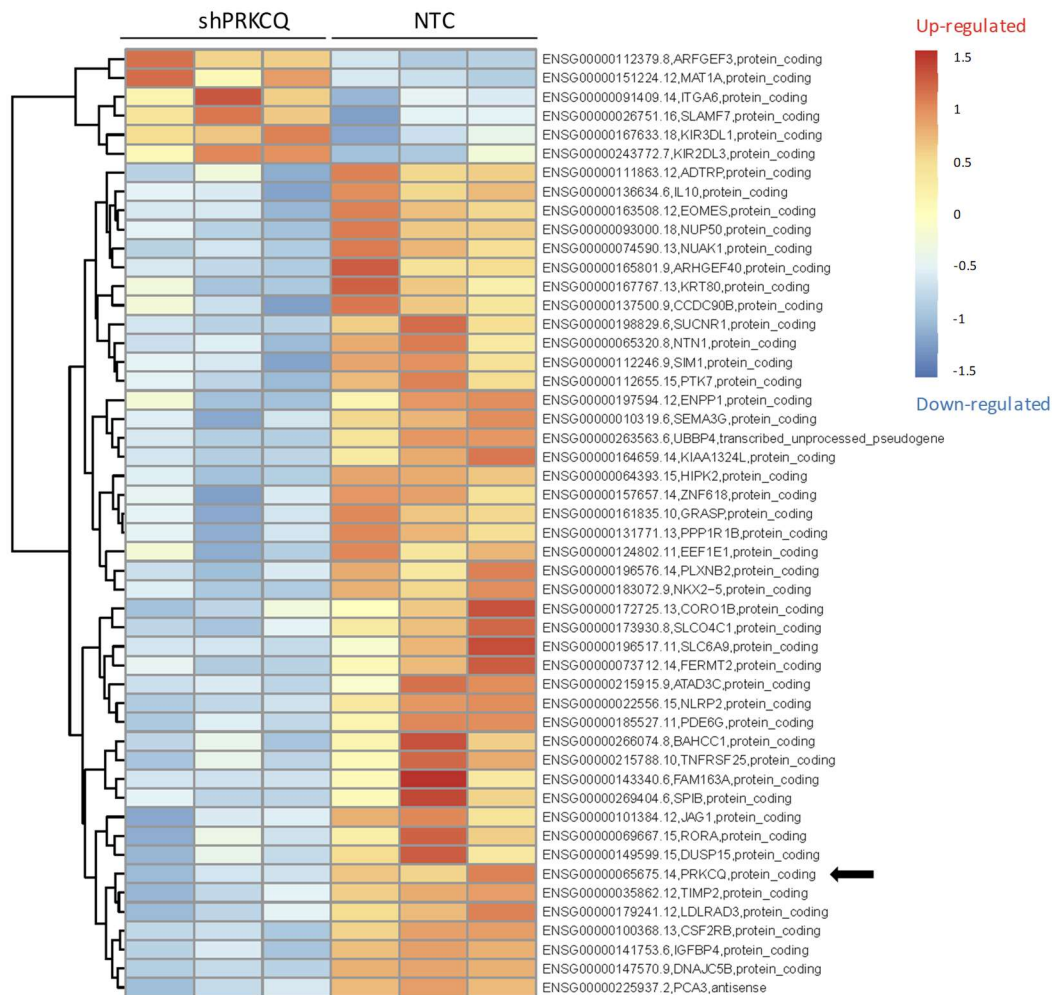


Figure 4.32. TPA-induced gene expression controlled by PRKCQ in HuT 78 cells. Gene expression of the top 50 more significantly deregulated genes in HuT 78 cells in inducible non targeting control (NTC) and short hairpin PRKCQ (shPRKCQ) and treated for 24 h with TPA (10 ng/ml) (n=3). Black arrow shows PRKCQ gene.

DISCUSSION

5. DISCUSSION

Currently the field of CTCLs lacks diagnostic markers and effective targeted therapies. This work challenges the biological roles and studies the mechanistic interplay between specific candidate proteins with potential to participate at different stages of the disease. We propose that these proteins and their signalling pathways are part of a malignant network of signalling mechanisms that drive CTCL. In this regard, and because of the genetic evidences accumulated in the recent years, we have considered that this network is highly influenced by deregulated PLCG1 activity towards the activation of specific transcription factors. Now, based on the generation of novel data, this work shows that downstream PLCG1, activation of STAT3 occurs via PRKCQ through JAK-dependent and JAK-independent mechanisms. Indeed, the pharmacological inhibition and knockdown of PRKCQ negatively affected STAT3 activation, cell proliferation and promoted apoptosis in CTCL cells. Interestingly, the effects on cell proliferation were synergistic when dual PRKCQ and JAK inhibition was performed. Finally, pharmacological inhibition and deficiency of PRKCQ abrogated MF tumour proliferation, angiogenesis, intravasation and prevented metastasis to distant organs *in vivo*.

5.1 STAT3 as a marker of MF progression

In the context of the aforementioned network, the activation of downstream effectors was studied in a cohort of 78 MF patients. The markers included IHC staining of transcription factors like NFAT, NF- κ B (canonical and non-canonical), P-STATs as well as PRKCQ amplification and/or polysomy by FISH. Importantly, JAK/STAT pathway was significantly activated in MF cases at advanced stages (**table 4.2**). Interestingly, no significant correlation was observed between different stages and positive expression of NFAT, NF- κ B, P-STAT1,

DISCUSSION

P-STAT5 and PRKCQ amplification or polysomy, hence suggesting that these may be activated alongside multiple stages of the disease. Of note, P-STAT1 was closer to significance. It is possible that, despite of the low incidence of this disease, assembling a larger cohort with equal number of cases, at early and advanced stages, could improve the outcome of such study. Importantly, cases with positive P-STAT3 staining were significantly correlated with advanced stages (47% of advanced patients showed activation of P-STAT3). This can constitute an important mechanistic feature with relevant clinical implications. Interestingly, STAT3 can form transcriptionally active dimers with STAT1 (Bromberg and Darnell 2000) which highlights the interest to further extend this study. To our knowledge, this is the first time that a comparative study in a large cohort of CTCL cases has been performed by studying NFAT, NF- κ B and STAT activities. Nevertheless, the positive expression of P-STAT3 in CTCL cases at tumour stages has been previously observed, although in cohorts with limited number of cases, probably impairing a statistical correlation (Eriksen et al. 2001; Sommer et al. 2004; R. C.T. McKenzie et al. 2012).

It is important to note that the percentage of cases with activated STATs observed in CTCL lesions can not only be explained by the acquisition of mutations in JAK genes (which can occur in approximately 4% of the total number of the cases analysed, see introduction, and unpublished data from our group). Alternative mechanisms are now under discussion including a pro-inflammatory microenvironment generated by malignant T-cells and other non-transformed reactive cells attracted to the lesions (Kim et al. 2005); as well as immune responses to bacterial colonization in the compromised skin barriers of CTCL lesions (Willerslev-Olsen, Krejsgaard, Lise M. Lindahl, et al. 2016; Fanok et al. 2018). Moreover, it is also possible that mutations and deregulated activity of different members of the malignant CTCL signalling network can also trigger STAT activation. Supporting this hypothesis, additional molecular studies using our cohort of MF cases (not included in this

thesis) were performed by using targeted enrichment sequencing to detect mutations in *PLCG1*, JAKs, and STATs genes among others (Pérez et al. 2019). Interestingly, and to serve as an example, two patients harbouring *PLCG1* S345F mutation displayed P-STAT3 staining in the absence of mutated JAK kinases. In addition, consecutive samples (initial and advanced stages) collected from MF patients showed an acquired JAK3 mutation in its pseudokinase domain (A573V), which on the other hand, was detected alongside positive P-STAT1 and P-STAT5 staining at an advanced stage (IIB) (Pérez et al. 2019). Finally, mutations and amplifications in STAT genes can also account for a deregulated STAT activity in CTCL samples (Park et al. 2017).

Thus, malignant STAT3 activation that participates in CTCL progression can be triggered by deregulated extracellular stimuli (usually JAK-dependent), mutations in JAKs and/or other mechanisms like deregulated TCR/*PLCG1* downstream signalling (probably JAK-independent).

5.2 Role of JAK/STAT signalling in CTCL

Numerous studies, including our own, have revealed multiple alterations in JAK kinases in CTCL samples. These mutations primarily affect the pseudokinase domain of JAK1 and JAK3 which is believed to regulate their kinase activity. To our best knowledge there is few data regarding the mechanistic nature derived from such mutations (Degryse et al. 2014; Degryse et al. 2018). Here, we analysed two JAK1 mutants (R659C and Y654F) for their unknown ability to activate downstream signalling. To this end, we used two different reporter approaches alongside western-blotting using P-STAT3 antibodies in HEK-IL6 cells. In basal conditions, JAK1 Y654F showed gain-of-function activity over STAT3 phosphorylation and transcriptional activity (using a STAT3 luciferase construct) (**figure 4.3**). On the other

hand, this same mutant required IL-6 stimulation to further induce STAT3 phosphorylation and transcriptional activation (using quanti-blue). These differences may be due to the differential sensitivities between the reporter assays used and explained as follows: a) Using a quanti-blue assay, upon STAT3 activation, the SEAP phosphatase is released extracellularly and its alkaline activity measured colorimetrically only using a small quantity of the supernatant, b) In the luciferase assays, the activity of both *renilla* and firefly are measured by luminescence using whole cell lysates. It is also possible that differences in the STAT3 consensus reporter sequences may account for these differences. Our data also show that STAT3 activation depends on JAK kinase activity (since it is inhibited by ruxolitinib), but nevertheless it is not clear whether this mutation provides a constitutively active kinase activity *per se* or just improves the ability of JAKs to promote STAT3 phosphorylation upon extracellular stimulation, like IL-6 in this case.

The deregulation of JAK/STAT pathway in CTCL has provided a rationale to treat this disease using targeted inhibition of JAK kinases. Currently, specific JAK inhibitors such as ruxolitinib and tofacitinib are being used for the treatment of myeloproliferative disorders (harbouring an activated JAK2 V617F mutant) and autoimmune diseases, such as rheumatoid arthritis (with a deregulated JAK/STAT activity) (Lee et al. 2014; de Freitas and da Costa Maranduba 2015; Malemud 2018). Therefore, it is conceivable that they may be effective to treat CTCL patients. Active clinical trials using ruxolitinib or tofacitinib in relapsed T or NK cell lymphomas, but not in CTCLs, are being conducted with an estimated study completion time finishing November 2020 and December 2021 (NCT02974647 and NCT03598959 respectively). To explore this possibility in a preclinical context, we treated CTCL cells with increasing concentrations of ruxolitinib and tested its effects on cell proliferation and apoptosis. We particularly used MyLa and HuT 78 cells (MF and SS cells respectively). Although only HuT 78 cells harbour JAK1 and JAK3 mutations, both cell lines showed

activated STAT1 and STAT3 proteins under serum-deprived conditions (**figure 4.12**), which could be due to multiple activating mechanisms not restricted to JAK kinases. In these cells, ruxolitinib caused a dose-dependent inhibition of cell proliferation but a moderate effect on cell death (**figure 4.18**). Thus, it seems that blocking JAK/STAT signalling, instead of provoking cytotoxic effects and subsequent cell death, may induce growth inhibition by cytostatic mechanisms like for example a decrease in DNA synthesis (Cristina Pérez et al. 2015).

5.3 PLCG1/PRKCQ signalling towards NFAT and NF- κ B activation

As part of a malignant CTCL signalling network, deregulated PLCG1 can control the activation of downstream nuclear effectors like NFAT and NF- κ B. Here, the activation of NFAT was confirmed in HEK-IL6 cells by cotransfecting a constitutively active PLCG1 mutant alongside specific reporter constructs. As could be anticipated, PLCG1 activated NFAT by a mechanism involving CaN and PRKCQ as shown by using specific inhibitors (**figure 4.4**) (G Werlen et al. 1998). In this regard, based on our original observations regarding PLCG1 activity towards CaN and NFAT activation (Vaqué et al. 2014), our working team is currently finishing a clinical trial using topical pimecrolimus (a CaN inhibitor) in early stage MFs with promising results (>60% ORR) (PimTo-MF study, EudraCT number: 2014-001377-14; Dr. Pablo L. Ortiz-Romero). Thus, in this work, the pre-clinical data can suggest that combinations of CaN and PRKCQ inhibitors may increase the efficacy of the treatment in early stages and/or provide rational to treat non-responders, or even advanced CTCL patients.

On the other hand, we also confirmed NF- κ B activation by transforming PLCG1 (**figure 4.4**), a result that has been recently described in HEK293 cells (Patel et al. 2019). It is widely

accepted that NF- κ B is a major target downstream of PKCs (Lin et al. 2000; Coudronniere et al. 2012). Interestingly, in our hands specific blockage of PRKCQ significantly but modestly impaired NF- κ B activity downstream of PLCG1 (**figure 4.4C**), hence suggesting that, at least in this system, PRKCQ may not participate as major PLCG1 effector to promote NF- κ B activation. This striking result was further confirmed by using a constitutively activated PRKCQ mutant that triggered activation of NFAT but failed at inducing NF- κ B activity (**figure 4.14**). On the other hand, TPA prompted the activation of NFAT and NF- κ B, which were abrogated by specific PRKCQ inhibition (**figure 4.8**). A possible but controversial explanation for these results implies that PRKCQ may not be the principal PKC isoform to connect with NF- κ B activation. Although these results should be confirmed in CTCL models, our research has focused in the mechanisms that activate STAT3 since it correlated with advanced MF stages, in contrast to NF- κ B (**table 4.2**).

5.4 PLCG1/PRKCQ signalling towards STAT3 activation

We provide robust and original evidence that PLCG1 S345F, a recurrent mutant found in advanced CTCL cases, can promote the activation of STAT3 (and STAT1, which was studied to a minor extent). This was assessed by multiple experimental approaches that included quanti-blue or luciferase reporter assays and western-blots using specific STAT3 antibodies to detect phosphorylated Y705 and S727 residues. Using specific inhibitors, we show that downstream PLCG1, STAT3 can be activated by JAK-dependent (P-STAT3 Y705) and JAK-independent (S727) mechanisms. Interestingly our data highlights the acting role of PRKCQ participating in both pathways (**figures 4.5, 4.6 and 4.7**). Furthermore, TPA induced phosphorylation of STAT1 and STAT3 in HEK-IL6, Jurkat, MyLa and HuT 78 cells (**figures 4.10 and 4.12**). In this regard, we noticed that TPA failed at promoting STAT3-Y705

phosphorylation in Jurkat (no signal) and MyLa (saturated signal in serum-deprived conditions) cells (**figure 4.12**). Alongside these results, TPA also activated STAT3-mediated transcription in HEK-IL6 and Hut 78 cells (**figures 4.9, 4.10 and 4.12**). In order to detect important effectors acting downstream of TPA towards STAT3 activation, a number of specific inhibitors were utilized in HEK-IL6 cells: the previously mentioned tacrolimus (CaNi), sotrastaurin (PRKCQi) and ruxolitinib (JAKi) alongside ibrutinib (BTKi), dasatinib (inhibitor of ABL, SRC and C-KIT), fostamatinib (SYKi) and MK-2206 (AKTi). Remarkably, in these conditions only sotrastaurin impaired TPA-mediated STAT3 phosphorylation at both Y705 and S727 residues as well as STAT3 transcriptional activity (**figure 4.10**). Other inhibitors just prevented STAT3 Y705 phosphorylation but failed to inhibit its transcriptional activity. Of note, when comparing the effects of PRKCQ and JAK inhibitors in HUT78 cells, both inhibited STAT3 activity (**figure 4.12**), which suggests that in a CTCL context, STAT3 activity can be controlled by mechanisms that are dependent on PRKCQ and JAK kinases.

Moreover, using inducible PRKCQ knockdown cells, PRKCQ deficiency impaired basal STAT3 phosphorylation at both residues, transcriptional activity and cell proliferation (**figures 4.20 and 4.21**). These data suggest that PRKCQ can play an important role in the control of essential CTCL mechanisms involving STAT3 activation by JAK-dependent and JAK-independent mechanisms.

To gain further knowledge about the mechanisms that can connect PRKCQ with STAT3 activation we performed mass spectrometry of PRKCQ-enriched immunoprecipitates in CTCL cells. A number of interacting proteins were significantly detected. Interestingly STAT3 was not included amongst these. This was independently confirmed by co-immunoprecipitation analysis (**figure 4.22**). Of note, whereas PRKCQ does not directly interact with STAT3 in CTCL cells, other works have shown that alternative PKC isoforms

like PRKCD (isoform δ) can bind to and phosphorylate STAT3 in S727, in alternative cellular contexts (Jain et al. 1999). Our data do not discard that a different PKC isoform can participate alongside PRKCQ in STAT3 activation in CTCL. Interestingly, amongst our results, ASK1 (MAP3K5) was significantly the most abundant PRKCQ interacting protein, and this was further confirmed using an independent approach (**figure 4.24**). ASK1 is a member of the MAPK family of serine/threonine kinases acting upstream of ERK1/2 and JNK1, which have been shown to interact with and phosphorylate STAT3 in S727 (Jain et al. 1998; Lim and Cao 1999). In support of the potential role of PRKCQ-ASK1 at regulating STAT3 via MAPKs, another PRKCQ-interacting protein identified was PGAM5. It is a phosphatase that activates ASK1, JNKs and p38MAPKs (Takeda et al. 2009). On the other hand, RACK1 was also detected, it binds to and stabilizes activated PKCs, thereby increasing PKC-mediated phosphorylation (Mochly-Rosen et al. 1995) and, remarkably, has also been shown to directly interact with JAK1, STAT1/3, IL-2R and IL-4R (Mochly-Rosen et al. 1995; Zhang et al. 2006).

Thus, these data provide plausible mechanisms downstream of PRKCQ to trigger STAT3 phosphorylation at S727 via ASK1 (JAK-independent) and at Y705 via RACK1/JAK kinases. Further work will be required to confirm these results and/or identify alternative mechanisms to explain STAT3 activation downstream of PRKCQ in CTCL. Upon validation, these effectors may provide potential targets for therapy and thus provide strong rational to develop novel strategies to manage specific cases of CTCL.

5.5 PRKCQ participates in essential CTCL activities *ex vivo* and *in vivo*

Based on the data presented in this work, STAT3 can exert a relevant biological activity in the tumoral progression of CTCL patients. Moreover, PRKCQ may control STAT3 activation through a combination of different molecular mechanisms. Also, in CTCL cells, pharmacological inhibition of PRKCQ or JAK abrogated STAT3 activity and impaired cell proliferation (**figures 4.16 and 4.18**). To further explore their potential anti-CTCL activities, the combined inhibition of both kinases was analysed. This combination exerted a synergistic anti-proliferative effect (**figure 4.19**). Thus, it is possible that developing specific therapy combinations of inhibitors to abrogate STAT3 activity alongside other targets relevant to the biology of CTCL (like for example CaN or other PKCQ downstream effectors), may improve the clinical management of CTCL patients with special focus on those at advanced stages.

To directly challenge the biological role of PRKCQ in CTCL, we generated inducible PRKCQ knockdown MyLa and HuT 78 cells. This approach provoked a dramatic decrease of PRKCQ expression (>90% of the protein; **figure 4.21**). In the absence of PRKCQ, STAT3 phosphorylation in Y705 and S727 and its transcriptional activity were impaired alongside cell proliferation, although not completely. These results suggest that PRKCQ can control important CTCL activities through mechanisms that include but that are probably not restricted to those exerted over STAT3. Nevertheless, these results were obtained using cell-based models *in vitro*.

The CTCL translational field can currently take advantage of only few *in vivo* models where to test essential biological processes. In this regard, and to serve as an example, a NSG mouse model has recently been developed to explore malignant activities of human SS cells

after injection in the dorsal ear surface of such mice (Gallardo et al. 2018). Alternatively, this work has applied a novel *in vivo* approach to this field by using chicken embryos. This model offers the possibility to generate primary tumours and study its metastatic potential in a timely and cost-effective manner. In this regard, MF cells deficient for PRKCQ expression had greatly impaired the ability to grow tumours, promote angiogenesis (see representative images in **figure 4.26**), intravasate blood vessels and metastasize to distant organs. Moreover, pharmacological treatment using sotrastaurin provoked similar effects in this system (**figure 4.27**). These *in vivo* data strongly robust the idea that PRKCQ plays a central role at controlling tumorigenesis and progression of CTCLs.

In addition, it will be highly interesting to study PRKCQ downstream effectors including actionable proteins and target genes to offer novel possibilities to diagnose and treat this disease at different stages. In an attempt to identify PRKCQ-controlled genes, a comparative mRNA-seq study using MyLa and HuT 78 cells deficient for PRKCQ expression was performed. After a preliminary analysis that needs further confirmation, a number of transcriptional PRKCQ targets were highly significant and, but to name a few examples, are described as follows (those targets negatively regulated include the symbol (-)): i) Rho/actin cytoskeleton genes such as *LCP1* (L-Plastin, which also was detected as a PRKCQ-interacting protein), *LSP1*, *CIT* and *LIMK1*, ii) genes associated with TNF/NF- κ B signalling, such as *BCL3*, *TANK*, *TNFRSF25* (-) and *TRAF3*, and iii) genes related to JAK/STAT signalling: *IL10*, *IL15* (-) and *SOCS2* (-). Interestingly, pro-apoptotic genes like *TNFRSF25*, also known as DR3 (Death receptor 3), (Chinnaiyan et al. 1996) or negative regulators of STAT activation like *SOCS2* (Yoshimura et al. 2007) were repressed in control cells and their expression increased after PRKCQ depletion. These data show that, downstream PRKCQ, there is a connection with the activation of NF- κ B-related genes like *TRAF3* (He et al. 2004) or *TANK* (Chariot et al. 2002), hence suggesting that despite no direct connexion between PRKCQ and NF- κ B

activity was found in this work, NF- κ B may still participate downstream PRKCQ. Finally, a large number of significant genes are involved in Rho GTPase signalling and the dynamic control of the actin cytoskeleton. This is a well-known mechanism used by multiple types of cancers, like for example cutaneous melanoma, to initiate and establish metastasis (Orgazy et al. 2014; Pandya et al. 2017).

In summary, this thesis has characterized, from molecular and biological perspectives, the role and mechanistic interplay of important members of the malignant network proposed to control the biology of CTCLs (**figure 5.1**). Moreover, from a translational perspective the

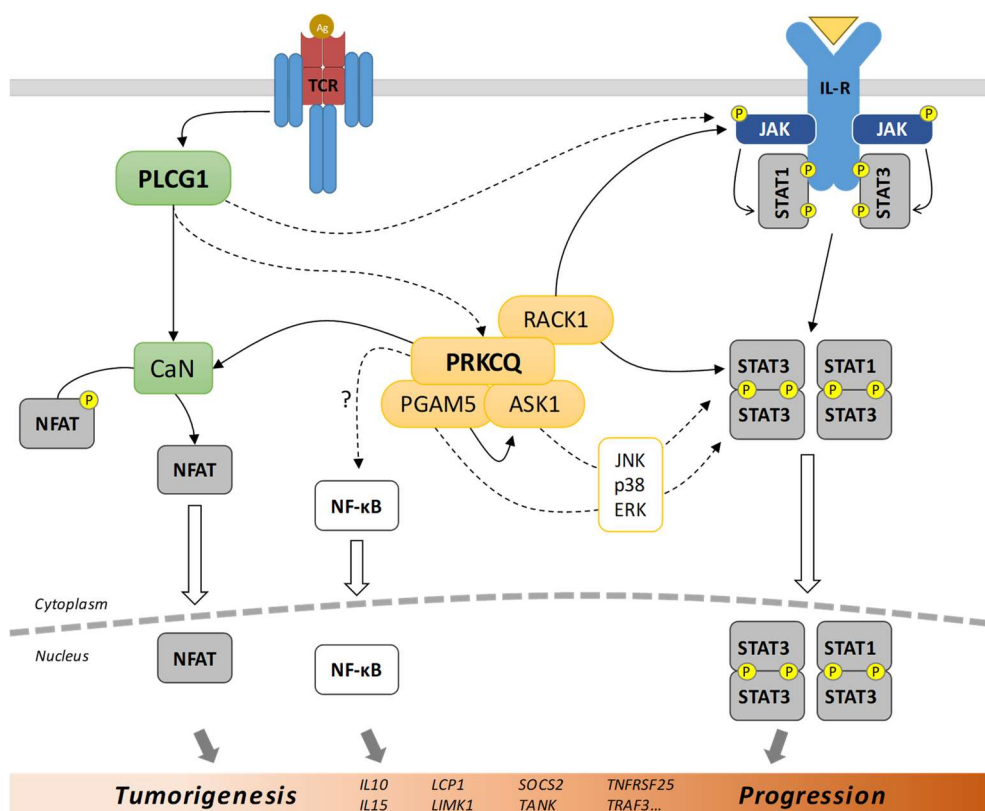


Figure 5.1. A malignant signalling network controlling tumorigenesis and progression of CTCL. Schematic representation showing the mechanistic interplay between different T-cell signalling pathways that may promote tumorigenesis and progression in CTCL. As part of this network, PRKCQ plays a pivotal role by controlling NFAT and STAT activation through specific protein interactions and target genes. Black arrows: direct mechanism, black dashed arrows: indirect mechanism, white arrows: nuclear translocation.

DISCUSSION

data: i) describe novel markers, like for example the expression of activated STAT proteins, to potentially serve for CTCL diagnosis; ii) proposes novel rational approaches to develop targeted therapy, including CaN, PRKCQ and JAK inhibitors used alone or in combination, and iii) identifies a number of PRKCQ interacting proteins and target genes that might play essential roles in CTCLs.

CONCLUSIONS

6. CONCLUSIONS

1. STAT3 activation is a common finding in advanced stages of MF patients.
2. STAT3 activation can be triggered by multiple mechanisms such as JAK, PLCG1 and PRKCQ signalling:
 - a. Through activating JAK1 Y654F mutation.
 - b. Downstream activated PLCG1 and mediated by PRKCQ and/or JAK.
 - c. Via activated PRKCQ both dependent and independent of JAK activity.
3. Specific pharmacological inhibition of PRKCQ and JAK synergistically impairs cell proliferation and promotes apoptosis.
4. PRKCQ interacts with effector proteins, such as ASK1, RACK1 and PGAM5, that can potentially mediate STAT3 activation.
5. PRKCQ is essential for CTCL tumour development, intravasation and metastasis.
6. Transcriptomic analysis reveals novel PRKCQ target genes, such as *LCP1*, *IL10* and *SOCS2*, with potential to participate in malignant CTCL mechanisms.

BIBLIOGRAPHY

- Agar NS, Wedgeworth E, Crichton S, Mitchell TJ, Cox M, Ferreira S, Robson A, Calonje E, Stefanato CM, Wain EM, et al. 2010. Survival outcomes and prognostic factors in mycosis fungoides/Sézary syndrome: Validation of the revised International Society for Cutaneous Lymphomas/European Organisation for Research and Treatment of Cancer staging proposal. *J Clin Oncol.* 28(31):4730–4739. doi:10.1200/JCO.2009.27.7665.
- Alcover A, Alar B, Bartolo V Di. 2018. Cell Biology of T Cell Receptor Expression and Regulation. *Annu Rev Immunol.* 36:103–25. doi:10.1146/annurev-immunol.
- Altman A, Kong K-F. 2016. Protein Kinase C Enzymes in the Hematopoietic and Immune Systems. *Annu Rev Immunol.* 34:511–38. doi:10.1146/annurev-immunol-041015-055347.
- Axelrod PI, Lorber B, Vonderheid EC. 1992. Infections Complicating Mycosis Fungoides and Sézary Syndrome. *JAMA.*
- Aziz MH, Manoharan HT, Verma AK. 2007. Protein kinase C ϵ , which sensitizes skin to sun's UV radiation-induced cutaneous damage and development of squamous cell carcinomas, associates with Stat3. *Cancer Res.* 67(3):1385–1394. doi:10.1158/0008-5472.CAN-06-3350.
- Bagot M, Porcu P, Marie-Cardine A, Battistella M, William BM, Vermeer M, Whittaker S, Rotolo F, Ram-Wolff C, Khodadoust MS, et al. 2019. IIPH4102, a first-in-class anti-KIR3DL2 monoclonal antibody, in patients with relapsed or refractory cutaneous T-cell lymphoma: an international, first-in-human, open-label, phase 1 trial. *Lancet Oncol.* doi:10.1016/s1470-2045(19)30320-1.
- Baier-Bitterlich G, Berall F, Bauer B, Fresser F, Wachter H, Grunicke H, Utermann G, Altman A, Baier G. 1996. Protein Kinase C- ζ Isoenzyme Selective Stimulation of the Transcription Factor Complex AP-1 in T Lymphocytes. *Mol Cell Biol.* 16(4):1842–1850.
- Baier G, Telford D, Giampa L, Coggeshall KM, Baier-Bitterlich G, Isakov N, Altman a. 1993. Molecular cloning and characterization of PKC theta, a novel member of the protein kinase C (PKC) gene family expressed predominantly in hematopoietic cells. *J Biol Chem.* 268(7):4997–5004.
- Bastidas Torres AN, Cats D, Mei H, Suzhai K, Willemze R, Vermeer MH, Tensen CP. 2018. Genomic analysis reveals recurrent deletion of JAK-STAT signaling inhibitors HNRNPK and SOCS1 in mycosis fungoides. doi:10.1002/gcc.22679.
- Benedek TG. 2010. Methotrexate: From its introduction to non-oncologic therapeutics to anti-TNF- α . *Clin Exp Rheumatol.* 28(5 SUPPL. 61).
- Blaizot R, Ouattara E, Fauconneau A, Beylot-Barry M, Pham-Ledard A. 2018. Infectious events and associated risk factors in mycosis fungoides/Sézary syndrome: a retrospective cohort study. *Br J Dermatol.* 179(6):1322–1328. doi:10.1111/bjd.17073.
- Bradford PT, Devesa SS, Anderson WF, Toro JR. 2009. Cutaneous lymphoma incidence patterns in the United States: a population-based study of 3884 cases. *Blood.* 113(21):5064–5073. doi:10.1182/blood-2008-10-184168.
- Bromberg J, Darnell JE. 2000. The role of STATs in transcriptional control and their impact on cellular function. *Oncogene.* 19(21):2468–2473. doi:10.1038/sj.onc.1203476.
- Bromberg JF, Wrzeszczynska MH, Devgan G, Zhao Y, Pestell RG, Albanese C, Darnell JE. 1999. Stat3 as an oncogene. *Cell.* doi:10.1016/S0092-8674(00)81959-5.

BIBLIOGRAPHY

- Calò V, Migliavacca M, Bazan V, Macaluso M, Buscemi M, Gebbia N, Russo A. 2003. STAT proteins: From normal control of cellular events to tumorigenesis. *J Cell Physiol.* 197(2):157–168. doi:10.1002/jcp.10364.
- Campbell JJ, Clark RA, Watanabe R, Kupper TS. 2010. Sézary syndrome and mycosis fungoides arise from distinct T-cell subsets: A biologic rationale for their distinct clinical behaviors. *Blood.* 116(5):767–771. doi:10.1182/blood-2009-11-251926.
- Cathcart Ashish Bhattacharjee MK, Xu B, Frank DA. 2019. Tyrosine-Phosphorylated Stat3 and δ Complex with Protein Kinase C Regulated by a Novel Cytosolic Signaling Monocyte 15-Lipoxygenase Expression Is. doi:10.4049/jimmunol.177.6.3771.
- Chariot A, Leonardi A, Müller J, Bonif M, Brown K, Siebenlist U. 2002. Association of the adaptor TANK with the I κ B kinase (IKK) regulator NEMO connects IKK complexes with IKK ϵ and TBK1 kinases. *J Biol Chem.* doi:10.1074/jbc.M205069200.
- Chinnaiyan AM, O'Rourke K, Yu GL, Lyons RH, Garg M, Duan DR, Xing L, Gentz R, Ni J, Dixit VM. 1996. Signal transduction by DR3, a death domain-containing receptor related to TNFR-1 and CD95. *Science* (80-). 274(5289):990–992. doi:10.1126/science.274.5289.990.
- Choi J, Goh G, Walradt T, Hong BS, Bunick CG, Chen K, Bjornson RD, Maman Y, Wang T, Tordoff J, et al. 2015. Genomic landscape of cutaneous T cell lymphoma. *Nat Genet.* 47(July):1–11. doi:10.1038/ng.3356.
- Chou TC, Talalay P. 1984. Quantitative analysis of dose-effect relationships: the combined effects of multiple drugs or enzyme inhibitors. *Adv Enzyme Regul.* doi:10.1016/0065-2571(84)90007-4.
- Clark RA, Chong B, Mirchandani N, Brinster NK, Yamanaka K-I, Dowgiert RK, Kupper TS. 2006. The vast majority of CLA+ T cells are resident in normal skin. *J Immunol.* 176(7):4431–9.
- Coudronniere N, Villalba M, Englund N, Altman A. 2012. NF- κ B activation induced by T cell receptor/CD28 costimulation is mediated by protein kinase C- θ . *Proc Natl Acad Sci.* 97(7):3394–3399. doi:10.1073/pnas.97.7.3394.
- Crespo P, Casar B. 2016. The Chick Embryo Chorioallantoic Membrane as an in vivo Model to Study Metastasis. *Bio-Protocol.* 6(20):1–11. doi:10.21769/BioProtoc.1962.
- Dawson MA, Bannister AJ, Göttgens B, Foster SD, Bartke T, Green AR, Kouzarides T. 2009. JAK2 phosphorylates histone H3Y41 and excludes HP1 α from chromatin. *Nature.* doi:10.1038/nature08448.
- Degryse S, De Bock CE, Cox L, Demeyer S, Gielen O, Mentens N, Jacobs K, Geerdens E, Gianfelici V, Hulselmans G, et al. 2014. JAK3 mutants transform hematopoietic cells through JAK1 activation, causing T-cell acute lymphoblastic leukemia in a mouse model. *Blood.* doi:10.1182/blood-2014-04-566687.
- Degryse S, Bornschein S, De Bock CE, Leroy E, Bempt M Vanden, Demeyer S, Jacobs K, Geerdens E, Gielen O, Soulier J, et al. 2018. Mutant JAK3 signaling is increased by loss of wild-type JAK3 or by acquisition of secondary JAK3 mutations in T-ALL. *Blood.* doi:10.1182/blood-2017-07-797597.
- Deng C, Pan B, O'Connor OA. 2013. Brentuximab Vedotin. *Clin Cancer Res.* 19(1):22–27. doi:10.1158/1078-0432.CCR-12-0290.

- Dobin A, Davis CA, Schlesinger F, Drenkow J, Zaleski C, Jha S, Batut P, Chaisson M, Gingeras TR. 2013. STAR: Ultrafast universal RNA-seq aligner. *Bioinformatics*. 29(1):15–21. doi:10.1093/bioinformatics/bts635.
- Dong D, Zheng L, Lin J, Zhang B, Zhu Y, Li N, Xie S, Wang Y, Gao N, Huang Z. 2019. Structural basis of assembly of the human T cell receptor–CD3 complex. *Nature*. 573(7775):546–552. doi:10.1038/s41586-019-1537-0.
- Duarte RF, Boumendil A, Onida F, Gabriel I, Arranz R, Arcese W, Poiré X, Kobbe G, Narni F, Corteleezi A, et al. 2014. Long-term outcome of allogeneic hematopoietic cell transplantation for patients with mycosis fungoides and sézary syndrome: A European society for blood and marrow transplantation lymphoma working party extended analysis. *J Clin Oncol*. 32(29):3347–3348. doi:10.1200/JCO.2014.57.5597.
- Duvic M, Hymes K, Heald P, Breneman D, Martin AG, Myskowski P, Crowley C, Yocum RC. 2017. Bexarotene Is Effective and Safe for Treatment of Refractory Advanced-Stage Cutaneous T-Cell Lymphoma: Multinational Phase II-III Trial Results. *J Clin Oncol*. 19(9):2456–2471. doi:10.1200/jco.2001.19.9.2456.
- Elenitoba-Johnson KSJ, Wilcox R. 2017. A new molecular paradigm in mycosis fungoides and Sézary syndrome. *Semin Diagn Pathol*. 34(1):15–21. doi:10.1053/j.semdp.2016.11.002.
- Eriksen KW, Kaltoft K, Mikkelsen G, Nielsen M, Zhang Q, Geisler C, Nissen MH, Röpke C, Wasik MA, Ødum N. 2001. Constitutive STAT3-activation in Sezary syndrome: Tyrphostin AG490 inhibits STAT3-activation, interleukin-2 receptor expression and growth of leukemic Sezary cells. *Leukemia*. 15(5):787–793. doi:10.1038/sj.leu.2402093.
- Fanok MH, Sun A, Fogli LK, Narendran V, Eckstein M, Kannan K, Dolgalev I, Lazaris C, Heguy A, Laird ME, et al. 2018. Role of Dysregulated Cytokine Signaling and Bacterial Triggers in the Pathogenesis of Cutaneous T-Cell Lymphoma. *J Invest Dermatol*. 138(5):1116–1125. doi:10.1016/j.jid.2017.10.028.
- Fiorentino DF, Zlotnik A, Mosmann TR, Howard M, O'Garra A. 1991. IL-10 inhibits cytokine production by activated macrophages. *J Immunol*. 147(11):3815–22.
- de Freitas RM, da Costa Maranduba CM. 2015. Myeloproliferative neoplasms and the JAK/STAT signaling pathway: An overview. *Rev Bras Hematol Hemoter*. 37(5):348–353. doi:10.1016/j.bjhh.2014.10.001.
- Furqan M, Mukhi N, Lee B, Liu D. 2013. Dysregulation of JAK-STAT pathway in hematological malignancies and JAK inhibitors for clinical application. *Biomark Res*. 1(1). doi:10.1186/2050-7771-1-5.
- Gallardo F, Bertran J, López-Arribillaga E, González J, Menéndez S, Sánchez I, Colomo L, Iglesias M, Garrido M, Santamaría-Babí LF, et al. 2018. Novel phosphorylated TAK1 species with functional impact on NF- κ B and β -catenin signaling in human Cutaneous T-cell lymphoma. *Leukemia.(Imim)*:1–13. doi:10.1038/s41375-018-0066-4.
- Georgakopoulos I, Papadavid E, Platoni K, Dilvoi M, Patatoukas G, Kypraiou E, Nikolaou V, Efsthathopoulos E, Kelekis N, Kouloulas V. 2018. Clinical application of Total Skin Electron Beam (TSEB) therapy for the management of T cell cutaneous lymphomas. The evolving role of low dose (12 Gy) treatment schedule. *Clin Transl Radiat Oncol*. 15:26–30. doi:10.1016/j.ctro.2018.12.002.

BIBLIOGRAPHY

- Geskin LJ, Viragova S, Stolz DB, Fuschiotti P. 2015. Interleukin-13 is overexpressed in cutaneous T-cell lymphoma cells and regulates their proliferation. *Blood*. 125(18):2798–2805. doi:10.1182/blood-2014-07-590398.
- Girardi M, Heald PW, Wilson LD. 2004. The Pathogenesis of Mycosis Fungoides. *N Engl J Med*. 350(19):1978–1988. doi:10.1056/NEJMra032810.
- Goswami R, Kaplan MH. 2017. STAT Transcription Factors in T Cell Control of Health and Disease. In: *International Review of Cell and Molecular Biology*. Vol. 331. Elsevier Inc. p. 123–180.
- Gough DJ, Corlett A, Schlessinger K, Wegrzyn J, Lerner AC, Levy DE. 2009. Mitochondrial Stat3 Supports Ras-Dependent Oncogenic Transformation. *Science* (80-). 324(5935):1713–1716. doi:10.1126/science.1171721.Mitochondrial.
- Gough DJ, Koetz L, Levy DE. 2013. The MEK-ERK Pathway Is Necessary for Serine Phosphorylation of Mitochondrial STAT3 and Ras-Mediated Transformation. *PLoS One*. 8(11):83395. doi:10.1371/journal.pone.0083395.
- Guenova E, Watanabe R, Teague JE, Desimone JA, Jiang Y, Dowlatshahi M, Schlapbach C, Schaekel K, Rook AH, Tawa M, et al. 2013. TH2 cytokines from malignant cells suppress TH1 responses and enforce a global TH2 bias in leukemic cutaneous T-cell lymphoma. *Clin Cancer Res*. 19(14):3755–3763. doi:10.1158/1078-0432.CCR-12-3488.
- Guenther L, Lynde C, Poulin Y. 2019. Off-Label Use of Topical Calcineurin Inhibitors in Dermatologic Disorders. *J Cutan Med Surg*. 23(4_suppl):27S-34S. doi:10.1177/1203475419857668.
- Hamrouni A, Fogh H, Zak ZL, Odum N, Gniadecki R. 2019. Clonotypic diversity of the T-cell receptor corroborates the immature precursor origin of cutaneous T-cell lymphoma. *Clin Cancer Res*:clincanres.4099.2018. doi:10.1158/1078-0432.CCR-18-4099.
- He L, Grammer AC, Wu X, Lipsky PE. 2004. TRAF3 forms heterotrimers with TRAF2 and modulates its ability to mediate NF-κB activation. *J Biol Chem*. doi:10.1074/jbc.M407284200.
- Hristov AC, Tejasvi T, Wilcox RA. 2019. Mycosis Fungoides and Sézary Syndrome: 2019 update on diagnosis, risk-stratification, and management. *Am J Hematol*.(734):ajh.25577. doi:10.1002/ajh.25577.
- Hu X, Dutta P, Tsurumi A, Li J, Wang J, Land H, Li WX. 2013. Unphosphorylated STAT5A stabilizes heterochromatin and suppresses tumor growth. *Proc Natl Acad Sci U S A*. doi:10.1073/pnas.1221243110.
- Hughes CFM, Khot A, McCormack C, Lade S, Westerman DA, Twigger R, Buelens O, Newland K, Tam C, Dickinson M, et al. 2015. Lack of durable disease control with chemotherapy for mycosis fungoides and Sézary syndrome: a comparative study of systemic therapy. doi:10.1182/blood-2014-07.
- Isakov N, Altman A. 2002. Protein Kinase Cθ in T Cell Activation. *Annu Rev Immunol*. 20:761–94. doi:10.1146/annurev.immunol.20.120701.074321.
- Ishii T, Ishida T, Utsunomiya A, Inagaki A, Yano H, Komatsu H, Iida S, Imada K, Uchiyama T, Akinaga S, et al. 2010. Defucosylated humanized anti-CCR4 monoclonal antibody KW-0761 as a novel immunotherapeutic agent for adult T-cell leukemia/lymphoma. *Clin Cancer Res*. 16(5):1520–31. doi:10.1158/1078-0432.CCR-09-2697.

- Iyer A, Hennessey D, O’Keefe S, Patterson J, Wang W, Salopek T, Wong GKS, Gniadecki R. 2019. Clonotypic heterogeneity in cutaneous T-cell lymphoma (mycosis fungoides) revealed by comprehensive whole-exome sequencing. *Blood Adv.* 3(7):1175–1184. doi:10.1182/bloodadvances.2018027482.
- Izban KF, Ergin M, Qin J-Z, Martinez RL, Pooley RJ, Saeed S, Alkan S. 2000. Constitutive expression of NF- κ B is a characteristic feature of mycosis fungoides: Implications for apoptosis resistance and pathogenesis. *Hum Pathol.* 31(12):1482–1490. doi:10.1053/HUPA.2000.20370.
- Jain N, Zhang T, Fong SL, Lim CP, Cao X. 1998. Repression of Stat3 activity by activation of mitogen-activated protein kinase (MAPK). *Oncogene.* doi:10.1038/sj.onc.1202238.
- Jain N, Zhang T, Kee WH, Li W, Cao X. 1999. Protein kinase C δ associates with and phosphorylates Stat3 in an interleukin-6-dependent manner. *J Biol Chem.* 274(34):24392–24400. doi:10.1074/jbc.274.34.24392.
- Kadamur G, Ross EM. 2013. Mammalian Phospholipase C. *Annu Rev Physiol.* 75(1):127–154. doi:10.1146/annurev-physiol-030212-183750.
- Khodadoust MS, Rook AH, Porcu P, Foss F, Moskowitz AJ, Shustov A, Shanbhag S, Sokol L, Fling SP, Ramchurren N, et al. 2019. Pembrolizumab in Relapsed and Refractory Mycosis Fungoides and Sézary Syndrome: A Multicenter Phase II Study. *J Clin Oncol.:JCO.* 19.01056. doi:10.1200/jco.19.01056.
- Kim EJ, Hess S, Richardson SK, Newton S, Showe LC, Benoit BM, Ubriani R, Vittorio CC, Junkins-Hopkins JM, Wysocka M, et al. 2005. Immunopathogenesis and therapy of cutaneous T cell lymphoma. *J Clin Invest.* 115(4):798–812. doi:10.1172/JCI200524826.
- Kim SW, Han YW, Lee ST, Jeong HJ, Kim Seong Hun, Kim IH, Lee SO, Kim DG, Kim Suh Hee, Kim SZ, et al. 2008. Protein Kinase C epsilon interacts with Stat3 and regulates its activation that is essential for the development of skin cancer. *Mol Carcinog.* 47(May):114–125. doi:10.1002/mc.
- Kim YH, Bagot M, Pinter-Brown L, Rook AH, Porcu P, Horwitz SM, Whittaker S, Tokura Y, Vermeer M, Zinzani PL, et al. 2018. Mogamulizumab versus vorinostat in previously treated cutaneous T-cell lymphoma (MAVORIC): an international, open-label, randomised, controlled phase 3 trial. *Lancet Oncol.* 19(September). doi:10.1016/S1470-2045(18)30379-6.
- Knobler R, Berlin G, Calzavara-Pinton P, Greinix H, Jaksch P, Laroche L, Ludvigsson J, Quaglino P, Reinisch W, Scarisbrick J, et al. 2014. Guidelines on the use of extracorporeal photopheresis. *J Eur Acad Dermatol Venereol.* 28(SUPPL. 1):1–37. doi:10.1111/jdv.12311.
- Kong KF, Yokosuka T, Canonigo-Balancio AJ, Isakov N, Saito T, Altman A. 2011. A motif in the V3 domain of the kinase PKC- θ determines its localization in the immunological synapse and functions in T cells via association with CD28. *Nat Immunol.* 12(11):1105–1112. doi:10.1038/ni.2120.
- Krejsgaard T, Lindahl LM, Mongan NP, Wasik MA, Litvinov I V, Iversen L, Langhoff E, Woetmann A, Odum N. 2017. Malignant inflammation in cutaneous T-cell lymphoma—a hostile takeover. *Semin Immunopathol.* 39(3):269–282. doi:10.1007/s00281-016-0594-9.
- Krejsgaard T, Litvinov I V., Wang Y, Xia L, Willerslev-Olsen A, Koralov SB, Kopp KL, Bonefeld CM, Wasik MA, Geisler C, et al. 2013. Elucidating the role of interleukin-17F in cutaneous T-cell lymphoma. *Blood.* 122(6):943–950. doi:10.1182/blood-2013-01-480889.
- Krejsgaard T, Odum N, Geisler C, Wasik MA, Woetmann A. 2012. Regulatory T cells and

BIBLIOGRAPHY

- immunodeficiency in mycosis fungoides and Sézary syndrome. *Leukemia*. 26(3):424–32. doi:10.1038/leu.2011.237.
- Krejsgaard T, Ralfkiaer U, Clasen-Linde E, Eriksen KW, Kopp KL, Bonefeld CM, Geisler C, Dabelsteen S, Wasik MA, Ralfkiaer E, et al. 2011. Malignant cutaneous T-cell lymphoma cells express IL-17 utilizing the Jak3/stat3 signaling pathway. *J Invest Dermatol*. 131(6):1331–1338. doi:10.1038/jid.2011.27.
- Kwon M-J, Ma J, Ding Y, Wang R, Sun Z. 2012. Protein Kinase C- θ promotes Th17 Differentiation via Upregulation of Stat3. *J Immunol*. 188(12):5887–5897. doi:10.4049/jimmunol.1102941.
- Laharanne E, Oumouhou N, Bonnet F, Carlotti M, Gentil C, Chevret E, Jouary T, Longy M, Vergier B, Beylot-Barry M, et al. 2010. Genome-wide analysis of cutaneous T-cell lymphomas identifies three clinically relevant classes. *J Invest Dermatol*. 130(6):1707–1718. doi:10.1038/jid.2010.8.
- Lee E, Koo J, Berger T. 2005. UVB phototherapy and skin cancer risk: A review of the literature. *Int J Dermatol*. 44(5):355–360. doi:10.1111/j.1365-4632.2004.02186.x.
- Lee EB, Fleischmann R, Hall S, Wilkinson B, Bradley JD, Gruben D, Koncz T, Krishnaswami S, Wallenstein G V., Zang C, et al. 2014. Tofacitinib versus methotrexate in rheumatoid arthritis. *N Engl J Med*. doi:10.1056/NEJMoa1310476.
- Lee Harris N, Jaffe ES, Stein H, Banks PM, Chan JKC, Cleary ML, Delsol G, Wolf-peeters C De, Falini B, Gatter KC, et al. 1994. A Revised European-American Classification of Lymphoid Neoplasms : *Blood J*. 84(5):1361–1392.
- Lessin SR, Duvic M, Guitart J, Pandya AG, Strober BE, Olsen EA, Hull CM, Knobler EH, Rook AH, Kim EJ, et al. 2013. Topical Chemotherapy in Cutaneous T-cell Lymphoma. *JAMA Dermatology*. 149(1):25. doi:10.1001/2013.jamadermatol.541.
- Li B, Dewey CN. 2014. RSEM: Accurate transcript quantification from RNA-seq data with or without a reference genome. In: *Bioinformatics: The Impact of Accurate Quantification on Proteomic and Genetic Analysis and Research*. p. 41–74.
- Li J, Gao H, Huang J, Wang P, Huang Y, Luo W, Zhang X, Shen P, You J, Cai S, et al. 2016. PKC ζ interacts with STAT3 and promotes its activation in cardiomyocyte hypertrophy. *J Pharmacol Sci*. 132(1):15–23. doi:10.1016/j.jphs.2016.03.010.
- Lim CP, Cao X. 1999. Serine phosphorylation and negative regulation of Stat3 by JNK. *J Biol Chem*. doi:10.1074/jbc.274.43.31055.
- Lim CP, Cao X. 2006. Structure, function, and regulation of STAT proteins. *Mol Biosyst*. 2(11):536–550. doi:10.1039/b606246f.
- Lin X, O'Mahony A, Mu Y, Geleziunas R, Greene WC. 2000. Protein kinase C-theta participates in NF-kappaB activation induced by CD3-CD28 costimulation through selective activation of IkappaB kinase beta. *Mol Cell Biol*. 20(8):2933–40. doi:10.1128/mcb.20.8.2933-2940.2000.
- Livak KJ, Schmittgen TD. 2001. Analysis of relative gene expression data using real-time quantitative PCR and the 2- $\Delta\Delta$ CT method. *Methods*. 25(4):402–408. doi:10.1006/meth.2001.1262.
- Lopez-Bergami P, Habelhah H, Bhoomik A, Zhang W, Wang LH, Ronai Z. 2005. RACK1 mediates activation of JNK by protein kinase C [corrected]. *Mol Cell*. 19(3):309–320. doi:10.1016/j.molcel.2005.06.025.

- Love MI, Huber W, Anders S. 2014. Moderated estimation of fold change and dispersion for RNA-seq data with DESeq2. *Genome Biol.* 15(12):550. doi:10.1186/s13059-014-0550-8.
- Luo J, Liu S, Leung S, Gru AA, Tao Y, Hoog J, Ho J, Davies SR, Allred DC, Salavaggione AL, et al. 2017. An mRNA Gene Expression–Based Signature to Identify FGFR1-Amplified Estrogen Receptor–Positive Breast Tumors. *J Mol Diagnostics.* 19(1):147–161. doi:10.1016/j.jmoldx.2016.09.007.
- Maingon P, Truc G, Dalac S, Barillot I, Lambert D, Petrella T, Naudy S, Horiot JC. 2000. Radiotherapy of advanced mycosis fungoides: indications and results of total skin electron beam and photon beam irradiation. *Radiother Oncol.* 54(1):73–78. doi:10.1016/S0167-8140(99)00162-0.
- Malemud CJ. 2018. The role of the JAK/STAT signal pathway in rheumatoid arthritis. *Ther Adv Musculoskelet Dis.* 10(5–6):117–127. doi:10.1177/1759720X18776224.
- Mao X, Lillington DM, Czepulkowski B, Russell-Jones R, Young BD, Whittaker S. 2003. Molecular cytogenetic characterization of Sézary syndrome. *Genes Chromosomes Cancer.* 36(3):250–60. doi:10.1002/gcc.10152.
- Marsland BJ, Soos TJ, Späth G, Littman DR, Kopf M. 2004. Protein kinase C θ is critical for the development of in vivo T helper (Th)2 cell but not Th-1 cell responses. *J Exp Med.* doi:10.1084/jem.20032229.
- Mcgirt LY, Jia P, Baerenwald DA, Duszynski RJ, Dahlman KB, Zic JA, Zwerner JP, Hucks D, Dave U, Zhao Z, et al. 2015. Whole-genome sequencing reveals oncogenic mutations in mycosis fungoides. *Blood.* doi:10.1182/blood-2014-11.
- McKenzie R C T, Jones CL, Tosi I, Caesar JA, Whittaker SJ, Mitchell TJ. 2012. Constitutive activation of STAT3 in Sézary syndrome is independent of SHP-1. *Leukemia.* 26(2):323–31. doi:10.1038/leu.2011.198.
- McKenzie R. C.T., Jones CL, Tosi I, Caesar JA, Whittaker SJ, Mitchell TJ. 2012. Constitutive activation of STAT3 in Sézary syndrome is independent of SHP-1. *Leukemia.* 26(2):323–331. doi:10.1038/leu.2011.198.
- Meller N, Altman A, Isakov N. 1998. New perspectives on PKC θ , a member of the novel subfamily of protein kinase C. *Stem Cells.* 16(3):178–192. doi:10.1002/stem.160178.
- Micaily B, Miyamoto C, Kantor G, Lessin S, Rook A, Brady L, Goodman R, Vonderheid EC. 1998. Radiotherapy for unilesional mycosis fungoides. *Int J Radiat Oncol Biol Phys.* 42(2):361–364. doi:10.1016/S0360-3016(98)00218-1.
- Mochly-Rosen D, Smith BL, Chen C-H, Disatnik M-H, Ron D. 1995. Interaction of protein kinase C with RACK1, a receptor for activated C-kinase: a role in β protein kinase C mediated signal transduction. *Biochem Soc Trans.* 23(3):596–600. doi:10.1042/bst0230596.
- Monks CRF, Kupfer H, Tamir I, Barlow A, Kupfer A. 1997. Selective modulation of protein kinase C- θ during T-cell activation. *Nature.* doi:10.1038/385083a0.
- Netchiporouk E, Litvinov I V., Moreau L, Gilbert M, Sasseville D, Duvic M. 2014. Deregulation in STAT signaling is important for cutaneous T-cell lymphoma (CTCL) pathogenesis and cancer progression. *Cell Cycle.* 13(21):3331–3335. doi:10.4161/15384101.2014.965061.
- Nguyen V, Huggins RH, Lertsburapa T, Bauer K, Rademaker A, Gerami P, Guitart J. 2008. Cutaneous

BIBLIOGRAPHY

T-cell lymphoma and *Staphylococcus aureus* colonization. *J Am Acad Dermatol.* 59(6):949–952. doi:10.1016/j.jaad.2008.08.030.

Oka T, Miyagaki T. 2019. Novel and Future Therapeutic Drugs for Advanced Mycosis Fungoides and Sézary Syndrome. *Front Med.* 6:116. doi:10.3389/fmed.2019.00116.

Olsen E, Vonderheid E, Pimpinelli N, Willemze R, Kim Y, Knobler R, Zackheim H, Duvic M, Estrach T, Lamberg S, et al. 2007. Revisions to the staging and classification of mycosis fungoides and Sézary syndrome: A proposal of the International Society for Cutaneous Lymphomas (ISCL) and the cutaneous lymphoma task force of the European Organization of Research and Treatment of Ca. Blood. 110(6):1713–1722. doi:10.1182/blood-2007-03-055749.

Olsen EA. 2003. Interferon in the treatment of cutaneous T-cell lymphoma. *Dermatol Ther.* 16(4):311–321. doi:10.1111/j.1396-0296.2003.01643.x.

Olsen EA, Hodak E, Anderson T, Carter JB, Henderson M, Cooper K, Lim HW. 2016. Guidelines for phototherapy of mycosis fungoides and Sézary syndrome: A consensus statement of the United States Cutaneous Lymphoma Consortium. *J Am Acad Dermatol.* 74(1):27–58. doi:10.1016/j.jaad.2015.09.033.

Orgazy JL, Herraizy C, Sanz-Moreno V. 2014. Rho GTPases modulate malignant transformation of tumor cells. *Small GTPases.* 5(4). doi:10.4161/sgtp.29019.

Pandya P, Orgaz JL, Sanz-Moreno V. 2017. Modes of invasion during tumour dissemination. *Mol Oncol.* 11(1):5–27. doi:10.1002/1878-0261.12019.

Papadavid E, Economidou J, Psarra A, Kapsimali V, Mantzana V, Antoniou C, Limas K, Stratigos A, Stavrianeas N, Avgerinou G, et al. 2003. The relevance of peripheral blood T-helper 1 and 2 cytokine pattern in the evaluation of patients with mycosis fungoides and Sézary syndrome. *Br J Dermatol.* 148(4):709–718. doi:10.1046/j.1365-2133.2003.05224.x.

Park J, Yang J, Wenzel AT, Ramachandran A, Lee WJ, Daniels JC, Kim J, Martinez-Escala E, Amankulor N, Pro B, et al. 2017. Genomic analysis of 220 CTCLs identifies a novel recurrent gain-of-function alteration in RLTPR (p.Q575E). *Blood.* 130(12):1430–1440. doi:10.1182/blood-2017-02-768234.

Patel VM, Flanagan CE, Martins M, Jones CL, Butler M, Woollard WJ, Bakr FS, Yoxall A, Begum N, Katan M, et al. 2019. Frequent and persistent PLCG1 mutations in Sézary cells directly enhance PLCγ1 activity and stimulate NFκB, AP-1 and NFAT signaling. *Society for Investigative Dermatology.*

Pérez C., González-Rincón J, Onaindia A, Almaráz C, García-Díaz N, Pisonero H, Curiel-Olmo S, Gómez S, Cereceda L, Madureira R, et al. 2015. Mutated JAK kinases and deregulated STAT activity are potential therapeutic targets in cutaneous T-cell lymphoma. *Haematologica.* 100(11). doi:10.3324/haematol.2015.132837.

Pérez Cristina, González-Rincón J, Onaindia A, Almaráz C, García-Díaz N, Pisonero H, Curiel-Olmo S, Gómez S, Cereceda L, Madureira R, et al. 2015. Mutated JAK kinases and deregulated STAT activity are potential therapeutic targets in cutaneous T-cell lymphoma. *Haematologica.* 100(11):e450–e453. doi:10.3324/haematol.2015.132837.

Pérez C, Mondéjar R, García-Díaz N, Cereceda L, León A, Montes S, Durán Vian C, Pérez Paredes MG, González-Morán A, Alegre de Miguel V, et al. 2019. Advanced-stage Mycosis Fungoides. Role of STAT3, NFκB and NFAT pathways. *Br J Dermatol.:*bjd.18098. doi:10.1111/bjd.18098.

- Phetsouphanh C, Kelleher AD. 2015. The role of PKC- θ in CD4⁺ T cells and HIV infection: To the nucleus and back again. *Front Immunol.* 6(JUL). doi:10.3389/fimmu.2015.00391.
- Pimpinelli N, Olsen EA, Santucci M, Vonderheid E, Haeffner AC, Stevens S, Burg G, Cerroni L, Dreno B, Glusac E, et al. 2005. Defining early mycosis fungoides. *J Am Acad Dermatol.* 53(6):1053–1063. doi:10.1016/j.jaad.2005.08.057.
- Prasad A, Rabionet R, Espinet B, Zapata L, Puiggros A, Melero C, Puig A, Sarria-Trujillo Y, Ossowski S, Garcia-Muret MP, et al. 2016. Identification of Gene Mutations and Fusion Genes in Patients with Sézary Syndrome. *J Invest Dermatol.* 136(7):1490–1499. doi:10.1016/J.JID.2016.03.024.
- Prince HM, Kim YH, Horwitz SM, Dummer R, Scarisbrick J, Quaglino P, Zinzani PL, Wolter P, Sanches JA, Ortiz-Romero PL, et al. 2017. Brentuximab vedotin or physician's choice in CD30-positive cutaneous T-cell lymphoma (ALCANZA): an international, open-label, randomised, phase 3, multicentre trial. *Lancet.* 390(10094):555–566. doi:10.1016/S0140-6736(17)31266-7.
- Querfeld C, Rosen ST, Kuze TM, Kirby KA, Henry H, Roenigk J, Prinz BM, Guitart J. 2005. Long-term Follow-up of Patients With Early-Stage Cutaneous T-Cell Lymphoma Who Achieved Complete Remission With Psoralen Plus UV-A Monotherapy. *Arch Dermatol.* 141:305–311. doi:10.1001/archpedi.161.4.356.
- Saed G, Fivenson DP, Naidu Y, Nickoloff BJ. 1994. Mycosis fungoides exhibits a Th1-type cell-mediated cytokine profile whereas sezary syndrome expresses a Th2-type profile. *J Invest Dermatol.* 103(1):29–33. doi:10.1111/1523-1747.ep12388985.
- Scarisbrick JJ, Quaglino P, Prince HM, Papadavid E, Hodak E, Bagot M, Servitje O, Berti E, Ortiz-Romero P, Stadler R, et al. 2018 Nov 25. The PROCLIP international registry of early-stage mycosis fungoides identifies substantial diagnostic delay in most patients. *Br J Dermatol.* doi:10.1111/bjd.17258.
- Shahmarvand N, Nagy A, Shahryari J, Ohgami RS. 2018. Mutations in the signal transducer and activator of transcription family of genes in cancer. *Cancer Sci.* 109(4):926–933. doi:10.1111/cas.13525.
- Sommer VH, Clemmensen OJ, Nielsen O, Wasik M, Lovato P, Brender C, Eriksen KW, Woetmann A, Kaestel CG, Nissen MH, et al. 2004. In vivo activation of STAT3 in cutaneous T-cell lymphoma. Evidence for an antiapoptotic function of STAT3. *Leukemia.* 18(7):1288–1295. doi:10.1038/sj.leu.2403385.
- Steinberg SF. 2008. Structural Basis of Protein Kinase C Isoform Function. *Physiol Rev.* 88(4):1341–1378. doi:10.1152/physrev.00034.2007.
- Sun Z, Arendt CW, Ellmeier W, Schaeffer EM, Sunshine MJ, Gandhi L, Annes J, Petrzilka D, Kupfer A, Schwartzberg PL, et al. 2000. PKC- θ is required for TCR-induced NF- κ B activation in mature but not immature T lymphocytes. *Nature.* 404(6776):402–407. doi:10.1038/35006090.
- Sutcliffe EL, Bunting KL, Qing He Y, Li J, Phetsouphanh C, Seddiki N, Zafar A, Hindmarsh EJ, Parish CR, Kelleher AD, et al. 2011. Chromatin-Associated Protein Kinase C- θ Regulates an Inducible Gene Expression Program and MicroRNAs in Human T Lymphocytes. *Mol Cell.* 41:704–719. doi:10.1016/j.molcel.2011.02.030.
- Takeda K, Komuro Y, Hayakawa T, Oguchi H, Ishida Y, Murakami S, Noguchi T, Kinoshita H, Sekine Y, Iemura S, et al. 2009. Mitochondrial phosphoglycerate mutase 5 uses alternate catalytic activity as a

BIBLIOGRAPHY

protein serine/threonine phosphatase to activate ASK1. *Proc Natl Acad Sci U S A.* 106(30):12301–5. doi:10.1073/pnas.0901823106.

Talpur R, Bassett R, Duvic M. 2008. Prevalence and treatment of *Staphylococcus aureus* colonization in patients with mycosis fungoides and Sézary syndrome. *Br J Dermatol.* 159(1):105–112. doi:10.1111/j.1365-2133.2008.08612.x.

Tan S-L, Zhao J, Bi C, Chen XC, Hepburn DL, Wang J, Sedgwick JD, Chintalacharuvu SR, Na S. 2006. Resistance to Experimental Autoimmune Encephalomyelitis and Impaired IL-17 Production in Protein Kinase C θ -Deficient Mice. *J Immunol.* doi:10.4049/jimmunol.176.5.2872.

Thomas SJ, Snowden JA, Zeidler MP, Danson SJ. 2015. The role of JAK/STAT signalling in the pathogenesis, prognosis and treatment of solid tumours. *Br J Cancer.* 113(3):365–371. doi:10.1038/bjc.2015.233.

Trautinger F, Eder J, Assaf C, Bagot M, Cozzio A, Dummer R, Gniadecki R, Klemke C-D, Ortiz-Romero PL, Papadavid E, et al. 2017. European Organisation for Research and Treatment of Cancer consensus recommendations for the treatment of mycosis fungoides/Sézary syndrome – Update 2017. *Eur J Cancer.* 77:57–74. doi:10.1016/J.EJCA.2017.02.027.

Turriziani B, Garcia-Munoz A, Pilkington R, Raso C, Kolch W, von Kriegsheim A. 2014. On-Beads Digestion in Conjunction with Data-Dependent Mass Spectrometry: A Shortcut to Quantitative and Dynamic Interaction Proteomics. *Biology (Basel).* 3(2):320–332. doi:10.3390/biology3020320.

Tuzova M, Richmond J, Wolpowitz D, Curiel-Lewandrowski C, Chaney K, Kupper T, Cruikshank W. 2015. CCR4 + T cell recruitment to the skin in mycosis fungoides: Potential contributions by thymic stromal lymphopoietin and interleukin-16. *Leuk Lymphoma.* 56(2):440–449. doi:10.3109/10428194.2014.919634.

Ungewickell A, Bhaduri A, Rios E, Reuter J, Lee CS, Mah A, Zehnder A, Ohgami R, Kulkarni S, Armstrong R, et al. 2015. Genomic analysis of mycosis fungoides and Sézary syndrome identifies recurrent alterations in TNFR2. *Nat Genet.* 47(9):1056–60. doi:10.1038/ng.3370.

Vantourout P, Hayday A. 2013. Six-of-the-best: unique contributions of $\gamma\delta$ T cells to immunology. *Nat Rev Immunol.* 13(2):88–100. doi:10.1038/nri3384.

Vaqué JP, Gómez-López G, Monsálvez V, Varela I, Martínez N, Pérez C, Domínguez O, Graña O, Rodríguez-Peralto JL, Rodríguez-Pinilla SM, et al. 2014. PLCG1 mutations in cutaneous T-cell lymphomas. *Blood.* 123(13):2034–2044. doi:10.1182/blood-2013-05-504308.P.L.O.-R.

Vermeer MH, van Doorn R, Dijkman R, Mao X, Whittaker S, van Voorst Vader PC, Gerritsen M-JP, Geerts M-L, Gellrich S, Söderberg O, et al. 2008. Novel and highly recurrent chromosomal alterations in Sézary syndrome. *Cancer Res.* 68(8):2689–98. doi:10.1158/0008-5472.CAN-07-6398.

Vermeer MH, van Doorn R, Dukers D, Bekkenk MW, Meijer CJ, Willemze R. 2001. CD8+ T cells in cutaneous T-cell lymphoma: expression of cytotoxic proteins, Fas Ligand, and killing inhibitory receptors and their relationship with clinical behavior. *J Clin Oncol.* 19(23):4322–9. doi:10.1200/JCO.2001.19.23.4322.

Villarino A V, Kanno Y, O'Shea JJ. 2017. Mechanisms and consequences of Jak-STAT signaling in the immune system. *Nat Immunol.* 18(4):374–384. doi:10.1038/ni.3691.

Vonderheid EC, Bernengo MG, Burg G, Duvic M, Heald P, Laroche L, Olsen E, Pittelkow M, Russell-

- Jones R, Takigawa M, et al. 2002. Update on erythrodermic cutaneous T-cell lymphoma: Report of the International Society for Cutaneous Lymphomas. *J Am Acad Dermatol*. 46(1):95–106. doi:10.1067/mjd.2002.118538.
- Waldmann TA, Chen J. 2017. Disorders of the JAK/STAT Pathway in T Cell Lymphoma Pathogenesis: Implications for Immunotherapy. *Annu Rev Immunol*. 35(1):533–550. doi:10.1146/annurev-immunol-110416-120628.
- Wang L, Ni X, Covington KR, Yang BY, Shiu J, Zhang X, Xi L, Meng Q, Langridge T, Drummond J, et al. 2015. Genomic profiling of Sézary syndrome identifies alterations of key T cell signaling and differentiation genes. *Nat Genet*. 47(12):1426–1434. doi:10.1038/ng.3444.
- Wang X, Chuang H-C, Li J-P, Tan T-H. 2012. Regulation of PKC- θ function by phosphorylation in T cell receptor signaling. *Front Immunol*. 3:197. doi:10.3389/fimmu.2012.00197.
- Watanabe R, Gehad A, Yang C, Scott LL, Teague JE, Schlapbach C, Elco CP, Huang V, Matos TR, Kupper TS, et al. 2015. Human skin is protected by four functionally and phenotypically discrete populations of resident and recirculating memory T cells. *Sci Transl Med*. 7(279). doi:10.1126/scitranslmed.3010302.
- Weiss A, Koretzky G, Schatzman RC, Kadlecsek T. 1991. Functional activation of the T-cell antigen receptor induces tyrosine phosphorylation of phospholipase C-gamma 1. *Proc Natl Acad Sci U S A*. 88(13):5484–8. doi:10.1073/pnas.88.13.5484.
- Wen Z, Zhong Z, Darnell JE. 1995. Maximal activation of transcription by stat1 and stat3 requires both tyrosine and serine phosphorylation. *Cell*. 82(2):241–250. doi:10.1016/0092-8674(95)90311-9.
- Werlen G, Jacinto E, Xia Y, Karin M. 1998. Calcineurin preferentially synergizes with PKC-theta to activate JNK and IL-2 promoter in T lymphocytes. *EMBO J*. 17(11):3101–11. doi:10.1093/emboj/17.11.3101.
- Werlen Guy, Jacinto E, Xia Y, Karin M. 1998. Calcineurin preferentially synergizes with PKC- θ to activate JNK and IL-2 promoter in T lymphocytes.
- Wilcox RA. 2016. A three-signal model of T-cell lymphoma pathogenesis. *Am J Hematol*. 91(1):113–122. doi:10.1002/ajh.24203.
- Wilcox RA. 2017. Cutaneous T-cell lymphomas: 2017 update on diagnosis, risk stratification, and management. *Annu Clin Updat Hematol Malig*. 92:1085–1102. doi:10.1002/ajh.25224.
- Wilcox RA, Wada DA, Ziesmer SC, Elsawa SF, Comfere NI, Dietz AB, Novak AJ, Witzig TE, Feldman AL, Pittelkow MR, et al. 2009. Monocytes promote tumor cell survival in T-cell lymphoproliferative disorders and are impaired in their ability to differentiate into mature dendritic cells. *Blood*. 114(14):2936–2944. doi:10.1182/blood-2009-05-220111.
- Willemze R, Cerroni L, Kempf W, Berti E, Facchetti F, Swerdlow SH, Jaffe ES. 2019. The 2018 update of the WHO-EORTC classification for primary cutaneous lymphomas. *Blood*. 133(16):1703–1714. doi:10.1182/blood-2018-11-881268.
- Willemze R, Jaffe ES, Cerroni L, Berti E, Swerdlow SH, Ralfkiaer E, Chimenti S, Duncan LM, Grange F, Harris NL, et al. 2005. WHO-EORTC classification for cutaneous lymphomas. *Hematology*. 105(10):3768–3785. doi:10.1182/blood-2004-09-3502.An.

BIBLIOGRAPHY

Willemze R, Kerl H, Sterry W, Berti E, Cerroni L, Chimenti S, Diaz-Peréz JL, Geerts ML, Goos M, Knobler R, et al. 1997. EORTC classification for primary cutaneous lymphomas: a proposal from the Cutaneous Lymphoma Study Group of the European Organization for Research and Treatment of Cancer. *Blood*. 90(1):354–71.

Willerslev-Olsen A, Krejsgaard T, Lindahl Lise M., Litvinov I V., Fredholm S, Petersen DL, Nastasi C, Gniadecki R, Mongan NP, Sasseville D, et al. 2016. Staphylococcal enterotoxin A (SEA) stimulates STAT3 activation and IL-17 expression in cutaneous T-cell lymphoma. *Blood*. 127(10):1287–1296. doi:10.1182/blood-2015-08-662353.

Willerslev-Olsen A, Krejsgaard T, Lindahl Lise M, Litvinov I V, Fredholm S, Petersen DL, Nastasi C, Gniadecki R, Mongan NP, Sasseville D, et al. 2016. Staphylococcal enterotoxin A (SEA) stimulates STAT3 activation and IL-17 expression in cutaneous T-cell lymphoma. *Blood*. 127(10):1287–96. doi:10.1182/blood-2015-08-662353.

Woollard WJ, Pullabhatla V, Lorenc A, Patel VM, Butler RM, Bayega A, Begum N, Bakr F, Dedhia K, Fisher J, et al. 2016. Candidate driver genes in Sézary syndrome: frequent perturbations of genes involved in genome maintenance and DNA repair. *Blood*. 127(26):blood-2016-02-699843. doi:10.1182/blood-2016-02-699843.

Yamaoka K, Saharinen P, Pesu M, Holt VET, Silvennoinen O, O'Shea JJ. 2004. The Janus kinases (Jaks). *Genome Biol*. 5(12). doi:10.1186/gb-2004-5-12-253.

Yoshimura A, Naka T, Kubo M. 2007. SOCS proteins, cytokine signalling and immune regulation. *Nat Rev Immunol*. doi:10.1038/nri2093.

Zackheim HS, Kashani-Sabet M, Amin S. 1998. Topical Corticosteroids for Mycosis Fungoides. *Arch Dermatol*. 134(8):949–954. doi:10.1001/archderm.134.8.949.

Zhang W, Zong CS, Hermanto U, Lopez-Bergami P, Ronai Z, Wang L-H. 2006. RACK1 recruits STAT3 specifically to insulin and insulin-like growth factor 1 receptors for activation, which is important for regulating anchorage-independent growth. *Mol Cell Biol*. 26(2):413–24. doi:10.1128/MCB.26.2.413-424.2006.

Zhou L, Chong MMW, Littman DR. 2009. Plasticity of CD4+ T Cell Lineage Differentiation. *Immunity*. 30(5):646–655. doi:10.1016/j.immuni.2009.05.001.

RESUMEN EN CASTELLANO

8. RESUMEN EN CASTELLANO

8.1 Introducción

El linfoma cutáneo de células T (LCCT de aquí en adelante) es un grupo de linfomas no Hodgkin caracterizado por la proliferación clonal de linfocitos T malignos CD4⁺ en la piel. Dentro de los LCCT clásicos, la Micosis Fungoides (MF) y el Síndrome de Sézary (SS) son los subtipos más comunes.

MF supone aproximadamente el 45% de los LCCT. Tiene un curso indolente con una progresión lenta a lo largo de los años. Puede presentarse en diferentes estadios, desde parches aislados hasta una mayor implicación de la piel con la aparición de placas y tumores, aunque también puede localizarse extracutáneamente cuando progresa a estadios más avanzados como por ejemplo en hígado o bazo. Tiene una prevalencia de 4.1 por millón de personas, mayor en hombres que en mujeres (con una ratio de hombre-mujer de 1.72) y en pacientes de piel negra (casi 6 por millón). MF afecta típicamente a adultos con una media de edad al diagnóstico de 55-60 años.

SS es un subtipo leucémico raro de LCCT. Está caracterizado por una eritrodermia, linfadenopatía generalizada, hiperqueratosis y la presencia de linfocitos T neoplásicos con el núcleo cerebriforme (llamados células de Sézary) en la piel, los nódulos linfáticos y la sangre periférica.

Aunque MF y SS son clasificadas como entidades separadas, actualmente se utiliza el mismo sistema de estadiaje para ambos subtipos, propuesto por la Sociedad Internacional de Linfomas Cutáneos (ISCL en inglés), y la Organización Europea para la Investigación y Tratamiento del Cáncer (EORTC). Este sistema está basado en la clasificación TNMB (en inglés T: tumor, N: nódulo linfático, M: metástasis y B: sangre) con la que se determina el

estadio del paciente desde IA hasta IVB. Los estadios IA, IB y IIA son estadios iniciales de la enfermedad, mientras que los estadios IIB, IIIA, IIIB, IVA₁, IVA₂ y IVB corresponden a enfermedad más avanzada.

MF puede resultar difícil de diagnosticar ya que los pacientes desarrollan características clínicas muy parecidas a enfermedades cutáneas benignas como por ejemplo la dermatitis, por lo que el diagnóstico final se basa en un conjunto de pruebas clínicas, histopatológicas, moleculares e inmunofenotípicas. Para el diagnóstico de SS también es necesario la demostración eventual de clonalidad linfocitaria en la piel y la sangre periférica. Mientras que el pronóstico de MF depende del estadio, concretamente el tipo de lesiones de la piel y su extensión o la presencia de linfocitos extracutáneamente, el pronóstico de SS es generalmente malo. La supervivencia media de MF es de 20 años mientras que la de SS solo 3.13 años.

Actualmente no hay tratamiento curativo para los pacientes con LCCT. El tratamiento de MF y SS es meramente paliativo y está enfocado a la mejora de los síntomas y la calidad de vida. La única excepción es el trasplante alogénico de células madre, el único tratamiento con intenciones curativas, aunque está restringido a un número muy limitado de pacientes generalmente jóvenes con baja carga tumoral y alto riesgo de progresar. La elección de tratamiento está adaptada al estadio, extensión de las lesiones, estado general del paciente y si han recibido tratamiento con anterioridad. En general, los estadios iniciales se tratan con terapias directas en la piel como corticosteroides tópicos, fototerapia o radioterapia localizada; mientras que las terapias sistémicas, como retinoides, quimioterapia o fotoféresis extracorpórea, se utilizan para estadios más avanzados. Debido a la falta de tratamientos curativos, se están estudiando numerosos tratamientos dirigidos contra moléculas esenciales para la supervivencia de los linfocitos malignos con resultados

prometedores. Algunos ejemplos son anticuerpos anti-CD30 y anti-CCR4, moléculas inhibitoras del control inmune, inhibidores de quinasas como PI3K y mTOR e inhibidores tópicos de la fosfatasa calcineurina (cuyo ensayo clínico se está realizando por el dermatólogo y colaborador Pablo Ortiz-Romero).

El origen del LCCT no está del todo claro. Actualmente los mecanismos inmunológicos y moleculares responsables de la formación del tumor están siendo estudiados en profundidad. Por un lado, se ha demostrado que MF y SS se originan de diferentes poblaciones de linfocitos T: mientras que SS tienen un fenotipo de linfocitos T de memoria capaces de circular entre la piel, los nódulos linfáticos y la sangre, características consistentes con las manifestaciones clínicas de este subtipo; los linfocitos que originan la MF tienen un fenotipo efector, quedando retenidos en la piel produciendo citoquinas inflamatorias capaces de atraer linfocitos T no malignos al microambiente tumoral, formando así las características placas y parches de este subtipo. Además, se ha descrito que en estadios tempranos de MF, estos linfocitos no malignos son de tipo colaborador 1 (Th1), mientras que en estadios avanzados y en SS tienen un fenotipo Th2, lo que facilitaría la progresión de la enfermedad. Esta progresión también se ha postulado que podría ser debida a un cambio en la expresión de quimiocinas e interleucinas tanto de las células tumorales como las que forman el microambiente tumoral.

Por otro lado, en los últimos años se ha descrito un gran número de alteraciones moleculares en los linfocitos que afectan generalmente a cinco procesos celulares o vías de señalización como i) regulación del ciclo celular, ii) señalización por JAK/STAT, iii) la vía de señalización de las quinasas MAPK, iv) señalización por TCR/NF- κ B y v) modificación de la cromatina; probablemente indicando la gran importancia de estos mecanismos para la formación del LCCT. Anteriormente en nuestro laboratorio se identificaron mutaciones

recurrentes (en el 21% de los pacientes) en el gen *PLCG1* (mutaciones con ganancia de función), una fosfolipasa efectora de la señalización del receptor de linfocitos T (TCR), y también en las quinasas JAK, más concretamente en JAK1 y JAK3, en un 15% de los pacientes, entre otros genes. Estas mutaciones fueron también validadas por otros estudios los cuales, además, identificaron amplificaciones recurrentes del gen *PRKCQ* (isoforma θ de las PKCs) en un 20-30% de los pacientes, aunque las consecuencias de estas alteraciones no han sido estudiadas en detalle. En conjunto, estos y otros estudios moleculares han revelado una serie de vías de señalización desreguladas con potencial de promover la proliferación, supervivencia y la diferenciación de los linfocitos T, y que nosotros creemos son importantes para el desarrollo y progresión de la enfermedad. En concreto, estas vías formarían parte de una red maligna de señalización que conducirían a la activación aberrante de mecanismos moleculares esenciales para el LCCT y serían: TCR-*PLCG1*, TNF/*PRKCQ* y JAK hacia la activación de los factores de transcripción NFAT, NF- κ B, y STATs respectivamente.

8.2 Hipótesis y objetivos

La hipótesis de esta tesis doctoral se basa en que la red maligna de mecanismos de señalización que se encuentran actuando por debajo de *PLCG1* conduce a la tumorigénesis y progresión del LCCT. Además, *PRKCQ* puede estar jugando un papel esencial en la activación de los factores de transcripción NFAT, NF- κ B y STAT promoviendo su potencial papel neoplásico.

Con el fin de analizar la interacción de los diferentes miembros de la red maligna de señalización y, más detalladamente, estudiar el papel de *PRKCQ* en esta enfermedad, se han planteado los siguientes objetivos:

1. Explorar el papel biológico de NFAT, NF- κ B y STAT y su potencial uso como biomarcadores para el diagnóstico de LCCT en una cohorte de pacientes.
2. Estudiar la actividad de NFAT, NF- κ B y STAT3 en modelos celulares.
3. Identificar proteínas que interaccionen con PRKCQ en célula de LCCT.
4. Investigar las implicaciones biológicas de la actividad de PRKCQ *in vivo*.
5. Determinar potenciales genes regulados por PRKCQ en células de LCCT.

8.3 Resultados y discusión

En el contexto de la red maligna de señalización mencionada anteriormente, se ha estudiado en una cohorte de 78 pacientes de MF la activación de los factores de transcripción que se encuentran por debajo de estas vías. Concretamente se ha estudiado, por inmunohistoquímica, la activación de NFAT, NF- κ B (tanto de la vía canónica como no canónica) y STATs (STAT1, 3 y 5) además de la amplificación del gen *PRKCQ* o la polisomía de la región del cromosoma donde se encuentra. Este análisis nos ha permitido identificar la fosforilación de STAT3 (P-STAT3) como potencial biomarcador de progresión ya que se ha encontrado más activado en aquellos pacientes con estadios avanzados (47% en estadios avanzados vs. 12% en estadios iniciales), lo que podría constituir una característica mecanística importante con implicaciones clínicas relevantes. A pesar de que esta observación ya ha sido descrita anteriormente, ha sido realizada en cohortes muy pequeñas lo que probablemente ha impedido una correlación estadística con los estadios de la enfermedad.

Es importante destacar que la presencia de una mayor activación de P-STAT3 en estadios avanzados no puede correlacionarse solo por la adquisición de mutaciones de JAKs, quinasas que se encuentran por encima de estos factores de transcripción, ya que estas

alteraciones solo han sido descritas en un 4% del total de casos analizados. Por lo tanto, actualmente se están estudiando posibles mecanismos alternativos que lleven a una activación de las STATs como por ejemplo una desregulación en la estimulación extracelular a través de citoquinas e interleucinas provenientes del microambiente tumoral (generalmente a través de JAK) o la señalización alterada de otras vías como TCR/PLCG1 (probablemente independientes de JAK).

Numerosos estudios, incluidos los de nuestro laboratorio, han revelado mutaciones en JAK1 y JAK3, pero la implicación biológica de estas mutaciones no ha sido estudiada. Para ello, en este trabajo se ha demostrado que la mutación Y654F en JAK1 induce una activación de la transcripción mediada por STAT3 y su fosforilación en el residuo Y705.

Debido a la desregulación observada en la vía JAK/STAT en estos pacientes, se ha estudiado el uso de inhibidores de las quinasas JAK como potencial tratamiento de LCCT. Actualmente pacientes con enfermedades autoinmunes y mieloproliferativas están siendo tratados con inhibidores de JAK, por lo que su uso en LCCT podría ser beneficioso. Para explorar esta posibilidad hemos estudiado el efecto del ruxolitinib, un inhibidor de JAK, en células de LCCT y hemos visto que este inhibidor tiene un efecto dosis-dependiente en la proliferación celular pero en cambio provoca un efecto moderado en la muerte celular. Por lo que bloquear esta vía de señalización podría inducir efectos citostáticos como un descenso de la síntesis de ADN en lugar de provocar efectos citotóxicos.

Como se ha descrito anteriormente, nuestro laboratorio identificó previamente mutaciones en PLCG1 en el 21% de los pacientes de LCCT. En este trabajo hemos confirmado que esta mutación tiene una ganancia de función debido al aumento de la transcripción mediada por los factores de transcripción NFAT y NF- κ B, factores ampliamente descritos por encontrarse por debajo de TCR/PLCG1. Además, a través del uso

de inhibidores específicos hemos descrito que la activación de NFAT es dependiente de la calcineurina, una enzima que activa NFAT, y de PRKCQ. Sin embargo, la activación de NF- κ B no parece estar mediada en gran parte por PRKCQ, a pesar de que está descrito que NF- κ B es un efector de las PKCs. A pesar de que este sorprendente resultado tendría que ser confirmado en células de LCCT, esta tesis doctoral se ha centrado en estudiar los mecanismos que conllevan a la activación de STAT3, ya que ha sido el único marcador que correlaciona con estadios avanzados de MF, al contrario que NF- κ B.

Para estudiar estos mecanismos, hemos analizado la vía de señalización de PLCG1 y el posible papel mediador de PRKCQ hacia la activación de STAT3. Tanto en células HEK-IL6 como en células de LCCT, hemos demostrado que STAT3 es activado por debajo de PLCG1, tanto de manera dependiente de las JAK como de manera independiente a través de PRKCQ. Además, el silenciamiento de PRKCQ a través de shRNAs inducibles, ha demostrado un efecto negativo tanto en la proliferación celular como en la fosforilación de STAT3 y su actividad transcripcional, lo que nos sugiere que PRKCQ podría estar jugando un papel importante en el control de procesos esenciales del LCCT a través de la activación de STAT3.

Para determinar qué proteínas podrían estar participando en esta activación de STAT3, realizamos un análisis del interactoma de PRKCQ a través de espectrofotometría de masas. Este abordaje nos ha permitido identificar un número de proteínas que interactúan con PRKCQ y que podrían estar activando STAT3 como por ejemplo ASK1, cuya interacción hemos validado por un método alternativo. ASK1 es una quinasa que se activa por encima de ERK1/2 y JNK1, las cuales ha sido descrita su interacción con STAT3. PGAM5, una fosfatasa que activa las quinasas ASK1, JNKs y p38MAPKs, también se ha visto que interactúa con PRKCQ; o RACK1 que activa ASK1 y además se ha descrito su interacción con JAK1 o STAT1/3 entre otras. Todas estas interacciones podrían estar contribuyendo a

la fosforilación y activación de STAT3 y, a falta de validarlas a través de métodos alternativos, podrían ser diana de terapia, así como proporcionar la base para desarrollar estrategias para el manejo de casos específicos de LCCT.

Por otro lado, el papel de PRKCQ en el LCCT ha sido también estudiado en un modelo *in vivo* de embriones de pollo a través de la implantación de células de MF con PRKCQ silenciado. Esta reducción de la expresión de PRKCQ ha afectado negativamente tanto al crecimiento del tumor primario como a la angiogénesis, la intravasación a los vasos sanguíneos y la metástasis a órganos distales como el pulmón o el hígado. Estos efectos también han sido observados cuando al tumor formado con células MF ha sido tratado con un inhibidor farmacológico específico para PRKCQ. Estos resultados refuerzan la idea de que PRKCQ podría ser un importante mediador del control de la tumorigénesis y la progresión de los LCCT.

Finalmente, para determinar qué genes podrían estar mediando estos procesos biológicos a través de PRKCQ, se ha realizado una secuenciación comparativa del ARN en células de LCCT deficientes para la expresión de PRKCQ. Después de un primer análisis, y a falta de validaciones, se han identificado una serie de genes significativamente desregulados como por ejemplo genes involucrados en el citoesqueleto de actina, genes asociados a la vía de señalización mediada por TNF/ NF- κ B y genes relacionados con la vía JAK/STAT.

En resumen, el trabajo realizado en esta tesis doctoral ha sido caracterizar, desde un punto de vista molecular y biológico, el papel y la interacción mecanística de algunos de los miembros de la red de señalización maligna propuesta como controladora de los procesos biológicos del LCCT. Además, desde un punto de vista traslacional, estos resultados: i) describen nuevos marcadores de diagnóstico del LCCT como STAT3, ii) propone abordajes novedosos para el desarrollo de terapias dirigidas, incluyendo inhibidores de la

calcineurina, PRKCQ o JAK utilizados tanto individualmente como en combinación y iii) identifica una serie de proteínas de interacción con PRKCQ y genes diana que podrían estar jugando un papel importante en esta enfermedad.

8.4 Conclusiones

1. STAT3 está significativamente más activado en pacientes con MF en estadio avanzado.
2. La activación de STAT3 puede producirse a través de múltiples mecanismos como la señalización de JAK, PLCG1 y PRKCQ:
 - a. A través de la mutación activante JAK1 Y654F.
 - b. Por debajo de la activación de PLCG1 y mediado por PRKCQ y/o JAK.
 - c. A través de la activación de PRKCQ, tanto de manera dependiente como independiente de la actividad de JAK.
3. La inhibición farmacológica específica de PRKCQ y JAK afecta a la proliferación celular de manera sinérgica y promueve la apoptosis.
4. PRKCQ interacciona con proteínas efectoras como ASK1, RACK1 y PGAM5, que podrían mediar la activación de STAT3.
5. PRKCQ es esencial para el desarrollo tumoral del LCCT, la intravasación y la metástasis.
6. El transcriptoma de PRKCQ revela nuevos genes diana como *LCP1*, *IL10* y *SOCS2*, que podrían potencialmente participar en los mecanismos malignos de LCCT.

ANNEXES

Annex 1. Proteins interacting with PRKCQ in starved HuT 78 cells. List of significantly proteins ($p < 0,05$) found interacting with PRKCQ in starved HuT 78 cells by mass spectrometry. The table includes proteins showing a fold change ≥ 2 in peptide abundance of non-targeting control (NTC) HuT 78 versus HuT 78 cells knocked down for PRKCQ (inducible short hairpin PRKCQ), as negative control, both starved for 2 h and treated with control vehicle. PRKCQ is highlighted in bold.

Protein IDs	Protein name	Gene names	Fold change (NTC vs. shPRKCQ)	p value (t-test)
Q99683	Mitogen-activated protein kinase kinase kinase 5	MAP3K5	2461725	0.001077381
Q08554	Desmocollin-1	DSC1	2336325	0.005851605
E5RIW3	Tubulin-specific chaperone A	TBCA	1769295	0.004142811
Q9Y6N5	Sulfide:quinone oxidoreductase	SQRDL	1231175	9.75822E-08
F1T0B3	ATP-dependent RNA helicase DDX1	DDX1	715035.25	0.039567974
F5H8D7	DNA repair protein XRCC1	XRCC1	682090.25	0.031776565
Q04759	Protein kinase C theta	PRKCQ	22.24856006	3.04375E-05
Q9ULD5	Zinc finger protein 777	ZNF777	10.37721926	0.020092261
Q15056	Eukaryotic translation initiation factor 4H	EIF4H	8.049541801	0.006357335
Q15046	Lysine--tRNA ligase	KARS	6.943062873	0.001240356
P13796	Plastin-2	LCP1	6.910884582	0.048287157
P10606	Cytochrome c oxidase subunit 5B	COX5B	6.410414667	0.024993365
H0YM70	Proteasome activator complex subunit 2	PSME2	6.357235864	0.002503926
I3L1P8	Mitochondrial 2-oxoglutarate/malate carrier protein	SLC25A11	6.326229688	0.003845903
K7EMZ9	Protein LSM14 homolog A	LSM14A	6.074080498	0.012416837
Q12904	Aminoacyl tRNA synthase complex-interacting multifunctional protein 1	AIMP1	5.540481409	0.008661107
F5H1M8	Protein-L-isoaspartate O-methyltransferase domain-containing protein 1	PCMTD1	4.724995259	0.002092984
A0A140T9Z4	HLA class I histocompatibility antigen	HLA-B	4.100228553	0.020514832
C9JRZ6	MICOS complex subunit MIC19	CHCHD3	4.075644027	0.005030918
M0QYZ0	Heterogeneous nuclear ribonucleoprotein U-like protein 1	HNRNPUL1	4.036925719	0.012430385
P14868	Aspartate-tRNA ligase	DARS	3.886434618	0.0065828
Q9UHD8	Septin-9	SEPT9	3.857295839	0.009021613
S4R456	40S ribosomal protein S15	RPS15	3.676418164	0.0164265
Q96HS1	Serine/threonine-protein phosphatase PGAM5	PGAM5	3.302332839	0.008605287
P78527	DNA-dependent protein kinase catalytic subunit	PRKDC	3.259533875	0.035373215
P31146	Coronin-1A	CORO1A	3.259485463	0.001231769
E7EU96	Casein kinase II subunit alpha 3	CSNK2A1	3.162883574	0.000277277
P07814	Bifunctional glutamate/proline-tRNA ligase	EPRS	3.059275635	0.006225407
H7C2W1	D-beta-hydroxybutyrate dehydrogenase	BDH1	3.056083086	0.026065921

ANNEXES

B1AMS2	Septin-6	SEPT6	2.959891099	0.027355989
Q14257	Reticulocalbin-2	RCN2	2.904697959	0.004131998
P54136	Arginine--tRNA ligase	RARS	2.83854658	0.005386576
F8WDS9	LanC-like protein 1	LANCL1	2.800149018	0.003383402
P62273	40S ribosomal protein S29	RPS29	2.771622333	0.032204729
P26038	Moesin	MSN	2.728533998	0.000558371
A2NJV5	Immunoglobulin kappa variable 2-29	IGKV2-29	2.713965347	0.00447154
Q9H6R7	WD repeat and coiled-coil-containing protein C2orf44	C2orf44	2.504336328	0.000202718
P14923	Junction plakoglobin	JUP	2.465707921	0.004043865
F1T011	Protein transport protein Sec16A	SEC16A	2.4179183	0.010408321
P26583	High mobility group protein B2	HMGB2	2.340773329	0.043471029
Q5H8X8	Urotensin-2	UTS2	2.307916458	9.55283E-05
P47914	60S ribosomal protein L29	RPL29	2.256817949	0.012385994
B9A067	MICOS complex subunit MIC60	IMMT	2.256264867	0.005327345
J3KR24	Isoleucine--tRNA ligase	IARS	2.252026666	0.00641985
A0A087WXM6	60S ribosomal protein L17	RPL17	2.239674605	0.027412913
P31948	Stress-induced-phosphoprotein 1	STIP1	2.215720623	0.042911806
F6S8N6	Protein-L-isoaspartate O-methyltransferase	PCMT1	2.2097106	0.007389246
P20340	Ras-related protein Rab-6A	RAB6A	2.197290039	0.045468174
B1AN99	Trypsin-3	PRSS3	2.181494078	0.008041391
P11021	78 kDa glucose-regulated protein	HSPA5	2.100940031	1.22396E-06
P05455	Lupus La protein	SSB	2.099525472	0.043822648
R4GMY8	Transcription elongation factor B polypeptide 1	TCEB1	2.063062407	0.000162119
P17066	Heat shock 70 kDa protein 6	HSPA6	2.059406514	0.000121144
P35908	Keratin	KRT2	2.058704203	0.000853763
E9PK01	Elongation factor 1-delta	EEF1D	2.038162011	0.019854821
P38646	Stress-70 protein	HSPA9	2.032543554	0.000429743
F8W7C6	60S ribosomal protein L10	RPL10	2.023733857	0.019093706
F8WAG1	Ras-related protein Rab-17	RAB17	2.005239091	0.000497343

Annex 2. Proteins interacting with PRKCQ in TPA-stimulated HuT 78 cells. List of significantly proteins ($p < 0,05$) found interacting with PRKCQ in TPA-stimulated HuT 78 cells by mass spectrometry. The table includes proteins showing a fold change ≥ 2 in peptide abundance of non-targeting control (NTC) HuT 78 versus HuT 78 cells knocked down for PRKCQ (inducible short hairpin PRKCQ), as negative control, both starved for 2 h and treated with TPA (10 ng/ml) for 1 h. PRKCQ is highlighted in bold.

Protein IDs	Protein name	Gene names	Fold change (NTC vs. shPRKCQ)	p value (t-test)
Q04759	Protein kinase C theta	PRKCQ	7786500	0.049939003
H7BZJ3	Protein disulfide-isomerase A3	PDIA3	2075350.25	0.037523783
P36542	ATP synthase subunit gamma, mitochondrial	ATP5C1	2041675	4.20679E-05
Q9UHD8	Septin-9	SEPT9	1627300.25	0.046678388
K7EMN2	6-phosphogluconate dehydrogenase, decarboxylating	PGD	1245575.25	0.033672934
Q99683	Mitogen-activated protein kinase kinase kinase 5	MAP3K5	1126850.25	0.027793451
G3V3U4	Proteasome subunit alpha type	PSMA6	787645.25	0.044456677
O15144	Actin-related protein 2/3 complex subunit 2	ARPC2	598897.75	0.033849071
P31939	Bifunctional purine biosynthesis protein PURH	ATIC	13.80229174	0.043042697
P32119	Peroxiredoxin-2	PRDX2	5.469118276	0.038264499
A0A0A0MRZ8	Ig kappa chain V-III region VG	IGKV3D-11	4.383148567	0.049987987
P34897	Serine hydroxymethyltransferase, mitochondrial	SHMT2	2.581351703	0.040112381
F8W7C6	60S ribosomal protein L10	RPL10;RPL10L	2.330020289	0.043043936
P63244	Guanine nucleotide-binding protein subunit beta-2-like 1	GNB2L1	2.27296519	0.011302741

Annex 3. Gene expression changes upon PRKCQ knockdown in MyLa and HuT 78 cells. mRNA levels of whole transcriptome were determined by RNA sequencing. The table includes genes showing significant differential expression (blue, down-regulated, red: up-regulated) upon inducible PRKCQ knockdown in MyLa and HuT 78 cells treated with control vehicle for 24 h. PRKCQ gene is highlighted in bold.

MyLa (NTC vs shPRKCQ) - Vehicle			HuT 78 (NTC vs shPRKCQ) - Vehicle		
Gene	Fold change	p value	Gene	Fold change	p value
FGFR1	-5.12	1.9645E-74	MPO	-6.53	2.3136E-04
PRKACB	-2.62	1.6988E-32	GOLGA8G	-5.84	4.9626E-03
PRKCQ	-2.47	1.0619E-07	CD27	-5.60	8.8265E-03
NRCAM	-1.50	5.7992E-03	CHRNA2	-5.27	4.8963E-03
COL5A2	-1.29	3.8563E-02	NLRP2	-4.72	1.3488E-31
CU634019.1	-1.26	5.4645E-03	FAM163A	-4.62	1.8152E-02
HIGD2A	-1.23	7.3073E-04	NLRP7	-4.37	2.9259E-14
DUSP6	-1.17	3.5559E-04	AZGP1	-4.31	8.2983E-07
LCP1	-1.08	1.2680E-15	SRL	-4.19	1.5573E-11
AC008012.1	-1.05	1.3589E-04	DNAJC5B	-4.05	3.1545E-19
ARL6IP6	-1.03	4.9260E-03	ATAD3C	-3.98	4.2950E-05
ADA2	-1.00	1.1571E-04	ABHD8	-3.55	3.5739E-07
MSMO1	-0.96	1.8047E-04	ROBO1	-3.46	1.0725E-02
LDLRAD3	-0.96	2.0952E-07	ALOX12P2	-3.44	4.6747E-08
ULK4	-0.93	3.8174E-02	SEZ6L	-3.36	3.1742E-04
ST3GAL1	-0.92	9.3963E-03	SPATC1L	-3.30	1.1602E-02
SUCLG2	-0.88	1.9093E-14	SLC6A9	-3.13	1.3119E-04
LIMK1	-0.86	3.2510E-03	CA6	-2.93	4.3807E-08
MCFD2	-0.84	3.7649E-14	KIAA1324L	-2.91	4.5111E-16
DHCR7	-0.82	5.7992E-03	CXCR5	-2.90	3.3258E-02
PPP2R1B	-0.80	8.6198E-11	RORA	-2.89	3.2539E-06
METTL9	-0.79	8.3790E-15	NRCAM	-2.89	6.1990E-03
PCYT1A	-0.76	2.4281E-18	DOK3	-2.81	3.6966E-18
PKIA	-0.73	5.3473E-04	UBBP4	-2.80	9.9352E-25
SCD	-0.72	4.7069E-02	GAS6	-2.76	1.4860E-03
VKORC1	-0.72	2.9384E-05	MTUS1	-2.72	1.7934E-02
EPB41L4B	-0.72	5.5782E-03	SUCNR1	-2.68	2.4160E-08
RBM47	-0.67	1.1971E-02	RYR2	-2.62	3.2591E-10
FAM107B	-0.67	1.3659E-08	UNC13C	-2.59	7.0698E-03
UBXN8	-0.62	2.1708E-02	GALNT9	-2.57	2.1967E-02
TAB3	-0.62	8.4631E-04	TREX1	-2.46	4.6553E-02
OSBP	-0.62	2.0484E-06	PKHD1	-2.44	2.1220E-02
TMEM230	-0.58	1.9115E-06	SATB1	-2.34	2.5286E-05
RFLNB	-0.58	2.8262E-04	BIRC7	-2.26	5.9406E-03
CELF2	-0.57	1.3188E-02	ABCA12	-2.25	1.5421E-03
GTF2E2	-0.57	5.8044E-03	TNFRSF25	-2.23	1.4606E-06
B4GALT1	-0.56	1.0652E-03	NME4	-2.13	3.8058E-02
AGRN	-0.56	4.9643E-02	POU2AF1	-2.03	1.2075E-04
AC010422.8	-0.55	3.7366E-02	NUAK1	-2.02	2.1062E-06
ETS1	-0.54	2.2709E-10	NT5E	-2.00	1.8010E-03
NFATC2	-0.54	4.8014E-02	CDK6	-1.87	4.2633E-02
SEMA4B	-0.53	6.6056E-03	PRKCQ	-1.83	3.6966E-18
BCL9	-0.53	1.5663E-04	PDE6G	-1.83	7.9641E-05

EAFF1	-0.51	9.2318E-05	ENPEP	-1.79	5.9406E-03
GMFB	-0.51	4.9260E-03	PTK7	-1.78	1.1530E-05
FBXW7	-0.50	2.3174E-02	APOC2	-1.78	2.0642E-02
IDH1	-0.50	3.9287E-07	LDLRAD3	-1.76	9.8904E-13
ELL2	-0.50	4.3609E-02	CHD5	-1.76	1.8824E-02
KIRREL2	-0.48	4.1954E-02	SERPINF1	-1.73	8.2523E-03
TMC8	-0.47	2.3927E-02	IRF6	-1.71	4.3199E-02
ADAM19	-0.47	5.4645E-03	ACPP	-1.69	1.3491E-02
RPP21	-0.46	4.8398E-02	SPIB	-1.66	3.0202E-03
LIMA1	-0.46	9.3963E-03	OLFML2A	-1.61	3.5498E-02
ARID3B	-0.45	4.0987E-02	RHOXF1-AS1	-1.60	1.1276E-03
FAF2	-0.45	4.8372E-02	ACOXL	-1.60	1.2957E-04
SLFN13	-0.45	7.0760E-03	ALDH1A3	-1.54	8.6014E-06
CCDC32	-0.45	4.5626E-03	GSDMA	-1.53	4.3695E-02
SRXN1	-0.44	3.0841E-02	GRB7	-1.52	2.5599E-02
CCDC28A	-0.43	2.7436E-02	ACE	-1.48	1.3291E-03
TMEM33	-0.40	7.3922E-03	STAR	-1.44	7.2641E-03
PTPN18	-0.40	1.1971E-02	CBFA2T3	-1.41	6.7867E-03
FADS1	-0.38	2.0798E-02	PPP1R1B	-1.40	2.3840E-09
SCOC	-0.38	2.3927E-02	SLC35F3	-1.38	5.9406E-03
SFXN1	-0.38	9.9118E-03	CACNA1E	-1.38	2.3296E-03
SCYL3	-0.37	9.9118E-03	RYR1	-1.37	3.8092E-02
UBALD2	-0.37	3.5684E-02	YBX2	-1.36	1.1606E-03
BLOC1S2	-0.37	1.1267E-02	LGALS9C	-1.34	2.4117E-04
SMC1A	-0.37	3.3445E-06	ARHGEF40	-1.29	4.8711E-03
ERLIN2	-0.36	9.5233E-03	APOD	-1.28	2.1255E-02
PANX1	-0.36	3.0841E-02	GJC1	-1.28	4.9245E-02
AHR	-0.35	5.7306E-03	CD79B	-1.28	2.0724E-02
FNDC3B	-0.34	2.6736E-03	CRACR2B	-1.26	1.8538E-03
FNIP2	-0.34	1.4674E-03	LRRC18	-1.25	4.2047E-02
GID4	-0.34	1.3638E-02	FERMT2	-1.23	2.3423E-02
DGCR2	-0.33	3.0076E-03	INAVA	-1.22	3.1513E-02
SLC50A1	-0.33	1.0652E-03	JAG1	-1.20	8.8164E-08
CASK	-0.33	1.2380E-04	GRASP	-1.19	3.8898E-02
ANKRD13C	-0.33	1.1661E-02	AC019117.2	-1.19	1.8824E-02
TNRC6A	-0.32	1.1611E-02	PTPN14	-1.18	8.5723E-05
SENP1	-0.31	7.0760E-03	ENPP1	-1.15	9.7717E-04
COPS7B	-0.31	2.3927E-02	NHSL2	-1.15	3.7035E-02
ZBTB7A	-0.31	8.1321E-03	NKX2-5	-1.14	3.7064E-02
JPT2	-0.28	3.4377E-02	LOXL1	-1.13	2.3263E-02
AIM2	-0.27	3.7366E-02	BEGAIN	-1.13	9.0581E-05
HACD2	-0.27	3.1794E-02	LTBP1	-1.12	1.6223E-02
OS9	-0.26	8.8647E-03	RAPGEF3	-1.10	1.8824E-02
CPNE8	-0.26	4.3257E-02	FGFR3	-1.09	4.1667E-03
CDC23	-0.25	4.9926E-02	PTGER2	-1.08	4.6908E-02
TM7SF3	-0.24	1.1051E-02	DUSP15	-1.08	5.4879E-03
SPTLC2	-0.24	2.3927E-02	RHOBTB1	-1.07	9.0903E-05
TEX264	-0.24	3.9521E-02	FZD7	-1.06	3.5888E-02
GAK	-0.22	3.0904E-02	EPAS1	-1.05	1.0725E-02
GLO1	0.20	7.3922E-03	MROH6	-1.04	1.7094E-02
WDR48	0.25	7.1709E-03	NTN1	-1.04	9.1828E-04

ANNEXES

CRLF3	0.28	2.9071E-02	HMOX1	-1.03	2.1246E-02
ELMO1	0.28	4.8987E-02	TRIO	-1.00	3.1779E-02
SUB1	0.28	9.3963E-03	LAMA4	-1.00	3.1299E-05
MINDY3	0.28	1.0227E-02	CD244	-0.99	4.2633E-02
ANXA1	0.28	2.3927E-02	IQSEC3	-0.99	2.7026E-02
WDR44	0.28	3.4377E-02	CD81	-0.99	7.0887E-03
ATG13	0.29	2.0798E-02	PTPRG	-0.98	1.6223E-02
SPAST	0.29	1.8400E-02	F2RL3	-0.96	5.4879E-03
RAB11FIP1	0.29	7.3748E-06	RASA4B	-0.95	6.3325E-03
WDR26	0.29	2.3927E-02	SIM1	-0.95	3.3258E-02
KIAA0232	0.30	4.7226E-02	FAR2P1	-0.95	1.8824E-02
LAPTM5	0.30	7.8922E-03	DAB2IP	-0.94	7.7901E-05
GPSM3	0.31	1.2455E-02	DERL3	-0.94	1.4132E-02
CHMP7	0.31	4.8036E-02	LAT2	-0.91	4.5767E-02
NKIRAS2	0.31	2.1881E-03	FHDC1	-0.91	1.2731E-02
PPP3R1	0.31	5.6168E-04	STS	-0.88	1.1276E-03
ARL2BP	0.32	3.9247E-02	TIMP2	-0.87	2.0204E-06
MAP4K4	0.32	1.8526E-02	KIAA1211	-0.83	3.3258E-02
SLC35D1	0.32	1.8526E-02	PFKFB2	-0.83	1.8824E-02
PHYH	0.32	6.5624E-03	AC136475.9	-0.80	3.5863E-02
COMMD8	0.33	2.1769E-02	RASA4	-0.79	7.2746E-03
PRKY	0.33	5.4690E-03	ZNF618	-0.79	5.7229E-04
SLC20A1	0.34	2.1873E-04	PLXNB2	-0.75	1.8538E-03
HSDL1	0.34	2.9615E-02	NFATC2	-0.75	4.7587E-02
ZNF581	0.34	3.6427E-02	SPRYD3	-0.73	1.0725E-02
TRUB1	0.34	3.2478E-02	PLXND1	-0.72	3.5498E-02
UBA3	0.35	2.5617E-03	ISYNA1	-0.72	4.3199E-02
MMGT1	0.35	1.1111E-03	LYN	-0.68	9.2249E-03
CAMSAP2	0.35	1.8349E-03	SLC12A7	-0.68	2.1967E-02
SOD2	0.35	1.1611E-02	GREB1	-0.68	3.5545E-04
AMFR	0.36	2.1955E-02	PALLD	-0.66	4.2187E-02
VOPP1	0.36	2.8262E-04	HSH2D	-0.66	2.7352E-02
DVL3	0.37	5.6494E-06	CCDC90B	-0.66	1.1396E-02
FAM69A	0.37	4.3609E-02	PHF7	-0.65	3.7064E-02
KDM5D	0.37	1.1661E-02	TMEM245	-0.64	2.0642E-02
TRAFD1	0.37	1.1179E-02	CABIN1	-0.63	2.7004E-05
OSBPL8	0.37	3.5371E-06	CDC42EP3	-0.63	3.5863E-02
ORMDL3	0.38	2.0287E-05	MLC1	-0.61	4.3199E-02
BTG3	0.38	9.5807E-06	HIPK2	-0.60	3.3258E-02
ERC1	0.38	3.1794E-02	PPT2	-0.59	4.7667E-02
GOPC	0.40	2.1349E-04	NUP50	-0.59	1.1684E-03
MPI	0.40	2.0484E-06	SH3BP1	-0.56	2.5972E-02
CDCA4	0.40	2.3927E-02	NOTCH1	-0.56	1.1396E-02
SNX7	0.41	7.8955E-07	RHOBTB2	-0.56	5.4462E-03
ZNF182	0.41	3.8563E-02	TMEM120B	-0.54	4.8383E-02
PAQR3	0.41	2.1708E-02	GINM1	-0.50	5.5456E-04
EVI5	0.41	3.0308E-02	ZCCHC3	-0.47	1.3491E-02
MACO1	0.43	5.6494E-06	MTHFD2	-0.45	3.2433E-02
ATXN10	0.43	2.3692E-03	ATXN7L3	-0.45	4.6553E-02
NUP58	0.44	3.6590E-02	VPS4A	-0.43	2.7641E-02
RNF19B	0.44	1.9610E-02	APOBEC3F	-0.41	4.3847E-02

RCOR1	0.44	4.0987E-02	BCR	-0.39	3.1513E-02
ZSWIM1	0.45	4.8858E-02	ATP9A	-0.38	4.1120E-02
C5orf24	0.45	9.9118E-03	EMILIN2	-0.35	4.6908E-02
BAZ2A	0.45	3.3117E-04	LASP1	-0.31	3.5498E-02
CLOCK	0.45	1.7073E-05	STXBP1	0.64	4.3199E-02
PPP1R3F	0.46	1.3076E-03	TMEM136	0.82	4.9561E-02
CREBL2	0.46	7.1054E-07	MYO18B	0.84	8.8671E-03
LSP1	0.46	2.4292E-04	KIR2DL3	0.87	1.7723E-02
MEF2D	0.47	6.6056E-03	ECHDC2	0.88	5.0180E-03
PDE7A	0.47	7.0760E-03	RHOU	0.91	1.7958E-04
IFIH1	0.47	1.8349E-03	C15orf38-AP3S2	0.94	4.3199E-02
DUSP10	0.48	1.9888E-09	NCALD	0.95	1.6616E-03
TRIM23	0.49	7.2006E-03	C16orf45	0.97	1.3941E-02
TRBV6-5	0.49	1.9041E-02	SYT11	1.04	2.5972E-02
YPEL5	0.50	1.7600E-07	TCEAL4	1.06	8.8265E-03
HIPK1	0.51	2.6113E-06	PKIB	1.15	4.3695E-02
CHIC1	0.51	1.9028E-02	KIR3DL1	1.19	1.1555E-03
TRIM37	0.52	1.2155E-05	ARFGEF3	2.14	1.4364E-07
SPIRE1	0.53	5.6783E-03	PEG10	2.36	4.9306E-08
SDC4	0.53	1.2463E-02	STMND1	2.70	2.5186E-05
RPS4Y1	0.53	2.3927E-02	MT-RNR1	2.97	1.2548E-03
GDF11	0.55	1.8623E-03	SNORD17	3.01	5.9406E-03
SH3KBP1	0.57	1.1971E-02	SGCE	3.24	1.8538E-03
RDX	0.58	2.0932E-02	HIST1H4J	3.30	6.1529E-03
CD79A	0.60	3.7232E-03	FAT4	4.79	3.6124E-03
RNF11	0.61	7.9841E-22	SNORD3A	5.22	5.0180E-03
KSR1	0.62	3.7649E-14	RN7SK	5.65	2.2159E-04
ERO1B	0.63	7.3922E-03	CCNA1	5.66	5.6050E-03
AGPAT4	0.63	9.9079E-03	RNA5-8SN2	6.77	1.0649E-05
ZFY	0.63	2.1352E-12	RNA5-8SN2	6.77	1.0649E-05
ORAI2	0.63	4.3257E-02	RNA5-8SN2	6.77	1.0649E-05
MAP3K4	0.64	1.3222E-02	RNA5-8SN2	6.77	1.0649E-05
CLIP2	0.64	1.7693E-04	RNA5-8SN2	6.77	1.0649E-05
PIM3	0.67	1.9196E-03	RNA5-8SN4	6.77	1.0649E-05
IRX3	0.68	4.8372E-02	RNA5-8SN2	6.77	1.0649E-05
CHST7	0.68	1.1661E-02	RNA5-8SN2	6.77	1.0649E-05
APBB1	0.69	3.0700E-03	RPPH1	6.88	4.0451E-06
TTY15	0.71	3.0700E-03			
LY6E	0.71	1.2535E-03			
STX6	0.72	2.4292E-04			
KLHL5	0.76	3.0700E-03			
NRAV	0.76	6.2529E-03			
KLHDC7B	0.77	2.7101E-02			
MRFAP1	0.78	6.5274E-09			
TMOD1	0.79	3.0245E-05			
SAMSN1	0.80	5.3997E-06			
RIMS3	0.80	2.1180E-02			
FREM2	0.85	1.2463E-02			
MYRF	0.86	2.5156E-02			
COL4A6	0.88	1.8069E-02			
CAPSL	0.93	1.8349E-03			

ANNEXES

RGS12	0.97	4.4670E-06
CACNA1E	0.98	2.0750E-09
AL139393.2	1.06	1.1661E-02
SPINK5	1.16	1.8349E-03
CACNB4	1.17	1.5814E-04
OASL	1.17	2.7482E-03
TCF7	1.25	6.3881E-07
PIK3R5	1.27	4.0455E-09
IFIT3	1.29	7.8955E-07
ISG15	1.31	3.1716E-08
GBP4	1.33	5.0809E-07
RNF38	1.35	4.6866E-11
AP3B2	1.39	2.3927E-02
JPH4	1.39	1.8926E-03
ANKRD55	1.40	1.3638E-02
CFI	1.42	3.9486E-02
SERPINE1	1.45	5.7992E-03
LPA	1.50	3.4377E-02
NAV2	1.51	6.5736E-05
RASSF4	1.52	4.6597E-02
IGFBP2	1.57	1.3574E-03
BMF	1.58	7.6465E-08
IFIT1	1.61	4.1411E-03
LINC002481	1.64	1.2463E-02
LHX2	1.64	6.4474E-03
AUTS2	1.66	3.1051E-02
IFIT2	1.70	2.6797E-16
CSAG3	1.71	1.1232E-03
RARRES3	1.85	7.2006E-03
GBP2	1.87	7.8922E-03
DGKI	1.90	1.3638E-02
BCAS1	2.08	5.5169E-04
AC026904.1	2.11	1.0227E-02
IL6R	2.13	3.4045E-07
MPP4	2.21	4.8916E-02
CEACAM1	2.21	9.6657E-04
KCNJ18	2.25	4.1452E-05
KCNJ12	2.26	1.0969E-06
TEAD2	2.64	5.0516E-04
PLD1	2.73	4.8036E-02
CYP4F12	2.80	1.2463E-02
AP000547.3	2.90	4.2782E-02
S100P	3.01	2.6288E-02
PLA2G2F	3.71	7.4464E-07
IGHM	6.28	1.6833E-02

Annex 4. Gene expression changes upon PRKCQ knockdown in MyLa and HuT 78 cells. mRNA levels of whole transcriptome were determined by RNA sequencing. The table includes genes showing significant differential expression (blue, down-regulated, red: up-regulated) upon inducible PRKCQ knockdown in MyLa and HuT 78 cells treated with TPA (10 ng/ml) for 24 h. PRKCQ gene is highlighted in bold.

MyLa (NTC vs shPRKCQ) - TPA			HuT 78 (NTC vs shPRKCQ) - TPA		
Gene	Fold change	p value	Gene	Fold change	p value
FGFR1	-5.81	1.5641E-64	SEPT5-GP1BB	-5.90	1.9198E-02
PRKCQ	-2.84	1.7762E-10	SEZ6L	-4.76	6.6235E-03
PRKACB	-2.65	7.7668E-33	DNAJC5B	-4.70	1.1647E-13
CU634019.1	-1.54	1.0518E-03	ATAD3C	-4.11	3.5368E-03
LNCOC1	-1.36	3.8602E-02	AZGP1	-3.79	2.8100E-02
DHCR7	-1.26	1.9345E-06	NLRP2	-3.69	1.0208E-17
FBXO43	-1.16	3.7880E-02	MTUS1	-3.66	3.0275E-02
TMEM132D	-1.11	2.8270E-03	CDH17	-3.57	1.0936E-02
HIGD2A	-1.02	8.3508E-27	FAM163A	-3.51	1.8494E-04
KIF15	-1.01	4.9757E-04	PCA3	-3.34	1.7208E-04
ADA2	-1.00	1.3677E-04	RIMBP3B	-3.34	1.8602E-02
LINC00184	-0.99	2.5962E-02	NRCAM	-3.19	2.1946E-02
AURKB	-0.97	2.6687E-02	SRL	-3.14	8.9861E-03
SUCLG2	-0.97	2.1105E-17	SLC6A9	-2.94	2.0367E-03
ARL6IP6	-0.96	9.7373E-03	NLRP7	-2.81	5.4155E-03
GAS2L3	-0.95	3.3966E-03	UNC13C	-2.72	7.2576E-03
ST3GAL1	-0.94	5.3789E-03	NME4	-2.71	3.6912E-02
CIT	-0.94	5.7915E-04	PDE6G	-2.61	7.7909E-09
FAM72D	-0.93	3.8944E-02	ARHGAP29	-2.52	1.7263E-02
TMEM143	-0.91	1.1901E-02	ABHD8	-2.49	1.4422E-02
DEPTOR	-0.91	4.1327E-03	UBBP4	-2.38	1.0037E-16
MCIDAS	-0.90	1.3193E-05	RORA	-2.34	1.3129E-03
GPRIN3	-0.88	4.9833E-02	KIAA1324L	-2.23	7.7909E-09
SKA1	-0.88	1.0518E-03	FARP1	-2.16	2.5948E-02
KIF14	-0.87	1.3369E-04	SUCNR1	-2.06	1.7208E-04
LDLRAD3	-0.86	3.2044E-05	NUAK1	-2.01	3.2624E-06
LCP1	-0.86	8.3362E-10	KRT80	-2.00	4.7392E-05
MATK	-0.86	4.6291E-02	PTK7	-1.94	3.0619E-03
CYB5RL	-0.84	8.3826E-03	COL4A4	-1.89	3.6912E-02
MXD3	-0.81	1.6452E-02	SIM1	-1.81	1.9622E-06
GNMT2	-0.81	4.1758E-04	TNFRSF25	-1.75	1.3129E-03
RNF26	-0.80	1.4818E-02	NKX2-5	-1.75	9.4721E-05
CKAP2L	-0.80	1.5485E-03	IGFBP4	-1.71	1.8571E-03
TOP2A	-0.78	3.4429E-02	SPIB	-1.68	4.2707E-03
FAM86JP	-0.78	2.6249E-03	PRKCQ	-1.68	2.3601E-14
AC068831.7	-0.77	1.6420E-02	SLCO4C1	-1.67	4.7434E-03
AC112777.1	-0.77	2.1671E-02	POU2AF1	-1.64	1.1635E-02
FAM107B	-0.75	8.7888E-11	RHOXF1-AS1	-1.58	5.5074E-03
MCFD2	-0.75	3.4235E-11	IL10	-1.56	1.9622E-06
HASPIN	-0.75	6.3172E-04	FERMT2	-1.50	2.2955E-03
FAM72B	-0.73	2.5510E-02	ARHGEF40	-1.48	2.0825E-03
TCF19	-0.73	1.5920E-02	OLFML2A	-1.45	3.8475E-02
SGO1	-0.72	4.1363E-02	ACE	-1.43	3.9169E-02

ANNEXES

GPSM2	-0.70	4.3731E-04	GRASP	-1.43	1.0556E-03
TRAF3	-0.69	8.1740E-07	INAVA	-1.39	1.2364E-02
CAMK2N2	-0.68	3.4701E-02	CNKSR2	-1.39	3.9000E-02
RBM47	-0.68	8.6077E-03	DOK7	-1.38	8.6152E-03
LRG1	-0.68	1.0388E-02	CBFA2T3	-1.38	1.5692E-02
NFAM1	-0.67	1.8604E-02	CD79B	-1.37	3.9000E-02
TYMS	-0.67	2.0221E-02	DUSP15	-1.37	1.5407E-03
MSMO1	-0.66	3.0362E-02	LDLRAD3	-1.36	1.5495E-07
VKORC1	-0.65	2.7099E-04	BAHCC1	-1.35	7.2710E-05
MYH10	-0.65	3.4701E-02	ACOXL	-1.30	7.8268E-03
NUP210	-0.65	2.6562E-14	TIMP2	-1.30	7.6194E-12
DHRS2	-0.64	1.5553E-03	RYR2	-1.28	4.9242E-02
SLC37A4	-0.63	2.6687E-02	GJC1	-1.24	3.6245E-02
WDHD1	-0.63	3.1400E-02	ZNF91	-1.24	2.2411E-02
SEMA4B	-0.62	4.2948E-04	ADTRP	-1.23	4.3151E-03
H2AFX	-0.62	3.7261E-02	ZBTB46	-1.18	5.4155E-03
CPPED1	-0.62	1.6178E-03	RASSF4	-1.17	1.9243E-02
VEGFB	-0.62	1.7305E-02	SEMA3G	-1.16	1.1892E-03
PCYT1A	-0.62	6.5410E-12	SALL4	-1.12	1.7515E-02
AC091057.6	-0.62	2.4124E-02	CIITA	-1.12	3.7191E-02
METTL9	-0.61	2.0640E-08	ENPP1	-1.09	3.8199E-03
PRPF40B	-0.60	8.5219E-05	CORO1B	-1.08	4.2177E-03
ELL2	-0.60	4.0312E-03	DUSP4	-1.06	4.9494E-02
PPP2R1B	-0.60	1.1821E-05	CLIC5	-1.05	4.9699E-02
SCN11A	-0.59	8.3558E-03	C14orf132	-1.04	3.8389E-02
SIPA1	-0.57	6.7812E-04	NTN1	-1.02	3.3025E-03
BCL3	-0.57	4.3731E-04	DERL3	-1.01	2.2411E-02
LIMA1	-0.56	2.5473E-04	PPP1R1B	-1.00	3.8926E-03
CHST14	-0.56	1.1155E-03	SYNPO	-1.00	2.0914E-02
ULBP2	-0.54	6.5490E-03	EOMES	-1.00	5.1997E-06
POLD1	-0.54	2.2508E-03	PLEKHA3	-0.98	1.9621E-02
FNDC3B	-0.53	9.6004E-10	PLXNB2	-0.96	1.5214E-05
TBC1D31	-0.53	1.1547E-02	CD109	-0.94	2.9192E-02
FANCI	-0.53	4.2304E-04	TRABD2A	-0.94	4.4054E-02
LIMK2	-0.52	3.0718E-04	TSC2	-0.93	7.8268E-03
MPZ	-0.52	1.6284E-02	PALM	-0.90	3.4540E-02
IFT88	-0.52	3.2264E-02	FAR2P1	-0.89	4.4035E-02
TLE2	-0.52	3.1813E-02	KREMEN1	-0.87	1.8575E-02
KIRREL2	-0.52	1.4588E-02	HIPK2	-0.85	1.9465E-04
PRKAA1	-0.51	2.3056E-02	KREMEN2	-0.85	3.6245E-02
JADE3	-0.51	1.5824E-02	JAG1	-0.79	2.7973E-03
RGS18	-0.51	8.3084E-04	RASGEF1B	-0.79	1.9198E-02
SMC1A	-0.50	6.6887E-12	GLCCI1	-0.78	1.9198E-02
MAPK13	-0.50	1.5553E-03	ZNF618	-0.78	4.2355E-03
ETS1	-0.50	7.7313E-09	AGTRAP	-0.76	3.0710E-02
TMEM230	-0.50	1.6802E-04	NUP50	-0.75	7.2972E-06
RFLNB	-0.49	4.3252E-03	CCDC90B	-0.74	4.2177E-03
NSD2	-0.49	4.8962E-05	SPRYD3	-0.72	1.7263E-02
OSBP	-0.49	6.3172E-04	LSP1	-0.71	5.4155E-03
LMAN1	-0.47	6.8083E-03	PALLD	-0.69	3.4540E-02
TAB3	-0.47	2.4124E-02	LYN	-0.67	2.2411E-02

FBXO5	-0.47	1.6707E-02	ASB7	-0.64	1.3393E-02
NAAA	-0.47	1.1901E-02	TMEM245	-0.64	2.4780E-02
GAA	-0.47	1.5824E-02	CSF2RB	-0.63	6.2502E-04
RMI1	-0.46	4.0195E-02	CKAP4	-0.61	7.2576E-03
PRKRA	-0.46	8.7673E-03	EEF1E1	-0.61	4.3151E-03
C4orf46	-0.46	8.6077E-03	RHOBTB2	-0.59	3.8199E-03
RFX5	-0.46	4.2675E-03	CBX6	-0.56	2.8768E-02
PRIMPOL	-0.45	4.0900E-02	LGALS3	-0.56	4.5986E-02
RBL1	-0.45	3.1400E-02	ALKBH8	-0.55	4.5372E-02
MAD2L2	-0.45	2.4124E-02	HLA-DMB	-0.54	3.5642E-02
CENPL	-0.44	2.9554E-03	CABIN1	-0.51	4.3151E-03
FAF2	-0.44	4.6291E-02	EAF1	-0.50	1.3393E-02
BCL9	-0.43	4.8838E-03	CCDC32	-0.49	3.4540E-02
C19orf54	-0.42	6.9001E-04	RTL10	-0.47	4.0113E-02
SENP1	-0.42	3.8186E-05	ATP9A	-0.46	1.3393E-02
SFXN1	-0.42	1.6858E-03	ZCCHC3	-0.44	3.4613E-02
SDHAF3	-0.42	3.6506E-02	PPM1D	-0.42	4.8458E-02
SLC8B1	-0.41	3.7880E-02	APOL3	-0.41	4.0326E-02
ARHGEF19	-0.39	1.4298E-02	VPS4A	-0.41	4.4054E-02
ERLIN2	-0.38	4.2546E-03	GINM1	-0.38	3.4540E-02
TOPBP1	-0.38	1.9387E-02	POM121C	-0.33	1.7320E-02
HINT2	-0.37	4.7170E-03	HOXA9	0.44	2.2411E-02
SCOC	-0.37	2.2235E-02	APBA2	0.45	3.4540E-02
CCDC32	-0.37	1.6420E-02	NEDD4L	0.52	3.6853E-02
ZNF76	-0.37	1.2370E-02	PAIP2B	0.55	1.7263E-02
TAF4B	-0.37	2.8693E-02	TFCP2L1	0.56	1.6307E-03
FADS1	-0.37	3.1277E-02	PPP1R21	0.59	4.2707E-03
ZDHHC4	-0.35	3.1400E-02	KIR2DS4	0.60	6.9280E-03
MYO18A	-0.35	2.5962E-02	NFIA	0.63	1.7597E-02
PIGS	-0.35	2.8315E-02	TLDC1	0.67	7.1356E-03
S100A10	-0.35	2.0293E-02	GALNT12	0.69	3.4540E-02
SBNO2	-0.35	3.7395E-02	ZG16B	0.77	1.7263E-02
TKFC	-0.35	1.5920E-02	RNLS	0.77	3.7191E-02
SUMO3	-0.34	2.4124E-02	NCALD	0.78	1.4422E-02
SMC4	-0.33	4.2840E-02	ECHDC2	0.80	2.5948E-02
KCTD3	-0.33	2.3272E-02	C16orf45	0.92	2.9192E-02
PRKX	-0.32	4.9880E-02	AP000295.1	0.95	8.3603E-03
NAGA	-0.32	1.9739E-03	RETREG1	0.96	3.6912E-02
CDC23	-0.30	5.7748E-03	RNASE6	0.98	4.9242E-02
LEMD2	-0.30	4.1000E-02	KIR2DL3	1.03	2.6212E-03
PICALM	-0.29	1.8502E-04	KLRC4-KLRK1	1.14	5.0279E-03
DGCR2	-0.29	1.2806E-02	SLAMF7	1.33	3.3025E-03
PKP4	-0.29	1.5775E-02	COL27A1	1.36	1.7263E-02
ADAM10	-0.29	2.6643E-02	AC005842.1	1.44	4.0326E-02
CASK	-0.29	1.5553E-03	SOCS2	1.54	1.9243E-02
AHR	-0.28	3.6592E-02	ZNF311	1.54	1.5933E-02
JPT2	-0.27	4.4431E-02	KIR3DL1	1.63	6.1040E-07
DROSHA	-0.27	8.4953E-03	ARFGEF3	1.72	4.7392E-05
CELSR3	-0.27	4.6754E-03	ITGA6	1.82	5.8297E-04
SH2D1A	-0.27	1.2903E-02	MAT1A	1.95	9.7543E-04
PANK2	-0.26	1.6012E-02	MAEL	1.98	4.1055E-02

ANNEXES

SLC50A1	-0.26	2.1020E-02	STMND1	2.05	1.1682E-02
STAG2	-0.25	1.0518E-03	KCNJ13	2.97	1.7263E-02
TM7SF3	-0.24	1.1202E-02			
KCMF1	-0.23	1.1514E-02			
ACAP1	-0.23	3.4429E-02			
GAK	-0.22	1.8784E-02			
PTDSS1	-0.16	4.1613E-02			
ST13	0.21	1.8643E-02			
BTG3	0.22	4.2766E-02			
MBTPS2	0.24	2.4291E-02			
SNX7	0.25	1.9749E-02			
KPNA4	0.25	3.4429E-02			
MMGT1	0.26	3.1400E-02			
CAMSAP2	0.26	4.1379E-02			
NKIRAS2	0.26	1.2418E-02			
ELMO2	0.26	4.4785E-02			
CAND1	0.26	1.2320E-02			
ACOX1	0.27	2.6881E-02			
TMEM9B	0.28	4.2802E-02			
LAPTM5	0.28	1.5775E-02			
FMR1	0.28	2.6529E-02			
EIF1B	0.28	1.2320E-02			
GOPC	0.29	2.3173E-02			
CREBL2	0.29	5.3824E-03			
HIPK1	0.30	3.5703E-02			
SLC35D1	0.30	3.3130E-02			
SYTL2	0.30	3.9928E-02			
OSBPL8	0.30	4.8903E-04			
SUB1	0.30	2.3389E-03			
CDK18	0.31	1.5803E-02			
C15orf39	0.31	6.5435E-03			
PFDN4	0.31	2.0293E-02			
PDCD7	0.31	2.3508E-03			
LSP1	0.31	4.1363E-02			
MFN1	0.31	4.6225E-02			
PPP3R1	0.32	2.7818E-04			
WDR26	0.32	6.5490E-03			
DVL3	0.32	1.6802E-04			
RFTN1	0.33	3.2044E-05			
ANXA1	0.33	2.4266E-03			
GFOD1	0.34	4.9880E-02			
ATXN10	0.34	3.1718E-02			
FOXO1	0.34	3.0645E-02			
EIF4A2	0.35	7.4913E-03			
FGFR1OP2	0.35	1.8946E-04			
KSR1	0.35	3.7928E-04			
PRKY	0.35	1.6561E-03			
CLOCK	0.36	2.9251E-03			
LTA4H	0.36	9.3256E-04			
ZNF827	0.36	4.8903E-04			
ACTG1	0.36	3.7840E-02			

TRIM37	0.37	1.1547E-02
AKAP17A	0.37	3.7880E-02
EGLN3	0.37	8.6503E-04
ARL2BP	0.37	7.2563E-03
KDM5D	0.37	8.5321E-03
UBE2B	0.38	1.4057E-05
TRAFD1	0.38	6.2768E-03
ZFY	0.38	4.3731E-04
SH2D3C	0.38	1.0205E-03
TRIM23	0.39	4.7813E-02
WBP1	0.39	2.5962E-02
TAF10	0.39	4.1636E-02
ITM2A	0.39	3.2301E-02
POLD4	0.40	3.2708E-02
CD44	0.40	2.7858E-07
TANK	0.40	1.4272E-02
SIK3	0.40	8.5321E-03
TMEM200A	0.40	3.1718E-02
GPSM3	0.40	8.0440E-05
PAQR3	0.40	2.5796E-02
C5orf24	0.40	2.5796E-02
IFIH1	0.40	1.2806E-02
NUP58	0.42	3.9227E-02
ARRB1	0.42	1.4768E-02
KIAA0232	0.42	4.0303E-04
ACVR1B	0.43	2.6881E-02
ADO	0.43	1.1910E-04
UBE2H	0.44	1.1487E-02
PRKAB2	0.44	3.9495E-03
GNAI1	0.45	3.1400E-02
VPS37B	0.45	3.4766E-03
ZSWIM6	0.46	8.9380E-03
TNFRSF25	0.47	3.5761E-06
IL15	0.47	9.4069E-03
BAZ2A	0.47	1.0713E-04
SEPT9	0.48	3.1400E-02
SPIRE1	0.48	1.1547E-02
FUT8	0.50	1.3147E-03
SLC25A4	0.51	1.5803E-02
SH3TC1	0.51	4.6754E-03
OSM	0.51	3.9698E-05
EFHD2	0.51	4.5297E-03
HEXIM1	0.52	1.8101E-02
LY6E	0.52	4.6284E-02
STX3	0.52	1.5920E-02
NCF2	0.52	3.6506E-02
STIMATE	0.52	6.5435E-03

ANNEXES

LCP2	0.53	4.2699E-10
PCED1B-AS1	0.54	1.7179E-02
TTY15	0.55	4.1363E-02
MAP4K3	0.55	4.7170E-03
ST3GAL2	0.56	1.9973E-05
CASP9	0.56	1.3278E-04
PIK3R5	0.57	1.6452E-02
MEF2D	0.60	3.3620E-05
TWF1	0.60	9.0282E-03
PHACTR2	0.61	5.8310E-03
DUSP10	0.61	9.8213E-17
VCAN	0.62	3.9580E-02
TRIB1	0.62	4.5186E-02
FAM131A	0.63	3.2087E-03
TEX19	0.64	1.5920E-02
RNF11	0.64	1.0471E-27
RPS4Y1	0.65	1.5553E-03
CYP4F35P	0.65	3.7567E-02
TAX1BP3	0.69	7.8714E-03
AC111188.1	0.69	3.9227E-02
ASAP1	0.69	1.7073E-02
MRFAP1	0.71	2.9249E-07
CRK	0.73	9.4271E-03
RGS16	0.74	7.7598E-03
GRID1	0.74	4.7147E-03
IKZF4	0.75	1.1230E-02
ASB2	0.77	3.5716E-03
GEM	0.77	1.7711E-03
STX6	0.77	3.7351E-05
TMC6	0.77	1.3394E-02
GPR35	0.81	5.2270E-03
AP002008.1	0.82	4.3588E-02
FHL3	0.84	1.1155E-03
PCED1B	0.84	6.2460E-08
SAMSN1	0.84	7.2797E-07
AC055854.1	0.84	3.9227E-02
DGKA	0.86	8.7362E-10
LINC01619	0.87	5.4043E-03
AC131254.1	0.89	3.0391E-03
PRF1	0.92	6.8964E-11
ZCCHC24	0.93	8.6077E-03
ERICD	0.93	5.5656E-03
TMEM91	0.96	2.6167E-02
DCUN1D3	0.99	1.2475E-10
PCLO	0.99	4.6786E-02
RGS12	1.00	5.0148E-07

GBP5	1.01	1.5485E-03
JUN	1.02	4.0222E-02
GABARAPL1	1.04	3.3207E-02
CACNB4	1.04	7.0877E-04
OASL	1.04	8.2139E-03
MAGEB2	1.05	1.5803E-02
AL139393.2	1.05	1.1372E-02
FGFR3	1.06	1.6256E-02
USP46	1.06	2.3173E-02
MICAL2	1.07	9.4235E-05
TNRC6C-AS1	1.10	2.8476E-07
LINC01588	1.11	1.2912E-02
CSF2	1.11	2.2508E-03
AKR1C4	1.12	3.3130E-02
GBP4	1.13	1.4962E-05
ACVRL1	1.13	3.7840E-02
BCL9L	1.13	7.2056E-03
CHST2	1.14	7.0877E-04
FCGR2A	1.15	2.0642E-02
ISG15	1.18	3.3718E-07
STAC	1.19	3.3966E-03
MAF	1.19	4.4875E-02
PDLIM2	1.19	8.5936E-03
CCR8	1.20	3.7378E-02
SERPINE1	1.23	6.5490E-03
CLCF1	1.23	1.7785E-02
AC025164.1	1.24	3.7880E-02
PSD	1.25	1.9558E-03
IFIT3	1.28	4.8838E-07
RGS3	1.28	1.6015E-02
VCAM1	1.29	1.6610E-03
RNF38	1.29	3.3960E-10
EGR2	1.30	1.0518E-03
AC002454.1	1.31	1.3831E-02
GBP2	1.35	1.4117E-21
JPH4	1.35	2.6249E-03
POU2F2	1.39	1.5745E-03
SNX9	1.42	4.7452E-03
IFIT1	1.45	4.9647E-03
APOBEC3G	1.48	1.6012E-02
KCNJ12	1.48	3.8253E-02
PPIAP45	1.50	1.3677E-04
IFIT2	1.51	7.8517E-14
VGf	1.52	3.5947E-05
MXRA7	1.57	3.9590E-02
BMF	1.61	4.6827E-11
STARD4-AS1	1.65	2.3973E-02
NEK6	1.65	2.8726E-03
SPINK5	1.74	1.8560E-06
IER5L	1.75	3.7378E-02
CPM	1.81	8.0000E-03
SPP1	1.94	6.3172E-04
TNFRSF9	2.02	4.6424E-18
BCAS1	2.03	3.4132E-04
GBP1	2.10	1.8337E-05
LCN10	2.26	4.8342E-02
RHOB	2.38	4.5186E-02
CGA	2.52	6.5417E-09
UCN2	2.66	3.5762E-02
APOD	2.66	4.8903E-04
S100P	2.66	4.6574E-02
ATP1B1	2.67	1.5824E-02
PLA2G2F	2.91	1.7230E-03
A2M	3.32	1.4677E-03
PARM1	4.32	4.9907E-02

PUBLICATIONS

PUBLICATIONS



RELATED TO THIS THESIS

- › Pérez C, Mondéjar R, **García-Díaz N**, Cereceda L, León A, Montes S, Durán Vian C, Pérez Paredes MG, González-Morán A, Alegre de Miguel V, Sanz Anquela JM, Frías J, Limeres MA, González LM, Martín Dávila F, Beltrán M, Mollejo M, Méndez JR, González MA, González García J, López R, Gómez A, Izquierdo F, Ramos R, Camacho C, Rodríguez-Pinilla SM, Martínez N, Vaqué JP, Ortiz-Romero PL, Piris MA. **Advanced-stage mycosis fungoides: role of the signal transducer and activator of transcription 3, nuclear factor- κ B and nuclear factor of activated T cells pathways.** *The British journal of dermatology*. 2019 May 3. doi: 10.1111/bjd.18098
- › Pérez C, González-Rincón J, Onaindia A, Almaráz C, **García-Díaz N**, Pisonero H, Curiel-Olmo S, Gómez S, Cereceda L, Madureira R, Hospital M, Suárez-Massa D, Rodríguez-Peralto JL, Postigo C, Leon-Castillo A, González-Vela C, Martinez N, Ortiz-Romero P, Sánchez-Beato M, Piris MÁ, Vaqué JP. **Mutated JAK kinases and deregulated STAT activity are potential therapeutic targets in cutaneous T-cell lymphoma.** *Haematologica*. 2015 Nov;100(11):e450-3. doi: 10.3324/haematol.2015.132837

OTHER PUBLICATIONS

- › Ruso-Julve F, Pombero A, Pilar-Cuéllar F, **García-Díaz N**, Garcia-Lopez R, Juncal-Ruiz M, Castro E, Díaz A, Vazquez-Bourgón J, García-Blanco A, Garro-Martinez E, Pisonero E, Estirado A, Ayesa-Arriola R, López-Giménez J, Mayor Jr. F, Valdizán E, Meana J, Gonzalez-Maeso J, Martínez S, Vaqué JP, Crespo-Facorro B. **Dopaminergic control of ADAMTS2 expression through cAMP/CREB and ERK molecular effects of antipsychotics.** *Translational Psychiatry*. 2019 Nov 9 (1), 306.
- › Llerena S*, **García-Díaz N***, Curiel-Olmo S, Agraz-Doblas A, García-Blanco A, Pisonero H, Varela M, Santibáñez M, Almaraz C, Cereceda L, Martínez N, Arias-Loste MT, Puente Á, Martín-Ramos L, de Lope CR, Castillo-Suescun F, Cagigas-Fernandez C, Isidro P, Lopez-López C, Lopez-Hoyos M, Llorca J, Agüero J, Crespo-Facorro B, Varela I, Piris MÁ, Crespo J, Vaqué JP. **Applied diagnostics in liver cancer. Efficient combinations of sorafenib with targeted inhibitors blocking AKT/mTOR.** *Oncotarget*. 2018 Jul 20;9(56):30869-30882. doi: 10.18632/oncotarget.25766 *Contributed equally
- › Curiel-Olmo S, García-Castaño A, Vidal R, Pisonero H, Varela I, León-Castillo A, Trillo E, González-Vela C, **García-Díaz N**, Almaraz C, Moreno T, Cereceda L, Madureira R, Martinez N, Ortiz-Romero P, Valdizán E Piris MA1, Vaqué JP. **Individualized strategies to target specific mechanisms of disease in malignant melanoma patients displaying unique mutational signatures.** *Oncotarget*. 2015 Sep 22;6(28):25452-65. doi: 10.18632/oncotarget.4545.

Advanced-stage mycosis fungoides: role of the signal transducer and activator of transcription 3, nuclear factor- κ B and nuclear factor of activated T cells pathways

C. Pérez,^{1,2} R. Mondéjar^{1,2,3} , N. García-Díaz,⁴ L. Cereceda,^{2,3} A. León,⁵ S. Montes,^{2,5} C. Durán Vian^{1,6} , M.G. Pérez Paredes,⁶ A. González-Morán,⁷ V. Alegre de Miguel,⁸ J.M. Sanz Anquela,⁹ J. Frias,¹⁰ M.A. Limeres,¹¹ L.M. González,¹² F. Martín Dávila,¹² M. Beltrán,¹³ M. Mollejo,¹⁴ J.R. Méndez,¹⁵ M.A. González,¹⁶ J. González García,¹² R. López,¹² A. Gómez,¹⁷ F. Izquierdo,¹⁸ R. Ramos,¹⁹ C. Camacho,²⁰ S.M. Rodríguez-Pinilla,^{2,3} N. Martínez,^{1,2} J.P. Vaqué,⁴ P.L. Ortiz-Romero^{2,21} and M.A. Piris^{2,3}

¹Translational Hematopathology, Instituto de Investigación Marqués de Valdecilla, IDIVAL, Santander, Spain

²Centro de Investigación Biomédica en Red Cáncer, Madrid, Spain

³Service of Pathology, Fundación Jiménez Díaz University Hospital, Madrid, Spain

⁴Departamento de Biología Molecular, Universidad de Cantabria, Infección, Inmunidad y Patología Digestive, Instituto de Investigación Marqués de Valdecilla, IDIVAL, Santander, Spain

⁵Pathology Service and ⁶Dermatology Service, Marqués de Valdecilla University Hospital, Santander, Spain

⁷Dermatology Service, Complejo Hospitalario de Ávila, Ávila, Spain

⁸Dermatology Service, Hospital General Universitario de Valencia, Valencia, Spain

⁹Cancer Registry and Pathology Department, Hospital Universitario Príncipe de Asturias and Department of Medicine and Medical Specialties, Faculty of Medicine, University of Alcalá, Alcalá de Henares, Madrid, Spain

¹⁰Dermatology Service, Hospital Clínico Universitario Virgen de la Arrixaca, Murcia, Spain

¹¹Pathology Department, Hospital Universitario de Gran Canaria Doctor Negrín, Gran Canaria, Canarias, Spain

¹²Pathology Service, Hospital General Universitario de Ciudad Real, Ciudad Real, Spain

¹³Pathology Service, Hospital Universitario Puerta del Mar, Cádiz, Spain

¹⁴Pathology Service, Complejo Hospitalario de Toledo, Toledo, Spain

¹⁵Pathology Service, Centro Médico de Asturias, Asturias, Spain

¹⁶Pathology Service, Hospital San Pedro de Alcántara, Cáceres, Spain

¹⁷Pathology Service, Hospital de la Marina Baixa, Alicante, Spain

¹⁸Pathology Service, Complejo Asistencial Universitario de León, León, Spain

¹⁹Pathology Service, University Hospital Son Espases, Palma de Mallorca, Spain

²⁰Pathology Service, C.H.U. Insular – Materno Infantil, Gran Canarias, Spain

²¹Dermatology Service, Hospital 12 de Octubre, Institute i+12 Medical School, University Complutense, Centro de Investigación Biomédica en Red Cáncer, Madrid, Spain

Summary

Correspondence

Miguel Ángel Piris.

E-mail: miguel.piris@quironsalud.es

Accepted for publication

23 April 2019

Funding sources

This study has been supported by grants from the Instituto de Salud Carlos III, from the Ministerio de Economía, Industria y Competitividad [SAF2013-47416-R, CIBERONC-ISCHII, ISCHII-MINECO-AES-FEDER (Plan Estatal I + D + I 2013-2016): PI14/00221, PIE14/0064, PIE15/0081, PIE16/01294 and FIS 17/0957], Asociación Española Contra el Cáncer (AECC), Comunidad Autónoma de Madrid and Instituto Formación e Investigación, Hospital

Background The malignant mechanisms that control the development of cutaneous T-cell lymphoma (CTCL) are beginning to be identified. Recent evidence suggests that disturbances in specific intracellular signalling pathways, such as RAS–mitogen-activated protein kinase, T-cell receptor (TCR)–phospholipase C gamma 1 (PLCG1)–nuclear factor of activated T cells (NFAT) and Janus kinase (JAK)–signal transducer and activator of transcription (STAT), may play an essential role in the pathogenesis of CTCL.

Objectives To investigate the mechanisms controlling disease development and progression in mycosis fungoides (MF), the most common form of CTCL.

Methods We collected 100 samples that were submitted for diagnosis of, or a second opinion regarding, MF between 2001 and 2018, 80% of which were in the early clinical stages of the disease. Formalin-fixed paraffin-embedded tissues were used for histological review and to measure the expression by immunohistochemistry of surrogate markers of activation of the TCR–PLCG1–NFAT, JAK–STAT and NF- κ B pathways. Folliculotropism and large-cell transformation were also examined.

Universitario Marqués de Valdecilla (IDIVAL): NVAL16/18.

Conflicts of interest

M.A.P. has received lecture fees and advisory committee fees from Janssen, Takeda, Celgene, Kyowa Kirin and Gilead. Research developed at the lymphoma laboratories at both IDIVAL and the Fundación Jiménez Díaz receives grants from Kura, Takeda and Gilead.

C.P. and R.M. contributed equally to this work.

DOI 10.1111/bjd.18098

Results NFAT and nuclear factor kappa B (NF- κ B) markers showed a comparable activation status in early and advanced stages, while STAT3 activation was more frequent in advanced stages and was associated with large-cell transformation. Consistently with this observation, STAT3 activation occurred in parallel with MF progression in two initially MF-negative cases. A significant association of NFAT with NF- κ B markers was also found, reflecting a common mechanism of activation in the two pathways. Genomic studies identified nine mutations in seven genes known to play a potential role in tumorigenesis in T-cell leukaemia/lymphoma, including *PLCG1*, *JAK3* and *STAT3*, which underlies the activation of these key cell-survival pathways. A higher mutational allele frequency was detected in advanced stages.

Conclusions Our results show that STAT3 is activated in advanced cases and is associated with large-cell transformation, while the activation of NFAT and NF- κ B is maintained throughout the disease. These findings could have important diagnostic and therapeutic implications.

What's already known about this topic?

- Mycosis fungoides is characterized by a clonal expansion of T cells in the skin.
- The mechanisms controlling disease development and progression are not fully understood.

What does this study add?

- An association of the nuclear factor of activated T cells and nuclear factor kappa B pathways was found, which could reflect a common mechanism of activation. These pathways were activated in early and advanced stages at the same level.
- Signal transducer and activator of transcription 3 activation was associated with large-cell transformation and was more frequent in advanced stages.
- A genomic analysis of cutaneous T-cell lymphoma-associated genes was performed. Nine mutations were detected.

What is the translational message?

- These results could have important implications for the treatment of MF in the near future.

Introduction

Cutaneous T-cell lymphoma (CTCL) is defined as a non-Hodgkin lymphoma comprising a group of disorders characterized by clonal expansion of malignant T cells present in the skin.¹ Mycosis fungoides (MF) is the most common type of CTCL, accounting for around 55% of cases.¹ The clinicopathological conditions of MF are broad, from single lesions to more generalized skin involvement with patches, plaques, tumours or erythroderma. Accurate staging, based on TNMB (tumour, node, metastasis, blood), is required because of its great prognostic value.² Patients in early stages (stage IA–IIA) have a good prognosis (52–100% 10-year overall survival) and a relatively low risk of disease progression (12–33% in 10 years). However, patients in advanced stages (stage IIB–IVB) have a

worse prognosis (< 38% 10-year overall survival) and more than 58% of them progress.² Patients with MF are usually clinically diagnosed based on the presentation of patches and/or plaques with indolent behaviour that cover the skin surface; these are defined as classic patch/plaque. Patients in early stages can be kept stable for several decades, with a 5–10% or 17–39% risk of progression to advanced stages in the first 10 years following diagnosis, depending on the proportion of the body surface involved (< 10% and \geq 10%, respectively).³

The malignant mechanisms controlling disease development and progression are not fully understood, although some of them have been identified. Recent evidence suggests that disturbances in specific intracellular signalling pathways can play an essential role in the pathogenesis of CTCL.^{4–6} These include RAS–mitogen-activated protein kinase, T-cell receptor (TCR)–

phospholipase C gamma 1 (PLCG1)—nuclear factor of activated T cells (NFAT) and Janus kinase (JAK)—signal transducer and activator of transcription (STAT), among others. Deregulated JAK–STAT signalling is involved in many types of cancer. In fact, somatically acquired genetic alterations of JAK or STAT genes that induce aberrant activation of downstream signalling, via STAT phosphorylation, have been reported in some human haematological malignancies, including CTCLs.^{4,7–13}

This study aimed to investigate the activation status of these three main survival pathways – NFAT, nuclear factor kappa B (NF-κB) and JAK–STAT – in a cohort of sequential patients with MF by assessing the frequency, clinical relevance and interactions among them. To identify the possible genomic alterations contributing to the activation of these pathways, we performed targeted sequencing in a panel of T-cell lymphoma-associated genes.

Material and methods

Clinical samples

Cases submitted for an MF diagnosis or a second opinion in different institutions of the Spanish national health system between 2001 and 2018 were included in the study. Diagnostic criteria were based on World Health Organization–European Organisation for Research and Treatment of Cancer classification.¹⁴ Cases of CTCL other than MF were excluded. Clinical stage was established on the basis of the TNMB classification.¹⁵ This study was conducted in accordance with the Declaration of Helsinki and was supervised by the ethical committee of the Hospital Universitario Marqués de Valdecilla, Santander, Spain.

We used only samples from skin biopsies. Formalin-fixed paraffin-embedded (FFPE) tissues were used for histological examination and DNA sequencing. Immunohistochemical and molecular studies were performed using the initial diagnostic samples. Survival analysis was performed from the date of the initial diagnosis of MF.

Immunohistochemistry

A panel of antibodies was used to quantify the levels of TCR–PLCG1–NFAT, NF-κB and JAK–STAT expression in 112 samples from 99 patients. Folliculotropism and large-cell transformation were also assessed.¹⁵ Immunohistochemical staining was performed on slides using the following antibodies: NFAT-C1, phospho (p)STAT1, pSTAT3, pSTAT5, p50, p52, p65 and RelB (Table S1; see Supporting Information). Each slide was reviewed by two independent pathologists, who examined the nuclear staining in each case. Specific thresholds are described in Table S1. Positive staining was defined as a score higher than 1. Immunohistochemical controls were taken from samples of inflammatory cutaneous disorders. Each immunostained slide included positive controls. Negative controls were routinely used for each marker (Fig. S1; see Supporting Information).

Targeted enrichment and sequencing

DNA was extracted from FFPE tissue with High Pure FFPE DNA Isolation Kit following the manufacturer's instructions (Roche Diagnostics Limited, Burgess Hill, U.K.). DNA was quantified using Qubit dsDNA HS Assay Kit (Thermo Fisher Scientific Inc., Waltham, MA, U.S.A.), with a range of 0.5–390 ng µL^{−1} (median 7.55). DNA quality was tested by quantitative polymerase chain reaction (PCR) using Infinium FFPE QC following the manufacturer's instructions (Illumina, San Diego, CA, U.S.A.). Targeted enrichment of 16 genes known to play a potential role in tumorigenesis in T-cell leukaemia¹⁶ was performed with Truseq Custom Amplicon Low Input (Illumina) (Table S2; see Supporting Information). Samples of 20–100 ng were used to perform Truseq enrichment. Samples with ΔCq > 6 were discarded. We also carried out adaptor-anchored PCR-based targeted enrichment in frequently mutated regions of PLCG1, JAK1 and JAK3 (Table S3; see Supporting Information) for Truseq validation (Table S4 and Fig. S2; see Supporting Information).

Variants were called using MiSeq Reporter (Illumina), employing the default settings, and were visually inspected within Integrative Genomics Viewer (www.broadinstitute.org/igv). Variants were annotated with Variant Effect Predictor (GRCh37, <http://grch37.ensembl.org/Tools/VEP>). Known single-nucleotide polymorphisms with an allelic frequency > 1% in public databases (dbSNP138, 1000 Genomes Project, Exome Sequencing Project, Exome Aggregation Consortium) were filtered out.

Table 1 Clinical and demographic characteristics of the patients included in the study at the time of biopsy

	All	Early stages	Advanced stages
Age at MF diagnosis (years), median (range) ^a	64 (12–87)	63 (12–87)	66 (38–87)
Sex, n (%) ^a			
Male	47 (61)	36 (59)	11 (69)
Female	30 (39)	25 (41)	5 (31)
Not available	23		
Clinical stage at diagnosis, n (%)			
Early (IA–IIA)	61 (78)	61 (100)	0
Advanced (IIB–IVB)	17 (22)	0	17 (100)
Not available	22		
MF variant at diagnosis, n (%)			
Classical patch/plaque	61 (78)	57 (93)	4 (24)
Follicular MF	5 (6)	4 (7)	1 (6)
Erythrodermic	5 (6)	0	5 (29)
Tumour	7 (9)	0	7 (41)
Not available	22		

MF, mycosis fungoides. Early stages are IA, IB and IIA; advanced stages are IIB, III, IVA1, IVA2 and IVB. ^aP > 0.05.

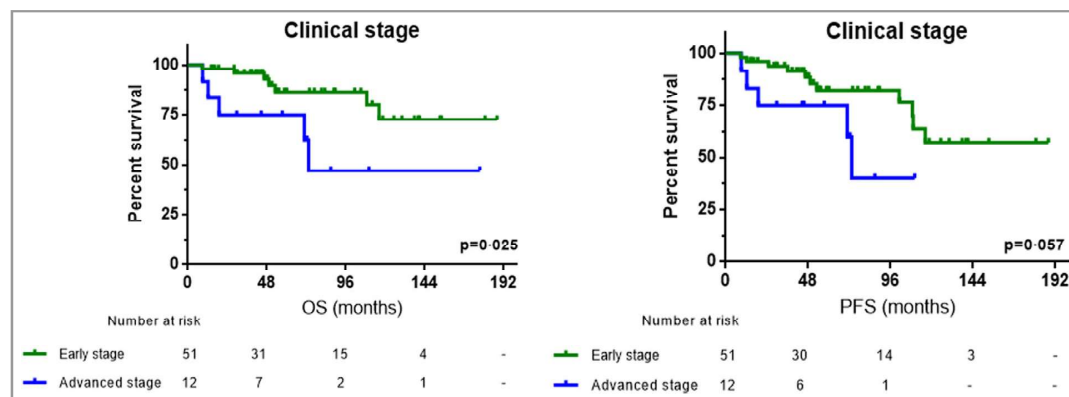


Fig 1. Kaplan–Meier curves for early and advanced clinical stages. OS, overall survival; PFS, progression-free survival.

Statistical analysis

The χ^2 -test or Fisher exact test was used, as appropriate, to determine associations between the presence and absence of markers. Overall survival (OS) was taken to be the period between the initial diagnosis and the date of death from any cause, or of the last contact in the case of living patients. Progression-free survival (PFS) was measured as the period between the initial diagnosis and the date of death from any cause, or of progression of the lymphoma disease to a higher clinical stage, or of the last contact for living patients with no disease progression. Kaplan–Meier survival analyses were carried out for OS and PFS using the log-rank test to examine differences between groups. A multivariate Cox regression model was also derived. Estimates were considered statistically significant for two-tailed P-values < 0.05. All analyses were carried out using SPSS for Windows version 15 (IBM, Armonk, NY, U.S.A.).

Results

Activation of signal transducer and activator of transcription 3 in advanced stages of mycosis fungoides

The initial series included 106 patients and 119 samples. After case-by-case revision, six patients were excluded because they were judged to have other CTCL subtypes. The clinical characteristics of the 100 patients with MF are summarized in Table 1. The median follow-up time was 55 months. We dichotomized the patients into early (stage IA, IB and IIA) or advanced (stage IIB, III, IVA1, IVA2 and IVB) clinical stages. At the time of initial diagnosis, this series consisted mainly of patients in early stages (78%). Most of the patients presented with classic patch/plaque MF (78%). Advanced-stage patients (22%) were characterized by classic patches and plaques (69%), erythroderma (50%), tumour skin lesions (38%) and extracutaneous lesions (visceral, blood and bone marrow

Table 2 Relationships between immunohistochemical (IHC) markers and clinical stage. The first biopsy (diagnostic biopsy) and the clinical stage at diagnosis were taken into account for χ^2 calculations. Positive staining was established as an IHC score higher than 1 (Table S1; see Supporting Information)

	All samples n/N (%)	Early stage n/N (%)	Advanced stage n/N (%)	P-value (χ^2)
NEAT	30/111 (27.0)	13/59 (22)	6/17 (35)	0.34
pSTAT1	11/94 (12)	3/56 (5)	3/13 (23)	0.076
pSTAT3	28/110 (25.5)	6/58 (10)	9/17 (53)	< 0.001
pSTAT5	82/93 (88)	9/58 (16)	4/17 (24)	0.48
p50	28/110 (25.5)	31/59 (53)	8/17 (47)	0.69
p65	87/115 (75.6)	27/57 (47)	9/17 (53)	0.50
p52	23/110 (20.9)	11/57 (19)	5/17 (29)	0.69
RelB	55/78 (71)	12/58 (21)	6/17 (35)	0.33
Large-cell transformation	56/111 (50.5)	14/59 (24)	8/17 (47)	0.075
Folliculotropism	59/115 (51.3)	10/59 (17)	3/17 (18)	1.00

Early stages are IA, IB and IIA; advanced stages are IIB, III, IVA1, IVA2 and IVB. NEAT, nuclear factor of activated T cells; pSTAT, phosphorylated signal transducer and activator of transcription.

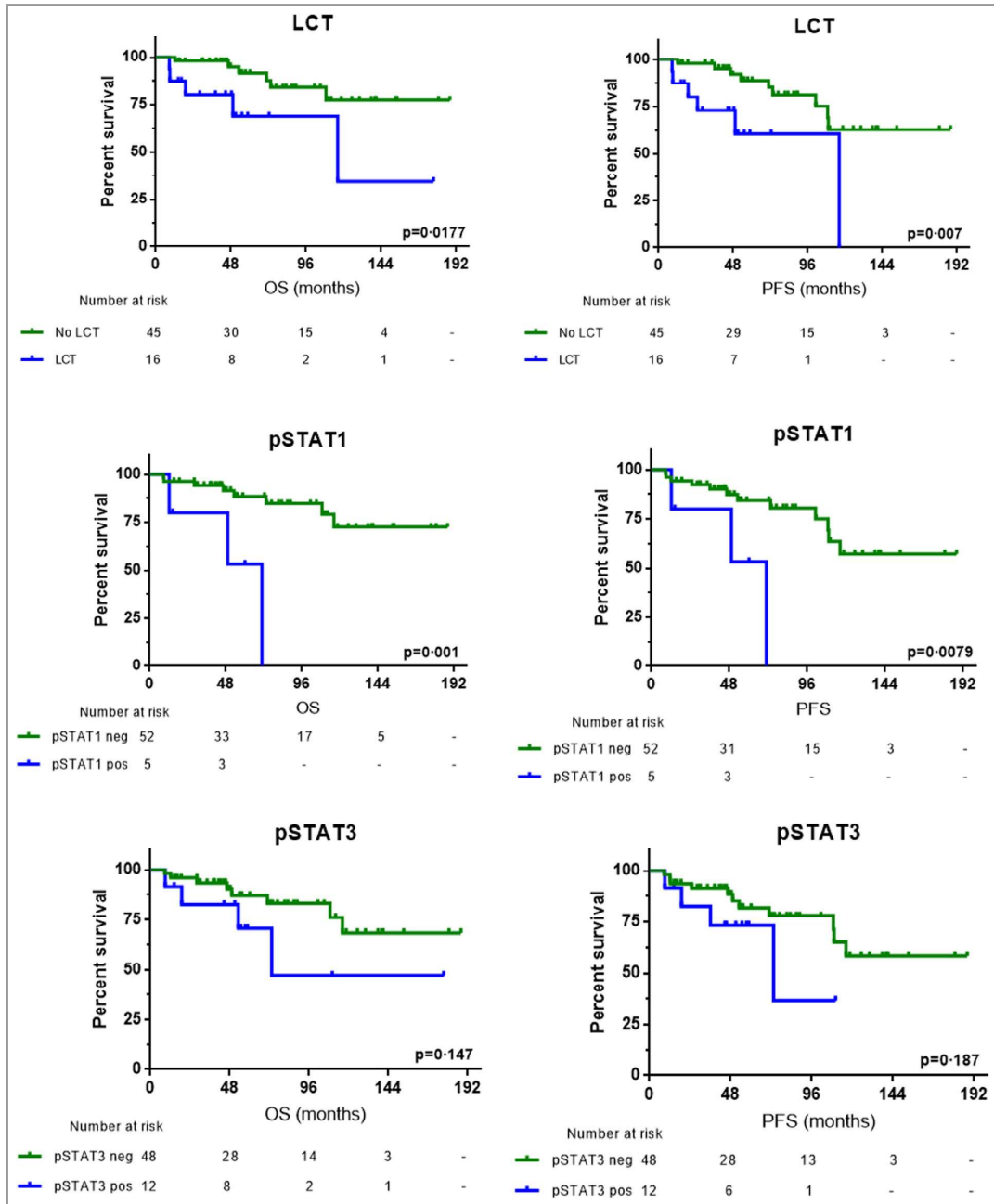


Fig 2. Kaplan-Meier curves for the main markers found to be associated with advanced clinical stages. Overall survival (OS) and progression-free survival (PFS) are expressed in months. LCT, large-cell transformation; pSTAT, phosphorylated signal transducer and activator of transcription.

involvement; 13%, 13% and 6%, respectively). At the time of data analysis, 12 patients had died, 58 patients were censored by their last appointment, eight patients had been lost to follow-up, and clinical data could not be obtained for 22 patients. Early-stage patients showed better OS and PFS than

those in advanced stages ($P = 0.025$ and $P = 0.057$, respectively; Fig. 1).

Immunohistochemical analysis of the TCR-PLCG1-NFAT, NF- κ B and JAK-STAT pathways was performed in 111 samples, taking only nuclear staining into account. We also

Table 3 Multivariate Cox analysis to identify independent predictors of overall survival and progression-free survival

	n (%)	Overall survival			Progression-free survival		
		HR	95% CI	P-value	HR	95% CI	P-value
Male	37 (63)	9.10	0.39–213	0.17	4.56	0.66–31.3	0.12
Age ≥ 60 years	30 (48)	10.8	1.13–104	0.039	2.45	0.63–9.53	0.20
Advanced stage	13 (21)	0.27	0.017–4.19	0.35	0.62	0.081–4.82	0.65
LCT > 25%	16 (25)	7.22	0.70–74.3	0.097	4.63	1.03–20.8	0.046
NFAT (+) ^a	15 (25)	2.31	0.46–11.7	0.31	1.43	0.36–5.73	0.62
pSTAT1 (+) ^a	5 (8)	10.4	1.14–95.3	0.038	5.28	0.96–29.2	0.057
pSTAT3 (+) ^a	10 (17)	6.19	0.63–61.2	0.12	3.13	0.57–17.2	0.19
p50 (+) ^a	33 (56)	4.34	0.42–44.9	0.22	4.12	0.75–22.5	0.10

HR, hazard ratio; CI, confidence interval; LCT, large-cell transformation; NFAT, nuclear factor of activated T cells; pSTAT, phosphorylated signal transducer and activator of transcription. ^aA positive marker (+) was established as an immunohistochemical score higher than 1 (Table S1; see Supporting Information).

analysed large-cell transformation and folliculotropism. We observed different ranges of activation of the assessed markers of NFAT (27%), NF-κB (25.9–50.5%) and STAT (11.7–25.5%) (Table 2; and Fig. S3a; see Supporting Information). Regarding the relationship between the presence of pairs of markers, we found an association between pSTAT3 and large-cell transformation ($P < 0.001$, Fig. S3b; see Supporting Information), and a relationship between the expression of the NFAT and NF-κB pathway markers ($P \leq 0.017$, Fig. S3b). No differences were found when comparing all patients and those with follow-up (data not shown).

When patients were grouped by clinical stage, only pSTAT3 expression showed an association with advanced stages ($P < 0.001$, Table 2). Analysis of the histological variables showed that large-cell transformation was associated with shorter OS and PFS ($P = 0.018$ and $P = 0.007$, respectively; Fig. 2). Patients with activated STAT3 also showed shorter OS and PFS, although the differences were not statistically significant ($P = 0.15$ and $P = 0.19$, respectively; Fig. 2). None of the other markers showed differences in OS and PFS between positive and negative markers, except for pSTAT1 ($P = 0.001$ and $P = 0.008$, for OS and PFS, respectively) (Fig. 2; and Fig. S4; see Supporting Information). The multivariate analysis showed that age at diagnosis and activation of STAT1 were independent predictors of OS, while large-cell transformation was independently associated with risk of progression (Table 3).

In four cases, paired samples were available for initial and progressed stages. Strikingly, three of these four patients showed expression of pSTAT3 only in the more advanced sample (Fig. S5; see Supporting Information). The other patient who progressed showed STAT1 and STAT5 but not STAT3 expression (Fig. 3). The three patients with parallel samples who did not progress showed no expression of STAT3 in the second sample.

Mutational profile and activation of pathways in patients with mycosis fungoides

After checking quality and quantity, samples from 73% of the patients included in the study were sequenced. We detected

nine mutations in seven genes from eight patients (Table S5a; see Supporting Information). Among them, the recurrent mutations p.S345F and p.A573V in PLCG1 and JAK3, respectively, were found in advanced-stage patients. Samples with PLCG1 mutations had concurrently activated NFAT, NF-κB and STAT (pSTAT3) pathways. We also found mutations in TNFRSF1B, CCR4, IDH2, TET2 and STAT3. Regarding JAK3 mutations, the sample harbouring p.Q507P, which was predicted to be benign, did not show pSTAT3 staining. Conversely, cases with p.A573V and p.R70H (predicted to be deleterious) did show STAT3 activation.

Discussion

The molecular mechanisms controlling the development of MF are not well understood. Several pathways and aberrant molecular findings have been associated with CTCL genesis or progression, but specific markers of progression have not previously been confirmed. Most of the molecular studies of this disease have considered patients with advanced-stage MF and Sézary syndrome;^{4,8,11–13} only two studies included early-stage patients.^{13,17}

Our study concentrated on a series of patients, mainly represented by early stages with classic patches and plaques, in whom we immunohistochemically tested activation markers of three of the possible pathways involved in MF pathogenesis and progression, namely the NFAT, NF-κB and JAK–STAT pathways.^{4,18} Approximately one-quarter of the patients showed activation of the NFAT pathway, with no significant differences between early and advanced stages. This proportion of activated cases was similar to that observed in our previous study in a smaller, independent series of advanced-stage cases.⁴ Vaqué *et al.* showed that the use of calcineurin inhibitors was able to decrease NFAT signalling, reducing cell proliferation and viability.⁴ Following these findings, a proof-of-concept clinical trial was conceived in which patients with early-stage MF were treated with a topical calcineurin inhibitor, pimecrolimus (PimTo-MF; EudraCT Number 2014-001377-14).

The NF-κB pathway is involved in proliferation, survival, apoptosis and cytokine production in T cells. In MF and Sézary

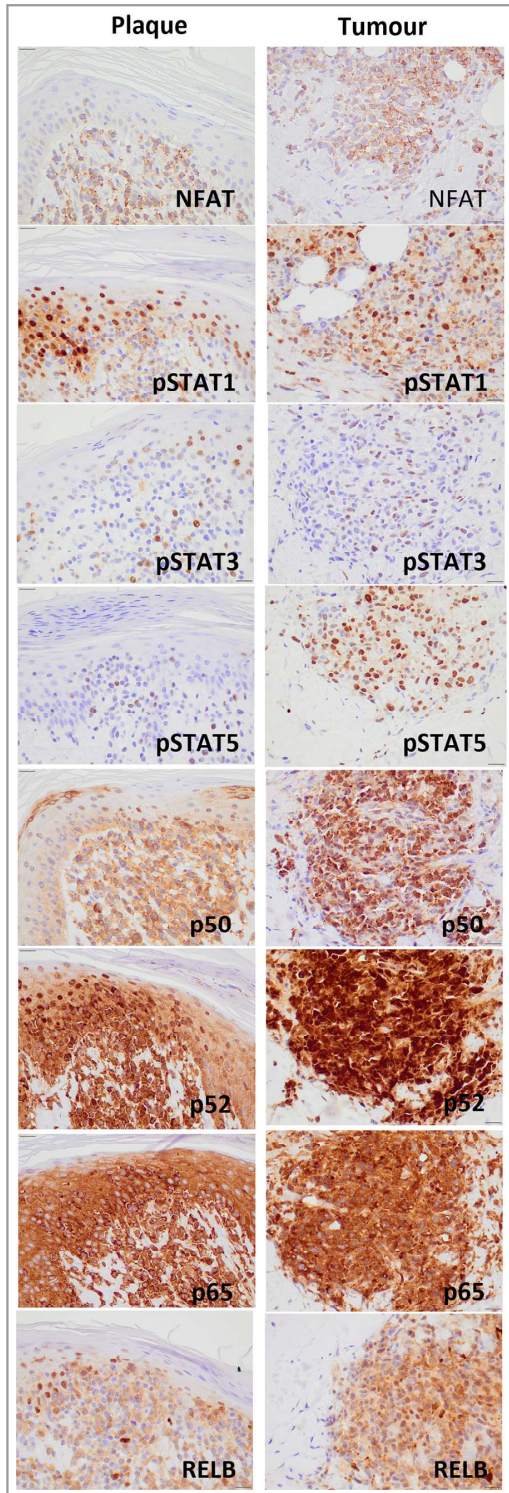


Fig 3. Expression of immunomarkers in formalin-fixed paraffin-embedded samples of a patient with mycosis fungoides (patient 107) with lesions in the plaque phase who developed tumour lesions. Images were taken at 40 × magnification. The nuclear factor of activated T cells (NFAT) pathway was not activated in either plaque or tumour lesions; only cytoplasmic staining was detected. The Janus kinase–signal transducer and activator of transcription (STAT) pathway was activated only in the tumour lesion, through phosphorylation of STAT1 and STAT5. In the plaque phase, STAT1 was shown to be activated in keratinocytes but not in tumoral T cells. Regarding the nuclear factor (NF)- κ B pathway, the samples highlight the strong staining of p52 in the tumour. The NF- κ B subunits p50, p65 and RelB show increased activation in the tumour lesion.

syndrome, NF- κ B can be activated upon TCR¹⁹ and tumour necrosis factor signalling pathway activation, and by structural alterations in the pathway components.^{8,11,12,20} Recently, it has been shown that FK506-binding protein 51 and TAK1 (mitogen-activated protein kinase kinase 7) are involved in NF- κ B activation in CTCL.^{21,22} We detected variable nuclear expression levels of NF- κ B subunits (p50, p65, p52 and RelB). p50 and p52 were both detected in T-cell nuclei in around 50% of cases, while p65 and RelB were found in 25%. We found an association between the expression of NFAT and the four NF- κ B markers (Fig. S3b; see Supporting Information), which suggests the presence of a common upstream activator of both pathways, possibly due to the activation of TCR signalling. We did not find any differences in NF- κ B marker expression between early and advanced stages.

STAT3 activation is associated with tumour progression in different types of cancer, including CTCL.^{5,9,18,23–25} Analysis of tissue samples has already shown that STAT3 activation occurs frequently in patients with MF.^{18,23} Here we found that expression of pSTAT3, a marker of STAT3 activation, is associated with advanced stages, confirming previous observations by Sommer *et al.* in eight patients.¹⁸ Consistently with these observations, we also found large-cell transformation to be an independent predictor of progression, as previously described.²⁶ Although we did not find any statistically significant differences in OS and PFS between the positive and negative pSTAT3 groups, the high proportion of patients with advanced MF stages with increased expression of pSTAT3 suggests that this may be a marker of MF progression.

STAT1 activation proved to be an independent predictor of OS. However, as this is a relatively rare alteration in our series, larger studies should be carried out to confirm this result. The use of JAK inhibitors, such as ruxolitinib, has been proposed to treat patients with CTCL with an altered JAK–STAT pathway, as they are known to reduce STAT signalling, cell viability and DNA synthesis.⁹

From a genomic perspective, we used targeted sequencing to analyse 16 genes that are frequently mutated in T-cell lymphomas.¹⁶ We also performed targeted sequencing of hotspot regions in the PLCG1, JAK1 and JAK3 genes, in two

independent rounds of library preparation and sequencing. Finally, we were able to detect nine mutations (Table S5; see Supporting Information). It is worth noting that early-stage biopsies showed a low mutational frequency (0.5–11.2%), whereas advanced-stage biopsies had a higher mutation frequency (> 20%). The mutational data generated here are in line with those of McGirt *et al.*, who detected mutations of only about 1% of variant allelic frequency in a few early-stage cases.¹³ This apparent low mutational load could be due to the low number of tumour cells present in these lesions. A more sensitive strategy to detect genetic changes present in small subpopulations could be used in future to characterize this type of lymphoma.

Some of the mutated genes in this series are involved in the activation of the analysed pathways: (i) *PLCG1* in NFAT and NF- κ B, (ii) *TNFRSF1B* in NF- κ B and (iii) *JAK1*, *JAK3*, *STAT3*, *STAT5* in JAK–STAT. *PLCG1* p.S345F has been previously associated with NFAT activation.⁴ We detected only one patient bearing this mutation, who exhibited activation of STAT3 and NF- κ B, but not NFAT. We detected a sample carrying a previously unreported mutation, *PLCG1* p.K713N, in which the three pathways were concurrently activated. We observed that p.A573V (*JAK3*) and p.R70H (*STAT3*) were associated with activation of the JAK–STAT pathway, but p.Q507P (*JAK3*) was not. The first mutation had been reported as being present in early stages and at low frequency¹³ and in the Hut-78 cell line.¹⁶ A previous study by our group showed that *STAT3* is not constitutively activated in Hut-78 under basal conditions, suggesting that this mutation may require an additional contribution, perhaps mediated through cytokines or interleukins, to activate the pathway.²⁷ Interestingly, the coincidence of *PLCG1* mutations and activation of *STAT3* deserves special consideration, as it might constitute a novel mechanism for activating this pathway (work in preparation).

Analysis of consecutive biopsies in the same patients could theoretically confirm the role of STAT activation in MF progression (Fig. 3; and Fig. S5; see Supporting Information). Strikingly, the mutation p.A573V (*JAK3*; Table S5; see Supporting Information) was found in a progression biopsy (sample 1-B, stage IIB), but we did not find it in the first early-stage diagnostic biopsy (sample 1-A, stage IA-IB). This patient showed no activation of any marker at diagnosis but STAT activation (*STAT3* and *STAT5*), and large-cell transformation was present in the tumour lesion. Patient 107 developed a lesion showing activation of *STAT1* and *STAT5*, compared with the previous plaque-phase biopsy (Fig. 3). Another patient who developed tumours showed *STAT3* activation when the disease progressed (sample 10-B, stage IIB). In this case, we found no mutation in the JAK–STAT pathway, although we did detect mutations in *PLCG1* and *TET2*. Finally, patient 8, who developed erythroderma, showed activation of *STAT3* in the progression biopsy but had no detectable mutation in early or advanced samples.

Besides the accumulation of activating mutations by malignant T cells, other genetic or environmental events could drive

constitutive *STAT3* activation. *Staphylococcus aureus* has been reported to be common in MF and a primary cause of death in patients with advanced disease,^{28,29} triggering *STAT3* activation in primary malignant T cells.³⁰ Recurrent chromosomal alterations in *STAT3* and *STAT5*³¹ and deletion³² or hypermethylation³³ of JAK–STAT signalling inhibitors have also been reported in MF.

In summary, this study evaluates three important survival pathways involved in T-cell lymphomas and sets out future directions for possible therapeutic options that could block the progression of the disease. The activation of *STAT3* is associated with large-cell transformation, which is known to be a risk factor for progression.³⁴ For this reason, p*STAT3* could constitute a biomarker of advanced stages in MF and therefore be useful as a predictive marker for targeted therapy.

Acknowledgments

We especially thank José Revert from the Instituto Formación e Investigación Hospital Universitario Marqués de Valdecilla (IDIVAL), and the staff of the Biobank and the Pathology Service at the Hospital Universitario Marqués de Valdecilla for their exceptional work in sample collection and organization.

References

- Willemze R, Hodak E, Zinzani PL *et al.* Primary cutaneous lymphomas: ESMO Clinical Practice Guidelines for diagnosis, treatment and follow-up. *Ann Oncol* 2013; **24** (Suppl. 6):vi149–54.
- Agar NS, Wedgeworth E, Crichton S *et al.* Survival outcomes and prognostic factors in mycosis fungoides/Sézary syndrome: validation of the revised International Society for Cutaneous Lymphomas/European Organisation for Research and Treatment of Cancer staging proposal. *J Clin Oncol* 2010; **28**:4730–9.
- Quaglino P, Pimpinelli N, Berti E *et al.* Time course, clinical pathways, and long-term hazards risk trends of disease progression in patients with classic mycosis fungoides: a multicenter, retrospective follow-up study from the Italian Group of Cutaneous Lymphomas. *Cancer* 2012; **118**:5830–9.
- Vaqué JP, Gomez-Lopez G, Monsalvez V *et al.* *PLCG1* mutations in cutaneous T-cell lymphomas. *Blood* 2014; **123**:2034–43.
- Netchiporouk E, Litvinov IV, Moreau L *et al.* Deregulation in *STAT* signaling is important for cutaneous T-cell lymphoma (CTCL) pathogenesis and cancer progression. *Cell Cycle* 2014; **13**:3331–5.
- Krejsgaard T, Lindahl LM, Mongan NP *et al.* Malignant inflammation in cutaneous T-cell lymphoma – a hostile takeover. *Semin Immunopathol* 2017; **39**:269–82.
- Woollard WJ, Pullabhatla V, Lorenc A *et al.* Candidate driver genes involved in genome maintenance and DNA repair in Sézary syndrome. *Blood* 2016; **127**:3387–97.
- da Silva Almeida AC, Abate F, Khiabanian H *et al.* The mutational landscape of cutaneous T cell lymphoma and Sézary syndrome. *Nat Genet* 2015; **47**:1465–70.
- Perez C, Gonzalez-Rincon J, Onaindia A *et al.* Mutated JAK kinases and deregulated *STAT* activity are potential therapeutic targets in cutaneous T-cell lymphoma. *Haematologica* 2015; **100**:e450–3.
- Tensen CP. *PLCG1* gene mutations in cutaneous T-cell lymphomas revisited. *J Invest Dermatol* 2015; **135**:2153–4.

- 11 Ungewickell A, Bhaduri A, Rios E et al. Genomic analysis of mycosis fungoides and Sézary syndrome identifies recurrent alterations in TNFR2. *Nat Genet* 2015; **47**:1056–60.
- 12 Choi J, Goh G, Walradt T et al. Genomic landscape of cutaneous T cell lymphoma. *Nat Genet* 2015; **47**:1011–19.
- 13 McGirt LY, Jia P, Baerenwald DA et al. Whole-genome sequencing reveals oncogenic mutations in mycosis fungoides. *Blood* 2015; **126**:508–19.
- 14 Burg G, Kempf W, Cozzio A et al. WHO/EORTC classification of cutaneous lymphomas 2005: histological and molecular aspects. *J Cutan Pathol* 2005; **32**:647–74.
- 15 Olsen E, Vonderheid E, Pimpinelli N et al. Revisions to the staging and classification of mycosis fungoides and Sézary syndrome: a proposal of the International Society for Cutaneous Lymphomas (ISCL) and the cutaneous lymphoma task force of the European Organization of Research and Treatment of Cancer (EORTC). *Blood* 2007; **110**:1713–22.
- 16 Mondejar R, Perez C, Onaindia A et al. Molecular basis of targeted therapy in T/NK-cell lymphoma/leukemia: a comprehensive genomic and immunohistochemical analysis of a panel of 33 cell lines. *PLOS ONE* 2017; **12**:e0177524.
- 17 Tracey L, Villuendas R, Dotor AM et al. Mycosis fungoides shows concurrent deregulation of multiple genes involved in the TNF signaling pathway: an expression profile study. *Blood* 2003; **102**:1042–50.
- 18 Sommer VH, Clemmensen OJ, Nielsen O et al. In vivo activation of STAT3 in cutaneous T-cell lymphoma. Evidence for an antiapoptotic function of STAT3. *Leukemia* 2004; **18**:1288–95.
- 19 Briones J, Moga E, Espinosa I et al. Bcl-10 protein highly correlates with the expression of phosphorylated p65 NF- κ B in peripheral T-cell lymphomas and is associated with clinical outcome. *Histopathology* 2009; **54**:478–85.
- 20 Kiel MJ, Sahasrabudhe AA, Rolland DC et al. Genomic analyses reveal recurrent mutations in epigenetic modifiers and the JAK-STAT pathway in Sézary syndrome. *Nat Commun* 2015; **6**:8470.
- 21 Mascolo M, Romano MF, Ilardi G et al. Expression of FK506-binding protein 51 (FKBP51) in mycosis fungoides. *J Eur Acad Dermatol Venerol* 2018; **32**:735–44.
- 22 Gallardo F, Bertran J, Lopez-Arribilla E et al. Novel phosphorylated TAK1 species with functional impact on NF- κ B and β -catenin signaling in human cutaneous T-cell lymphoma. *Leukemia* 2018; **32**:2211–23.
- 23 Fantin VR, Loboda A, Paweletz CP et al. Constitutive activation of signal transducers and activators of transcription predicts vorinostat resistance in cutaneous T-cell lymphoma. *Cancer Res* 2008; **68**:3785–94.
- 24 Eriksen KW, Kaltoft K, Mikkelsen G et al. Constitutive STAT3-activation in Sézary syndrome: typhostin AG490 inhibits STAT3-activation, interleukin-2 receptor expression and growth of leukemic Sézary cells. *Leukemia* 2001; **15**:787–93.
- 25 Nielsen M, Kaltoft K, Nordahl M et al. Constitutive activation of a slowly migrating isoform of Stat3 in mycosis fungoides: typhostin AG490 inhibits Stat3 activation and growth of mycosis fungoides tumor cell lines. *Proc Natl Acad Sci U S A* 1997; **94**:6764–9.
- 26 Diamandidou E, Colome M, Fayad L et al. Prognostic factor analysis in mycosis fungoides/Sézary syndrome. *J Am Acad Dermatol* 1999; **40**:914–24.
- 27 Losdyck E, Hornakova T, Springuel L et al. Distinct acute lymphoblastic leukemia (ALL)-associated janus kinase 3 (JAK3) mutants exhibit different cytokine-receptor requirements and JAK inhibitor specificities. *J Biol Chem* 2015; **290**:29022–34.
- 28 Axelrod PI, Lorber B, Vonderheid EC. Infections complicating mycosis fungoides and Sézary syndrome. *JAMA* 1992; **267**:1354–8.
- 29 Blaizot R, Ouattara E, Fauconneau A et al. Infectious events and associated risk factors in mycosis fungoides/Sézary syndrome: a retrospective cohort study. *Br J Dermatol* 2018; **179**:1322–8.
- 30 Willerslev-Olsen A, Krejsgaard T, Lindahl LM et al. Staphylococcal enterotoxin A (SEA) stimulates STAT3 activation and IL-17 expression in cutaneous T-cell lymphoma. *Blood* 2016; **127**:1287–96.
- 31 Vermeer MH, van Doorn R, Dijkman R et al. Novel and highly recurrent chromosomal alterations in Sézary syndrome. *Cancer Res* 2008; **68**:2689–98.
- 32 Bastidas Torres AN, Cats D, Mei H et al. Genomic analysis reveals recurrent deletion of JAK-STAT signaling inhibitors HNRNPK and SOCS1 in mycosis fungoides. *Genes Chromosomes Cancer* 2018; **57**:653–64.
- 33 Ferrara G, Pancione M, Votino C et al. A specific DNA methylation profile correlates with a high risk of disease progression in stage I classical (Alibert–Bazin type) mycosis fungoides. *Br J Dermatol* 2014; **170**:1266–75.
- 34 Talpur R, Sui D, Gangar P et al. Retrospective analysis of prognostic factors in 187 cases of transformed mycosis fungoides. *Clin Lymphoma Myeloma Leuk* 2016; **16**:49–56.

Supporting Information

Additional Supporting Information may be found in the online version of this article at the publisher's website:

Fig S1. Expression of immunomarkers in a formalin-fixed paraffin-embedded sample of a patient with mycosis fungoides.

Fig S2. (a) Workflow followed in the mutational screening in the study. (b) Example of the quality control step in the Truseq methodology. (c) An agarose gel of a formalin-fixed paraffin-embedded sample.

Fig S3. Immunohistochemical data from patients with clinical information.

Fig S4. Kaplan–Meier curves for the immunomarkers not associated with the tumour phase or advanced clinical stage.

Fig S5. Immunohistochemical data in progression biopsies.

Table S1 Antibodies used in the immunohistochemical analysis.

Table S2 Information on the 547 probes included in pool A of the Truseq Custom Amplicon Low Input.

Table S3 Anchored-adaptor primers used for library preparation of hotspot mutations in PLCG1, JAK1 and JAK3.

Table S4 Anchored-adaptor primers used for Truseq validation of selected regions.

Table S5 Mutational landscape and phenotype–genotype association.



Mutated JAK kinases and deregulated STAT activity are potential therapeutic targets in cutaneous T cell lymphoma

by Cristina Pérez, Julia González-Rincón, Arantza Onaindia, Carmen Almaráz, Nuria García-Díaz, Helena Pisonero, Soraya Curiel-Olmo, Sagrario Gómez, Laura Cereceda, Rebeca Madureira, Mercedes Hospital, Dolores Suárez-Massa, José L. Rodríguez-Peralto, Concepción Postigo C., Alicia Leon-Castillo, Carmen González-Vela, Nerea Martínez, Pablo Ortiz-Romero, Margarita Sánchez-Beato, Miguel Á. Piris, and José P. Vaqué

Haematologica 2015 [Epub ahead of print]

*Citation: Pérez C, González-Rincón J, Onaindia A, Almaráz C, García-Díaz N, Pisonero H, Curiel-Olmo S, Gómez S, Cereceda L, Madureira R, Hospital M, Suárez-Massa D, Rodríguez-Peralto JL, Postigo C, Leon-Castillo A, González-Vela C, Martínez N, Ortiz-Romero P, Sánchez-Beato M, Piris MA, and Vaqué JP. Mutated JAK kinases and deregulated STAT activity are potential therapeutic targets in cutaneous T cell lymphoma. Haematologica. 2015; 100:xxx
doi:10.3324/haematol.2015.132837*

Publisher's Disclaimer.

E-publishing ahead of print is increasingly important for the rapid dissemination of science. Haematologica is, therefore, E-publishing PDF files of an early version of manuscripts that have completed a regular peer review and have been accepted for publication. E-publishing of this PDF file has been approved by the authors. After having E-published Ahead of Print, manuscripts will then undergo technical and English editing, typesetting, proof correction and be presented for the authors' final approval; the final version of the manuscript will then appear in print on a regular issue of the journal. All legal disclaimers that apply to the journal also pertain to this production process.

Mutated JAK kinases and deregulated STAT activity are potential therapeutic targets in cutaneous T cell lymphoma

Cristina Pérez¹, Julia González-Rincón², Arantza Onaindia³, Carmen Almaráz¹, Nuria García-Díaz¹, Helena Pisonero¹, Soraya Curiel-Olmo¹, Sagrario Gómez², Laura Cereceda¹, Rebeca Madureira¹, Mercedes Hospital⁴, Dolores Suárez-Massa⁵, José L. Rodríguez-Peralto⁶, Concepción Postigo C.⁷, Alicia Leon-Castillo³, Carmen González-Vela³, Nerea Martínez¹, Pablo Ortiz-Romero^{7#}, Margarita Sánchez-Beato^{2#}, Miguel Á. Piris^{1,3#} and José P. Vaqué^{1,8#+}.

¹Cancer Genomics Laboratory Instituto de Investigación Maques de Valdecilla, IDIVAL, Santander, Spain.

²Lymphoma Research Group (Medical Oncology Service) Oncohematology Area, Instituto Investigación Sanitaria Puerta de Hierro-Majadahonda (IDIPHIM), Madrid, Spain.

³Pathology Department, Hospital Universitario Marqués de Valdecilla, Santander, Spain.

⁴Dermatology Service , Hospital Universitario Puerta de Hierro-Majadahonda, Madrid, Spain.

⁵Pathology Department, Hospital Universitario Puerta de Hierro-Majadahonda, Madrid, Spain.

⁶Pathology Department, Institute i+12, Medical School, Universidad Complutense de Madrid, Madrid, Spain.

⁷Dermatology Service, Institute i+12, Medical School, Universidad Complutense de Madrid, Madrid, Spain.

⁸Instituto de Biomedicina y Biotecnología de Cantabria, IBBTEC (CSIC, Universidad de Cantabria), Departamento de Biología Molecular, Universidad de Cantabria, Santander, Spain.

[#]Senior authors

⁺Corresponding author

Corresponding author: José P. Vaqué

Address: PCTCAN-IBBTEC. C. Albert Einstein 22. 39011 Santander, Spain

e-mail: vaquej@unican.es

Phone number: +34942206858; Fax number: +34 942 266399

The malignant mechanisms that control the development of CTCL are starting to be identified. Recent evidence suggests that disturbances in specific intracellular signaling pathways, such as RAS-MAPK, TCR-PLCG1-NFAT and JAK-STAT, can play an essential role in the pathogenesis of CTCL^{1, 2}. Our group had previously reported a network of somatic mutations affecting genes with potential to affect critical T cell-signaling pathways in CTCL patients¹. As part of our findings we detected a number of some mutations potentially affecting JAK/STAT signaling. These results have recently been confirmed by an independent group hence suggesting that mutations in this pathway may contribute as mechanisms of disease in CTCL³. Deregulated JAK/STAT signaling is involved in many types of cancer. In fact, somatically acquired genetic alterations of *JAK* or *STAT* genes that induce aberrant activation of downstream signaling, via STAT phosphorylation, have been reported in some human hematological malignancies including T-cell lymphomas^{4, 5}. We decided to explore JAK/STAT signaling as part of an intricate network of malignant signaling that controls the pathogenesis of CTCL, on the basis of the following evidence: 1) we had detected 2/11 patients and one cell line that harbored mutations in the pseudokinase domain of *JAK1* and *JAK3*; 2) we had also found several mutations that can directly (i.e., IL6S/T) or indirectly (i.e., TRAF6, RELB and CARD11) activate JAK/STAT signaling; and 3) activated STAT3 had been detected in a large proportion of CTCL patients with advanced CTCL^{6, 7}.

To explore the mutational status of *JAK* genes in a larger cohort of human CTCL patient samples and cell lines, two independent state-of-the-art ultrasequencing approaches were used: a targeted gene-enrichment kit (HaloPlex) coupled to Ion-PGM (Life Technologies) sequencing, and a specific PCR-based amplification protocol targeting the pseudokinase domains of *JAK1*, *JAK2* and *JAK3* genes (PsTKd-PCR, hereafter), followed by specific indexing and sequencing with MiSeq (Illumina; see supplementary methods for details). These are two highly sensitive methods that may enable the detection of mutations even at low frequencies in neoplastic cells or in minority clones that may be found in CTCL samples. Thus, taken together, the data from our series (including those already described in¹) enabled us to detect and validate somatic mutations in either *JAK1* or *JAK3* genes in up to seven patients and one cell line (table 1) from a total of 46 CTCL patients (Clinical data described in Supplementary table 1)

and two cell lines. A recurrent mutation, JAK1-R659C, was found affecting two different samples, patients 3 and 4 (table 1). Most of the mutations were located within the pseudokinase domain of JAK proteins, a finding that is consistent with the results of other research groups that have found somatic mutations in the same domain of JAK1 and JAK3 kinases in prolymphocytic leukemia, other T cell leukemias including CTCL and various human malignancies^{3, 4, 8-10}. Thus, it has been shown that JAK pseudokinases are autoinhibitory domains that keep the kinase domain inactive until receptor dimerization stimulates transition to an active state¹¹.

Molecular analysis of deregulated JAK/STAT signaling has provided a novel rationale for treating human cancers using targeted inhibition of JAK kinases. To explore this possibility in CTCL, we decided to study JAK/STAT activity in a panel of CTCL cell lines including HuT-78 cells carrying mutated *JAK1* and *JAK3* genes (table 1 and ⁴). We first explored the biological effects of the specific inhibition of JAK/STAT signaling in human CTCL cells. MyLa, HuT-78 and HH cell lines were incubated with increasing doses of INCB018424, a specific JAK inhibitor (INCB018424, also known as Ruxolitinib), which is currently used in the treatment of myeloproliferative disorders, which caused a dose-dependent inhibition of cell proliferation (figure 1A-C) that enabled us to calculate the IC₅₀ concentration in each case. Molecularly, these cells showed activated basal STAT phosphorylation in the absence of serum, which could be due to multiple activating mechanisms including, but not restricted, to JAK mutations. In these conditions we incubated CTCL cells at different time points with IC₅₀ concentrations of ICBB018424 and observed a marked and rapid inhibition of STAT activation that was abolished after 3 hours of treatment. Remarkably, this effect was greatly accentuated in HuT-78 cells that harbor mutations in *JAK1* and in *JAK3* genes (figure 1D-F). Thus, we have detected basal activation of JAK/STAT signaling in CTCL cells that is highly sensitive to the use of JAK inhibitors. We also studied the cytotoxic effects induced by JAK inhibition by using AnnexinV/7AAD binding and PARP cleavage, by FACS and western blot analysis, respectively, and found a moderate effect on cell death (figures 2A-F). Instead, we found that incubation with INCB018424 led to a marked inhibition of cell proliferation by a mechanism that impinges on the control of DNA synthesis, as shown by the FACS analyses illustrated in figures 2G-I. Thus, blocking JAK/STAT signaling appears to target

CTCL mechanisms of malignant cell growth more efficiently than occurs by simply inducing cytotoxic effects.

In summary, we show that *JAK1* and *JAK3* somatic mutations can contribute to deregulated JAK/STAT signaling in CTCL. Our study also provides new information that could help develop novel tools for molecular diagnosis (i.e., JAK mutations or STAT activation) as well as novel targets for therapy using specific JAK inhibitors.

ACKNOWLEDGEMENTS

We are indebted to the patients who have contributed to this study. We especially thank José Revert and Carolina Santa Cruz from IDIVAL (Santander, Spain), and the staff members of the Biobank and the Pathology service at HUMV (Santander, Spain) for their exceptional work.

This work was supported by grants from the Instituto de Salud Carlos III of the Spanish Ministry of Economy and Competence (MINECO and RTIC) to MAP (SAF2013-47416-R and RD06/0020/0107-RD012/0036/0060) and from ISCIII-MINECO-AES-FEDER to JPV, MSB and POR (Plan Nacional I+D+I: 2012-2015-PI12/00357, 2011-2014-CP11/00018), and 2014-2017-FIS PI14/01784) and the Asociación Española Contra el Cáncer to MAP. CP is a recipient of a Sara Borrel contract from MINECO (CD13/00088). JG-R is a recipient of an iPFIS fellowship (IFI14/00003) from ISCIII-MINECO-AES-FEDER (P.E.I+D+I 2013-2016). Salary support to SG was provided by CP11/00018, from ISCIII-MINECO-AES-FEDER (P.N.I+D+I 2008-2011). MSB currently holds a Miguel Servet contract (CP11/00018) from the ISCIII- MINECO-AES-FEDER (P.N.I+D+I 2008-2011), Spain. JPV was partially supported by SODERCAN and is now supported by a Ramón y Cajal research program (RYC-2013-14097).

REFERENCES

1. Vaqué JP, Gómez-López G, Monsálvez V, et al. PLCG1 mutations in cutaneous T-cell lymphomas. *Blood*. 2014;123(13):2034-2043.

2. Kiessling MK, Oberholzer PA, Mondal C, et al. High-throughput mutation profiling of CTCL samples reveals KRAS and NRAS mutations sensitizing tumors toward inhibition of the RAS/RAF/MEK signaling cascade. *Blood*. 2011;117(8):2433-2440.
3. McGirt LY, Jia P, Baerenwald DA, et al. Whole genome sequencing reveals oncogenic mutations in mycosis fungoides. *Blood*. 2015;126(4):508-519.
4. Kiel MJ, Velusamy T, Rolland D, et al. Integrated genomic sequencing reveals mutational landscape of T-cell prolymphocytic leukemia. *Blood*. 2014;124(9):1460-1472.
5. Crescenzo R, Abate F, Lasorsa E, et al. Convergent Mutations and Kinase Fusions Lead to Oncogenic STAT3 Activation in Anaplastic Large Cell Lymphoma. *Cancer Cell*. 2015;27(4):516-532.
6. Netchiporouk E, Litvinov IV, Moreau L, Gilbert M, Sasseville D, Duvic M. Deregulation in STAT signaling is important for cutaneous T-cell lymphoma (CTCL) pathogenesis and cancer progression. *Cell Cycle*. 2014;13(21):3331-3335.
7. Sommer VH, Clemmensen OJ, Nielsen O, et al. In vivo activation of STAT3 in cutaneous T-cell lymphoma. Evidence for an antiapoptotic function of STAT3. *Leukemia*. 2004;18(7):1288-1295.
8. Flex E, Petrangeli V, Stella L, et al. Somatic acquired JAK1 mutations in adult acute lymphoblastic leukemia. *J Exp Med*. 2008;205(4):751-758.
9. Xiang Z, Zhao Y, Mitaksov V, et al. Identification of somatic JAK1 mutations in patients with acute myeloid leukemia. *Blood*. 2008 111(9):4809-4812.
10. Bergmann AK, Schneppenheim S, Seifert M, et al. Recurrent mutation of JAK3 in T-cell prolymphocytic leukemia. *Genes Chromosomes Cancer*. 2014;53(4):309-316.
11. Lupardus PJ, Ultsch M, Wallweber H, Bir Kohli P, Johnson AR, Eigenbrot C. Structure of the pseudokinase-kinase domains from protein kinase TYK2 reveals a mechanism for Janus kinase (JAK) autoinhibition. *Proc Natl Acad Sci U S A*. 2014;111(22):8025-8030.

TABLE LEGEND

Table 1. Somatic mutations of JAK in CTCL patient samples. Ref/Alt, reference/alters base; AA change, aminoacid change; Pos. protein, number of aminoacid changed in the protein; PsTKd-PCR, specific pseudokinase domain PCR-based amplification protocol; Depth, total number of reads in each position; Var. Freq., Frequency of the mutated read; Vaqué JP et al. 2014¹ and Kiel MJ et al.⁴. COSMIC, mutations can be found in COSMIC database.

Table 1. Somatic mutations of JAK in CTCL patient samples.

Case	Gene	Position (hg19)	Ref/Alt	AA change	Pos. protein	Consequence	Primary Analysis	Depth	Var. Freq.	REFERENCE	COSMIC
1	JAK1	1:65312365	A/T	Y/N	652	MISSENSE	HALOPLEX	1861	0,4	This study	No data
2	JAK1	1:65313323	G/C	I/M	597	MISSENSE	HALOPLEX	1707	0,5	This study	No data
3	JAK1	1:65312344	G/A	R/C	659	MISSENSE	PstKd-PCR	3565	0,3	Vaqué JP et al. 2014 + This study	COSMIC
7	JAK3	19:17945496	G/A	P/L	745	MISSENSE	PstKd-PCR	295	0,1	This study	No data
8	JAK3	19:17948745	ATGCAGTTCT/A	KNCM/M	563 565	INDEL (DELETION)	HALOPLEX	995	0,2	Kiel MJ et al. 2014 + This study	COSMIC
8	JAK3	19:17948760	T/G	K/T	561	MISSENSE	HALOPLEX	1552	0,1	This study	No data
4	JAK1	1:65312344	G/A	R/C	659	MISSENSE	SURESELECT	N/A	N/A	Vaqué JP et al. 2014	COSMIC
9	JAK3	19:17949108	C/T	M/I	511	MISSENSE	SURESELECT	N/A	N/A	Vaqué JP et al. 2014	COSMIC
HuT-78	JAK1	1:65312358	T/A	Y/F	654	MISSENSE	PstKd-PCR	4794	0,3	Vaqué JP et al. 2014 + this study	COSMIC
HuT-78	JAK3	19:17948006	G/A	A/V	573	MISSENSE	PstKd-PCR	3308	1,0	Kiel MJ et al. 2014 + this study	COSMIC

FIGURE LEGENDS

Figure 1. Treatment with Ruxolitinib inhibits CTCL cell proliferation and JAK/STAT activity in CTCL cell lines. Cell proliferation assay in MyLa (A) HuT-78 (B) and HH (C) cells incubated for 0, 24, or 48 hours, using DMSO (control) or the indicated amount of INCB018424 (μ M). N=3; error bars indicate SEM. Analysis of basal activation STAT-1, 3 and 5 activity by western blot using total cell lysates from previously starved CTCL cell lines incubated for the indicated times with a specific JAK inhibitor (INCB018424) using the specific IC_{50} concentrations in each case (D-E).

Figure 2. Treatment with Ruxolitinib activates apoptosis and inhibits DNA-synthesis in CTCL cells. Percentage of viable MyLa (A), HuT-78 (B) and HH (C) cells incubated for 24 hours with vehicle (DMSO) or the indicated 1x or 2x IC_{50} concentration of INCB018424. Right plots are representative examples of AnnexinV (X-axis)/7AAD (Y-axis) staining data in each case. N=3; error bars indicate SEM. Representative western blot analysis using anti-PARP and anti-tubulin antibodies in whole-protein extracts from MyLa (D) HuT-78 (E) and HH (F) cells treated with DMSO or the indicated concentrations of INCB018424. C+ indicates treatment of each cell line with 20 nM of okadaic acid for 48 hours as a positive control. Percentage of total DNA-synthesis in exponentially growing MyLa (G) HuT-78 (H) and HH (I) cells incubated for 24 hours with vehicle (DMSO) or the indicated concentration of INCB018424 (as explained in figure 2). Right plots are representative examples of FITC-A (X-axis) staining data and cell count (Y-axis) staining data in each case. N=3; error bars indicate SEM.

Figure 1.

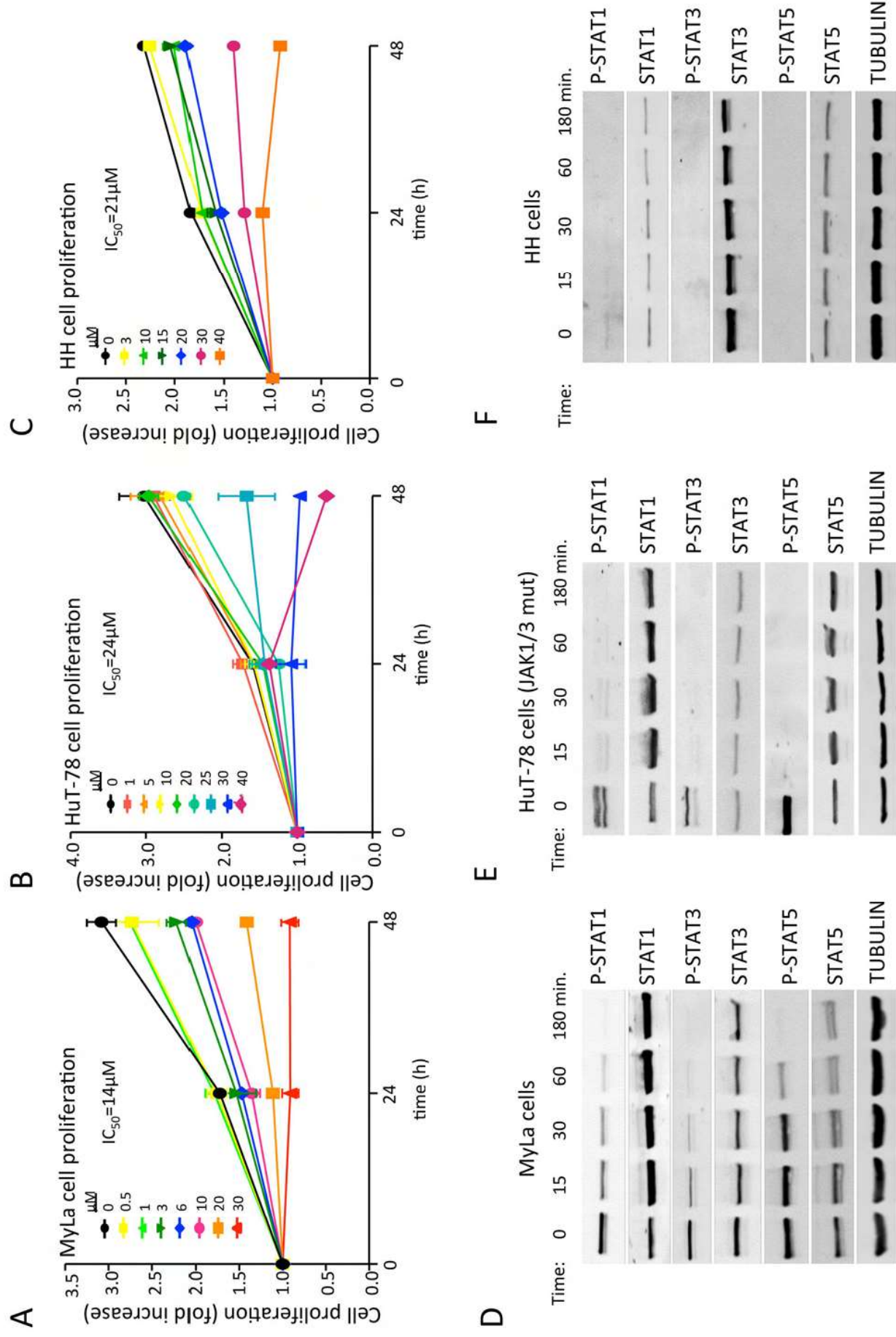
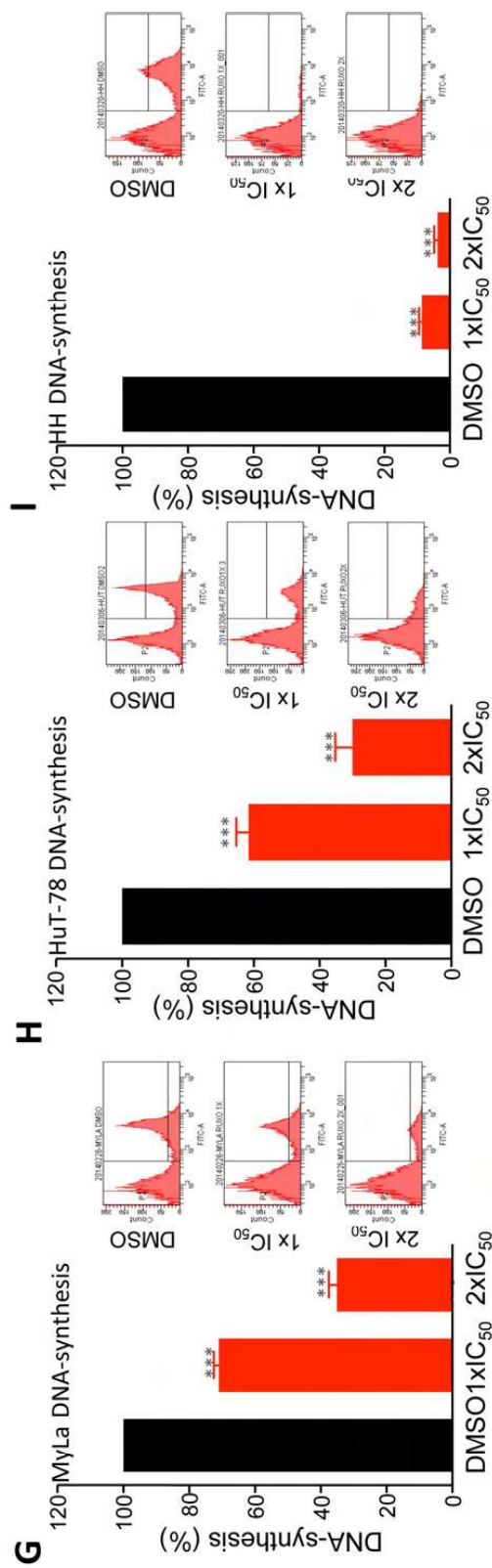
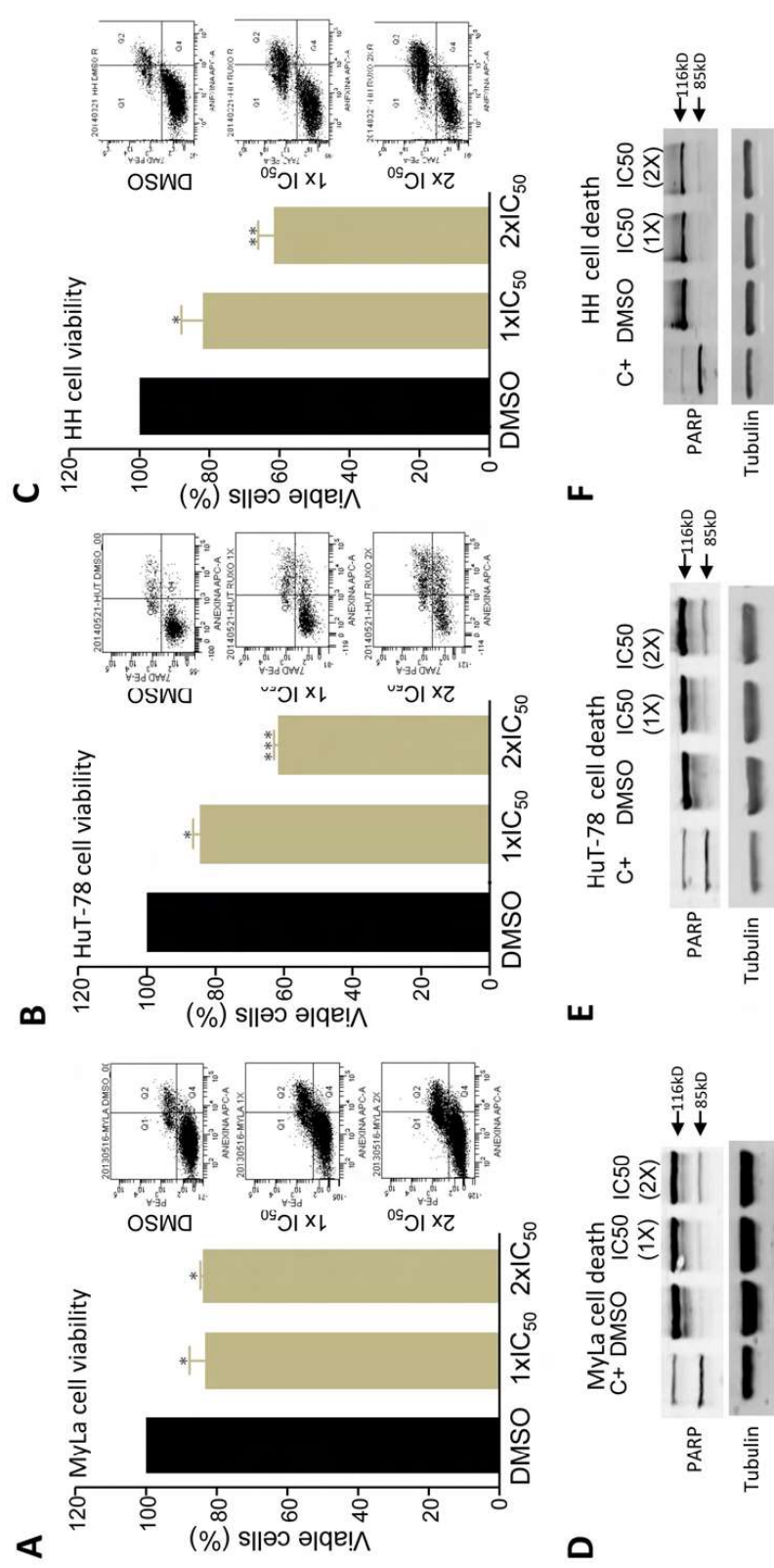


Figure 2.



ARTICLE

Open Access

Dopaminergic control of *ADAMTS2* expression through cAMP/CREB and ERK: molecular effects of antipsychotics

Fulgencio Ruso-Julve^{1,2,3}, Ana Pombero^{3,4}, Fuencisla Pilar-Cuellar^{3,5,6}, Nuria García-Díaz^{1,2,7}, Raquel Garcia-Lopez^{3,4}, María Juncal-Ruiz^{3,8}, Elena Castro^{3,5,6}, Álvaro Díaz^{3,5,6}, Javier Vazquez-Bourgón^{1,3}, Agustín García-Blanco^{1,2,7}, Emilio Garro-Martínez^{3,5,6}, Helena Pisonero^{2,7}, Alicia Estirado^{3,4}, Rosa Ayesa-Arriola^{1,3}, Juan López-Giménez⁹, Federico Mayor Jr.^{10,11}, Elsa Valdizán^{3,5,6}, Javier Meana^{1,2,3,12}, Javier Gonzalez-Maeso^{1,3}, Salvador Martínez^{3,4}, José Pedro Vaqué^{2,7} and Benedicto Crespo-Facorro^{1,3,14}

Abstract

A better understanding of the molecular mechanisms that participate in the development and clinical manifestations of schizophrenia can lead to improve our ability to diagnose and treat this disease. Previous data strongly associated the levels of deregulated *ADAMTS2* expression in peripheral blood mononuclear cells (PBMCs) from patients at first episode of psychosis (up) as well as in clinical responders to treatment with antipsychotic drugs (down). In this current work, we performed an independent validation of such data and studied the mechanisms implicated in the control of *ADAMTS2* gene expression. Using a new cohort of drug-naïve schizophrenia patients with clinical follow-up, we confirmed that the expression of *ADAMTS2* was highly upregulated in PBMCs at the onset (drug-naïve patients) and downregulated, in clinical responders, after treatment with antipsychotics. Mechanistically, *ADAMTS2* expression was activated by dopaminergic signalling (D₁-class receptors) and downstream by cAMP/CREB and mitogen-activated protein kinase (MAPK)/ERK signalling. Incubation with antipsychotic drugs and selective PKA and MEK inhibitors abrogated D₁-mediated activation of *ADAMTS2* in neuronal-like cells. Thus, D₁ receptors signalling towards CREB activation might participate in the onset and clinical responses to therapy in schizophrenia patients, by controlling *ADAMTS2* expression and activity. The unbiased investigation of molecular mechanisms triggered by antipsychotic drugs may provide a new landscape of novel targets potentially associated with clinical efficacy.

Introduction

Antipsychotic drugs (APDs) remain the standard pharmacological treatment for schizophrenia (SCZ) and psychotic disorders, mainly by targeting dopamine neurotransmission (primarily D₂ receptors)^{1–3}. APDs can be

classified into typical (i.e., haloperidol) and atypical (i.e., aripiprazole, risperidone or clozapine), the latter prescribed as first-line drugs and/or in refractory patients⁴. Despite the effectiveness of APDs in the clinical realm, there is a marked disparity among patients with respect to symptoms, responses and side effects^{5,6}. Whereas 50–60% of patients achieve an optimal degree of clinical improvement of positive symptoms, little to no improvement of negative symptoms or cognitive deficits is common⁵. Overall, estimates suggest that one-fifth to one-half of patients have treatment-resistant SCZ and about 30–60% of these respond to clozapine^{6–8}. These

Correspondence: José Pedro Vaqué (jose.vaque@unican.es) or Benedicto Crespo-Facorro (crespob@unican.es)

¹Department of Psychiatry, University Hospital Marqués de Valdecilla-IDIVAL, Santander 39011 Cantabria, Spain

²Department of Molecular Biology, School of Medicine, University of Cantabria, Santander 39011 Cantabria, Spain

Full list of author information is available at the end of the article.

These authors contributed equally: José Pedro Vaqué, Benedicto Crespo-Facorro

© The Author(s) 2019



Open Access This article is licensed under a Creative Commons Attribution 4.0 International License, which permits use, sharing, adaptation, distribution and reproduction in any medium or format, as long as you give appropriate credit to the original author(s) and the source, provide a link to the Creative Commons license, and indicate if changes were made. The images or other third party material in this article are included in the article's Creative Commons license, unless indicated otherwise in a credit line to the material. If material is not included in the article's Creative Commons license and your intended use is not permitted by statutory regulation or exceeds the permitted use, you will need to obtain permission directly from the copyright holder. To view a copy of this license, visit <http://creativecommons.org/licenses/by/4.0/>.

evidences suggest that although D₂ receptors is a direct target for all drugs used to treating SCZ, its blockade may not tackle the primary biological anomaly in a significant percentage of patients⁹. In this respect, the combined D₁ and D₂ receptors antagonism has been proposed to have synergic effects, which could account for the atypical clinical effectiveness of clozapine¹⁰. From a molecular perspective, the effects of APDs may also include the modulation of D₂ receptor-independent mechanisms through indirect effects, such as, e.g., those related to other metabotropic receptors implicated in the control cAMP-dependent signalling¹¹ and/or those related with receptor-biased agonism^{4,12}. Downstream of cAMP, the activation of protein kinase A (PKA) promotes phosphorylation of DARPP-32 (a cytosolic protein), which has been associated with the pathophysiology of SCZ^{13,14}. In addition, the glutamate hypothesis of SCZ led to explore its potential clinical application as targets for therapy¹⁵. The investigation of the mechanisms downstream of the receptors targeted by APDs will certainly guide to finding out new explanations for pathophysiological mechanisms and novel approaches for therapy⁴.

A new paradigm has emerged based on the investigation of transcriptional patterns associated with clinical responses in SCZ, raising the likelihood of revealing unknown molecular mechanisms associated with anti-psychotic action that may be crucial in accomplishing optimal clinical responses^{16,17}. Using an unbiased transcriptome approach, we have previously described a set of genes that are differentially expressed at the onset of SCZ¹⁶. In addition to this, we also showed significant differential gene expression elicited after a 3-month APD treatment in responder patients¹⁷. Among the above-mentioned results, *ADAMTS2* was the highest upregulated gene in SCZ patients at the onset of the disease and also was the most significant downregulated gene, back to 'healthy levels', in responder patients to treatment with APDs. The observation that the expression of *ADAMTS2* can be modulated by APDs and its association with clinical response, makes it an appealing candidate to investigate its interface with illness pathology and clinical efficacy¹⁷.

In the present work we initially performed an independent validation using a new cohort of drug-naïve non-affective psychosis patients. We confirmed that *ADAMTS2* expression was significantly overexpressed at diagnosis, and that treatment with APDs reduced their expression levels back to 'healthy' values, which, in turn, was associated with clinical responses (positive symptoms). However, the molecular or cellular mechanisms exerted by APDs to regulate *ADAMTS2* expression are unknown. Following a bottom-up strategy starting from the transcriptional data obtained in SCZ cases and taking advantage of neuronal-like cells towards the identification

of membrane receptors and the intracellular mechanism controlled by them, we herein provide new evidence that *ADAMTS2* expression is regulated by dopaminergic signalling cascade (D₁-class receptors) through ERK and cAMP/cAMP response element-binding protein (CREB) activities.

Materials and methods

Human samples and study setting

Human samples for this study were obtained from an ongoing epidemiological and 3-year longitudinal intervention programme of first-episode psychosis (PAFIP) conducted at the University Hospital Marques de Valdecilla (Cantabria, Spain) and biological samples were provided by the IDIVAL biobank. The study was approved by the Cantabria Ethics Institutional Review Board, conforming to international standards for research ethics. Patients meeting inclusion criteria and their families provided written informed consent to be included in the PAFIP.

A new independent set of 30 APD-naïve, first-episode non-affective individuals and 10 healthy individuals (without a history of neuropsychiatric disorders) were used to validate gene expression profiles related to clinical response (Table 1).

Briefly, all patients underwent a head-to-head risperidone and aripiprazole randomized (simple randomization procedure), flexible-dose, open-label study (EudraCT number 2013-005399-16). More detailed information about PAFIP and treatment protocol has been published elsewhere^{17,18} and also is briefly available in Supplementary Information.

RNA extraction

Peripheral blood from patients and controls was extracted using the Tempus™ Blood RNA Tube (Applied Biosystems, UK). Peripheral blood mononuclear cell (PBMC) isolation was performed using a Ficoll-Paque Premium reagent (Sigma) and total mRNA isolation using a Tempus™ Spin RNA Isolation Kit (Invitrogen, CA, USA), following the manufacturer's instructions. RNA Integrity Number (RIN) was characterized with a Bioanalyzer (Agilent Technologies) and samples with a RIN > 8 were selected. Total mRNA from culture cells was extracted using Trizol reagent (Invitrogen) and its concentration was determined using a Nanodrop 2000 spectrophotometer (Thermo Scientific, IL, USA).

RT-PCR and quantitative PCR

cDNA synthesis was performed using the SuperScript IV Reverse Transcriptase (Invitrogen). cDNA was amplified using the Power SYBR™ Green PCR Master Mix (Applied Biosystems) in a 7300 Fast Real-Time PCR System (Applied Biosystems). Specific oligos for human

Table 1 Psychopathological characteristics at baseline, at 3 months and clinical changes during the follow-up period. Comparison between aripiprazole and risperidone.

	Total (N = 30)		Statistics	p	Aripiprazole (n = 16)		Risperidone (n = 14)		Statistics	p
	Mean	SD			Mean	SD	Mean	SD		
CGI										
Baseline	6.5	0.6			6.56	0.51	6.43	0.65	t = 0.63 ^C	0.532
3 Months	1.8	1.2			1.63	1.20	2.00	1.24		
3-Month change from baseline	−4.7	1.2	z = 4.83 ^a	0.000	−4.90	0.30	−4.47	0.33	F = 0.96 ^d	0.336
YMRS										
Baseline	13.8	6.2			14.25	7.24	13.29	5.01	t = 0.42 ^C	0.679
3 Months	1.2	2.3			1.56	2.63	0.79	1.93		
3-Month change from baseline	−12.6	6.5	z = 4.78 ^a	0.000	−12.25	0.59	−13.00	0.63	F = 0.75 ^d	0.394
CDSS										
Baseline	1.5	3.0			2.06	3.82	0.86	1.75	t = 1.08 ^C	0.288
3 Months	1.2	2.3			1.19	2.34	1.14	2.25		
3-Month change from baseline	−0.3	3.7	z = 0.35 ^a	0.724	−0.34	0.59	−0.32	0.63	F = 0.00 ^d	0.985
BPRS										
Baseline	70.3	15.0			69.06	16.08	71.85	13.95	t = − 0.49 ^C	0.627
3 Months	29.9	7.1			29.06	7.07	30.92	7.48		
3-Month change from baseline	−40.4	15.2	t = 14.32 ^b	0.000	−41.13	1.81	−39.53	2.01	F = 0.35 ^d	0.561
SAPS										
Baseline	15.9	4.2			15.63	3.50	16.07	4.94	t = − 0.29 ^C	0.775
3 Months	0.6	1.7			0.69	1.89	0.71	1.49		
3-Month change from baseline	−15.4	4.3	t = 19.28 ^b	0.000	−15.14	0.44	−15.12	0.47	F = 0.00 ^d	0.975
SANS										
Baseline	4.8	6.9			3.47	6.56	5.93	7.43	t = − 0.95 ^C	0.352
3 Months	3.9	6.6			4.00	6.47	4.93	7.04		
3-Month change from baseline	−0.9	5.6	z = 1.14 ^a	0.255	−0.07	1.54	−0.36	1.59	F = 0.02 ^d	0.899

BPRS Brief Psychiatric Rating Scale, CDSS Calgary Depression Rating Scale for Schizophrenia, CGI Clinical Global Impression, SANS Scale for the Assessment of Negative Symptoms, SAPS Scale for the Assessment of Positive Symptoms, YMRS Young Mania Rating Scale

^aWilcoxon matched-pairs signed-rank test

^bPaired Student's t-test

^cComparison between aripiprazole and risperidone at baseline; unpaired Student's t-test

^dComparison between aripiprazole and risperidone following the antipsychotic treatment, using the total score of the clinical scales at baseline as covariate; analysis of covariance (ANCOVA)

ADAMTS2, *CREB1*, and *C-FOS* were designed using Primer-Blast (NCBI; see sequences in Supplementary Table S1). *ACTB* expression was used to normalize values. Gene expression changes were determined using $2^{(-\Delta\Delta Ct)}$ formula. A melting curve was generated for every run to confirm assay specificity.

Cell culture and treatments

Human neuroblastoma (SK-N-SH, ATCC HTB-11) and 293T (ATCC CRL-3216) cells were obtained from the American Type Cell Collection (Rockville, MD). Cells

were cultured in modified Eagle's medium and Dulbecco's Modified Eagle's Medium, respectively (Corning, VA, USA). Culture medium was supplemented with 10% dialysed fetal bovine serum (dFBS; HyClone, UT, USA), glucose, L-glutamine, streptomycin sulphate and potassium penicillin (10,000 U/L) (Lonza, Belgium).

Drugs and pharmacological agents

Aripiprazole, clozapine, haloperidol hydrochloride, H89 dihydrochloride, L 741,626, MDL 100907, paliperidone, risperidone, SKF 83822, SCH 39166, TCB-2, WAY

100635, 7-OH-DPAT and 8-OH-DPAT were purchased from Tocris Bioscience (Spain). Forskolin and selumetinib (AZD6244) were purchased from Selleckchem (Spain). Cholera toxin (CTX), pertussis toxin (PTX) and 12-O-tetradecanoylphorbol-13-acetate (TPA) were purchased from Sigma-Aldrich (MO, USA). YM-254890 was purchased from Adipogen Life Sciences (CA, USA). All were dissolved in dimethyl sulfoxide, except CTX and WAY 100635 that were dissolved in water.

Luciferase report assays

Luciferase report assays were performed by transfection with 0.5 µg DNA of the following plasmids mix (ratio 3:1): pGL4.29[luc2P/CRE/Hygro] containing firefly luciferase reporter, alongside pRL-Null containing *Renilla* luciferase used as control (Promega, WI, USA). Cells were transfected with Lipofectamine LTX with PLUS reagents (Invitrogen) in transient conditions. Firefly and *Renilla* levels were detected using Dual-Luciferase Reporter Assay System kit and quantified using a GloMax-Multi apparatus (Promega).

Western blotting

Cells were starved overnight before treatment. Whole cell lysates were obtained using RIPA buffer (Sigma) supplemented with phosphatase and protease inhibitors (Roche, Germany). Protein expression was analysed by western blotting as described previously¹⁹. Briefly, antibodies used were as follows: phospho-CREB, CREB, phospho-ERK1/2, ERK1/2, phospho-p38, p38, and phospho-PKA substrates (Cell Signaling, MA, USA), and β-Tubulin (Santa Cruz Biotechnology). Fluorophore conjugate antibodies were obtained from Invitrogen. Signals were visualized and recorded with an Odyssey Infrared Imaging scanner (LI-COR Biosciences, NE, USA). Immunoblot densitometry analysis on every band was calculated using Image Studio Software (LI-COR Biosciences). Phosphorylation and total protein densitometry values were normalized to β-Tubulin signal.

CREB knocked down reagents and procedures

ShCREB1-inducible SK-N-SH cells were generated by lentiviral infection of SK-N-SH cells with SMARTvector carrying tGFP and human inducible *CREB1* short hairpin RNA (shRNA) mCMV constructs or non-target control shRNA (Dharmacon, CO, USA). Lentiviral particles were produced by co-transfection of 293T cells using Trans-Lentiviral shRNA Packaging System (Dharmacon), according to the manufacturer's protocol. Cells were incubated with doxycycline (1 µg/ml) (Sigma) for 72 h to induce green fluorescent protein and shRNA expression. SK-N-SH cells expressing stable shCREB1 constructs were generated by direct transfection by Lipofectamine LTX with PLUS reagent (Invitrogen) using pGFP-V-RS-

CREB1 shRNA expression vectors or scrambled control (Origene, MD, USA). Transfected cells were selected with puromycin (1 µg/mL) at least 7 days.

Statistical analyses

Kolmogorov–Smirnov test and Levene test were used to test normality and equality of variances, respectively.

For patients' studies, to ensure group comparability between healthy volunteers and patients, socio-demographic and clinical characteristics at baseline were tested by unpaired Student's *t*-test or one-way analysis of variance (ANOVA) for continuous variables as necessary, and by Fisher's exact test for qualitative variables (Table 1 and Supplementary Table S2).

Wilcoxon's signed-rank test for independent data was used to compare the *ADAMTS2* mRNA expression level among healthy volunteers and drug-naïve patients at baseline. Wilcoxon's matched-pairs signed-rank test for paired data was performed to compare the change in the mRNA expression level from baseline to 3 months following the antipsychotic treatment ($\alpha = 0.05$). STATA 15.1 was used for statistical analysis.

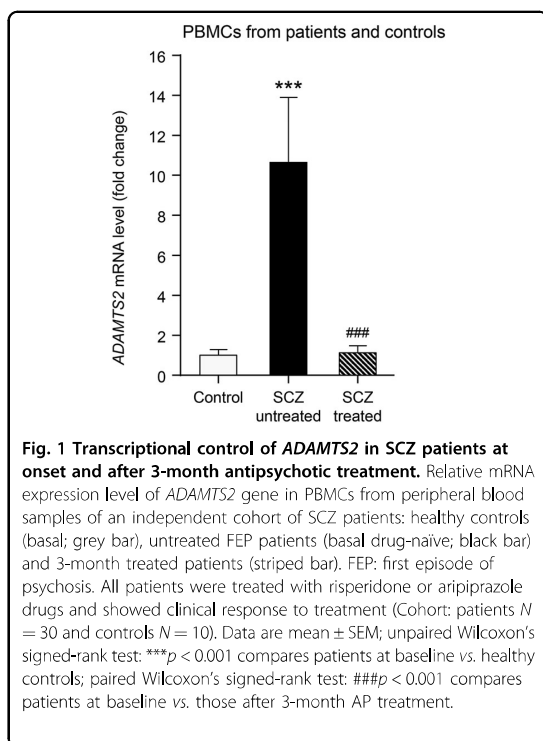
For in vitro studies, unless otherwise specified, all experiments were independent and numerical data were summarized as the mean ± SEM using GraphPad Prism6 software. Each global mean was compared using unpaired Student's *t*-test (two tailed; $\alpha = 0.05$) or one-way ANOVA followed by post-hoc test where appropriated, as described in each figure legend.

Results

ADAMTS2 expression is controlled by APD treatment in SCZ patients

To better evaluate the mechanistic effects of atypical APDs in SCZ patients, we prepared and studied a new cohort of 30 drug-naïve SCZ patients with baseline quantitative data (sociodemographic and clinical characteristics) and clinical follow-up data, after 3 months of treatment with APDs (Table 1). We found significant within-subject changes between baseline data and after 3 months of treatment in both risperidone and aripiprazole groups. These changes were observed in CGI (Clinical Global Impression, $p < 0.000$), YMRS (Young Mania Rating Scale, $p < 0.000$), BPRS (Brief Psychiatric Rating Scale, $p < 0.000$) and SAPS (Scale for the Assessment of Positive Symptoms, $p < 0.000$) total scores. However, as it is shown in Table 1, no differences were found in total scores of the clinical scales when the two APD groups were compared at baseline and after 3 months of treatment.

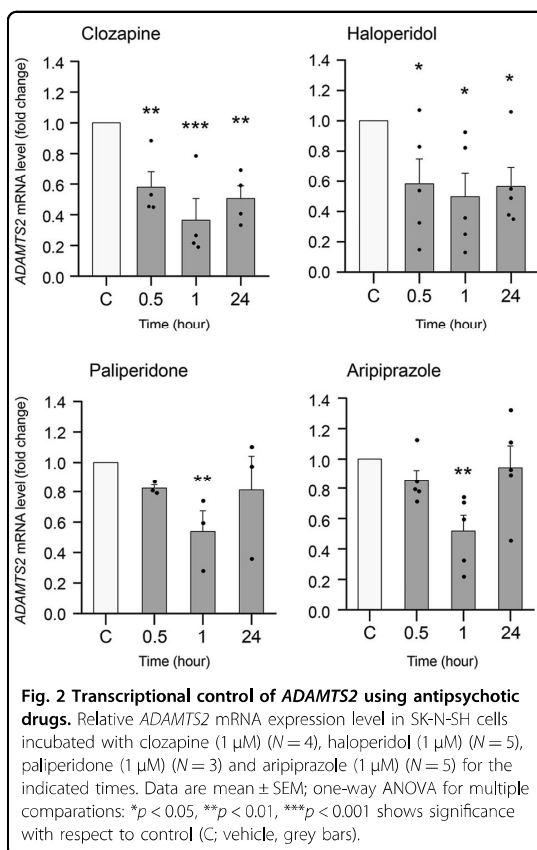
To analyse transcriptomic changes, we obtained PBMCs isolated from blood samples from SCZ patients, which were obtained at the first episode of psychosis (onset) and after a 3-month period of treatment with APDs. In this



context, using quantitative reverse transcriptase PCR (RT-qPCR), we performed an independent validation of transcriptional changes by focusing on *ADAMTS2*. Thus, we confirmed *ADAMTS2* as a significant gene that was highly overexpressed at the onset, with respect to healthy controls, and downregulated by APDs after 3 months of treatment (Fig. 1).

Dynamic control of *ADAMTS2* transcription by APDs in neuronal-like cells

To gain mechanistic insight into the transcriptional control of *ADAMTS2*, we analysed the effects of APDs in SK-N-SH cells using dFBS. No significant differences in *ADAMTS2* expression were observed when dFBS was not present in the culture medium (data not shown). These cells express cell surface receptors that are targets of APDs (i.e., D_1 , D_2 , 5-HT_{1A} and 5-HT_{2A} receptors) as well as detectable basal expression of *ADAMTS2* mRNA. Our data showed that incubation with APDs in these cells induced dynamic changes in *ADAMTS2* mRNA expression along time. Incubation with atypical APDs such as paliperidone, aripiprazole (Fig. 2) and risperidone (Supplementary Fig. S1), provoked a dynamic inhibition of *ADAMTS2* basal mRNA expression in these cells with fast (<1 h) but transitory responses. Interestingly, clozapine (atypical APD) and haloperidol (typical APD) induced a



fast and sustained (up to 24 h) inhibition of *ADAMTS2* expression (Fig. 2).

Neurotransmitter receptors and associated signalling pathways involved in the control of *ADAMTS2* gene expression

Using selective agonists for D_1 , D_2 , 5-HT_{1A} and 5-HT_{2A} receptors in SK-N-SH cells, we observed that SKF 83822 (a D_1 -class receptor agonist) significantly triggered *ADAMTS2* mRNA expression compared with the lack of effect of 7-OH-DPAT, 8-OH-DPAT and TCB-2 (agonists of D_2 , 5-HT_{1A} and 5-HT_{2A} receptors, respectively) (Fig. 3a). In addition, using selective antagonists for these receptors, we observed that only SCH 39166 (a D_1 -class receptor antagonist) significantly downregulated *ADAMTS2* mRNA expression, whereas L 741,626, WAY 100635 and MDL 100907 (antagonists of D_2 , 5-HT_{1A} and 5-HT_{2A} receptors, respectively) were devoid of this effect (Fig. 3a). Furthermore, we analysed *ADAMTS2* mRNA and protein expression profiles in the brain of developing and early postnatal mice (see Supplementary Methods). Interestingly and in support of our previous results in

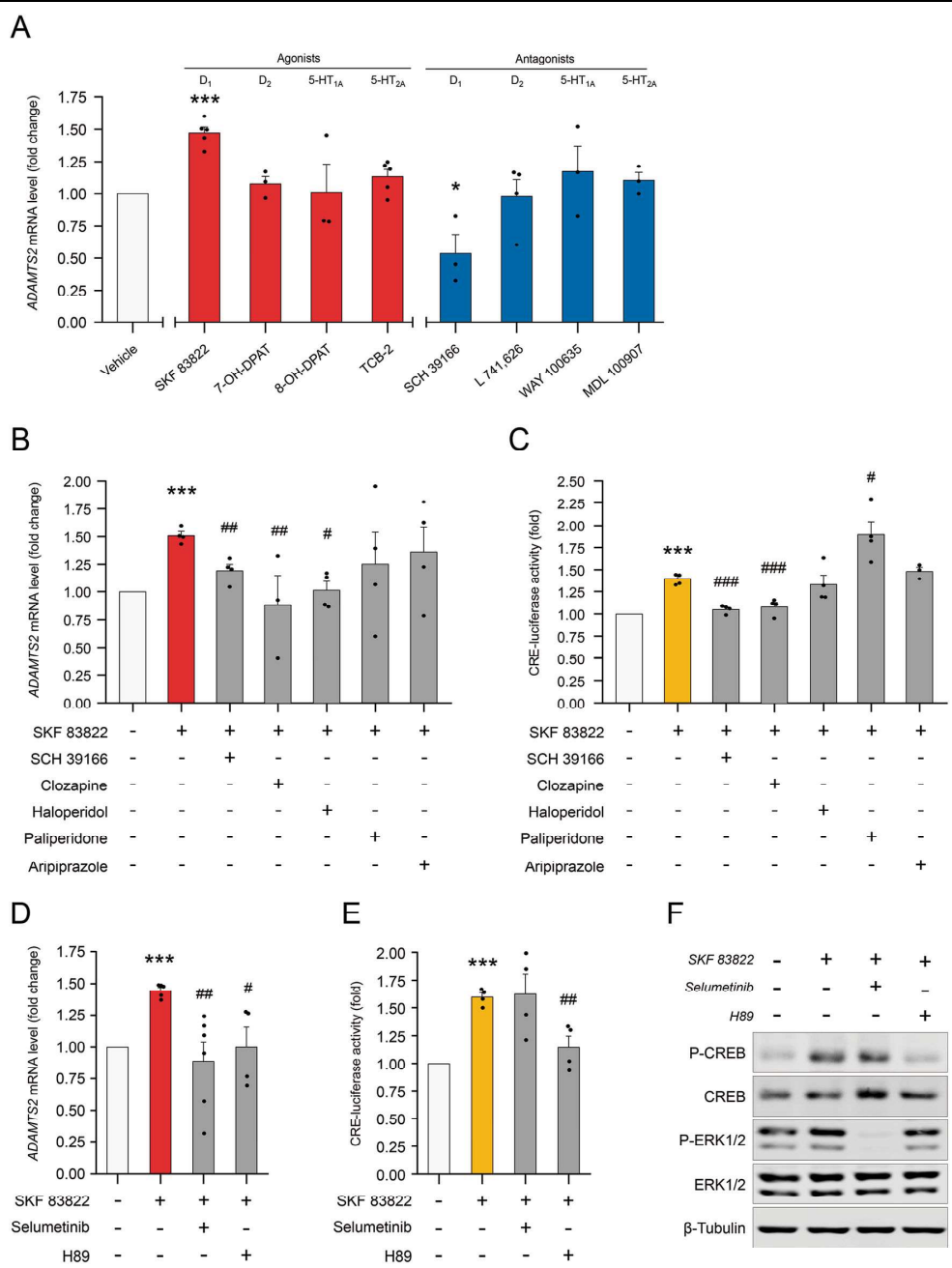


Fig. 3 (See legend on next page.)

(see figure on previous page)

Fig. 3 Neurotransmitter receptors and associated signalling pathways involved in the control of *ADAMTS2* gene expression. **a** *ADAMTS2* mRNA levels by RT-qPCR in SK-N-SH cells incubated 1 h with the indicated selective receptor agonist (red bars): SKF 83822 (D_1 -class receptors) ($N = 5$), 7-OH-DPAT (D_2 -class receptors) ($N = 3$), 8-OH-DPAT (5-HT $_{1A}$ receptor) ($N = 3$) and TCB-2 (5-HT $_{2A/2C}$ receptors) ($N = 5$); and selective antagonist (blue bars): SCH 39166 (D_1 -class receptors) ($N = 3$), L 741,626 (D_2 -class receptors) ($N = 4$), WAY 100635 (5-HT $_{1A}$ receptors) ($N = 3$) and MDL 100907 (5-HT $_{2A}$ receptors) ($N = 3$) (Drug concentration 1 μ M). **b** *ADAMTS2* mRNA levels by RT-qPCR in cells incubated for 1 h with SKF 83822 ($N = 4$) and pre-incubated also for 30 min with SCH 39166 ($N = 4$), clozapine ($N = 3$), haloperidol ($N = 4$), paliperidone ($N = 4$) or aripiprazole ($N = 4$) (Drug concentration 1 μ M). **c** CREB activity in cells transfected with CRE-Luc alongside pRL-Null: cells were pre-incubated for 1 h with the indicated APDs and then, incubated for 24 h with SKF 82833 (10 μ M) ($N = 4$). **d** *ADAMTS2* mRNA levels by RT-qPCR: SK-N-SH cells were pre-incubated for 30 min with MAPK/ERK and cAMP-PKA inhibitors (selumetinib 1 μ M $N = 6$ and H89 10 μ M $N = 4$, respectively) and then, incubated for 1 h with SKF 82833 (1 μ M) ($N = 5$). **e** CREB activity in cells transfected with CRE-Luc alongside pRL-Null ($N = 4$): SK-N-SH cells were pre-incubated for 1 h with the indicated inhibitors and then incubated for 24 h with SKF 82833 (10 μ M). **f** Western blottings showing relative phosphorylation levels of CREB and ERK1/2: SK-N-SH cells were pre-incubated for 1 h with the indicated inhibitors and then incubated for 15 min with SKF 82833 (1 μ M) ($N = 3$). Blots are representative images of each western-blot. Data are mean \pm SEM; Student's t -test: * $p < 0.05$ and *** $p < 0.001$ vs. control condition (vehicle), and # $p < 0.05$, ## $p < 0.01$, ### $p < 0.001$ vs. SKF 83822 condition.

cells, *ADAMTS2* was specifically localized in brain regions that are part of the mesolimbic and mesocortical dopamine systems (Supplementary Fig. S2).

Next, we studied whether treatment with APDs could modulate *ADAMTS2* gene expression activated downstream of the D_1 receptor. Our results show that haloperidol and clozapine could significantly block SKF 83822-mediated transcriptional activation of *ADAMTS2*. As expected, SCH 39166, a selective D_1 receptor antagonist, also prevented D_1 receptor-mediated activation of *ADAMTS2* (Fig. 3b). In addition, the reduction in *ADAMTS2* expression induced by clozapine was prevented by L 741,626 and MDL 100907 (a D_2 and 5-HT $_{2A}$ receptor antagonists, respectively) (Supplementary Fig. S3).

As D_1 receptors are known to signal through $G_{\alpha s}$, we sought to confirm its role at controlling *ADAMTS2* expression in our system, alongside $G_{\alpha i}$ and $G_{\alpha q}$. For this purpose, we incubated SK-N-SH cells with CTX ($G_{\alpha s}$ activator), PTX ($G_{\alpha i}$ inhibitor) and YM-254890 (a specific $G_{\alpha q}$ inhibitor)²⁰, before activating D_1 receptors with SKF 83822. The activation of $G_{\alpha s}$ (Supplementary Fig. S4A) and the inhibition of $G_{\alpha i}$ (Supplementary Fig. S4B) per se significantly upregulated *ADAMTS2* expression. Moreover, the inhibition of $G_{\alpha i}$ potentiated *ADAMTS2* expression after D_1 receptor activation (Supplementary Fig. S4B). Finally, the inhibition of $G_{\alpha q}$ did not modify the basal and the SKF 83822-mediated increase of *ADAMTS2* expression (Supplementary Fig. S4C).

Incubation of neuronal-like cells with the selective D_1 receptor agonist (SKF 83822) provoked rapid phosphorylation of CREB and ERK1/2 (15 min), and no changes in p38 (Supplementary Fig. S4D-F). In addition, rapid phosphorylation of PKA substrates was detected in response to SKF 83822 (Supplementary Fig. S4G). To evaluate CREB-dependent transcriptional activity in neuronal-like cells, we took advantage of a CRE-luciferase reporter. We analysed if APDs could counteract the intracellular signalling activation mediated by selective SKF 83822 D_1 -class receptor agonist. Our results (Fig. 3c)

demonstrate that preincubation with clozapine, but not haloperidol, paliperidone, or aripiprazole, prevented SKF 83822-induced CREB activation using a specific reporter assay.

To evaluate the potential contribution of PKA and ERK to the activation of *ADAMTS2* expression, we incubated SK-N-SH cells with SKF 83822 D_1 receptor agonist in combination with selective MAPK/ERK (selumetinib-AZD6244) and cAMP/PKA (H89 dihydrochloride) inhibitors. Both inhibitors prevented D_1 receptor induced expression of *ADAMTS2* (Fig. 3d), although only a cAMP/PKA inhibitor abrogated CREB-dependent transcription and phosphorylation (Fig. 3e, f).

Transcriptional mechanisms controlling *ADAMTS2* gene expression downstream of dopamine D_1 receptors

Our previous data suggest that there is a rapid activation of the signalling mechanisms controlling CREB activation after D_1 receptor activation that can be modulated pharmacologically. We decided to challenge the contribution of cAMP/CREB signalling to the transcriptional activation of *ADAMTS2* (Fig. 4a). We initially evaluated the activation of *ADAMTS2* gene expression together with that of *C-FOS*, an 'early response gene' known to be a direct transcriptional target of CREB that was used as control. Our data showed that SKF 83822 activated mRNA expression of both *ADAMTS2* and *C-FOS*. Interestingly, incubation with forskolin alone (a selective adenylyl cyclase activator) was sufficient to trigger the transcription of both genes, whereas TPA (a PKC/MAPK activator) uniquely activated *C-FOS* transcription.

To explore the implication of CREB in D_1 receptor-mediated *ADAMTS2* expression, we generated stable SK-N-SH cells with inducible expression of control or *CREB1* shRNAs upon addition of doxycycline to the culture media. Using this approach, we reduced *CREB1* mRNA and protein expression, as shown in Fig. 4b. Under these settings, SKF 83822 and forskolin failed to induce the expression of *ADAMTS2* (Fig. 4c). Interestingly, SKF

83822 did not significantly activate *C-FOS* expression in *CREB1* knocked down cells when compared with control cells; in contrast, TPA did (Fig. 4d). A schematic representation of the signalling pathways and the molecules used in this work is illustrated in Fig. 5 for explanatory purposes. The above-mentioned results were further confirmed using SK-N-SH cells stably expressing control or *CREB1* shRNAs (Supplementary Fig. S5). Mechanistically, reduced *CREB* expression did not impair ERK phosphorylation elicited downstream of *D*₁ receptor activation by SKF 83822 (Fig. 4e). In this context, we also used forskolin and TPA as controls for selective activation of *CREB* and ERK, respectively (Fig. 4e and Supplementary Fig. S6). Thus, activation of *CREB* seems to play a key role in the control of *ADAMTS2* gene expression downstream of *D*₁ receptors.

Discussion

Our results revealed that treatment with APDs control *ADAMTS2* expression, which is directly associated with dopaminergic signalling, primarily with the *D*₁-class receptors and downstream through cAMP/*CREB* and MAPK signalling. Interestingly, *ADAMTS2* mRNA and protein were specifically found in mesolimbic and mesocortical dopaminergic regions in mice. Our data suggest that *D*₁ receptor signalling towards *CREB* activation and its effects on *ADAMTS2* expression may be linked to key biological mechanisms in SCZ and the clinical response to APDs^{21,22}.

In the context of the local PAFIP programme, we collected a new cohort of 30 drug-naïve SCZ patients with associated clinical data and follow-up. Using these cases alongside 'healthy' controls, we attempted an independent validation of our previous results using a different cohort of cases^{16,17}. In this cohort, we confirmed *ADAMTS2* as a significant gene that was highly overexpressed at baseline in PBMCs from drug-naïve SCZ individuals and which returned to 'normal' levels in clinical responders treated with APDs (clinical rate scales in Table 1). Although, there is not always a direct correlation between the biomarkers obtained in peripheral blood cells and the central nervous system (CNS) samples, a previous study in a rodent model of SCZ have shown a certain parallelism between the expression in human PBMCs^{16,17} and mouse frontal cortex samples²³. Supporting the previously mentioned data, *ADAMTS2* mRNA expression was quickly downregulated by all APDs in neuronal-like cells. Moreover, whereas the activities of paliperidone, risperidone, and aripiprazole downregulating *ADAMTS2* mRNA were transitory in such cells, those of clozapine and haloperidol were sustained to up to 24 h. The molecular effects exerted by clozapine and haloperidol as compared with other APDs might deserve further

investigations. In this respect, clozapine has shown superior efficacy for treatment-resistant and suicidality, as well as its apparent ability to decrease substance use in SCZ²⁴. Thus, *ADAMTS2* might play a key, and yet to be defined, mechanistic role in both the illness onset and clinical responses, regardless of the type of APD used.

There is scarce information regarding specific *ADAMTS2* expression and activity in the CNS. Therefore, we analysed the expression profiles of *ADAMTS2* mRNA and protein in mice. Interestingly, these were specifically localized in brain regions that are part of the mesolimbic and mesocortical dopamine systems (i.e., the dentate gyrus in the hippocampus and the ventral tegmental area^{21,22,25}). At a prenatal stage (E18.5), *ADAMTS2* protein was mapped in the neuropiles of anterior brain structures, anterior cingulate cortex, superficial striatum and lateral septum, where neuronal expression of dopamine *D*₁ and *D*₂ receptors was detected by in situ hybridization (<http://developingmouse.brain-map.org/>). The hypothesis that dopamine and dopaminergic mechanisms are essential to psychosis, and particularly to SCZ, has been one of the most enduring ideas about this disorder²⁶. Elevated presynaptic striatal dopamine correlates most closely with the symptom dimension of psychosis and blockade of this heightened transmission leads to a resolution of symptoms for most patients²⁷. Nonetheless, the functional association between *ADAMTS2* and the dopaminergic system has not been previously established, to our best knowledge. *ADAMTS2* is a member of the ADAM Metalloproteinase with Thrombospondin family^{28,29}, with a number of targets such as the *N*-propeptides of procollagens I–III, fibronectin, decorin and Dkk3 participating in extracellular matrix (ECM) organization, as well as in transforming growth factor (TGF)- β and WNT signalling^{30,31}. Alterations in the ECM as well as TGF- β and WNT signalling have been associated with SCZ^{32–34}. Moreover, deregulated mRNA expression of MMPs (MMP-16, -24 and -25) and ADAMTS (ADAMTS-1, -6 and -8) families of proteases have also been reported in SCZ^{35,36}. Thus, considering *ADAMTS2* expression and its associated activities in the CNS, as well as the data presented in this work, it is conceivable to speculate that it could participate in SCZ at different stages of the disease. In this regard, a selective *D*₁-class receptor agonist (SKF 83822) significantly activated *ADAMTS2* expression, and haloperidol and clozapine blocked this activation in neuronal-derived cells. It will be of interest, to address these appealing questions, within the next future, using SCZ and/or *ADAMTS2* transgenic mice models.

*D*₁ receptors are the most abundant dopaminergic receptor in CNS and their functional crosstalk with *D*₂ receptor is well documented^{11,37,38}. *D*₁ receptor activate adenylyl cyclase (AC), which in turn regulate intracellular cAMP levels leading to PKA activation and *CREB* phosphorylation^{39–41}. Our data have shown that selective *D*₁ receptor activation upregulated *ADAMTS2* expression

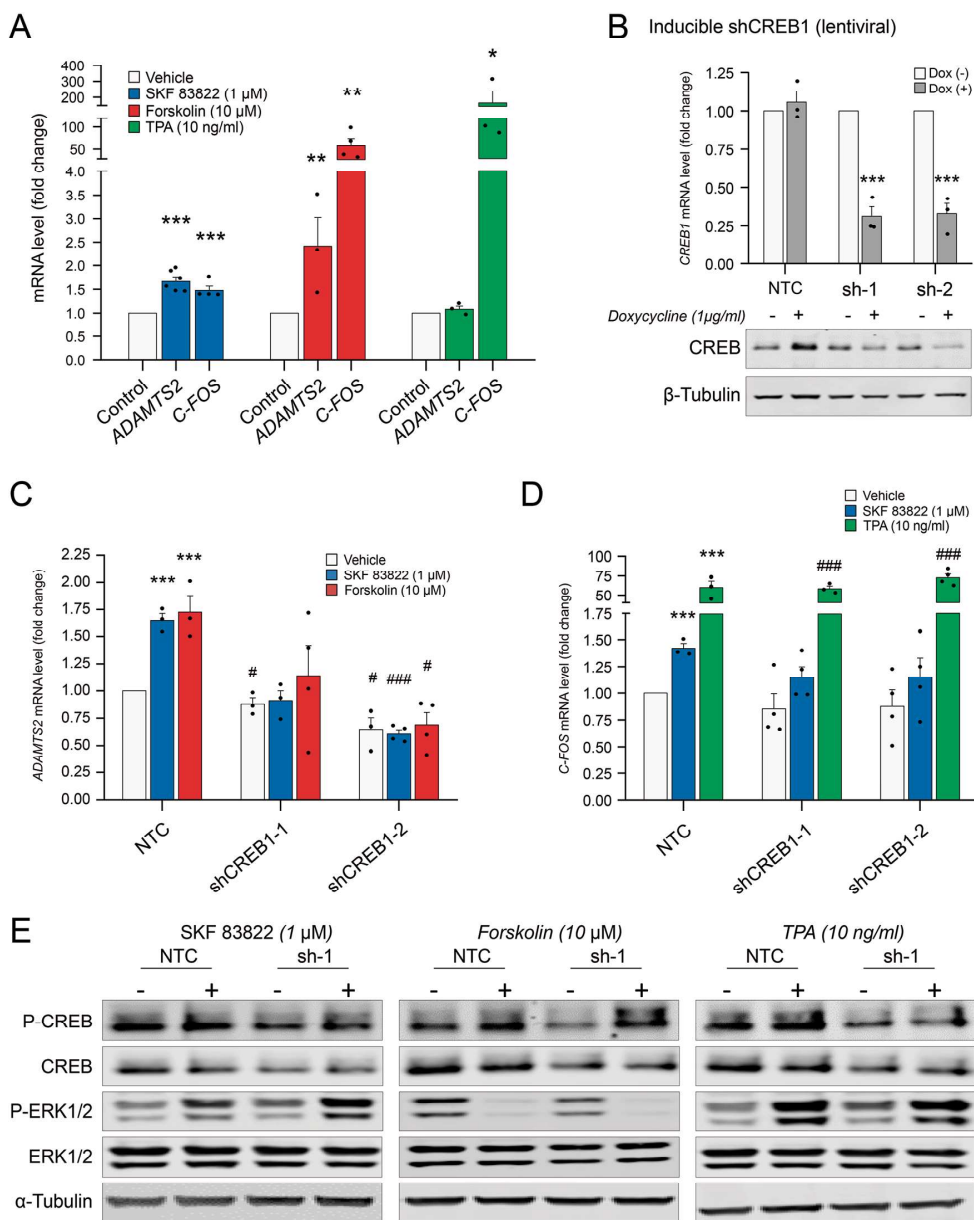
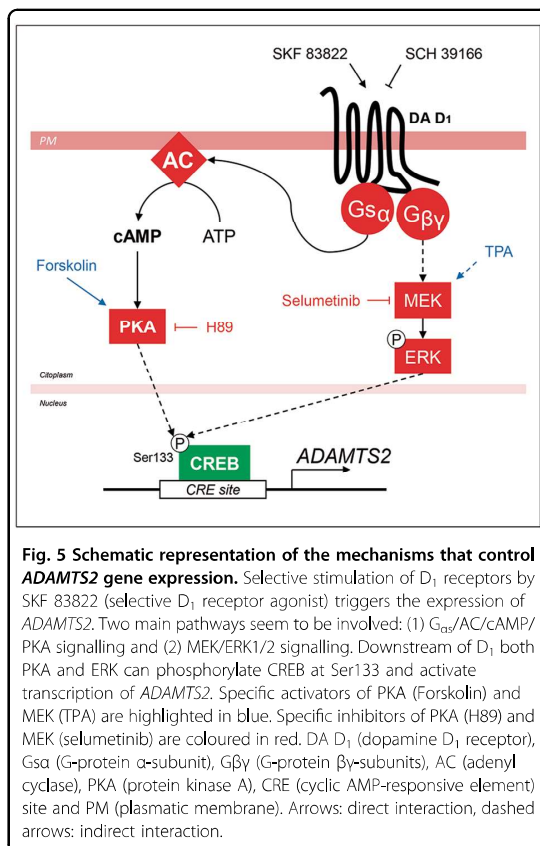


Fig. 4 Transcriptional mechanisms that control *ADAMTS2* gene expression downstream of dopamine D_1 -class receptors. **a** RT-qPCR showing *ADAMTS2* and *C-FOS* mRNA expression level in SK-N-SH cells incubated for 1 h with SKF 83822 (1 μ M; blue bars) ($N = 6$ and $N = 4$, respectively), forskolin (10 μ M; red bars) ($N = 3$ and $N = 4$, respectively) and TPA (10 ng/ml; green bars) ($N = 3$). **b** *CREB1* knockdown SK-N-SH cells by lentiviral inducible shRNA and GFP reporter construct (yellow bars), incubated with doxycycline (1 μ g/ml) for 72 h, *CREB1* mRNA level (up) and CREB protein total expression (down) in non-targeted control (NTC) or shCREB1 cells ($N = 3$). Inducible *CREB1* Knockdown SK-N-SH cells were incubated for 1 h with SKF 83822 (1 μ M, blue bars), forskolin (10 μ M, red bars) and TPA (10 ng/ml, green bars): RT-qPCR showing *ADAMTS2* (**c**) and *C-FOS* (**d**) mRNA expression in inducible shCREB1 or non-targeted control (NTC) cells incubated with doxycycline (1 μ g/ml) for 72 h ($N = 3-4$). **e** Shows western blottings using anti-phospho-CREB and anti-phospho-ERK, as well as anti-CREB and anti-ERK antibodies: inducible shCREB1 or non-targeted control (NTC) SK-N-SH cells incubated with doxycycline (1 μ g/ml) for 72 h and then incubated for 15 min with SKF 83822 (1 μ M), forskolin (10 μ M) and TPA (10 ng/ml) ($N = 3$). Inducible knockdown cells were selected with puromycin (1 μ g/ml) at least 7 days. Blots images are representative of independent experiments. Data are mean \pm SEM; Student's *t*-test: * $p < 0.05$, ** $p < 0.01$, *** $p < 0.001$ vs. vehicle or doxycycline (—); and # $p < 0.05$, ### $p < 0.001$ vs. each condition in NTC cells.



alongside a rapid phosphorylation of CREB and ERK proteins, which resulted in CREB-mediated transcriptional activity as detected by using specific reporter assays (Fig. 3). In support of this and in our system, *ADAMTS2* transcription was specifically triggered by activation of D₁ receptors (by SKF 83822), G_{sα} (using CTX) and AC (forskolin). Thus, it is possible that, as part of the dopaminergic activity, *ADAMTS2* could act as a major cAMP/CREB effector in SCZ. Interestingly, D₁ receptor-mediated CREB activation was abrogated by clozapine (Fig. 3c), providing evidence that cAMP/CREB signalling, and therefore *ADAMTS2* expression, can be modulated by APDs. Our findings reveal the contribution of D₁ receptors over *ADAMTS2* transcription, and also indicate the participation of D₂ and 5-HT_{2A} receptors in the effect of clozapine in the control of *ADAMTS2* expression. In this regard, it has been reported that clozapine can act as a biased agonist on 5-HT_{2A} receptors^{42,43} and/or affect the hetero-dimer D₂/5-HT_{2A}⁴⁴. Moreover, disrupting cAMP/CREB and ERK signalling using selective PKA and MEK inhibitors also impaired *ADAMTS2* expression and CREB activity (in this case, only when it was PKA dependent) in neuronal-like

cells. Supporting these observations, recent data pointed at cAMP/CREB signalling as an important mechanism linking dopaminergic signalling with the pathophysiology of SCZ⁴⁵. Moreover, incubating SK-N-SH cells with forskolin was sufficient to trigger *ADAMTS2* expression that occurred alongside PKA and CREB activation. Forskolin directly activates AC in mammals, thereby promoting a rapid phosphorylation of CREB via PKA^{46,47}. In addition, in CREB-knockdown cells, D₁ receptor activation failed to increase *ADAMTS2* gene expression, reinforcing the idea that cAMP/CREB is an essential mechanism to control *ADAMTS2* transcriptional activation.

Finally, a number of potential limitations could be considered when interpreting our data and the scope of our findings: (1) sample size in this study is rather small ($N=30$). Noteworthy, we selected a group of patients with a first episode of non-affective psychosis, who had not previously taken APDs (not even a single dose) at the time of baseline blood test to avoid any interference with the mRNA levels. Only those individuals who gave written consent and had mRNA samples at baseline and at 3 months were eligible for this study. Therefore, all these stringent inclusion criteria limited the number of patients in this cohort. Further investigations to replicate our findings using larger and more heterogeneous groups are warranted. (2) Transcriptomic data obtained from blood samples might not resemble that of the brain. (3) *ADAMTS2* protein and mRNA expression show modest but detectable levels in 'healthy' human and mouse brain samples (<https://www.proteinatlas.org>). Thus, it is conceivable to detect high fold increases when analysing diseased specimens, like in this case *ADAMTS2* in SCZ. (4) Failure of some APDs to inhibit CREB activity and/or *ADAMTS2* mRNA expression in a D₁ receptor-context. Our data herein do not discard that APDs might regulate *ADAMTS2* by indirect mechanisms like for example those involving β-arrestin, ERK or AKT signalling^{42,48}.

In conclusion, we have confirmed the association between *ADAMTS2* expression and SCZ disease including its potential role in the clinical efficacy of APDs. Transcription of *ADAMTS2* is primarily controlled by the activity of D₁-class receptors through cAMP/CREB and MAPK signalling. The unbiased investigation of the molecular mechanisms triggered by APDs, may provide a landscape of novel targets potentially associated with improved therapeutic responses.

Acknowledgements

We are highly indebted to the participants and their families for their cooperation in this study. We also thank IDIVAL biobank (Inés Santiuste and Jana Arozamena) for clinical samples and data as well as the PAFIP members (Marga Corredera) for the data collection. This work was supported by: SAF2016-76046-R and SAF2013-46292-R (MINECO and FEDER) to B.C.F., PI16/00156 (ISCIII and FEDER) to J.P.V., LUCHAMOS POR LA VIDA project to F.R.J. and J.P.V., SAF2017-83702-R (MINECO and FEDER), Red TERCEL RD12/0019/0024 (ISCIII) and GVA-PROMETEO 2018/041 (Generalitat Valenciana) to S.M. J.P.V. is

supported by the RyC research programme (RYC-2013-14097) and F.R.J. by the predoctoral research programme (BES-2014-070615), from MINECO and FEDER.

Author details

¹Department of Psychiatry, University Hospital Marqués de Valdecilla-IDIVAL, Santander 39011 Cantabria, Spain. ²Department of Molecular Biology, School of Medicine, University of Cantabria, Santander 39011 Cantabria, Spain. ³Centro de Investigación Biomédica en Red de Salud Mental (CIBERSAM), Instituto de Salud Carlos III, Madrid 28029, Spain. ⁴Instituto de Neurociencias, UMH-CSIC, Alicante 3550, Spain. ⁵Instituto de Biomedicina y Biotecnología de Cantabria, IBBTEC (Universidad de Cantabria, CSIC, SODERCAN), 39011 Santander, Cantabria, Spain. ⁶Department of Physiology and Pharmacology, School of Medicine, University of Cantabria, Santander 39011 Cantabria, Spain. ⁷Infection, Immunity and Digestive Pathology Group, University Hospital Marqués de Valdecilla-IDIVAL, Santander 39011 Cantabria, Spain. ⁸Department of Psychiatry, Sierrallana Hospital, Torrelavega 39300 Cantabria, Spain. ⁹Institute of Parasitology and Biomedicine “López-Neyra” (IPBLN-CSIC), Armilla 18016 Granada, Spain. ¹⁰Department of Molecular Biology, Centro de Biología Molecular “Severo Ochoa” (UAM-CSIC), Universidad Autónoma de Madrid, Madrid 28049, Spain. ¹¹Centro de Investigación Biomédica en Red de Enfermedades Cardiovasculares (CIBERCV), Instituto de Salud Carlos III, Madrid 28029, Spain. ¹²Department of Pharmacology, University of the Basque Country UPV/EHU, Leioa 48940 Bizkaia, Spain. ¹³Department of Physiology and Biophysics, Virginia Commonwealth University School of Medicine, P. O. Box 980551 Molecular Medicine Research Building 5-038, Richmond 23298 Virginia, USA. ¹⁴Department of Psychiatry, School of Medicine, University Hospital Virgen del Rocío-IBIS, Sevilla 41013, Spain

Conflict of interest

The authors declare that they have no conflict of interest.

Publisher's note

Springer Nature remains neutral with regard to jurisdictional claims in published maps and institutional affiliations.

Supplementary Information accompanies this paper at (<https://doi.org/10.1038/s41398-019-0647-7>).

Received: 8 May 2019 Revised: 8 October 2019 Accepted: 20 October 2019
Published online: 18 November 2019

References

- Chouinard, G. et al. Antipsychotic-induced dopamine supersensitivity psychosis: pharmacology, criteria, and therapy. *Psychother. Psychosom.* **86**, 189–219 (2017).
- Seeman, P. Targeting the dopamine D2 receptor in schizophrenia. *Expert Opin. Ther. Targets* **10**, 515–531 (2006).
- Rampino, A. et al. Antipsychotic drug responsiveness and dopamine receptor signaling: old players and new prospects. *Front. Psychiatry* **9**, 702 (2018).
- Aringhieri, S. et al. Molecular targets of atypical antipsychotics: from mechanism of action to clinical differences. *Pharm. Ther.* **192**, 20–41 (2018).
- Fusar-Poli, P. et al. Treatments of negative symptoms in schizophrenia: meta-analysis of 168 randomized placebo-controlled trials. *Schizophr. Bull.* **41**, 892–899 (2015).
- Meltzer, H. Y. Treatment-resistant schizophrenia—the role of clozapine. *Curr. Med. Res. Opin.* **14**, 1–20 (1997).
- Elkis, H. Treatment-resistant schizophrenia. *Psychiatr. Clin. North Am.* **30**, 511–533 (2007).
- Gillespie, A. L., Samanata, R., Mill, J., Egerton, A. & MacCabe, J. H. Is treatment-resistant schizophrenia categorically distinct from treatment-responsive schizophrenia? a systematic review. *BMC Psychiatry* **17**, 12 (2017).
- Stone, J. M. Glutamatergic antipsychotic drugs: a new dawn in the treatment of schizophrenia? *Ther. Adv. Psychopharmacol.* **1**, 5–18 (2011).
- Nordstrom, A. L. et al. D1, D2, and 5-HT2 receptor occupancy in relation to clozapine serum concentration: a PET study of schizophrenic patients. *Am. J. Psychiatry* **152**, 1444–1449 (1995).
- Miller, R. Mechanisms of action of antipsychotic drugs of different classes, refractoriness to therapeutic effects of classical neuroleptics, and individual variation in sensitivity to their actions: Part I. *Curr. Neuropharmacol.* **7**, 302–314 (2009).
- Wisler, J. W., Xiao, K., Thomsen, A. R. & Lefkowitz, R. J. Recent developments in biased agonism. *Curr. Opin. Cell Biol.* **27**, 18–24 (2014).
- Wang, H., Farhan, M., Xu, J., Lazarovici, P. & Zheng, W. The involvement of DARPP-32 in the pathophysiology of schizophrenia. *Oncotarget* **8**, 53791–53803 (2017).
- Nishi, A. et al. Glutamate counteracts dopamine/PKA signaling via dephosphorylation of DARPP-32 Ser-97 and alteration of its cytonuclear distribution. *J. Biol. Chem.* **292**, 1462–1476 (2017).
- Nicoletti, F., Bruno, V., Ngomba, R. T., Gradini, R. & Battaglia, G. Metabotropic glutamate receptors as drug targets: what's new? *Curr. Opin. Pharm.* **20**, 89–94 (2015).
- Sainz, J. et al. Inflammatory and immune response genes have significantly altered expression in schizophrenia. *Mol. Psychiatry* **18**, 1056–1057 (2013).
- Crespo-Facorro, B., Prieto, C., Sainz, J. Schizophrenia gene expression profile reverted to normal levels by antipsychotics. *Int. J. Neuropsychopharmacol.* **18**, pii: pyu066 (2014).
- Pelayo-Teran, J. M. et al. Epidemiological factors associated with treated incidence of first-episode non-affective psychosis in Cantabria: insights from the Clinical Programme on Early Phases of Psychosis. *Early Inter. Psychiatry* **2**, 178–187 (2008).
- Llerena, S. et al. Applied diagnostics in liver cancer. Efficient combinations of sorafenib with targeted inhibitors blocking AKT/mTOR. *Oncotarget* **9**, 30869–30882 (2018).
- Zhang, H., Nielsen, A. L., Stromgaard, K. Recent achievements in developing selective Gq inhibitors. *Med. Res. Rev.* **1**–23 (2019).
- Phillipson, O. T. Afferent projections to the ventral tegmental area of Tsai and interfascicular nucleus: a horseradish peroxidase study in the rat. *J. Comp. Neurol.* **187**, 117–143 (1979).
- Khilghatyan, J., Quintana, C., Parent, M., Beaulieu, J. M. High sensitivity mapping of cortical dopamine D2 receptor expressing neurons. *Cereb. Cortex* **29**, 3813–3827 (2018).
- Lopez-Gimenez, J. F. et al. Validation of schizophrenia gene expression profile in a preclinical model of maternal infection during pregnancy. *Schizophr. Res.* **189**, 217–218 (2017).
- Khokhar, J. Y., Henricks, A. M., Sullivan, E. D. K. & Green, A. I. Unique effects of clozapine: a pharmacological perspective. *Adv. Pharm.* **82**, 137–162 (2018).
- Rice, M. W., Roberts, R. C., Melendez-Ferro, M. & Perez-Costas, E. Mapping dopaminergic deficiencies in the substantia nigra/ventral tegmental area in schizophrenia. *Brain Struct. Funct.* **221**, 185–201 (2016).
- Howes, O. D. & Kapur, S. The dopamine hypothesis of schizophrenia: version III—the final common pathway. *Schizophr. Bull.* **35**, 549–562 (2009).
- Kapur, S., Zipursky, R., Jones, C., Remington, G. & Houle, S. Relationship between dopamine D(2) occupancy, clinical response, and side effects: a double-blind PET study of first-episode schizophrenia. *Am. J. Psychiatry* **157**, 514–520 (2000).
- Mead, T. J. & Apte, S. S. ADAMTS proteins in human disorders. *Matrix Biol.* **71–72**, 225–239 (2018).
- Kelwick, R., Desantis, L., Wheeler, G. N. & Edwards, D. R. The ADAMTS (a disintegrin and metalloproteinase with thrombospondin motifs) family. *Genome Biol.* **16**, 113 (2015).
- Colige, A. et al. Domains and maturation processes that regulate the activity of ADAMTS-2, a metalloproteinase cleaving the aminopeptide of fibrillar procollagens types I and V. *J. Biol. Chem.* **280**, 34397–34408 (2005).
- Bekhouche, M. et al. Determination of the substrate repertoire of ADAMTS2, 3, and 14 significantly broadens their functions and identifies extracellular matrix organization and TGF-beta signaling as primary targets. *FASEB J.* **30**, 1741–1756 (2016).
- Berretta, S. Extracellular matrix abnormalities in schizophrenia. *Neuropharmacology* **62**, 1584–1597 (2012).
- Benes, F. M. et al. Regulation of the GABA cell phenotype in hippocampus of schizophrenics and bipolars. *Proc. Natl Acad. Sci. USA* **104**, 10164–10169 (2007).
- Hoseth, E. Z. et al. Exploring the Wnt signaling pathway in schizophrenia and bipolar disorder. *Transl. Psychiatry* **8**, 55 (2018).
- Pietersen, C. Y. et al. Molecular profiles of parvalbumin-immunoreactive neurons in the superior temporal cortex in schizophrenia. *J. Neurogenet.* **28**, 70–85 (2014).

36. Pietersen, C. Y. et al. Molecular profiles of pyramidal neurons in the superior temporal cortex in schizophrenia. *J. Neurogenet.* **28**, 53–69 (2014).
37. Miller, R. Mechanisms of action of antipsychotic drugs of different classes, refractoriness to therapeutic effects of classical neuroleptics, and individual variation in sensitivity to their actions: Part II. *Curr. Neuropharmacol.* **7**, 315–330 (2009).
38. Paul, M. L., Graybiel, A. M., David, J. C. & Robertson, H. A. D1-like and D2-like dopamine receptors synergistically activate rotation and c-fos expression in the dopamine-depleted striatum in a rat model of Parkinson's disease. *J. Neurosci.* **12**, 3729–3742 (1992).
39. Belgacem, Y. H. & Borodinsky, L. N. CREB at the crossroads of activity-dependent regulation of nervous system development and function. *Adv. Exp. Med. Biol.* **1015**, 19–39 (2017).
40. Carlezon, W. A. Jr., Duman, R. S. & Nestler, E. J. The many faces of CREB. *Trends Neurosci.* **28**, 436–445 (2005).
41. Lonze, B. E. & Ginty, D. D. Function and regulation of CREB family transcription factors in the nervous system. *Neuron* **35**, 605–623 (2002).
42. Aringhieri, S. et al. Clozapine as the most efficacious antipsychotic for activating ERK 1/2 kinases: role of 5-HT_{2A} receptor agonism. *Eur. Neuropsychopharmacol.* **27**, 383–398 (2017).
43. Schmid, C. L., Streicher, J. M., Meltzer, H. Y. & Bohn, L. M. Clozapine acts as an agonist at serotonin 2A receptors to counter MK-801-induced behaviors through a betaarrestin2-independent activation of Akt. *Neuropsychopharmacology* **39**, 1902–1913 (2014).
44. Lukasiewicz, S., Faron-Gorecka, A., Kedracka-Krok, S. & Dziedzicka-Wasylewska, M. Effect of clozapine on the dimerization of serotonin 5-HT_{2A} receptor and its genetic variant 5-HT_{2A}H425Y with dopamine D₂ receptor. *Eur. J. Pharm.* **659**, 114–123 (2011).
45. Wang, H., Xu, J., Lazarovici, P., Quirion, R. & Zheng, W. cAMP response element-binding protein (CREB): a possible signaling molecule link in the pathophysiology of schizophrenia. *Front. Mol. Neurosci.* **11**, 255 (2018).
46. Seamon, K. B., Padgett, W. & Daly, J. W. Forskolin: unique diterpene activator of adenylate cyclase in membranes and in intact cells. *Proc. Natl Acad. Sci. USA* **78**, 3363–3367 (1981).
47. Zhang, G., Liu, Y., Ruoho, A. E. & Hurley, J. H. Structure of the adenylyl cyclase catalytic core. *Nature* **386**, 247–253 (1997).
48. Del'guidice, T., Lemasson, M. & Beaulieu, J. M. Role of beta-arrestin 2 downstream of dopamine receptors in the basal ganglia. *Front. Neuroanat.* **5**, 58 (2011).

Applied diagnostics in liver cancer. Efficient combinations of sorafenib with targeted inhibitors blocking AKT/mTOR

Susana Llerena^{1,2,*}, Nuria García-Díaz^{3,4,*}, Soraya Curiel-Olmo³, Antonio Agraz-Doblas^{4,5}, Agustín García-Blanco^{1,2}, Helena Pisonero^{2,4}, María Varela⁶, Miguel Santibáñez⁷, Carmen Almaraz³, Laura Cereceda³, Nerea Martínez³, María Teresa Arias-Loste^{1,2}, Ángela Puente^{1,2}, Luis Martín-Ramos^{1,2}, Carlos Rodríguez de Lope^{1,2}, Federico Castillo-Suescun⁸, Carmen Cagigas-Fernandez⁸, Pablo Isidro⁹, Carlos Lopez-López¹⁰, Marcos Lopez-Hoyos¹¹, Javier Llorca^{12,13}, Jesús Agüero¹⁴, Benedicto Crespo-Facorro^{15,16}, Ignacio Varela⁴, Miguel Ángel Piris^{17,**}, Javier Crespo^{1,2,**} and José Pedro Vaqué^{2,4,**}

¹Gastroenterology and Hepatology Unit, Hospital Universitario Marqués de Valdecilla, Santander, Spain

²Infection, Immunity and Digestive Pathology Group, IDIVAL, Santander, Spain

³Translational Hematopathology Group, IDIVAL, Instituto de Investigación Marqués de Valdecilla, Santander, Spain

⁴Departamento de Biología Molecular, Universidad de Cantabria (UC-IBBTEC), Santander, Spain

⁵Josep Carreras Leukemia Research Institute and School of Medicine, University of Barcelona, Barcelona, Spain

⁶Digestive Service, Hepatology Unit, Hospital Universitario Central de Asturias, Oviedo, Spain

⁷Universidad de Cantabria-IDIVAL, Santander, Spain

⁸General and Digestive Tract Surgery Service, Hospital Universitario Marqués de Valdecilla, Santander, Spain

⁹Biobanco-Hospital Universitario Central de Asturias, Oviedo, Spain

¹⁰Oncology Service, Hospital Universitario Marqués de Valdecilla, Santander, Spain

¹¹Immunology Service, Hospital Universitario Marqués de Valdecilla, Santander, Spain

¹²Department of Epidemiology and Computational Biology, School of Medicine, University of Cantabria, Santander, Spain

¹³CIBER Epidemiología y Salud Pública (CIBERESP), Madrid, Spain

¹⁴Microbiology Service, University Hospital Marques de Valdecilla-IDIVAL, Santander, Spain

¹⁵Department of Psychiatry, Marqués de Valdecilla University Hospital-IDIVAL, Santander, Spain

¹⁶CIBERSAM, Centro de Investigación Biomédica en Red Salud Mental, Madrid, Spain

¹⁷Department of Pathology, Fundación Jiménez Díaz, Madrid, Spain

*These authors have contributed equally to this work

**Senior author

Correspondence to: José Pedro Vaqué, **email:** vaquej@unican.es

Keywords: hepatocellular carcinoma; mutations; sorafenib; targeted therapy; AKT/mTOR

Received: January 16, 2018

Accepted: June 22, 2018

Published: July 20, 2018

Copyright: Llerena et al. This is an open-access article distributed under the terms of the Creative Commons Attribution License 3.0 (CC BY 3.0), which permits unrestricted use, distribution, and reproduction in any medium, provided the original author and source are credited.

ABSTRACT

Hepatocellular carcinoma (HCC) is the third most common cause of cancer-related deaths worldwide. There is increasing interest in developing specific markers to serve as predictors of response to sorafenib and to guide targeted therapy. Using a sequencing platform designed to study somatic mutations in a selection of 112 genes (HepatoExome), we aimed to characterize lesions from HCC patients and cell lines, and to use the data to study the biological and mechanistic effects of case-specific

targeted therapies used alone or in combination with sorafenib. We characterized 331 HCC cases in silico and 32 paired samples obtained prospectively from primary tumors of HCC patients. Each case was analyzed in a time compatible with the requirements of the clinic (within 15 days). In 53% of the discovery cohort cases, we detected unique mutational signatures, with up to 34% of them carrying mutated genes with the potential to guide therapy. In a panel of HCC cell lines, each characterized by a specific mutational signature, sorafenib elicited heterogeneous mechanistic and biological responses, whereas targeted therapy provoked the robust inhibition of cell proliferation and DNA synthesis along with the blockage of AKT/mTOR signaling. The combination of sorafenib with targeted therapies exhibited synergistic anti-HCC biological activity concomitantly with highly effective inhibition of MAPK and AKT/mTOR signaling. Thus, somatic mutations may lead to identify case-specific mechanisms of disease in HCC lesions arising from multiple etiologies. Moreover, targeted therapies guided by molecular characterization, used alone or in combination with sorafenib, can effectively block important HCC disease mechanisms.

INTRODUCTION

Hepatocellular carcinoma (HCC hereafter) is the fifth most prevalent cancer and the third most frequent cause of cancer-related death worldwide, with up to 800K deaths in 2012 [1]. It is a disease of increasing incidence and the leading cause of death among patients with cirrhosis. It can be related to multiple etiologies, including infections with hepatitis B or C viruses (HBV and HCV, respectively), alcohol and nonalcoholic steatohepatitis [2, 3]. HCC diagnosis is mainly guided by radiological criteria with only one third of patients being diagnosed at early stages (namely BCLC-0 and BCLC-A) [4]. This makes them candidates for liver transplantation, surgical resection or percutaneous ablation, which is associated with a 5-year recurrence rate of 70-80% [5, 6]. Outcomes are even worse for patients with intermediate or advanced stages (BCLC-B and C, respectively) [7]. Generally, these patients will receive specific therapy that includes transarterial chemoembolization (for BCLC-B patients), which yields an increase in median survival from 16 to 24 months [8], or therapy with sorafenib (for BCLC-C patients). Sorafenib is an oral multitarget kinase inhibitor that can increase median survival from 7.9 to 10.7 months [9]. The modest but significant clinical benefit from sorafenib has prompted further clinical trials based on the comparison of sorafenib with other inhibitors, alone or in combination, as first- and second-line treatment, but these have yielded poor results [10], [11]. It is important to note that we currently lack molecular evidence to optimize the clinical benefits that HCC patients may gain from any of these therapies.

From a genomic perspective, HCC is a very heterogeneous disease, possibly reflecting the multiple etiologies causing this type of cancer [12]. Much effort has been made to characterize HCC molecularly. On one hand, whole-transcriptome analyses have revealed deregulated expression of signaling molecules, such as the overexpression of well-known oncogenic genes

and pathways like MET (in 40-50% of patients) [13], IGF2 (in 10%) [14, 15], WNT/ β -catenin (in 25%) [16] and TGF- β [17]. These transcriptome findings helped establish a molecular classification of two different HCC subtypes: 1) a proliferation class, with activated signaling pathways like TGF- β , MYC or PI3K-AKT, promoting worse clinical outcomes; and 2) a non-proliferation class, displaying activated WNT signaling in up to 25% of cases [17]. On the other hand, recent next-generation sequencing (NGS) mutational studies have confirmed the heterogeneous nature of HCC. The main genes recurrently found to have mutations are tumor suppressors like *TP53*, which affects 20-24% of the patients analyzed [12, 18], and those involved in the WNT pathway, like *CTNNB1*, which is detected in 33-37% of cases, or *AXIN1* (in 11-15% of cases) [11, 12, 18]. Somatic mutations have also been found in genes like *ARID1A* (in 13-17% of patients) and *CDKN2A* (7-9%), and to a lesser extent in *IRF2* (5%), *KRAS* (1.6%) and *PIK3CA* (1.6%) [12, 18]. Finally, mutations affecting the *TERT* promoter associated with increased *TERT* expression have been described as an early event in HCC (60% of cases) [19]. However, our knowledge of the molecular mechanisms that can participate in the development of HCC has not so far improved our ability to diagnose or treat this disease.

Taking advantage of the NGS data already generated for HCC, in this study we aimed to characterize HCC lesions to potentially use the data for diagnosis and targeted therapy. To this end, we have designed a targeted approach based on the mutational analysis of a specific selection of 112 genes, which enabled us to prospectively characterize HCC cases from patients with multiple etiologies and in a time that was compatible with the requirements of the clinic (within 15 days). Moreover, we used the data to study the biological and mechanistic effects of case-specific therapies used alone or in combination with sorafenib in a panel of HCC cell lines. This approach can enable the generation of genomic data in early stage HCCs that could be useful for tracking

disease evolution and progression, and that might serve as a rationale for targeted therapy.

RESULTS

A targeted approach to characterizing specific mutational HCC signatures *in silico*

There is great interest in developing novel approaches for HCC diagnosis as well as in improving our ability to manage patients with advanced diseases. We hypothesized that case-specific mutational signatures within HCC cases could act as markers of important oncogenic mechanisms involved in HCC activities, including responses to sorafenib. To explore such specific mechanisms, we designed a targeted NGS approach that focused on mutations affecting the exonic regions of a selection of 112 genes (HepatoExome hereafter). For this purpose, we used the mutational data already available from a cohort of 41 cases comprising samples from patients and cell lines (see Supplementary Table 1). Within our selection of genes, we included those already known to play a potential role in the disease (i.e., *WNT*, *B-CATENIN* and *TP53*) and others that have been implicated in specific signaling networks and that might serve as targets for therapy, e.g., JAK-STAT, PI3K-mTOR, MAPK and Receptors with Tyrosine Kinase Activity (RTKs). To assess the feasibility of our approach to detecting mutated genes in HCC samples, we studied *in silico* the mutations in genes included in the HepatoExome in an independent cohort of 331 samples from HCC patients with a known mutational profile (validation cohort in Supplementary Table 1). In this setting, we were able to detect relevant mutated genes in 69.2% of the cases. The most frequently mutated genes detected in the validation cohort samples are described in Figure 1A and Supplementary Table 2. Amongst these, we detected mutations affecting the WNT pathway (*CTNNB1*, *AXIN1* and *APC*), PI3K-mTOR (*TSC2*, *TSC1*, *PTEN* and *MTOR*), RTKs (e.g., *FLT1*, *EGFR*, *INSR* and *RET*), chromatin regulation and repair (*HNFI1A*, *ATM*, *ATR* and *PRKDC*) and TP53. Interestingly, these hits belonged to multiple signaling pathways (Figure 1B), which may reflect the molecular heterogeneity associated with this disease.

Prospective mutational profiling of HCC cases in the discovery cohort

Next, we examined the translational application of this approach by prospectively studying a cohort of 32 HCC cases arising from multiple etiologies (discovery cohort). The clinical characteristics of these 32 patients are summarized in Supplementary Table 3. The majority were male (29/32; 90.6%), and the average age of the patients was 63.8 years. All patients developed HCC in a cirrhotic liver caused by various etiologies: alcohol (12/32; 37.5%),

hepatitis C virus (11/32; 34.4%), hepatitis B virus (3/32; 9.4%), hemochromatosis (3/32; 9.4%), hepatitis C virus + alcohol (2/32; 6.25%), and hepatitis B virus + alcohol (1/32; 3.2%). The samples were collected consecutively at initial stages, mostly from resection (28/32, 87.5%) but also from transplantation specimens (4/32, 12.5%). To detect somatic mutations in the HepatoExome, we compared the mutational data obtained from tumoral lesions with that from non-tumoral lesions (cirrhotic liver and blood when available). To this end, genomic DNA was extracted from paired samples from each patient and analyzed using a targeted primary ultrasequencing approach, followed by a secondary validation analysis (see supplementary methods for further details). These processes were completed within 15 days of sample reception. Interestingly, we detected somatic mutations in 17 of the 32 patients analyzed (53.1%); they had an average of 2.1 mutated genes each (Table 1).

Moreover, each patient showed a unique mutational profile with individualized combinations of mutations and mutated genes. Considered in greater detail, our results identified mutant genes that can participate in a number of signaling pathways, as would be expected from our previous *in silico* observations. Among these, we found mutations affecting WNT- β -CATENIN signaling (*CTNNB1* in 8/32 of the samples), the MAPK pathway (*RAF1* and *HRAS*; 3/32 samples), intracellular calcium signaling in 5/32 of the samples (*ITPR1* and *ITPR2*), and members of the PI3K/mTOR pathway (*MTOR*, *AKT1* and *RICTOR*; 3/32 samples) (Table 1). Somatic mutations were detected with average depths of 420-X and 3.25K-X in the primary and validation analyses, respectively.

Thus, it is possible to use this approach to characterize cancer lesions in up to 53% of patients with HCC with respect to the presence of genomic alterations that presumably affect specific signaling mechanisms.

Heterogeneous mechanistic effects on treatment with sorafenib in HCC cells

Sorafenib is the only inhibitor used to treat HCC at advanced stages in the clinic. We sought to explore the effects in proliferation that treatment with this inhibitor could elicit in a panel of HCC cell lines. We first performed an *in silico* characterization that enabled the detection of mutations in the genes included in the HepatoExome. As expected from our previous observations in lesions from HCC patients, each cell line showed an individual and unique mutational profile (Supplementary Table 4). In this setting, the IC₅₀ of sorafenib differed between cell lines over a range between 0.5 and 5 μ M (Supplementary Figure 1 and Supplementary Table 4). This observation led us to compare the mechanistic effects of sorafenib on the activity of some well-known intracellular cancer-related signaling pathways using an intracellular pathway array kit (see Methods). To this end, we incubated SNU-449, Hep-G2

and HUH-7 cells with their specific IC_{50} concentrations of sorafenib. Under these conditions, most of the pathways showed no response to this drug, e.g., JAK/STAT, JNK, p53, members of the PI3K/mTOR pathways (such as AKT, mTOR and PRAS40) or the proapoptotic CASPASE-3 and PARP (with the exception of P-BAD in Hep-G2 cells) (Figure 2A and Supplementary Table 5). On the other hand, treatment with sorafenib in HCC cells elicited heterogeneous inhibitions of ERK1/2 (MAPK) and RPS6 (S6) phosphorylation (PI3K/mTOR) alongside a consistent activation of P-AMPK between cell lines (Supplementary Table 5). Since MAPK and PI3K/mTOR are well known signaling pathways downstream of the intended molecular targets of sorafenib, we sought to confirm these data by using an independent approach in a larger panel of HCC cell lines. To this end, we performed western blot (WB) using lysates from starved cells treated with 1- and 2-fold IC_{50} concentrations of the drug. Confirming our previous results, sorafenib displayed differential abilities to inhibit the P-MEK and P-ERK signaling pathway in different cell lines, independently of the drug concentration (Figure 2B and 2C). In this regard, the effects of this inhibitor on MEK-ERK activity ranged from no inhibition (SNU-449 cells) through medium (SNU-182) to high (HUH-7) levels of inhibition. Finally, under these conditions, sorafenib inhibited P-S6 at different intensities (compare the IC_{50} responses in SNU-475, Hep-G2 and HUH-7 cells) and had no effect on P-AKT (Figure 2B and 2C). Thus, in the context of a variety of HCC cell lines, sorafenib elicited

heterogeneous proliferative and mechanistic responses downstream of its intended molecular targets.

Ex vivo effects of targeted therapies guided by individual mutational profiles

To gain insights into the biological and mechanistic effects that targeted therapy guided by mutational profiles could exert in HCC cells, we decided to focus on the potentially actionable mutations in our panel of human HCC cell lines. Using SNU-449 and HUH-7 cells as examples of low or high MAPK inhibition by sorafenib, respectively, we first detected mutations in specific genes (and validated them by Sanger sequencing; Supplementary Figure 2 and Supplementary Table 6). For SNU-449 cells, the mutated genes were *NTRK1* and *PTEN*, which were associated with the inhibitors lestaurtinib (Cep) and everolimus (Ev) respectively (Table 2). In HUH-7 cells, mutated genes like *INSR*, *SYK* and *PIK3C2G* were associated with fostamatinib (Fos), BMS-754807 (Bms) and buparlisib (Bkm) respectively, (Table 2). We then analyzed the anti-proliferative effects of each inhibitor, in the intended cell line, and calculated their IC_{50} concentrations, using them in the subsequent experiments (Table 2). In addition to the biological effects observed with targeted drugs, incubation of starved cells with 1- or 2-fold IC_{50} concentrations of each drug inhibited downstream signaling pathways associated with the activity of the mutated genes (Supplementary Figure 3). The biological and mechanistic effects of the

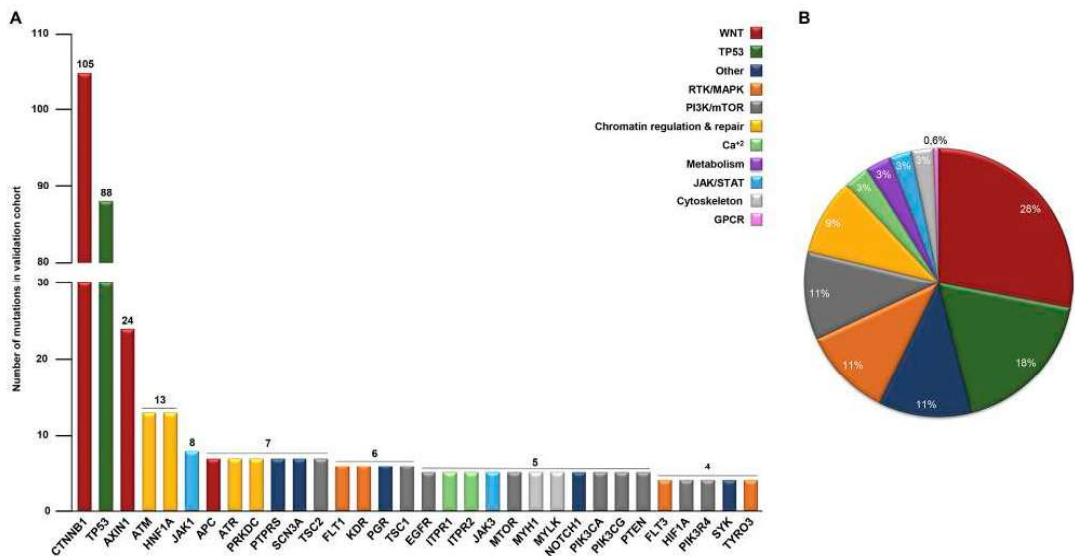


Figure 1: Molecular heterogeneity detected *in silico* in 331 HCC lesions with a known mutational profile. (A) *In silico* analysis showing the number of mutations (≥ 4) detected in 331 patients (validation cohorts). (B) Percentage of total hits involved in the indicated signaling pathways.

Table 1: Validated somatic mutations found in the discovery cohort using HepatoExome

Patient	Chr.	Position	Ref.	Alt.	AA change	Gene	Coverage	Etiology	Associated therapy
P-01	2	39605221	A	T	I47K	MAP4K3	675		N/A
	3	12627258	A	C	D486E	RAF1	576	Alcohol	Selumetinib/ Sorafenib
	17	7574003	G	A	R210*	TP53	704		N/A
P-02	3	41266110	A	C	H36P	CTNNB1	230	Alcohol	N/A
	3	12660100	G	A	R41W	RAF1	935		Selumetinib/ Sorafenib
P-05	3	41266100	T	G	S33A	CTNNB1	325		N/A
	11	100962605	G	T	Q434K	PGR	206	Alcohol	Mifepristona
	12	26749892	G	T	T1393N	ITPR2	502		Tacrolimus/ Cyclosporine
	22	36696277	C	A	A958S	MYH9	521		N/A
P-10	12	26568307	A	G	I2412T	ITPR2	45	Alcohol	Tacrolimus/ Cyclosporine
P-11	11	532737	A	C	Y157D	HRAS	1384	Alcohol	Selumetinib/ Sorafenib
P-13	1	11199401	G	A	T1697I	MTOR	387	HBV	Everolimus
P-14	14	105236685	G	A	T479M	AKT1	325	HBV	Everolimus/ Ipatasertib
P-16	12	26553126	C	A	V2489L	ITPR2	19		Tacrolimus/ Cyclosporine
P-17	11	108117799	G	A	R337H	ATM	27		N/A
	11	111625284	T	C	E196G	PPP2R1B	880	HCV	N/A
	17	7578370	C	A	Splice	TP53	743		N/A
P-18	3	4709191	T	C	Y600T	ITPR1	83		Tacrolimus/ Cyclosporine
	5	38962438	T	C	Y565C	RICTOR	251	HCV	Everolimus
	10	43610119	C	A	G691S	RET	697		Regorafenib
	17	7577535	C	T	R117K	TP53	666		N/A
	20	54961541	A	T	F311	AURKA	439		Barasertib
P-21	3	41266124	A	G	T41A	CTNNB1	270	HCV	N/A
	2	165997273	G	C	P636R	SCN3A	270		Zonisamida
P-22	2	165997274	G	T	P636T	SCN3A	270	HCV	Zonisamida
	3	41266137	C	T	Y157D	CTNNB1	161		N/A
P-23	3	41266110	A	C	H36P	CTNNB1	161	HCV	N/A
P-25	3	41268766	A	C	K335T	CTNNB1	108	HCV	N/A
P-26	3	41266113	C	A	S37Y	CTNNB1	87	HCV	N/A
	4	55981463	G	T	N158K	KDR	130		Sorafenib

(Continued)

Patient	Chr.	Position	Ref.	Alt.	AA change	Gene	Coverage	Etiology	Associated therapy
P-31	3	41266136	T	C	S45P	CTNNB1	343	Hemochr.	N/A
	6	44219910	A	T	D546V	HSP90AB1	934		N/A
	2	165948799	A	G	I1542T	SCN3A	928		Zonisamida
	3	41266101	C	G	S33C	CTNNB1	51		N/A
P-32	12	26636635	T	C	N2003S	ITPR2	278	Hemochr.	Tacrolimus/ Cyclosporine
	17	7577094	G	A	R150W	TP53	452		N/A

Patient: Patient number; Chr.: Chromosome number; Position: Genomic location of the mutation in the chromosome; Ref.: Normal nucleotide; Alt.: Altered nucleotide; AA change: Amino acid change; Gene: Gene name; Coverage: Number of reads analyzed at each position; Etiology: Etiology of each patient; Associated therapy: Possibly Associated Therapy for the indicated genes and/or signaling pathways. Hemochrom.: Hemochromatosis.

drugs, used alone or in combinations, were then compared in SNU-449 and HUH-7 HCC cells. In these settings, all combinations were highly effective at inhibiting cell proliferation compared with single treatments, suggesting that multiple mechanisms associated with case-specific mutations could participate in controlling essential HCC activities (Figure 3A and 3B). Furthermore, similar results were also obtained in other HCC cell lines like Hep-G2 (Table 2 and Supplementary Figure 4), SNU-182, SNU-475 and SNU-423 (Table 2 and Supplementary Figure 5). Following the example using SNU-449 and HUH-7 cells, we comparatively studied the molecular effects elicited by case-specific combinations of targeted therapy over multiple signaling pathways simultaneously. Interestingly, we only found significant inhibition over the activities of MAPK-ERK and a number of AKT/mTOR pathway effectors like AKT⁴⁷³, GSK-3B, S6 and PRAS40 (Figure 3C and Supplementary Table 5). These results were further confirmed alongside our panel of six different cell lines, each treated with a specific targeted therapy defined by their individual mutational signatures (Table 2). In these settings, targeted therapy provoked a robust inhibition of cell proliferation that occurred alongside a highly significant inhibition of PRAS40 and S6 activities, hence suggesting an important role for these molecules, which are downstream effectors of the AKT/mTOR pathway, in the biology of HCC (Figure 3D and Supplementary Table 7).

Biological and mechanistic effects of combinations of sorafenib with targeted therapies in HCC cell lines

In light of our findings, it is conceivable that case-specific targeted therapies could increase the anti-HCC effects of sorafenib. To explore this possibility, we compared the mechanistic effects elicited by incubating SNU-449 and HUH-7 cells with IC₅₀ concentrations of sorafenib plus cell-specific targeted therapies (see results

from Hep-G2 cells in Supplementary Figure 4). As expected from our previous findings, these combinations most strongly inhibited specific signaling mechanisms like MAPK-ERK (P-ERK-1/2) and AKT/mTOR (P-AKT⁴⁷³, P-GSK-3B and P-PRAS40 and P-S6), which are known to play an important role in the biology of HCC (Figure 4A and Supplementary Table 5). We next examined our data by using an alternative approach to explore the biological and mechanistic effects of treatment with sorafenib and targeted therapy used alone or in combination in SNU-449 and HUH-7 cells. The combination of sorafenib with targeted drugs most strongly inhibited cell proliferation and DNA synthesis in HCC cells (Figures 4B-4E). Interestingly, the combination of sorafenib with targeted inhibitors caused synergistic effects over the proliferation of SNU-449 and HUH-7 cells, with combination indexes below 1 (Supplementary Figure 6). Moreover, this occurred in parallel with higher blockages of MAPK and AKT/mTOR signaling pathways as assessed by western blot using anti-P-ERK-1/2, anti-P-AKT⁴⁷³ and anti-P-PRAS40 antibodies (Figures 4B-4E). Similar results were also obtained in other HCC cell lines like Hep-G2, SNU-182, SNU-475 and SNU-423 (Supplementary Figures 4 and 5). Finally, we interchanged the targeted inhibitors plus sorafenib between SNU-449 and HUH-7 cells and analyzed the effects in cell proliferation. Our data show higher efficiency when inhibitors were used in the appropriate mutational background (compare Supplementary Figures 7A with 4D and Supplementary Figure 7B with 4B). It is therefore possible that, using our targeted approach, we could detect and target specific mechanisms, like for example AKT/mTOR, that when used in combination with sorafenib, could increase its anti-HCC activities.

DISCUSSION

Considerable effort has been made to determine the main mechanisms that may be involved in the

pathogenesis and evolution of HCC. Based on the NGS data already available in the literature concerning HCC, we designed a targeted approach to characterize HCC cases from patients with multiple etiologies and in a time compatible with the requirements of clinics (within 15 days). This method enables us to show that sorafenib can produce heterogeneous cellular responses in different genomic contexts, and that case-specific targeted inhibitors can greatly increase its biological and mechanistic anti-HCC effects.

Taking advantage of the genetically heterogeneous nature of HCC, we set up a genomic platform consisting of an HCC customized HaloPlex™ enrichment library coupled to a MiSeq sequencing system. This enabled us to characterize HCC cases (in initial tumors) for the presence of somatic mutations in a selection of 112 genes cost-effectively and in suitably quick manner to meet the requirements of the clinic. We first performed an *in silico* analysis of 331 HCC cases (validation cohort) and a prospective *ex vivo* study of a cohort of 32 paired samples (discovery cohort) from multiple etiologies and low-stage

HCC. Independently of the etiology of the tumor, 60% of all cases displayed unique mutational profiles; up to 34% of the discovery cohort cases had mutated genes that could be associated with an inhibitor. In this regard, *RAF1* (patient-01; sorafenib or selumetinib), *MTOR* (patient-13; everolimus) and *RET* (patient-18; regorafenib) are but three examples of mutated genes potentially associated with specific therapy. We might be able to use the information obtained by this method to track disease progression, for example, using liquid biopsies, and to design case-specific approaches for therapy.

Treatment with sorafenib is the standard of care in HCC patients with advanced disease (BCLC-C) [9]. It is a multi-kinase inhibitor that can target VEGFR, PDGFR, c-Kit, c-RAF and B-RAF activities and currently offers limited clinical benefits [9, 20]. To study the molecular mechanisms targeted by sorafenib in a heterogeneous genetic context, we analyzed a panel of HCC cell lines, each of which had a unique mutational profile. Surprisingly, we found heterogeneous biological responses between the cell lines with respect to the range of IC₅₀

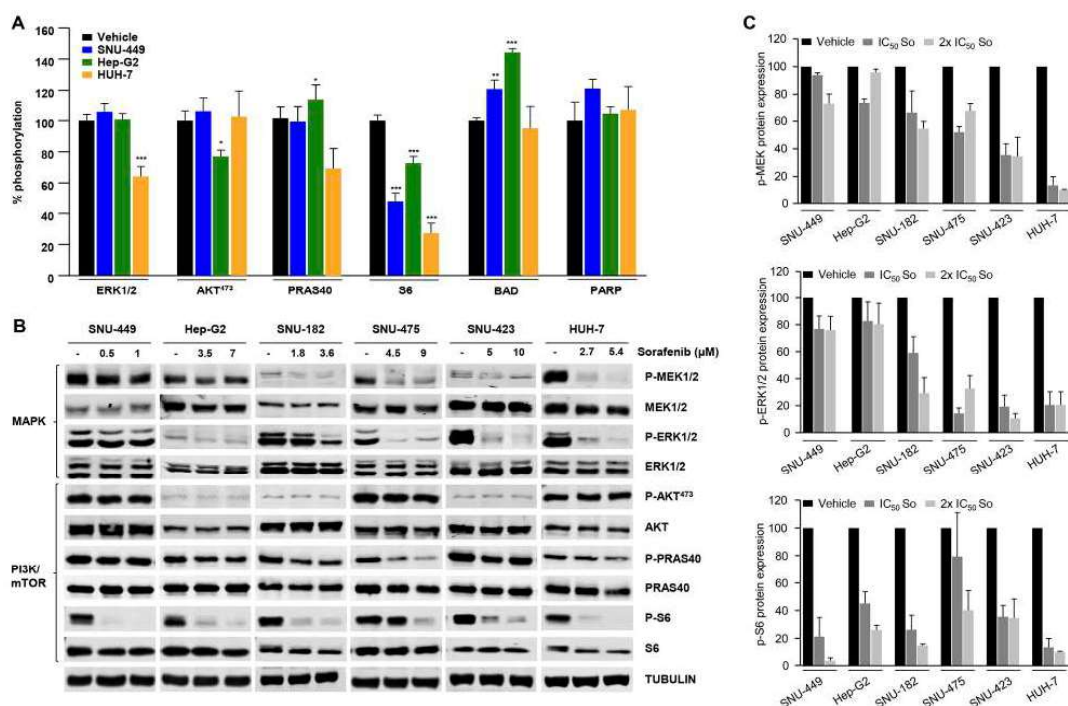


Figure 2: Mechanistic effects of sorafenib in a panel of HCC cell lines. (A) Intracellular signaling array of SNU-449, Hep-G2 and HUH-7 cells starved and treated for 1h with their IC₅₀ concentration of Sorafenib. (B) Western blotting analyses of SNU-449, Hep-G2, SNU-182, SNU-475, SNU-423 and HUH-7 cells starved and treated for 1h with control vehicle (-) and the IC₅₀ and 2x IC₅₀ concentrations of sorafenib, as indicated. Cell lysates were incubated with P-MEK1/2, MEK1/2, P-ERK1/2, ERK1/2, P-AKT173, AKT, P-PRAS40, PRAS40, P-S6, S6, and α-tubulin antibodies. (C) P-MEK, P-ERK1/2 and P-S6 relative to MEK, ERK1/2 and S6 protein expression in HCC cell lines treated with control vehicle, the IC₅₀, and 2 x IC₅₀ concentrations of sorafenib. Error bars show SEM. * compared with the control vehicle (* P < 0.05; **P < 0.01; ***P < 0.001).

concentrations observed. In addition, from a mechanistic perspective, treatment with sorafenib elicited inhibitory responses of different intensities to MAPK-ERK and PI3K/mTOR activities depending on the cell line tested. On the other hand, we observed steady P-AMPK activation, as have previously been described as potential

mechanisms involved in cellular responses to this drug [21, 22]. It is possible that, in different genomic contexts, as in this case of HCC cell lines with different mutational profiles, the intracellular mechanistic effects elicited by sorafenib may vary. It is also conceivable that this could be reflected in the heterogeneous population of patients

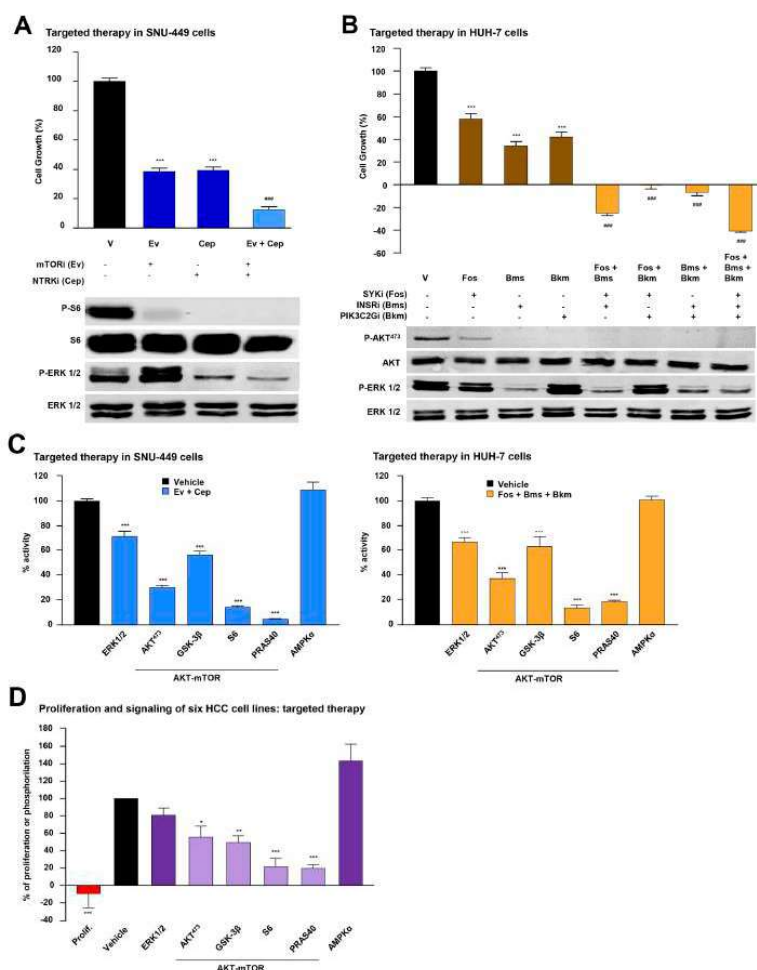


Figure 3: Biological effects of combined targeted therapies in HCC cells. (A) *Top*: Proliferation analysis of SNU-449 cells incubated 48h with control vehicle (V, black bar) or the IC₅₀ concentration of the indicated inhibitor (mTORi (Ev: Everolimus) and NTRKi (Cep: Lestaurtinib)) alone (dark blue bars) or in a double (light blue bar) combination. *Bottom*: Western Blotting analyses of SNU-449 cells starved and treated for 1h with control vehicle or the indicated inhibitor, or the combination of inhibitors under the same conditions as above, and incubated with P-S6, S6, P-ERK1/2 and ERK1/2 antibodies. (B) *Top*: Proliferation analysis of HUH-7 cells at 48h incubated with control vehicle (V, black bar) or the IC₅₀ concentration of the indicated inhibitor (SYKi (Fos: Fostamatinib), INSRi (Bms: BMS-754807) and PIK3R2i (Bkm: Buparlisib)) alone (dark brown bars), or in double or triple combination (light brown bars). *Bottom*: Western Blotting analysis of HUH-7 cells treated for 1h with control vehicle, the indicated inhibitor, or the combination of inhibitors under the same conditions as above. P-AKT^{T473}, AKT, P-ERK1/2 and ERK1/2, antibodies were used as indicated. (C) Intracellular signaling array of SNU-449 (*left*) and HUH-7 (*right*) cells starved and treated for 1h with control vehicle (black bar) or the combination of IC₅₀ concentration of the indicated targeted inhibitors. (D) Proliferation (red bar) and phosphorylation of the indicated antibodies (purple bars) within a panel of six HCC cell lines compared to control vehicle (black bar). Error bars show SEM. * compared with the control vehicle (* P < 0.05; **P < 0.01; ***P < 0.001). # compared with each inhibitor alone (### P < 0.001).

Table 2: Potentially actionable mutations found in silico in HCC cell lines and IC50 values associated to them. Table showing the mutational characteristics of six commercial cell lines (in silico comparison with Cancer Cell Line Encyclopedia (CCLE) data)

Cell line	Chr.	Position	Ref.	Alt.	AA change	Gene	Inhibitor name	Inhibitor	IC ₅₀ (μM)
Hep-G2	4	55976843	A	T	Y357N	KDR	KDRi (So)	SORAFENIB	3,5
	10	43608351	G	A	D567N	RET	RETi (Re)	REGORAFENIB	3,1
	19	18279692	C	A	Y655*	PIK3R2	PIK3R2i (Bkm)	BUPARLISIB (BKM-120)	2,8
SNU-449	1	156851421	A	C	D793A	NTRK1	NTRKi (Cep)	LESTAUTINIB (CEP-701)	1,6
	10	89717696	T	C	F241L	PTEN	mTORi (Ev)	EVEROLIMUS	14,6
	9	93606577	A	G	K133E	SYK	SYKi (Fos)	FOSTAMATINIB	12,9
HUH-7	12	18762561	A	C	I1394L	PIK3C2G	PIK3C2Gi (Bkm)	BUPARLISIB (BKM-120)	1,7
	19	7141798	T	C	T858A	INSR	INSRi (Bms)	BMS-754807	8,5
	3	130409498	T	A	R1033S	PIK3R4	PIK3R4i (Bkm)	BUPARLISIB (BKM-120)	0,8
SNU-182	13	29008268	T	A	E201D	FLT1	FLT1i (Re)	REGORAFENIB	4,7
	19	7184495	G	A	P269L	INSR	INSRi (Bms)	BMS-754807	1,5
SNU-475	13	28611336	G	A	T432M	FLT3	FLT3i (Cep)	LESTAUTINIB (CEP-701)	2,5
SNU-423	3	130452809	C	A	V345F	PIK3R4	PIK3R4i (Bkm)	BUPARLISIB (BKM-120)	1,7
	13	28913428	C	T	E789K	FLT1	FLT1i (Re)	REGORAFENIB	9,5

The table includes Cell line: Cell line name; Chr.: Chromosome number; Position: Genomic location of the mutation in the chromosome; Ref.: Normal nucleotide; Alt.: Altered nucleotide; AA Change: Amino acid change; Gene: Gene name; Inhibitor name: Used throughout this report; Inhibitor: General name and IC50 (μM): Micromolar IC50 concentration for the indicated inhibitor.

that are uniformly treated with sorafenib and develop variable and unpredictable clinical responses to this drug.

We examined the HepatoExome data obtained in a panel of HCC cell lines by analyzing the effects of targeted drugs guided by case-specific mutational profiles. We found that a rational combination of targeted inhibitors can strongly inhibit HCC cell proliferation. Moreover, case-specific combinatory therapies were highly effective at blocking important HCC signaling mechanisms like MAPK or AKT/mTOR. In this context, downstream of AKT/mTOR signaling axis, we detected two effectors like RPS6 (S6) and PRAS40, which were highly dephosphorylated and presumably inactivated in response to different targeted therapies. Phosphorylation of S6 by p70-S6K has been shown to regulate protein synthesis and promote cell growth and proliferation by selectively promoting the translation of specific mRNAs [23, 24]. PRAS40 can be directly phosphorylated by AKT and exert pro-tumorigenic activities. Interestingly, in its dephosphorylated form PRAS40 negatively regulates mTOR activity which can be

reversed by direct phosphorylation (reviewed in [25]). It is thus possible, that guided by molecular characterization of tumor lesions, we could use PI3K, AKT or mTOR inhibitors to disrupt AKT/mTOR signaling and inhibit S6 and PRAS40 activities as an effective approach to treat HCC. We believe this study highlights what targeted characterization of specific lesions might offer by way of diagnostic possibilities for human hepatocarcinoma in the near future. Using early stage hepatocarcinoma samples, we found highly heterogeneous genomic landscapes with unique mutational signatures. It is conceivable that these can trigger aberrant activation of multiple mechanisms that may contribute to the pathogenesis and progression of each disease. Following this line of evidence, it is also possible that upon molecular characterization we could use this heterogeneity as a molecular basis to detect specific mechanisms promoting HCC progression and resistance to treatment and to serve as potential targets for therapy. In this regard, multiple clinical trials have been conducted to explore the clinical benefit of other drugs when compared,

or used in combination, with sorafenib (reviewed in [11]). These have yielded poor results that could be partially explained by the inclusion of an uncharacterized population of patients in the studies. We also explored the effects of combinations of sorafenib with case-specific inhibitors in a panel of HCC cell lines. In each case, we

observed greater inhibition of cell proliferation and DNA synthesis of the drug combinations (targeted inhibitors + sorafenib) compared with sorafenib alone. Intriguingly, these inhibitory effects were more evident in HCC cells, in which treatment with sorafenib alone inhibited MAPK-ERK signaling compared with those in which it did not

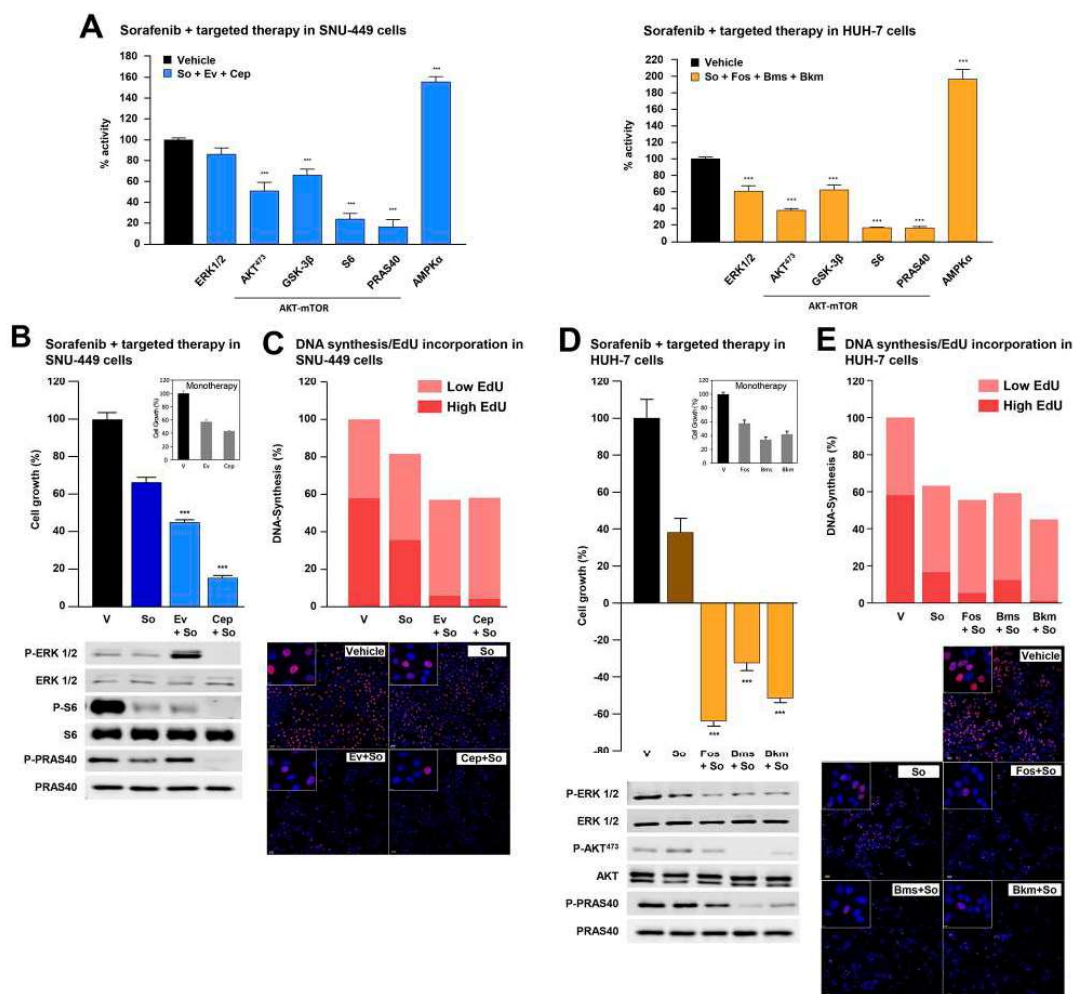


Figure 4: Combination of sorafenib and targeted therapy in HCC cells. (A) Intracellular signaling array of SNU-449 (left) and HUH-7 (right) cells starved and treated for 1h with control vehicle or the IC₅₀ concentrations of the indicated inhibitors. Proliferation analyses of SNU-449 (B, top) and HUH-7 cells (D, top) at 48h incubated with control vehicle (V) or the IC₅₀ concentration of sorafenib alone (dark blue and dark brown bars for SNU-449 and HUH-7 cells, respectively), the targeted inhibitors alone (inner squares) or combinations of sorafenib with targeted inhibitors (light blue and light brown bars for SNU-449 and HUH-7 cells, respectively). Western Blotting analyses of SNU-449 (B, bottom) and HUH-7 (D, bottom) cells starved, treated under the same conditions as above and incubated with P-ERK1/2, ERK1/2, P-S6, S6, P-PRAS40, PRAS40, P-AKT^{T27} and AKT antibodies. DNA synthesis assay using Click-iT® EdU in SNU-449 (C) and HUH-7 (E) cells incubated for 24h under the same conditions as in B or D respectively. Graph bars show percentage of low (light red) or high (intense red) EdU-stained cells in three photographic fields from a representative experiment. Representative pictures show the nucleus of the total number of cells (blue dots) and EdU-positive cells (red dots). Statistical analyses of targeted therapy or sorafenib plus targeted therapy versus sorafenib alone. Error bars show the SEM. * P ≤ 0.05; ** P ≤ 0.01; *** P ≤ 0.001.

(HUH-7 and SNU-449 cells, respectively; see data in Figures 2 and 4). Moreover, our results suggest that targeted blockage of MAPK-ERK signaling and AKT/mTOR used along with sorafenib can greatly inhibit cell proliferation and DNA synthesis of HCC cells. Thus, our results suggest that molecular characterization of HCC cases could help develop therapies that are more efficient. In this regard, a phase II trial of tivantinib used in the second line, showed no difference in survival compared with a placebo. This inhibitor is currently being tested as a highly selective MET inhibitor, although the exact mechanism of action is still unclear [26]. Nevertheless, a subgroup of patients with a high level of MET expression significantly benefited from this treatment although they had worse survival overall; a phase III trial in this specific population has since been designed [27].

Despite its potential applicability in routine clinical practice, our approach requires several limitations to be overcome in a similar way to those described in [28]. In the case of HCC, a solution would entail: 1) establishing efficient protocols to safely collect, manipulate and characterize specific lesions that are representative of the advanced steps of this disease; 2) considering other molecular approaches, such as transcriptome or copy number variation studies, in addition to targeted mutational analyses; 3) managing the toxicity due to drug combinations, particularly given that this disease usually appears in the context of a damaged liver; and 4) dealing with tumor heterogeneity and interactions with the immune system that may be responsible for the resistance eventually acquired after combination treatments.

In summary, adopting targeted approaches to characterize HCC lesions may make it possible to detect specific disease mechanisms, like for example AKT/mTOR, that can lead to: 1) develop biomarkers to support diagnosis and/or prognosis; 2) serve as targets for specific inhibitors rationally combined in individualized therapies to target case-specific mechanisms of hepatocyte transformation; and 3) design more effective combination therapies when used with sorafenib in advanced stages of HCC.

MATERIALS AND METHODS

Patient samples

Matched tumoral and non-tumoral samples from 32 patients with clinically characterized HCC who were surgically treated (resection or transplant) were obtained retrospectively and prospectively (discovery cohort; Supplementary Table 1): 17 patients from Hospital Universitario Marqués de Valdecilla (HUMV), Santander; and 15 from Hospital Universitario Central de Asturias (HUCA), Oviedo. Tumoral DNA samples were obtained from freshly frozen (FF) tissue samples and matched non-tumoral DNA was collected from FF adjacent cirrhotic tissue samples and/or peripheral blood from the available patients.

All human samples used in this study were collected following the Declaration of Helsinki protocols after obtaining written informed consent from each patient as required by the CEIC (Comité Ético de Investigación Clínica, Cantabria) and the CEAS (Comité de Ética para la Atención Sanitaria, Oviedo). No donor organs were obtained from executed prisoners or other institutionalized persons.

Genomic DNA samples

Genomic DNA was extracted from fresh (blood) and/or frozen (cirrhotic and tumoral liver) using standard procedures. Briefly, PBS-washed samples, were centrifuged and lysed using “Tissue and cell lysis solution” buffer for the MasterPure™ kit, complemented by proteinase K (5 µl/100 µl buffer) (Epicenter), shaking overnight at 56°C. DNA was extracted using phenol/chloroform/isoamyl alcohol (in proportions of 25:24:1, respectively) in a fast Lock Gel Light Eppendorf tube (Eppendorf), then washed and precipitated. Genomic DNA was quantified using a Qubit ds DNA BR assay kit and a Qubit 2.0 fluorimeter (Invitrogen).

Enrichment library design, preparation and sequencing

Targeted enrichment sequencing was performed on human FF tumor and non-tumor specimen and, when indicated, on blood samples. The custom probe design was constructed with SureDesign (Agilent Technologies; Design ID: 37503-1413372517). The design focused on the coding regions of a group of 112 genes known to be mutated in HCC, and which were selected based on the following criteria: i) genes of known relevance in HCC, ii) genes that may be associated with pharmacological inhibitors with potential clinical use and iii) genes shown mutated in HCC independently of the population frequency. DNA libraries were prepared with the HaloPlex Target Enrichment System, following the manufacturer's instructions and sequenced as described in [28].

Somatic mutation identification and validation

Somatic mutation identification was done by using Agilent Sure Call 2.1.1.13 software and IGV 2.3.46 software. In parallel Sequencing data were aligned against the human reference genome (hg19) using the BWA aligner [29]. The alignment was refined using SAMTOOLS fixmate and PICARD TOOLS cleanSam tools [30], (<http://broadinstitute.github.io/picard/>). The RAMSES application was used to detect nucleotide substitutions [31]. For validation, genomic DNA was amplified using the specific oligonucleotides described in Supplementary Table 5. Samples were prepared and analyzed as described in [28].

Cell cultures and reagents

Six human hepatocellular carcinoma cell lines were used. Hep-G2, SNU-449, SNU-475, SNU-423 and SNU-182 cells were obtained from the American Type Cell Collection (ATCC, Rockville, MD). HUH-7 cells were obtained from the Japanese Collection of Research Bioresources Cell Bank (JCRB, Japan). Genomic data from these cells, including the somatic mutations detected in this study, are publicly available at the Broad-Novartis Cancer Cell Line Encyclopedia website (CCLE: <http://www.broadinstitute.org>). Commercial cell lines were cultured as recommended by ATCC or JCRB. Hep-G2 and HUH-7 cells were cultured in EMEM medium (Lonza, Basel, Switzerland) and SNU-475, SNU-449, SNU-423 and SNU-182 cells were cultured in RPMI-1640 medium (Lonza, Basel, Switzerland). Both mediums were supplemented with 10% heat-inactivated fetal bovine serum (FBS) (Life Technologies), glucose (4.5 g/L), L-glutamine (292 mg/L), streptomycin sulfate (10 mg/L) and potassium penicillin (10000 U/L) (Lonza).

To perform functional analysis the following inhibitors used in this study were obtained from Selleck Chemicals (Houston, TX): BMS-754807, Buparlisib (BKM-120), Everolimus (RAD001), Fostamatinib (R788), Regorafenib (BAY 73-4506) and Sorafenib; and Lestaurtinib (Cep-701) inhibitor were obtained from Sigma Aldrich. These drugs were reconstituted in Dimethyl Sulfoxide (DMSO) and kept at -20°C until use.

Statistics

Unless otherwise specified, all experiments were done in independent triplicates and all numerical data were summarized as the average of the values \pm the standard error of the mean (SEM) using GraphPad Prism5 software. In Figure 3D and Supplementary Table 6, the significant effects of targeted therapy versus control were calculated for each cell line. Each global median was compared using t-Student test.

Author contributions

Experimental design: SL, NGD, JC, JPV; Experimental data: SL, NGD, SCO, AGB, HP, CA; Clinical data: SL, LC, MTAL, MV, AP, LMR, CLL, PI, MGG, MLH, FCS, CGF; Analysis: SL, NGD, SCO, AAD, AGB, MS, NM, MLH, JL, JA, BCF, IV, JPV; Manuscript drafting and revision: SL, NGD, MV, CRL, MAP, JC, JPV; Overall supervision: MAP, JC, JPV.

ACKNOWLEDGMENTS

We are indebted to the patients who have contributed to this study. We especially thank Dr. Fidel Madrazo, from IDIVAL, and José Revert and the staff members of the

Biobank and the Pathology and Digestive Tract Services at HUMV, and members of the Hospital General de Asturias Biobank for their exceptional work in sample collection and organization. We would also like to thank the Santander Super-Computation Service for their support.

CONFLICTS OF INTEREST

MV: Advisory boards, conferences, travel grants from Bayer. MAP has the following COI: Takeda-advisory board. Novartis, Amgen and Roche: Speaker bureau. CRL: Bayer HealthCare advisory board. JC: advisory board and conferences ABBVIE, MBS, GILEAD, JANSSEN, MSD and ROCHE. The other authors declare no conflicts of interest.

FUNDING

Grants from ISCIII, co-financed by the European Union (FEDER) (PI16/00156), Ramón and Cajal research program from MINECO (RYC-2013-14097) and FUNDACIÓN LUCHAMOS POR LA VIDA to JPV. Grants from ISCIII (RD06/0020/0107-RD012/0036/0060) to MAP. Grant from ISCIII (Ref. PIE15/00079) to JC & JPV. NGD is a recipient of a UC-IDIVAL pre-doctoral fellow. I.V. was also supported by the Ramón and Cajal research program.

REFERENCES

1. Ferlay J, Soerjomataram I, Dikshit R, Eser S, Mathers C, Rebelo M, Parkin DM, Forman D, Bray F. Cancer incidence and mortality worldwide: sources, methods and major patterns in GLOBOCAN 2012. *International Journal of Cancer*. 2015; 136:E359-86.
2. El-Serag HB. Hepatocellular carcinoma. *The New England Journal of Medicine*. 2011; 365:1118-27.
3. El-Serag HB. Epidemiology of viral hepatitis and hepatocellular carcinoma. *Gastroenterology*. 2012; 142:1264-73.e1.
4. Bruix J, Reig M, Sherman M. Evidence-based diagnosis, staging, and treatment of patients with hepatocellular carcinoma. *Gastroenterology*. 2016; 150:835-53.
5. Imamura H, Matsuyama Y, Tanaka E, Ohkubo T, Hasegawa K, Miyagawa S, Sugawara Y, Minagawa M, Takayama T, Kawasaki S, Makuuchi M. Risk factors contributing to early and late phase intrahepatic recurrence of hepatocellular carcinoma after hepatectomy. *Journal of Hepatology*. 2003; 38:200-7.
6. Forner A, Llovet JM, Bruix J. Hepatocellular carcinoma. *Lancet*. 2012; 379:1245-55.
7. Forner A, Reig M, Varela M, Burrel M, Feliu J, Briceno J, Sastre J, Marti-Bonmati L, Llovet JM, Bilbao JI, Sangro B, Pardo F, Ayuso C, et al. [Diagnosis and treatment of hepatocellular carcinoma. Update consensus document from

the AEEH, SEOM, SERAM, SERVEI and SETH]. [Article in Spanish]. *Medicina Clinica*. 2016; 146:511.e1-511.e22.

8. Burrell M, Reig M, Forner A, Barrufet M, de Lope CR, Tremosini S, Ayuso C, Llovet JM, Real MI, Bruix J. Survival of patients with hepatocellular carcinoma treated by transarterial chemoembolisation (TACE) using Drug Eluting Beads. Implications for clinical practice and trial design. *Journal of Hepatology*. 2012; 56:1330-5.
9. Llovet JM, Ricci S, Mazzaferro V, Hilgard P, Gane E, Blanc JF, de Oliveira AC, Santoro A, Raoul JL, Forner A, Schwartz M, Porta C, Zeuzem S, et al. Sorafenib in advanced hepatocellular carcinoma. *The New England Journal of Medicine*. 2008; 359:378-90.
10. Llovet JM, Hernandez-Gea V. Hepatocellular carcinoma: reasons for phase III failure and novel perspectives on trial design. *Clinical Cancer Research*. 2014; 20:2072-9.
11. Bruix J, Han KH, Gores G, Llovet JM, Mazzaferro V. Liver cancer: Approaching a personalized care. *Journal of Hepatology*. 2015; 62:S144-56.
12. Guichard C, Amaddeo G, Imbeaud S, Ladeiro Y, Pelletier L, Maad IB, Calderaro J, Bioulac-Sage P, Letexier M, Degos F, Clement B, Balabaud C, Chevet E, et al. Integrated analysis of somatic mutations and focal copy-number changes identifies key genes and pathways in hepatocellular carcinoma. *Nature Genetics*. 2012; 44:694-8.
13. Goyal L, Muzumdar MD, Zhu AX. Targeting the HGF/c-MET pathway in hepatocellular carcinoma. *Clinical Cancer Research*. 2013; 19:2310-8.
14. Tovar V, Alsinet C, Villanueva A, Hoshida Y, Chiang DY, Sole M, Thung S, Moyano S, Toffanin S, Minguez B, Cabellos L, Peix J, Schwartz M, et al. IGF activation in a molecular subclass of hepatocellular carcinoma and pre-clinical efficacy of IGF-1R blockage. *Journal of Hepatology*. 2010; 52:550-9.
15. Breuhahn K, Vreden S, Haddad R, Beckebaum S, Stippel D, Flemming P, Nussbaum T, Caselmann WH, Haab BB, Schirmacher P. Molecular profiling of human hepatocellular carcinoma defines mutually exclusive interferon regulation and insulin-like growth factor II overexpression. *Cancer Research*. 2004; 64:6058-64.
16. Zucman-Rossi J, Villanueva A, Nault JC, Llovet JM. Genetic landscape and biomarkers of hepatocellular carcinoma. *Gastroenterology*. 2015; 149:1226-39.e4.
17. Hoshida Y, Nijman SM, Kobayashi M, Chan JA, Brunet JP, Chiang DY, Villanueva A, Newell P, Ikeda K, Hashimoto M, Watanabe G, Gabriel S, Friedman SL, et al. Integrative transcriptome analysis reveals common molecular subclasses of human hepatocellular carcinoma. *Cancer Research*. 2009; 69:7385-92.
18. Schulze K, Imbeaud S, Letouze E, Alexandrov LB, Calderaro J, Rebouissou S, Couchy G, Meiller C, Shinde J, Soysouvanh F, Calatayud AL, Pinyol R, Pelletier L, et al. Exome sequencing of hepatocellular carcinomas identifies new mutational signatures and potential therapeutic targets. *Nature Genetics*. 2015; 47:505-11.
19. Nault JC, Mallet M, Pilati C, Calderaro J, Bioulac-Sage P, Laurent C, Laurent A, Cherqui D, Balabaud C, Zucman-Rossi J. High frequency of telomerase reverse-transcriptase promoter somatic mutations in hepatocellular carcinoma and preneoplastic lesions. *Nature Communications*. 2013; 4:2218.
20. Wilhelm SM, Adnane L, Newell P, Villanueva A, Llovet JM, Lynch M. Preclinical overview of sorafenib, a multikinase inhibitor that targets both Raf and VEGF and PDGF receptor tyrosine kinase signaling. *Molecular Cancer Therapeutics*. 2008; 7:3129-40.
21. Prieto-Dominguez N, Ordóñez R, Fernández A, García-Palomo A, Muntané J, González-Gallego J, Mauriz JL. Modulation of autophagy by sorafenib: effects on treatment response. *Frontiers in Pharmacology*. 2016; 7:151.
22. Rudalska R, Dauch D, Longerich T, McJunkin K, Wuestefeld T, Kang TW, Hohmeyer A, Pesic M, Leibold J, von Thun A, Schirmacher P, Zuber J, Weiss KH, et al. *In vivo* RNAi screening identifies a mechanism of sorafenib resistance in liver cancer. *Nature Medicine*. 2014; 20:1138-46.
23. Meyuhas O. Physiological roles of ribosomal protein S6: one of its kind. *International Review of Cell and Molecular Biology*. 2008; 268:1-37.
24. Villanueva A, Chiang DY, Newell P, Peix J, Thung S, Alsinet C, Tovar V, Roayaie S, Minguez B, Sole M, Battiston C, Van Laarhoven S, Fiel MI, et al. Pivotal role of mTOR signaling in hepatocellular carcinoma. *Gastroenterology*. 2008; 135:1972-83, 83.e1-11.
25. Lv D, Guo L, Zhang T, Huang L. PRAS40 signaling in tumor. *Oncotarget*. 2017; 8:69076-69085. <https://doi.org/10.18632/oncotarget.17299>.
26. Rebouissou S, La Bella T, Rekik S, Imbeaud S, Calatayud AL, Rohr-Udilova N, Martin Y, Couchy G, Bioulac-Sage P, Grasl-Kraupp B, de Koning L, Ganne-Carrie N, Nault JC, et al. Proliferation markers are associated with MET expression in hepatocellular carcinoma and predict tivantinib sensitivity *in vitro*. *Clinical Cancer Research*. 2017; 23:4364-4375.
27. Qi XS, Guo XZ, Han GH, Li HY, Chen J. MET inhibitors for treatment of advanced hepatocellular carcinoma: A review. *World Journal of Gastroenterology*. 2015; 21:5445-53.
28. Curiel-Olmo S, García-Castano A, Vidal R, Pisonero H, Varela I, Leon-Castillo A, Trillo E, González-Vela C, García-Díaz N, Almaraz C, Moreno T, Cereceda L, Madureira R, et al. Individualized strategies to target specific mechanisms of disease in malignant melanoma patients displaying unique mutational signatures. *Oncotarget*. 2015; 6:25452-65. <https://doi.org/10.18632/oncotarget.4545>

29. Li H, Durbin R. Fast and accurate short read alignment with Burrows-Wheeler transform. *Bioinformatics*. 2009; 25:1754-60.
30. McKenna A, Hanna M, Banks E, Sivachenko A, Cibulskis K, Kernytsky A, Garimella K, Altshuler D, Gabriel S, Daly M, DePristo MA. The genome analysis toolkit: a mapreduce framework for analyzing next-generation DNA sequencing data. *Genome Research*. 2010; 20:1297-303.
31. Martinez N, Almaraz C, Vaque JP, Varela I, Derdak S, Beltran S, Mollejo M, Campos-Martin Y, Agueda L, Rinaldi A, Kwee I, Gut M, Blanc J, et al. Whole-exome sequencing in splenic marginal zone lymphoma reveals mutations in genes involved in marginal zone differentiation. *Leukemia*. 2013; 28:1334-40.